Imaging and Analysis of the Uptake and Activity of Azoxystrobin in Plant and Fungal Cells

Samuel R. Swift

University of Edinburgh

Ph.D Thesis

October 2003

Abstract

The aims of this research were to develop and apply a variety of live-cell fluorescence imaging, phosphorimaging and scanning electron microscopy techniques to investigate fungicide/fungus interactions and uptake of the fungicide azoxystrobin into plant and fungal cells on the micro-scale. Radiolabelled fungicide uptake rates were further analysed using combustion analysis and scintillation counting.

Fungicide/fungus interactions were analysed on the wheat leaf surface using single 0.2 μl droplets of azoxystrobin and the pathogens *Blumeria graminis* and *Puccinia recondita*. Although no observable activity was observed on established colonies of *P. recondita*, azoxystrobin was shown to have potent curative and preventative activity on *B. graminis* over distances of up to 7 mm within 24 h. Micro-phosphorimaging of wheat leaves showed that azoxystrobin translocated up to 9 cm after 24 h. Wax stripping of leaves indicated that the majority of movement occurred acropetally. These results indicated that azoxystrobin diffusion through wax and epidermal cells was responsible for preventative and curative activity over short time periods (within 7 h of treatment). Quantitative analysis of radiolabelled fungicide uptake using combustion analysis and scintillation counting showed that approximately 9% of applied azoxystrobin from 0.2 μl fungicide droplets (125 g/L azoxystrobin) was taken into the leaf within 24 h.

Live-cell imaging techniques were developed to study the biology and physiology of mitochondria in hyphae of *Neurospora crassa, Aspergillus nidulans* and *Botrytis cinerea*. The vital fluorescent probes DASPMI, Mitotracker Green, Rhodamine 123, FM4-64 and FM1-43, and GFP targeted to mitochondria were assessed for this purpose. On the basis of these data an assay for mitochondrial activity was developed using the potentiometric marker Rhodamine 123.

Mitochondria were shown to be more tightly packed at the tips of growing hyphae than in sub-apical regions. Inhibitor studies (with azoxystrobin and FCCP) demonstrated that mitochondrial morphology was significantly altered during inhibition (mitochondria became spherical and retracted from the hyphal tip as growth rate decreased) and that membrane potential was significantly reduced. Fungicide uptake experiments supported the conclusion that the main uptake pathway for strobilurin fungicides is by diffusion.

Fluorescence lifetime imaging microscopy (FLIM) and two photon laser scanning microscopy (TPLSM) were assessed for their suitability for future live cell research on fungal mitochondria. Fluorescence lifetime data were collected for several fluorescent probes and lifetime data were recorded in hyphae for the first time. Differences in lifetime of the mitochondrial probe DASPMI were recorded in plasma membrane and mitochondria of the same hypha. Two photon laser scanning microscopy of fungal hyphae labelled with Rhodamine 123, FM4-64 and GFP suggested that the wavelengths and laser power required for imaging had a significantly more damaging effect on cells than confocal microscopy and no improvement in resolution was observed.

Acknowledgements

Many thanks go to the following people I have collaborated with and who provided useful discussion and inspiration:

Jill Foundling
Patrick Hickey
Rick Perry
Stephen MacGinnis
Logan MacKay
Richard Goodwin

People from the University of Edinburgh and Syngenta who have provided technical help and friendship:

Alex Zelter
Richard Parton
Anushka Howell
Anne Stalker
Gavin Hall
Ian Southworth
John Findlay
Gordon Bell
Avian Townley

Friends and family for their encouragement and support:

Mum and Dad
Fiona Edmonds
Cerys Thomas
Charles Taylor
Ewan Roche

The supervision and support of:

Nick Read
Dave Bartlett
Cliff 'TGC' Hart
Chris Jeffree

Registered Trademarks

Quadris and *Amistar* are registered trade marks belonging to Syngenta Ltd.

Mitotracker Green FM, FM 1-43 and FM 4-64 are registered trade marks belonging to Molecular Probes Inc.

Abbreviations

Standard SI (international System of Units) were used throughout this thesis. Non-SI units are as follows:

ADC	analogue to digital converter
AOD	alternative oxidase
Apo	apochromatic
ASAE	American Society of Agricultural Engineers
ASTM	American Society of Testing and Materials
ATP	adenosine triphosphate
AT-SEM	ambient temperature scanning electron microscopy
bas	BASF proprietary image format
BF	barrier filter
Bp	boiling point
C	centigrade
CCD	charge coupled device
CLSM	confocal laser scanning microscopy
cm	centimetre
conc	concentration
DC	dichroic (mirror)
DMSO	Dimethyl Sulfoxide
dps	discharges per second
Em	emission
EPS	encapsulated postscript
EtOH	ethanol
Exc	excitation
FADH	flavin adenine dinucleotide
FCCP	Carbonyl cyanide p-[trifluormethoxy]-phenyl-hydrazone
FGSC	fungal genetic stock company
FLIM	fluorescence lifetime imaging microscopy
fs	femtosecond (s)
g	gram
Gb	gigabyte
GFP	green fluorescent protein

GHS	green excitation filter set
GHz	Gigahertz
GPL	General Public licence
h	hour(s)
HeNe	helium neon
IR	infrared
IPA	ISO-propylaclohol
jpg	joint photographic experts group
kDa	kilodaltons
kg	kilogram
kV	kilovolt
L	litre (s)
LP	long pass filter
LSM	laser scanning microscopy
LTSEM	low temperature scanning electron microscopy
Max	maximum
Mb	megabyte
MEA	malt extract agar
MHz	megahertz
min	minute (s)
ml	millilitre
mm	millimetre
mV	millivolt
MW	molecular weight
μl	microlitre
μm	micrometer
NA	numerical aperture
NADH	nicotinamide adenine dinucleotide
No	number
ns	nanosecond (s)
PC	personal computer
pic	BioRad proprietary image format
PMT	photomultiplier tube
ppm	parts per million
prep	preparation
RAM	random access memory

RH	relative humidity
s	second (s)
SEM	scanning electron microscopy
Sp	species
TAC	time to amplitude converter
TCSPC	time correlated single photon counting
tif	tagged image format
TiSapph	titanium sapphire
TPLSM	two photon laser scanning microscopy
Tween20	Polyoxyethylenesorbitan monolaurate
txt	text only file
UV	Ultraviolet
W	watt
w/v	weight by volume

Contents

Declaration i
Abstract ii
Acknowledgements iv
Registered Trademarks v
Abbreviations vi

1 Review of the Literature **2**
1.1 General Introduction 2
1.1.1 Crop Losses and Disease 2
1.1.2 Fungal Penetration 4
1.2 A Brief History of Fungicides 5
1.2.1 Fungicides and Food Quality 5
1.2.2 Fungicide Modes of Action 6
1.3 Novel Fungicides and Natural Products 7
1.3.1 The Strobilurins 7
1.3.2 Azoxystrobin Mode of Action 9
1.4 Fungicide Resistance 9
1.5 Fungicide Formulation Chemistry 11
1.5.1 Leaf Surface Structures and Leaf Wettability 11
1.5.2 Influence of Formulation Physical Type on Fungicide Activity 12
1.5.3 Leaf Penetration by Fungicides 14
1.5.4 Droplet Deposition 15
1.6 Fungal Biology and Fungicide Research 17
1.6.1 Fungal Morphology and Hyphal Extension 18
1.6.2 Potential Pathways for Fungicide Uptake into Cells and Organelles 19
1.6.3 Passive Uptake 19

1.6.4 Mitochondria: Form and Function 20
1.6.5 Fungal Mitochondria 21
1.7 Introduction to Research in this Thesis 23

2 Materials and Methods **26**
2.1 Chemicals 26
2.1.1 Media and Inhibitors 26
2.1.2 Fungicides 26
2.1.3 Fungicide Formulations 26
2.2 Plant Material 28
2.3 Fungal Material 28
2.3.1 Growth Conditions for Fungal Infection *in planta* 29
2.3.2 Growth Conditions for Fungal Cultures 29
2.3.3 Media 29
2.4 Treatments 31
2.4.1 Droplet Application 31
2.4.2 Wax Stripping 32
2.4.3 Inhibitors 32
2.5 Light Microscopy 32
2.5.1 Sample Preparation for Light Microscopy 33
2.5.2 Image Processing 33
2.6 Scanning Electron Microscopy 33
2.6.1 Ambient Temperature Scanning Electron Microscopy 33
2.6.2 Low Temperature Scanning Electron Microscopy 34
2.6.3 Image Processing 34
2.7 Phosphorimaging 35
2.7.1 Radiolabelling Azoxystrobin 35
2.7.2 Image Plate 35
2.7.3 Digitiser 36
2.7.4 Image Processing 36
2.7.5 Combustion Analysis and Scintillation Counting 38
2.8 Live-Cell Imaging 39
2.8.1 Sample Preparation 39
2.8.2 Loading of Cell-Permeant Dyes 40
2.8.3 Introduction of Inhibitors and Fungicides to Samples 40
2.8.4 Confocal Laser Scanning Microscopy 41

2.8.5 Image Processing 43
2.8.6 Two Photon Laser Scanning Microscopy 44
2.8.7 Fluorescence Lifetime Imaging Microscopy 45
2.9 Image Processing for this Report 45

3 Azoxystrobin Droplet Deposition **46**
3.1 Introduction and Aims 46
3.1.1 Introduction 46
3.1.2 Aims 47
3.2 Results 47
3.2.1 Overview of Results 47
3.2.2 Light Microscopy of Drying Deposits 48
3.2.3 Comparison of LT-SEM and AT-SEM Image Quality and Complexity 52
3.2.4 Comparison of Azoxystrobin Formulation Deposits 56
3.3 Discussion 68
3.3.1 Mechanism of Annular Deposit Formation 68
3.3.2 SEM Techniques in the Study of Pesticide Deposits 69
3.3.3 Mechanical Damage and Deposit Consistency 71

4 Azoxystrobin Micro-Biokinetics **75**
4.1 Introduction and Aims 75
4.1.1 Introduction 75
4.1.2 Aims 76
4.2 Results 76
4.2.1 Overview of Results 76
4.2.2 Wheat Leaf Structures Imaged with LT-SEM 78
4.2.3 *Puccinia recondita* Infected Tissue Imaged with LT-SEM 80
4.2.4 Investigation into the Curative Activity of Azoxystrobin on *Puccinia recondita* 82
4.2.5 Investigation into the Curative and Preventative Activity of Azoxystrobin on *Blumeria graminis* 83
4.2.6 Ambient Temperature SEM and LT-SEM of Wheat Infected with *Blumeria graminis* 84
4.2.7 Curative Activity of Azoxystrobin on *Blumeria graminis* 87
4.2.8 Preventative Activity of Azoxystrobin on *Blumeria graminis* 93

4.3 Discussion 101
4.3.1 Curative Activity of Azoxystrobin on *Puccinia Recondita* 101
4.3.2 Comparison of AT-SEM and LT-SEM techniques in the Study of *Blumeria Graminis* 103
4.3.3 Curative Activity of Azoxystrobin on *Blumeria graminis* 104
4.3.4 Preventative Activity of Azoxystrobin on *Blumeria graminis* 106

5 Measuring Azoxystrobin Uptake and Translocation in Wheat 108
5.1 Introduction and Aims 108
5.1.1 Introduction 108
5.1.2 Aims 109
5.2 Results 109
5.2.1 Overview of Results 109
5.2.2 Phosphorimaging of Radiolabelled Azoxystrobin over 7 h 110
5.2.3 Low Temperature SEM of Wax Stripped Leaves 113
5.2.4 Phosphorimaging of Normal and Wax Stripped Leaves 116
5.2.5 Combustion Analysis and Scintillation Counting of Wax Stripped Leaves 117
5.3 Discussion 119
5.3.1 Redistribution of Azoxystrobin over 7 h 119
5.3.2 Uptake, Translocation and Redistribution of Azoxystrobin after 24 h 120

6 Live-Cell Imaging of Mitochondrial Spatial Location, Morphology and Physiology in Fungal Hyphae 123
6.1 Introduction and Aims 123
6.1.1 Introduction 123
6.1.2 Aims 125
6.2 Results 125
6.2.1 Overview of Results 125
6.2.2 Comparison of Mitochondrion-Selective Probes 126
6.2.3 Morphology and Spatial Location of Mitochondria in Filamentous Fungi 142
6.2.4 Physiology and Activity of Mitochondria in Filamentous Fungi 150
6.2.5 Morphological and Spatial Location of Mitochondria Following Treatment with FCCP and Azoxystrobin 153

6.3 Discussion . . . 160
6.3.1 Comparison of Mitochondrion-Selective Probes . . . 160
6.3.2 Mitochondrial Morphology and Dynamics . . . 160
6.3.3 Mitochondrial Physiology . . . 163
6.3.4 Mitochondrial Inhibition . . . 164

7 Live-Cell Two Photon Laser Scanning and Fluorescence Lifetime Imaging Microscopy of Filamentous Fungi **168**
7.1 Introduction and Aims . . . 168
7.1.1 Introduction . . . 168
7.1.2 Aims . . . 169
7.2 Overview of Technology . . . 170
7.2.1 Two Photon Scanning Microscopy . . . 170
7.2.2 Principles of 2 Photon Excitation . . . 170
7.2.3 Fluorescence Lifetime Imaging Microscopy . . . 173
7.3 Results . . . 176
7.3.1 Overview of Results . . . 176
7.3.2 Live-Cell TPLSM of Filamentous Fungi . . . 177
7.3.3 Live-Cell FLIM of Filamentous Fungi at High Temporal Resolution . . . 188
7.4 Discussion . . . 196
7.4.1 Two Photon Laser Scanning Microscopy . . . 196
7.4.2 Fluorescence Lifetime Imaging Microscopy . . . 199

8 Future Work **202**
8.1 Future Work . . . 202
8.1.1 Droplet and Deposit Characteristics . . . 203
8.1.2 Micro-scale of Infection Biokinetics . . . 204
8.1.3 Uptake and Translocation . . . 206
8.1.4 Fungicide Uptake and Mitochondrial Dysfunction . . . 207
8.1.5 New Techniques in Live-Cell Imaging . . . 208

9 References **210**

10 Appendix **234**
10.1 Azoxystrobin Micro-Biokinetics . . . 234
10.1.1 Curative Control of *Blumeria graminis* . . . 234

10.1.2 Preventative Control of *Blumeria graminis* 235
10.2 Azoxystrobin Uptake and Translocation in Wheat 236
10.2.1 Longitudinal Translocation of Azoxystrobin 236
10.2.2 Lateral Translocation of Azoxystrobin 246
10.2.3 Uptake of Azoxystrobin over 24 h 250
10.3 Uptake of Azoxystrobin into Fungal Cells 252

11 Publications and Presented Posters **253**
11.1 ICHC 2000 253
11.2 Scanning FAMS, 2001 255

Chapter 1

Review of the Literature

We see our cattle fall and our plants wither without being able to render them assistance, lacking as we do understanding of their condition.
J.C. Fabricus, 1745-1808.

1.1 General Introduction

The predicted growth of the world population from 6.1 billion in 2000 to approximately 8 billion by 2020 (United Nations, 2000) presents a major global challenge to meet the necessary increases in food production and distribution. Thousands of micro-organisms are known to cause plant diseases and, on average, each crop plant is affected by 50 or more diseases (Jackson and Taylor, 1996). Pathogens can be obligate on only one species, or opportunistic on hundreds of different plant species (Knogge, 1996). These pathogens are estimated to cause yield reductions of almost 20% in the principal food and cash crops worldwide, with more severe losses on highly susceptible crop varieties (Oerke et al., 1994; Schwinn, 1992). Furthermore, many crop pathogens pose health risks to humans e.g. carcinogens from mycotoxins produced by fungal pathogens (Knight et al., 1997; Jackson and Taylor, 1996; Schumann, 1991; Carefoot and Sprott, 1967).

1.1.1 Crop Losses and Disease

Plants come into contact with a constant barrage of insects, nematodes, fungi and bacterial pests and yet under natural conditions the majority of plants remain healthy most of the time. Plants have evolved with pathogens and insect pests and as a result any plant has a high degree of immunity to most of them (Keen, 1992). It is therefore unsurprising that in a natural ecosystem epidemics are the exception, due largely to this natural balance

between host, environment and pathogen. Conversely, in modern agriculture monocultures are usually planted and epidemics are often the result (Jackson and Taylor, 1996). However, the balance between host and pathogen is not static and the parameters of an epidemic can often be manipulated in favour of one or the other (Osbourn, 1996; Bennett and Wallsgrove, 1994).

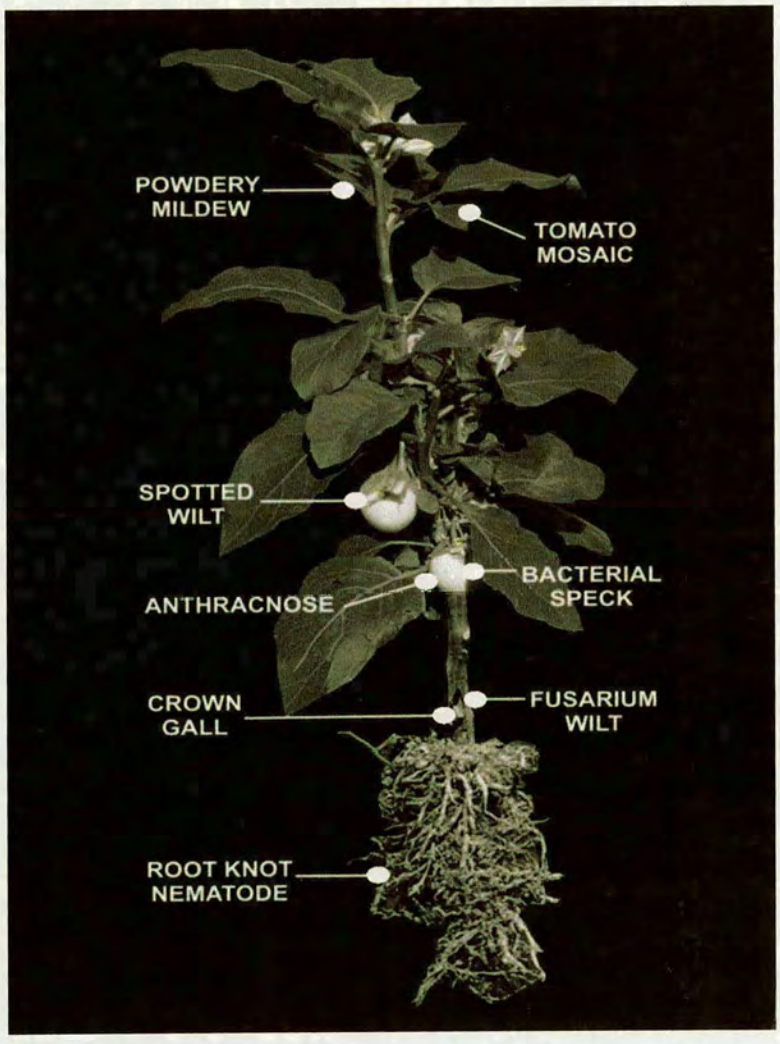

Figure 1.1: Examples of characteristic diseases of tomato caused by viruses, bacteria, fungi and nematodes (adapted from Jackson and Taylor, 1996).

Five major groups of organisms (bacteria, mycoplasmas, viruses and viroids, nematodes, and fungi) are responsible for plant diseases (Fig 1.1). Approximately 80 species of plant pathogenic bacteria are responsible for plant disease, including fruit rot, blight, galls, cankers, wilts and leaf spots. Mycoplasmas (wall-less micro-organisms) are known to be responsible

for over 200 distinct diseases in plants. These include chlorosis, stunting and progressive weakening. About a quarter of the 2000 known viruses attack and cause disease in plants. These include barley stripe, peanut mottle, cucumber mosaic, and potato leaf roll viruses. Hundreds of species of nematode feed on plants, causing disease symptoms which include root galls, root knots, root lesions, wilting and abnormal floral development.

However, of all the causal agents of infectious disease in crops, it is the phytopathogenic fungi which play the dominant role, by not only causing devastating epidemics, but also the chronic and commercially significant losses to crop yields every year (Jackson and Taylor, 1996; Knogge, 1996, Isaac, 1992). Fungi constitute a highly versatile group of eukaryotic heterotrophic organisms, which have colonised most natural habitats. The vast majority are saprotrophic, but even so, approximately 8% of the 100 000 recognised fungal species are capable of colonising plants, with a significant proportion responsible for disease (Knogge, 1996). Probably all of the 300 000 known species of flowering plant are attacked by pathogenic fungi, although a single plant species is typically susceptible to only a few fungal pathogens. Similarly, most fungi have only a limited host range (Scheffer, 1991).

1.1.2 Fungal Penetration

In order to colonise plants, fungal micro-organisms have evolved strategies to invade plant tissue, to optimise growth *in planta*, and to propagate. Whereas opportunistic fungi (as well as bacteria and viruses) depend on natural openings or wounds for invasion, many obligate pathogens have evolved mechanisms to actively penetrate the plant's outer structural barriers, namely the cuticle, and the cell wall. This generally involves the secretion of hydrolytic enzymes (e.g. cutinases, cellulases, pectinases and proteases), but in the more advanced species, specialised infection structures called appressoria allow the mechanical penetration of the germ tube (Knogge, 1996; Mendgen and Deising, 1993; Howard et al., 1991).

Certain fungal species, including some rusts, have developed mechanisms to actively locate stomatal openings on the host surface. This mechanism is poorly understood, but chemotaxis (movement up a concentration gradient either of gases, photosynthates or of hormones leaking from the stomata) and recognition of the host surface through touch sensing are thought to play an important role (Correa and Hoch, 1995; Huttenen, 1994; Read et al., 1992; Hoch et al., 1987; Tukey 1971).

1.2 A Brief History of Fungicides

The widespread use of fungicides in agriculture is relatively recent, and most of the major developments have taken place during the last 40 years (Clough and Godfrey, 1996). In the first half of this century, protection of many crops became possible with the advent of organic fungicides. In the 1960's, the development of systemic products able to penetrate plant tissue and deliver curative properties beyond the site of application permitted more flexible application regimes (Lyr, 1995; Brent, 1985).

Commercial fungicides account for approximately 20% of the agrochemical market value. World-wide sales in 1996 were put at about $5.9 billion (Wood Mackenzie, 1997). Agrochemical companies are constantly searching for new fungicides for the following reasons (Clough and Godfrey, 1996):

- to find compounds with marketable technical advantages over competing products.
- to find fungicides with novel modes of action to overcome pathogen resistance.
- to replace certain products with new ones displaying decreased toxicity on non-target species.

There are now at least 123 active ingredients registered as fungicides world-wide (Tomlin, 2002). Despite the choice of effective fungicides available, new antifungal chemicals are still required to deliver improved yield and quality benefits. Improved fungicides are also needed to combat diseases, such as vascular wilts and anthracnoses, that are poorly controlled by current products.

1.2.1 Fungicides and Food Quality

Fungicides not only improve crop yield, but also contribute to food safety by controlling many of the fungi that produce mycotoxins. Nearly one quarter of food crops world-wide are affected by mycotoxins such as aflatoxins, ergotamine, Fusarium toxins, patulin, and tenuazonic acid (Schneider and Dickert, 1994; Pohland, 1993). Most mycotoxicoses are caused by such common and widespread fungi as *Aspergillus, Penicillium, Fusarium* and *Stachybotrys*, and some may result in severe illness or death. Plant pathogenic fungi must be controlled if consumer demand in developed countries for premium quality, diverse foods is to be met.

1.2.2 Fungicide Modes of Action

The first fungicides, based on copper and sulphur, were discovered in 1846 and 1882, respectively. Today these early inorganic compounds are being superceded by more user-friendly organic compounds, which are active at low doses and effective against a wide range of fungi (Lucas, 1998; Deacon, 1997). Metal-based fungicides employing copper and mercury are still in use today and inhibit a wide variety of enzymes involved in a number of metabolic processes. The simultaneous fatal disruption of several core processes explains why few fungi have evolved resistance against the copper, sulphur, mercury or dithiocarbamate fungicides. Modern, systemic fungicides are usually much more site-specific (Fig 1.2), often acting on only a single site within the cell (Deacon, 1997; Lyr et al., 1995; Dixon et al., 1995).

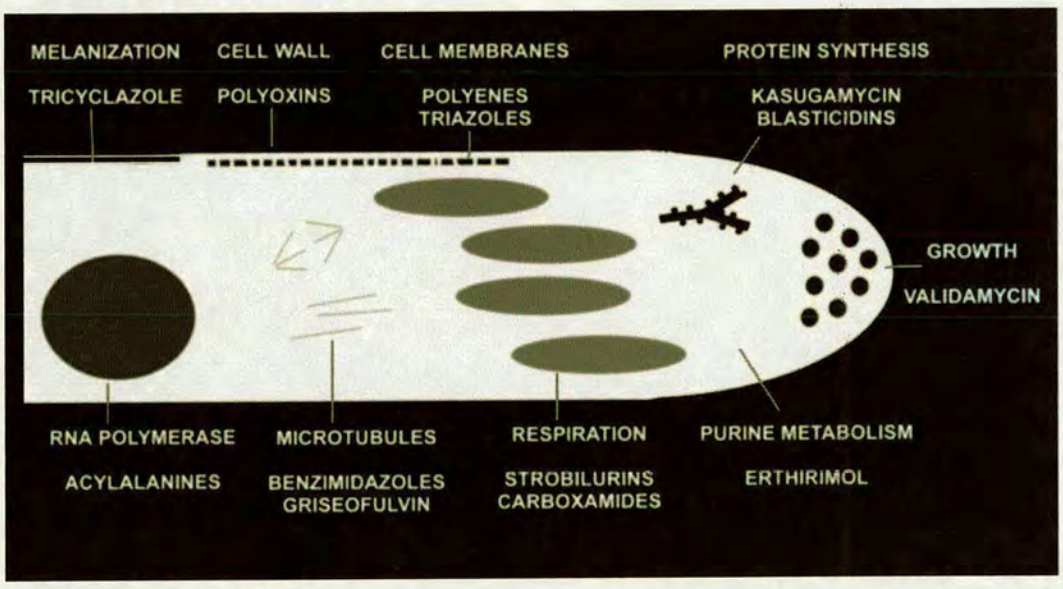

Figure 1.2: The main targets currently exploited for chemical control of fungi that cause plant diseases. Some examples of the chemical control agents are shown (adapted from Deacon, 1997).

Because these fungicides have specific modes of action, mutations in the fungal target protein can profoundly affect the efficacy of the compound. Often a single mutation has been found sufficient to abolish activity and lead to resistance (Steffens et al., 1996; Georgopolous et al., 1995). Consequently, agrochemical companies empirically screen many millions of compounds in an attempt to keep one step ahead of the constantly evolving target species. Recent estimations suggest that only 1 in 20 000 chemicals investigated may become a commercial product (Lucas, 1998; Clough et al., 1997).

1.3 Novel Fungicides and Natural Products

Fungicide research has recently delivered a diverse range of chemical structures with novel modes of action; these products are expected to have a significant impact on disease control in the 21st century. Naturally occurring substances found in fungi, bacteria, and higher plants are important sources of molecules with antifungal properties. They may be developed either as products *per se* or used as starting points for organic synthesis.

The first major natural products of microbial origin to be commercialised were the antibiotics blasticidin S, kasugamycin, and validamycin A. They were developed in Japan to control rice blast (*Magnaporthe grisea*) and sheath blight (*Rhizoctonia solani*) (Worthington, 1988). Another group of antibiotics, the polyoxins, have been used to protect against fungal disease of fruit trees and vegetables (Suzuki et al., 1965). The complex natural product soraphen A is a potent inhibitor of acetyl-coA-carboxylase in fungi; its discovery has stimulated further research for novel fungicides that act on this enzyme (Pridzun et al., 1995). Several natural fungicidal products with simpler structures are more suitable as leads for chemical synthesis. Extensive research on two of these, the phenylpyrrole antibiotic, pyrrolnitrin (Gehmann et al., 1990; Nevill et al., 1988; Arima et al., 1964), and strobilurin A, has yielded commercial products (Knight et al., 1997; Musilek, 1969). The strobilurins, and specifically azoxystrobin, were of primary interest to this research.

1.3.1 The Strobilurins

Strobilurin A and Oudemansin A are fungicidal natural products found in the basidiomycete fungi *Strobilurus tenacellus* and *Oudemansiella mucida* respectively (Anke et al., 1989; Musilek, 1969). These substances are members of a group of natural products, the strobilurins, oudemansins, and myxothiazols (Fig 1.3). They share a common mode of action, the inhibition of mitochondrial respiration in fungi (Bartlett et al., 2002; US Environmental Protection agency, 1996); oxidation of ubiquinol is blocked at the Q_o-site of the cytochrome b-c_1 complex, which is located on the inner mitochondrial membrane of fungi (Bartlett et al., 2002).

These natural products stimulated major independent programmes of synthetic chemistry by ICI and BASF. Subsequently, most leading crop production companies have researched this mode of action, and over 700 patents have been published by the industry (Bartlett et al., 2002; Knight et al., 1997). Strobilurin A is active *in vitro* against a range of plant pathogenic fungi, but its photochemical instability and relatively high volatility result in poor activity *in vivo* (Clough et al., 1997). Synthetic programmes were aimed at preparing

analogues with improved light stability, low acute mammalian toxicity, appropriate movement properties within the plant, and acceptable crop safety. The first synthetic strobilurins, azoxystrobin (Fig 1.4) and kresoxim-methyl, were launched in 1996, and others have been developed including trifloxystrobin, pyraclostrobin, picoxystrobin, dimoxystrobin and fluoxastrobin (Bartlett, personal communication; Bartlett et al., 2002; Knight et al., 1997).

Azoxystrobin is a broad spectrum fungicide controlling major economic pathogens from every taxonomic group of plant pathogens (Heaney and Knight, 1994; Godwin et al., 1992), and is currently registered in 72 countries for use on 84 crops and over 400 plant pathogens (Bartlett, personal communication). It strongly inhibits spore germination, showing excellent preventative activity, while demonstrating additional eradicant and anti-sporulant properties, depending on crop and pathogen. Kresoxim-methyl also controls fungi from each of the taxonomic groups and shows particular strength against powdery mildews and apple scab (Brunelli et al., 1996; Ammerman et al., 1992). Azoxystrobin was one of 1400 analogues tested (Godwin et al., 1993).

Figure 1.3: *Oudemansiella mucida*, the wood rotting fungus from which some of the strobilurin class of fungicide were isolated (from Siller and Turscanyi, 2002).

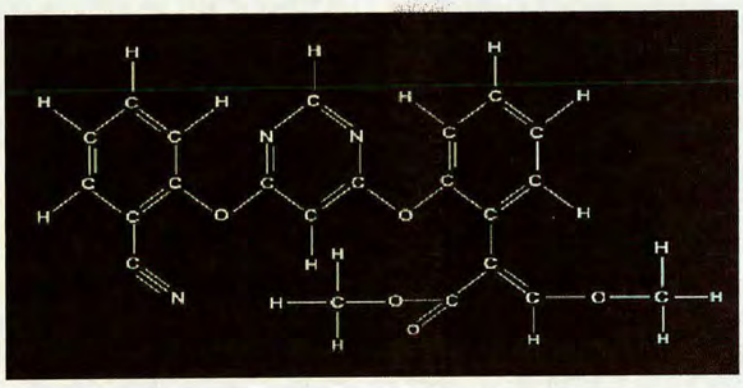

Figure 1.4: The molecular structure of the synthesised strobilurin, azoxystrobin (adapted from Clough and Godfrey, 1998).

The fungicidal activity of the synthetic strobilurins results directly from the inhibition of mitochondrial respiration, an essential process in both fungi and plants. It is believed that the combination of high fungicidal potency and good crop safety is attributable to differential penetration and degradation between plant and fungal species, rather than to differences between mitochondrial target sites (Gold et al., 1995). Since the strobilurins possess a novel mode of action, the synthetic strobilurins control fungi that are resistant to the other major classes of fungicide such as the 14-demethylase inhibitors, phenylamides, dicarboxamides, and benzimidazoles (Godwin et al., 1993).

1.3.2 Azoxystrobin Mode of Action

Azoxystrobin has a novel, single site mode of action, exerting its effect on fungi by blocking the ubiquinol:cytochrome c oxidoreductase complex (cytochrome bc_1) thus inhibiting the generation of ATP in the fungal cell (Wiggins and Jager, 1994; Becker et al., 1981). Given that strobilurins act as inhibitors of respiration in fungal cells, application of azoxystrobin is recommended early in disease development to maximise its potent effect against spore germination (a particularly energy-demanding phase of fungal development). By comparison, the most active ergosterol biosynthesis inhibitors demonstrate better late curative or eradicant activities against plant pathogens than azoxystrobin because the mycelium is growing rapidly at the time of application when ergosterol demands are high. A feature of azoxystrobin applied during the stem expansion phase of cereal growth is translaminar and systemic movement to give disease control on leaves not unfurled at the time of application (Bartlett et al., 2002; Clough and Godfrey, 1998).

1.4 Fungicide Resistance

The development of resistance by target pathogens to current products adds impetus to the search for novel fungicides. In the late 1960's, reports of resistance were limited (Georgopolous, 1967); by 1988, Eckert had identified over 60 fungal genera in which resistance had been recorded to 12 different fungicide groups.

All major systemic fungicide groups (benzimidazoles, phenylamides, dicarboxamides, sterol biosynthesis inhibitors and strobilurins) have been affected to a greater or lesser extent by the development of resistance in target populations (De Waard, 1994; Staub, 1991; Smith, 1988; Georgopolous, 1967). These modern fungicides, with their greater potency, persistence of effect, and more extensive distribution in the crop, exert strong selection pressures.

Resistance can evolve quickly where conditions are favourable for the epidemic if anti-resistance strategies have not been implemented. A novel fungicide with a multiple site of action is undoubtedly attractive from an anti-resistance viewpoint, yet even this is challenged by the recent discovery of a major gene (Dic1) controlling resistance to the old multiple site fungicide dichlofluanid in field isolates of *Botrytis cinerea* (Pollastro, 1996).

Strategies with the potential to contain or delay resistance development depend upon inherent 'fitness penalties' in resistant strains. Such strains are built around alternation or mixtures of fungicides from different cross resistance groups to reduce or diversify selection pressures. They have been successful in delaying or limiting the development of resistance to phenylamides, dicarboximides, and the ergosterol biosynthesis inhibitors (Felsenstein, 1994; Staub, 1991; Lorenz, 1988). However, the adoption of such schemes over large areas in a consistent fashion presents many practical problems and their success has been limited in the past because strategies were often introduced only in response to a major resistance problem (Staub, 1991).

When a new type of fungicide is introduced into major agricultural outlets, the risk of resistance has to be assessed and there are guidelines available from currently used fungicides indicating the important factors requiring consideration (Georgopolous et al, 1995).

Attempts to raise mutants to azoxystrobin have met with partial success; strains of *Neurospora crassa* with low levels of resistance and a more tolerant *Septoria tritici* mutant have been isolated (Ziogas et al, 1997). In mutant sporidia, instead of inhibition, stimulated respiration in the presence of a strobilurin compound was observed. This was due to the shift in fungal metabolism to the alternative oxidase. Ubiquinone is generally thought to be the branching point between the cytochrome and the alternative pathway (Ziogas et al, 1997; Moore and Siedow, 1991; Ziogas and Georgopolous, 1979). Thus, respiration is uninhibited by inhibitors of cytochrome III and IV in the organisms with an active alternative pathway. From the first studies on the genetic basis of the alternative pathway in *N. crassa*, it was concluded that the alternative oxidase activity is encoded by structural and regulatory genes (Bertrand et al, 1983).

1.5 Fungicide Formulation Chemistry

The activity of a foliar-applied pesticide must ultimately depend on the concentration of the active ingredient that reaches the site of action together with the intrinsic potency of the pesticide on the biochemical mechanisms taking place at these sites. A number of interrelated factors may influence uptake and movement, including the efficiency of foliar retention and cuticular penetration, tissue absorption and, in the case of systemic compounds, vascular loading and translocation. Pesticide metabolism or immobilisation may further reduce the amount of active ingredient reaching the target sites.

Although adjuvants have a significant effect on the biological activity of fungicides and leaf surface wettability, a variety of environmental, commercial, health and safety issues often take precedence in formulation development (Stock and Davies, 1992). To be effective, systemic fungicides must penetrate the leaf and be translocated throughout the plant. Azoxystrobin, for example, is a systemic fungicide, and is exclusively transported through the xylem in the direction of transpiration (Bartlett et al., 2002).

1.5.1 Leaf Surface Structures and Leaf Wettability

All primary aerial surfaces of vascular plants (and some bryophytes) are covered by a thin, superficial film called the cuticle. This membrane is composed of soluble and polymeric lipids whose function is to protect and waterproof the plant surface (Jeffree, 1996; Holloway, 1994). Comparison between cuticle preparations of extant plants and 400 million year old fossilised cuticles reveals anatomically indistinguishable guard cells as well as resilient and hydrophobic macromolecules on the leaf surface of both groups. It is acknowledged that the cuticle has evolved to serve the primary function of preventing water loss from within the plant via the epidermal surface, without unduly compromising the plant's ability to photosynthesise at an effective rate (Edwards et al., 1996; Jeffree, 1996; Raven, 1984).

Given that the plant cuticle controls the exchange of matter between leaf and atmosphere (not only loss of water from the leaf interior, but also the uptake of non-volatile chemicals deposited on the leaf surface) the properties of the cuticle are recognised as imposing a major barrier to the penetration of foliar-applied agrochemicals (Schreiber et al., 1996; Baker, 1992; Silcox and Holloway, 1989).

Furthermore, all plants carry an amorphous epicuticular wax film upon which plate, tube, ribbon, rod, filament or dendrite crystalline wax structures may be superimposed. Intracuticular wax embedded in the cuticle confers significant water resistance to the leaf, whereas leaf surface waxes and prominent surface wax structures are significant in water repellency (Percy and Baker, 1990; Juniper and Jeffree, 1983; Juniper and Bradley, 1958).

In an application of a pesticide, the retained quantity and distribution of the active ingredients on plant surfaces are largely influenced by wetting conditions as determined by the pesticide formulation and leaf surface wettability (Wattanabe and Yamaguchi, 1992). It is an obvious conclusion that the successful retention of an active ingredient on the leaf surface is an essential prerequisite for uptake, distribution and activity for all foliar-applied systemic fungicides although its chemical properties may significantly influence the options available to the formulation chemist. These issues are considered below.

1.5.2 Influence of Formulation Physical Type on Fungicide Activity

The influence of formulation and adjuvants on the biological activity of a pesticide active ingredient is a complex, interactive phenomenon and many factors can influence the final result (Stock and Briggs, 2000; Stock and Davies, 1992). The physical properties of the active ingredient and adjuvant both play an important part in the uptake of compounds, although the exact nature of each is often far from clear.

Surfactants are important ingredients of pesticidal formulations. In conjunction with other adjuvants they may function as spreaders, stickers, antifoamers, compatibility agents or as so called 'activators' (McWhorter, 1982). Activator adjuvants improve the efficacy of a formulation and are thought to function primarily by altering solubility relationships and hence affecting the ability of a pesticide to penetrate the plant cuticle (Van Valkenberg, 1982).

It is well established that surfactants can enhance the biological efficacy of active ingredients (Riederer and Schonherr, 1990; Silcox and Holloway, 1989). Adjuvants for use with fungicides have been identified since the first studies on formulation efficiency, and it is well known that the activity of systemic fungicides can be improved by a proper choice of adjuvant (Steurbaut, 1993).

In medicine, percutaneous drug absorption is recognised as relying on several factors. These are the release of a solid to solution, uptake from solution into the skin, clearance into the sub-barrier environment, and long distance movement and metabolism (Briggs and Bromilow, 1992, Higuchi, 1977). Similarly, general empirical rules govern foliar penetration: non-polar solutes are better absorbed than polar ones; lipoidal agents are more easily delivered than non-lipids; solids with low melting point are more easily absorbed than those with high melting point; liquids are better absorbed than solids (Briggs and Bromilow, 1992; McCall, 1982).

However, the majority of compounds penetrate most plants poorly when applied alone, with few exceptions (Baker et al., 1992). Hence, formulation chemistry is an important stage in the commercial development of any agrochemical. To penetrate readily, a compound must be either in the form of a liquid or in solution. Solubility is influenced by the physical properties of the compound, the solvent properties of the adjuvant and the adjuvant concentration (Briggs and Bromilow, 1992).

The physicochemical properties of the active ingredient influence, and often seriously limit, the type of formulation which can be produced (Holloway, 1992). Changes to the active ingredient's physicochemical properties are not always an option because the biological efficacy of the compound can be seriously impaired (Stock and Davies, 1992). It is also important to recognise that restrictions are also imposed by commercial requirements such as formulation reliability, storage stability and acceptable cost.

Active ingredients do not always have appropriate physicochemical properties to be formulated in their most biologically active form. For example, a high melting point systemic herbicide which requires efficient penetration for maximal activity is in its least active form if applied to the leaf surface as suspended particles, but this may be the only realistic option to the formulation chemist (Fig 1.5). Furthermore, small particle size of the active ingredient and high droplet surface area of applied pesticide generally improve uptake.

Although solvent based products, such as emulsifiable concentrates, are generally the most biologically active they tend to be the least favoured both environmentally, and in terms of operator safety and safe transportation. Of the major non-solvent based formulations in common use, those with a particular content, such as wettable powders and aqueous suspension concentrates, are often viewed as being less biologically active. Therefore, formulation chemistry is often a question of compromise (Stock and Davies, 1992).

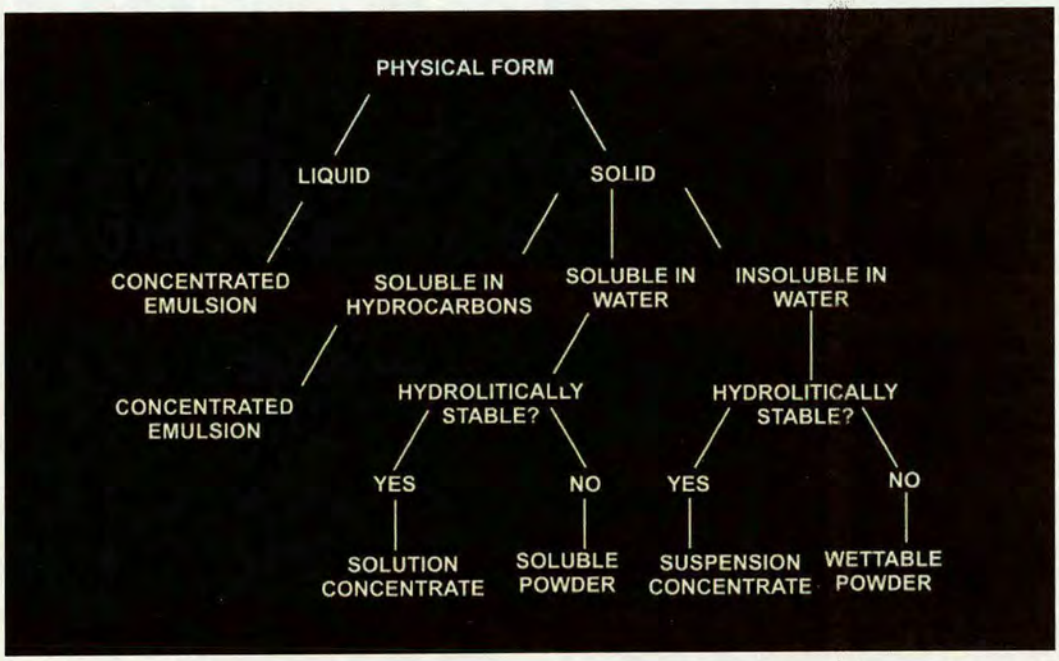

Figure 1.5: Overview of the formulation options available in fungicide development based on the physical properties of the active ingredient (adapted from Stock and Davies, 1992).

Historically, fungicide-specific adjuvant research was of limited interest because the first fungicides had only contact activity. Preventative activity was only possible through the formation of a uniform layer on the leaf surface, achieved by high volume and repeated applications with sufficient wetting. The introduction of systemic fungicides, which can penetrate the plant and translocate via the apoplast, has changed this situation entirely because a complete and uniform surface treatment is no longer necessary. Penetration and associated increases in translocation of fungicides can be greatly influenced by judicious choice of adjuvants.

1.5.3 Leaf Penetration by Fungicides

As previously discussed, the cuticle of most plants represents a major barrier to the penetration of foliar applied pesticides, based not only on an understanding of their fundamental physical and chemical properties (Baker, 1989; Holloway, 1982), but also on work with isolated cuticles (Schonherr and Baur, 1996; Davis et al., 1979). Surfactants play an important role in aiding the penetration of pesticides into leaves (Hartley and Bryce, 1980 ; Foy, 1969).

This may depend on one or more of the following factors (Anderson and Girling, 1983) -

- the dissolution/disruption of cuticular waxes
- the solubilisation of the active ingredient of the dried spray deposit
- the penetration of the leaf cuticle by the surfactant, thereby rendering the cuticle more permeable to the active ingredient
- the co-penetration of the active ingredient with the surfactant

Considerable attention has been given to the first three of these effects (Hartley and Bryce, 1980) but penetration has been investigated only to a small extent (Schonherr, 2001; McCall, 1982; Hart and Price, 1979).

1.5.4 Droplet Deposition

The residue of active ingredients deposited on the leaf following spray application will depend not only on the properties of the formulation, but also on the chemical and physical properties of the surface which has been treated. Drops resting on smooth, homogeneous surfaces take the shape of spherical caps provided they are of mass lower than 1 mg (larger drops are distorted by gravity). Two extreme modes of evaporation (Fig 1.6) are recognised under these circumstances although it is not unusual for both modes to occur simultaneously or alternately and discontinuously (Picknett and Bexton, 1976):

- the contact angle is unaltered during evaporation, the drop shape remaining that of a spherical cap but with diminishing area of contact between liquid and surface
- the contact area is unaltered during evaporation, evaporation takes place with unchanged surface area, the shape remaining that of a spherical cap but with diminishing contact angle

This is by no means the full story, however, for without exception the surfaces of plants are to varying extents chemically and structurally heterogeneous (due to surface structures such as trichomes, stomatal pores and surface bound crystalline structures such as waxes). Surface roughness is recognised as playing an important role in the spreading behaviour of surface liquids and to influence the macroscopic contact angle between liquid and surface (Schreiber et al., 1996; Oliver et al., 1977; Holloway, 1971; Holloway, 1969; Wenzel, 1949). Microscopic roughness is of particular influence to this contact angle and its movement during evaporation.

The lower spatial limit for the influence of surface roughness on spreading and wetting has been placed at only 50 nm by some authors (e.g. Oliver et al., 1977). Studies of contact angles on leaf surfaces suggest that although profoundly hydrophobic surface chemicals such as waxes are water repellent, the highest contact angles are exhibited on plant leaves with crystalline surface waxes which hold the droplet away from the 'true' surface of the leaf (Juniper and Jeffree, 1983; Oliver et al., 1980; Oliver et al., 1977; Holloway, 1971).

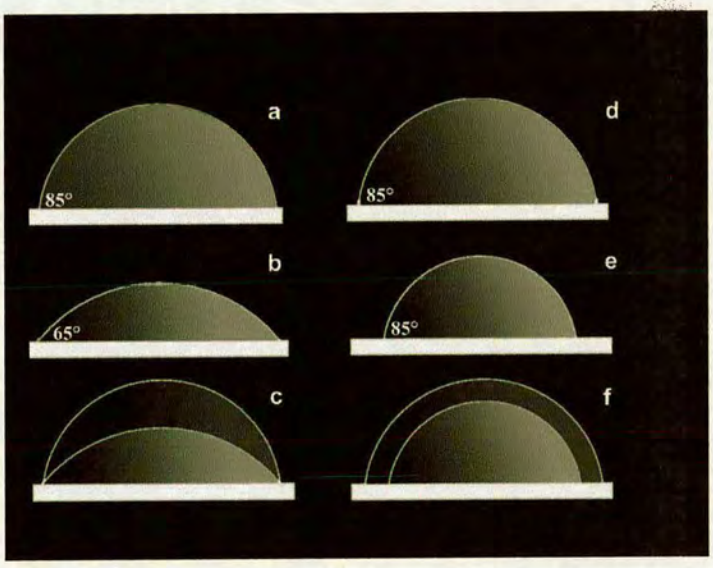

Figure 1.6: Water droplet contact angles are a convenient measure of leaf surface hydrophobicity. In the first example (a-c) the contact area remains unchanged with contact angle decreasing over time. In the second example (d-f) the contact angle remains unchanged and contact area decreases as the droplet dries (adapted from Juniper and Jeffree, 1983).

Two contact angles are often quoted; the advancing contact angle (that describes the wetting of fresh surface), and the receding contact angle (that describes the droplet angle on previously wetted surfaces as it recedes). Leaves typically display contact angle hysteresis i.e. advancing and receding contact angles have different values, which is due to surface structural heterogeneity. Further complications arise when one considers that for any droplet containing dispersed solids which evaporates on a given surface, the solid content (which is initially dispersed throughout the entire droplet) becomes concentrated into a tiny fraction of the volume of that droplet.

A form of capillary flow within the drying droplet significantly contributes to this effect in that the contact line of the drying drop is pinned and causes liquid from the drop interior to replenish liquid evaporating from the edge i.e. a solid rim is produced by the effects of a centrifugal liquid flow within the droplet. The outward movement associated with this has been shown to carry virtually all the previously dispersed solid to the periphery of the droplet.

This effect is consistent for a variety of solvents and solutes providing the solvent meets the surface at a non-zero contact angle, the contact line remains pinned to its original position, and that the solvent evaporates. Relative solubility of the dissolved solute may also be of importance because solids of high solubility will remain solubilised for longer in a droplet of decreasing volume, whereas solids of low solubility will fall out of solution more readily and be more immediately available to the effects described above (Deegan et al., 1997).

It is clear, then, that the drying of fungicide droplets on the leaf surface is a complex and interactive phenomenon, with potentially significant differences in droplet behaviour and deposit characteristics resulting from relatively minor differences to leaf surface structure and fungicide formulation chemistry.

1.6 Fungal Biology and Fungicide Research

Although the discovery and development of novel products remains an essential aspect of fungicide research, the improvement of fungicide delivery systems which can reduce the quantities of fungicide active ingredient to be applied to crops is increasingly recognised as a priority by agrochemical manufacturers. Most research into fungicides has focused on leaf application and uptake, with apparently little or no emphasis placed on uptake into fungal cells or subsequent delivery of active ingredients to their target sites. Adjuvant systems in fungicidal formulations generally exist to improve spray and droplet retention, foliar uptake and translocation throughout the plant. Appropriate adjuvant systems can provide similar levels of disease control despite reductions in the concentration of active ingredient within the formulation.

However, it remains clear that the same rationale has not been applied to the fungal cell. That is, no adjuvants have been specifically developed which exploit the uptake and translocation pathways within the target cell. In fact, the mechanisms by which fungicides enter fungal cells, are transported within them and inhibit metabolic processes at recognised and specific active sites remain largely unknown.

Furthermore, whereas large scale studies, e.g. field trials and glasshouse studies, provide general information about the fungicidal formulation such as photostability, application rate and leaf retention there is often no clear understanding of the micro-scale interactions between host, pathogen and formulation.

A novel approach to fungicide research exploring micro-scale interactions at the pathogen/ host interface, and attempting to answer basic questions relating to fungal cell and organelle biology and the uptake and distribution of fungicides within fungal cells could provide agrochemical companies with previously unrecognised opportunities to develop new formulations which improve the efficacy of existing and novel fungicides and enable further reductions in active ingredient concentrations and increased toxicity on target organisms.

1.6.1 Fungal Morphology and Hyphal Extension

Fungi exhibit highly polarised growth involving the extension of hyphae at their apices. In a growing hypha, new cell wall and plasma membrane is predominantly laid down at the tip through localised secretion and cell wall synthesis (Harold, 1997, Gow, 1994). The energy requirements of this region of the mycelium must be considerable, with hyphal elongation rates of up to 2 μm per second being reported by some authors (Bracker et al., 1997). It would be predicted that the energy requirements of the sub-apical region of the cell are less substantial, although they are the sites of energy-dependent processes such as protein synthesis and organelle and cytoskeleton assembly (Harold, 1997).

Hyphae often contain extensive regions along which considerable movement of cytoplasm and organelles can occur. In most fungi, this movement commonly involves the transport of material through septal pores between adjacent hyphal compartments (Gull 1978). The relatively high surface area to volume ratio makes hyphae well adapted for absorption, secretion and excretion and their tubular nature coupled with a tendency to form branched networks, provides an efficient means for the interchange of materials and organelles between different regions of a colony (Read, 1994).

1.6.2 Potential Pathways for Fungicide Uptake into Cells and Organelles

Uptake of molecules into fungal cells and their subsequent delivery to intracellular organelles is poorly understood. Two membranes (the outer and inner) surround each mitochondrion. The outer membrane contains many copies of the transport protein porin, which forms large aqueous channels through the lipid bilayer. This membrane is permeable to all molecules of less than 5 kDa. The major working part of the mitochondrion is the matrix space and the inner membrane that surrounds it (Wallace, 1999; Childs, 1996; Voet and Voet, 1995).

The inner membrane is especially impermeable to ions, and also contains a variety of transport proteins. This makes it selectively permeable to small molecules that are metabolised or required by the mitochondrial enzymes located in the matrix space (Alberts et al., 1994). Potential pathways for the uptake of fungicides into fungal cells are described below (Fig 1.7).

1.6.3 Passive Uptake

When considering the passage of fungicides from the external medium to the mitochondria, it is important to remember that the compound must pass through at least three membranes in order to reach a site of activity in the matrix or on the inner membrane (Fig 1.7). Small molecules will be able to diffuse freely through both the cell's plasma membrane and the mitochondrion's outer membrane. The mitochondrion's inner membrane is, however, highly selective and passage may depend upon active uptake mechanisms.

The primary pathway for fungicide uptake into fungal cells is generally thought to be by diffusion across the plasma membrane (Karpuk, 1996; Lyr et al., 1995). This membrane is a lipid bilayer, which is relatively impermeable to the flow of most water-soluble molecules. The smaller and more hydrophobic a molecule is, the faster it will diffuse across the plasma membrane. Azoxystrobin is a small (molecular weight approximately 300), profoundly hydrophobic molecule and was anticipated to diffuse freely into cells and mitochondria. An alternative pathway, endocytosis, may prove significant in the uptake of larger or more hydrophilic molecules (Read and Hickey, 2001), but has been somewhat overlooked in the past.

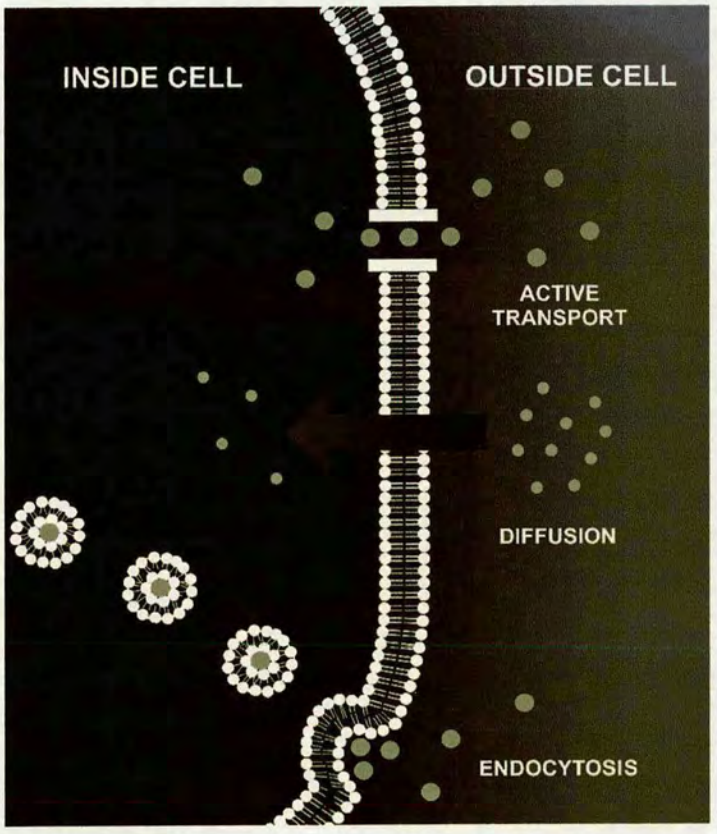

Figure 1.7: Potential pathways for fungicide uptake. Molecules and ions can generally enter cells through three different pathways: active uptake (e.g. an ion pump); diffusion, and endocytosis (whereby plasma membrane containing external molecules is pinched off, internalised, and subsequently delivered to intracellular organelles) (Swift and Read, unpublished)

1.6.4 Mitochondria: Form and Function

Mitochondria occupy a substantial portion of the cytoplasmic volume of eukaryotic cells. They are surprisingly mobile and plastic organelles that constantly change their shape and are even able to fuse with each other and separate again (Yaffe, 1999; Alberts et al., 1994). Mitochondria are primarily energy producing organelles. ATP is required to drive most of the energy-requiring reactions in all living things. The mitochondrion is the site of eukaryotic oxidative metabolism, and contains the enzymes that mediate this process. The energy required for ATP production is extracted through the oxidation of NADPH and $FADH_2$ by the electron transport chain; a series of four protein complexes through which electrons pass from lower to higher standard reduction potentials (Fig 1.8).

This enables the maintenance of a transmembrane proton electrochemical gradient, negative inside of approximately 150-200 mV which provides the energy required by ATP synthase to produce ATP (Duchen, 1999; Wallace, 1999; Voet and Voet, 1995; Duchen and Biscoe 1992).

The rate of ATP synthesis shows a very strong dependency on membrane potential (Zoratti et al., 1982; Maloney et al., 1980) so that relatively small depolarisations of membrane potential can alter ATP production significantly. Furthermore, in mammalian systems, cells with high energy requirements (e.g. cardiac cells) are shown to have increased numbers of mitochondria per unit volume of cell (Diaz et al., 1999; Duchen, 1999; Duchen et al., 1993).

Because mitochondria play a crucial role in the life of the cell, it is unsurprising that mitochondrial dysfunction can cause acute energy failure and cell death. A variety of toxins are known that block respiration at different sites on the protein complexes of the respiratory chain, inhibit ATP synthase, or (in the case of protonophores) cause the uncoupling of respiration from phosphorylation. Their application can provide insight into mitochondrial activity, and certain energy-dependent cellular processes (Duchen, 1999; Morgan-Hughes et al., 1990).

1.6.5 Fungal Mitochondria

The respiratory pathway elucidated for mitochondria in animal cells is present in most fungal mitochondria. A few fungi, such as *Saccharomyces cerevisiae* and *Schizosaccharamyce pombe*, lack complex I. More commonly, however, fungi have additional components, such as alternative NADH dehydrogenases and an alternative terminal oxidase (Joseph-Horne et al., 2001).

The alternative oxidase (AOD) is a secondary terminal oxidase present in plants and most fungi. Some differences have been recognised, particularly in their regulation, but their functionality appears to be identical (Umbach and Siedow, 2000; Vanderleyden et al., 1980). The AOD is located in the inner mitochondrial membrane and catalyses the reduction of oxygen to water after receiving electrons directly from reduced ubiquinone (circumventing complex III and IV). Consequently they are insensitive to certain respiratory inhibitors such as antimycin A and cyanide (Joseph-Horne et al., 2001; Michea-Hamzehpour and Turian, 1987).

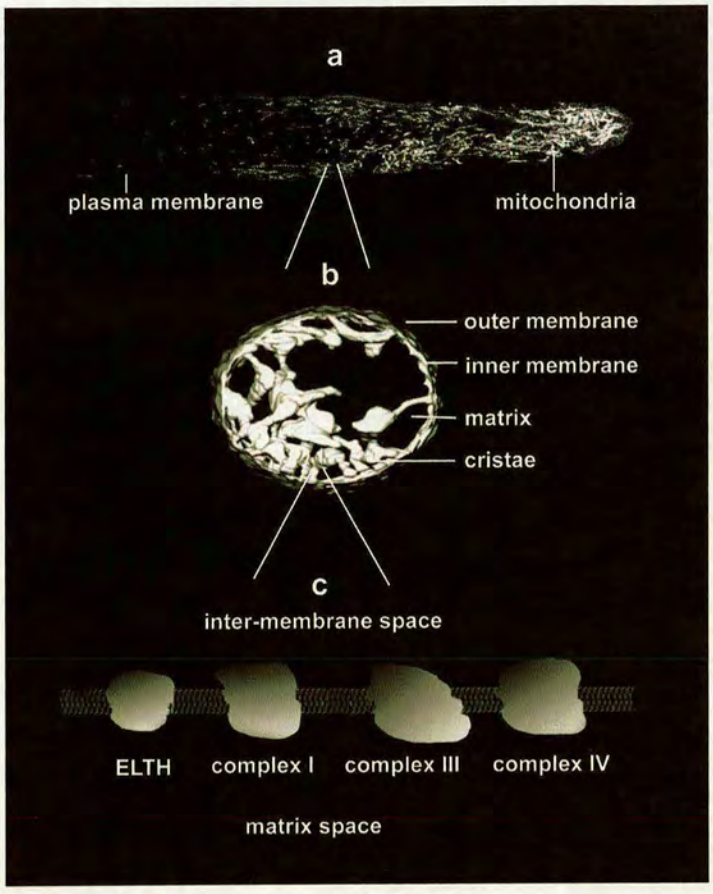

Figure 1.8: Mitochondria. A: confocal image showing mitochondria located at the hyphal tip. B: SEM image showing the internal organisation of mitochondrial structures. C: stylised image of the mitochondrial membrane showing the protein complexes I, III and IV, and the energy-linked tranhydrogenase protein (1.8a Swift, unpublished; 1.8b Skepper, 2003, 1.8c adapted from Terry, 2003).

In most systems studied, alternative oxidase generally operates only under conditions that inhibit normal electron transport. Induction of this pathway is believed to be of particular importance to fungal plant pathogens that are exposed to compounds that inhibit the cytochrome oxidase pathway, for example NO released by plants expressing the hyper-sensitive response (Joseph-Horne et al., 2001). Other studies have identified further differences between animal and fungal mitochondria. For example, the filamentous fungus *Fusarium oxysporum* has the ability to denitrify nitrate to N_2O through a process within the mitochondria coupled to ATP synthesis (Kobayashi et al., 1996). These components, additional to those in animal cells, no doubt provide fungi with a greater versatility in aerobic respiration by enabling them to adjust their metabolic capacity when encountering different energy sources or in the presence of cytochrome oxidase inhibitors.

1.7 Introduction to Research in this Thesis

The study of micro-environment interactions between fungicide, pathogen and host represents a novel approach in the analysis of fungicide translocation and localised control. The development of new techniques and approaches towards micro-scale studies of fungicide/fungus interactions has proved an important aspect of this research. The focus of the research described in this thesis has been to analyse mitochondrial biology and physiology of filamentous fungi and describe and analyse micro-scale interactions of the fungicide azoxystrobin on plant pathogens and experimental fungal systems.

The initial aim in this study was to analyse efficacy of azoxystrobin on the micro-scale in pseudo-field conditions for laboratory application. Chapter 3 is therefore concerned with the comparison of different fungicide formulation characteristics on wheat leaf surfaces using scanning electron and light microscopy. For the first time, small differences between formulations were shown to have a profound impact on droplet characteristics and on ease of handling under experimental conditions.

In Chapter 4, the activity of azoxystrobin on established *Puccinia recondita* colonies and established colonies and germinating spores of *Blumeria graminis* was examined *in planta* using the low temperature scanning electron microscope (LT-SEM) and ambient temperature scanning electron microscope (AT-SEM) respectively. No curative effect was observed on established *P. recondita* colonies. Excellent curative and preventative control was observed on *B. graminis* at low doses. A zone of inhibition around single azoxystrobin deposits was identified and its effect on germinating *B. graminis* spores over time was analysed. This demonstrated that azoxstrobin was a potent germination inhibitor, even at low doses, and suggested that azoxystrobin moves quickly through surface waxes and epidermal cells to provide localised control within several hours.

In Chapter 5, short time period, micro-environment studies of the uptake of radiolabelled azoxystrobin were performed to analyse uptake and redistribution events on the micro-scale. Phosphorimaging and combustion analysis of similarly treated wheat leaves was performed, and supported the hypothesis that azoxystrobin immediately diffuses through surface waxes and epidermal cells and begins translocating through xylem vessels within 7 h of application. No symplastic movement through the phloem was observed.

Phosphorimaging demonstrated that azoxystrobin had translocated beyond the zone of inhibition identified in Chapter 4. This was probably due to the fungicide being unavailable for uptake into the fungal cell, rather than as a result of too low a dose rate.

Azoxystrobin's target site is in the mitochondrial respiratory chain. Despite the importance of this mode of action to current fungicide development, little is known about mitochondrial morphology and physiology within the fungal cell, or how fungicides and other small molecules enter the cell. In Chapter 6, a variety of mitochondrion-selective fluorescent markers were assessed using confocal laser scanning microscopy (CLSM) in *Aspergillus nidulans, Botrytis cinerea* and *Neurospora crassa.* The most appropriate of these were used to study fungal mitochondria. Important conclusions from this research were that mitochondria are densely packed at the hyphal tip and that these mitochondria are more active than mitochondria situated in sub-apical regions. This is probably a requisite for hyphal tip growth, which is thought to require a considerable amount of energy from ATP. Further to this, an assay for mitochondrial activity was developed using the potentiometric marker Rhodamine 123.

The effects of the respiratory inhibitors FCCP and azoxytrobin on mitochondrial physiology and fungal cell growth were analysed in *Bot. cinerea, N. crassa* and *A. nidulans.* Time courses for azoxystrobin uptake strongly suggested diffusion as the primary pathway for entry into the fungal cell. This was unsurprising given the relative size and hydrophobicity reported for azoxystrobin. Processes in mitochondrial degradation and subsequent cell death were observed.

The recent commercial availability of two photon laser scanning microscopy (TPLSM) and fluorescence lifetime imaging microscopy (FLIM) provided the opportunity to technically assess these relatively novel approaches to live cell imaging of filamentous fungi. Chapter 7 describes the development and application of these techniques to the study of fungal mitochondria. Multiphoton microscopy represents an advance in live cell imaging and offers a potential solution to a variety of technical problems in fungal cell research, e.g. phototoxicity associated with UV excitation and light penetration into thick samples. Critical analysis of two photon excitation of mitochondrion-selective probes was carried out, focusing on phototoxicity from potentially useful wavelengths for live cell research.

Until recently, biological applications of fluorescence microscopy have involved analysis of fluorescence intensity only. Fluorescence lifetime imaging microscopy offers an alternative approach to live cell imaging because it enables the visualisation of fluorescence lifetime, rather than fluorescence intensity. Two photon FLIM was done on *N. crassa* cells stained with DASPMI, GFP and FM4-64. Differences in lifetime between dyes was recorded in different cells, and different lifetimes of DASPMI were recorded between different membranes in the same cell. For the first time, visualisation of charged and non-charged membranes in the same cell was possible.

Chapter 2

Materials and Methods

Man is a credulous animal and must believe in something; in the absence of good grounds for belief, he will be satisfied with bad ones.
Bertrand Russell, Unpopular Essays (1950).

2.1 Chemicals

2.1.1 Media and Inhibitors

Unless stated otherwise, chemicals were purchased from BDH Ltd. (Poole, Dorset, UK), Sigma Chemical Co. (Poole, Dorset UK) or Fluka (UK).

2.1.2 Fungicides

All fungicide active ingredients and adjuvants were provided by Syngenta (Jeallot's Hill, UK). In the EU, azoxystrobin is marketed as *Amistar* for cereal applications and *Quadris* for vines. The adjuvant difference between these two formulations is that *Amistar* contains a wetting agent and *Quadris* does not.

2.1.3 Fungicide Formulations

In field applications, *Amistar* spray droplets vary considerably in diameter. Very coarse droplets (ASAE S-572 spray nozzle standard) have a volume mean diameter (VMD) of 250 μm with a volume of approximately 0.00815 μl (C.A. Hart, personal communication; Hewit, 1998).

Field application rates also vary based on a combination of disease pressure, crop variety and profit margin over fungicide cost analysis. Rates are typically between 0.5 and 0.8 L product per hectare. However, the application rate shown below (1.25g/L) is not uncommon.

Amistar product contains 250 g of azoxystrobin in 1 L. The maximum registered application rate of *Amistar* is 1 L of formulate product per hectare. Volumes of between 150 and 300 L of water per hectare are typical in the EU. Application of maximum registered rate gives a spray concentration of 1.25 g azoxystrobin/L, which is 0.125 azoxystrobin w/v, equivalent to 1250 ppm.

Amistar formulation also contains an adjuvant (hereafter referred to as *'Amistar adjuvant'* at 125 g/L (625 ppm). This is known to marginally increase droplet spread and leaf wettability (Hart, personal communication). Application rates for *Quadris* are identical to *Amistar*. In this study the following formulations were variously applied to either glass slides or the adaxial or abaxial surface of wheat leaves -

- Formulation 1: Azoxystrobin technical active ingredient milled to a powder (concentration 99.7 w/w in water, density 1.25 g/ml) and diluted in distilled, deionised water to a concentration of 10g azoxystrobin/L.
- Formulation 2: *Quadris* product (250 g azoxystrobin/L, no adjuvant, was diluted in 25% ISO-propylalcohol (IPA), 75% distilled, deionised water to a concentration of 0.125g azoxystrobin/L.
- Formulation 3: Azoxystrobin technical active ingredient milled to a powder (concentration 99.7 w/w in water, density 1.25 g/ml) and diluted in 25% IPA, 75% distilled, deionised water to a concentration of 0.01 g azoxystrobin/L.
- Formulation 4: *Amistar* product (250 g azoxystrobin/L, 125g *Amistar adjuvant*/L) was diluted in distilled, deionised water to a concentration of 1.25 g azoxystrobin, 0.625 g *Amistar adjuvant.*
- Formulation 5: *Quadris* product (250 g azoxystrobin/L, no wetting agent, batch reference unknown) and *Amistar adjuvant* were diluted in distilled, deionised water to a concentration of 0.125 g azoxystrobin/L and 0.125 g *Amistar adjuvant*/L (twice the concentration of adjuvant in *Amistar* product).
- Formulation 6: *Amistar adjuvant* (concentration 99.99%) diluted in distilled, deionised water to a concentration of 10g/L (160 times the concentration of adjuvant in *Amistar* product).

Azoxystrobin has low water solubility (solubility in water 6.0 mg/L at 20°C) with a high melting point (mp 114-116°C) (Clough and Godfrey, 1998). Therefore, complete solubility would not be possible in the above formulations. All formulations were prepared in 10 ml vials. Vials containing these formulations were placed in a 20°C sonic bath for 20 min prior to application to ensure chemicals were homogeneously dispersed.

2.2 Plant Material

The winter wheat cultivar Kanzler was selected due to its low resistance to *Puccinia recondita* and *Blumeria graminis* (Humphreys, 1991). Seeds were sown in 37 mm pots containing John Innes No. 2 potting compost (Foremost, Croxden Horticultural products Ltd., UK) with 5 seeds per pot.

Pots were transferred to either the microscope laboratory several days before imaging, or to a controlled environment room prior to phosphorimaging (16 h day, 20°C, 16°C night temperature with relative humidity of approximately 45%). Illumination in the controlled environment room was provided by 400 W metal halide lamps (Hipka, Thorn industries, UK). In both cases, pots were placed on capillary matting and watered from below twice daily.

2.3 Fungal Material

Experiments were performed using the wild type and transformants indicated in Table 2.1.

Table 2.1 Species and strains used.

Species	Strain	Source
Neurospora crassa	Shear and Dodge wild type (74A)	FGSC no. 2489
Neurospora crassa	GFP-H1-nucleus	Freitag
Aspergillus nidulans	wild type (R-153)	X. Xiang
Aspergillus nidulans	GFP-mitochondria	A. Brakhage
Botrytis cinerea	wild type	C.E. Bracker
Blumeria graminis	K1812	Syngenta (UK)
Puccinia recondita	K2039	Syngenta (UK)

2.3.1 Growth Conditions for Fungal Infection *in planta*

Plants for micro-arena of infection studies were infected with *B. graminis* or *P. recondita* under the conditions described below.

Puccinia recondita

Uredospores were collected from infected wheat plants using a cyclone spore collector (De-Vilvis, UK) 10 days after inoculation. Seven day old seedlings were inoculated by spraying with a spore suspension (approximately $1x10^5$ spores per ml, prepared in distilled water containing 0.05% v/v Tween 20) to the point of maximum leaf retention. Plants were immediately placed in a darkened growth room with high humidity (100% RH, 21°C) for 48 h and then transferred to a glasshouse for 5 days (supplementary halogen lamps provided a 16 h photoperiod). Plants were taken directly from here to the scanning electron microscope (SEM) preparation room and cryopreserved (see section 4.2.4 for a full account) immediately to minimise desiccation.

Blumeria graminis

Blumeria graminis cultivars were maintained on whole plants by shaking the spores from a heavily diseased stock plant (1-2 weeks post inoculation) over 7-14 day old seedlings. These were maintained in a glasshouse reserved for plants infected with mildew only, to avoid cross contamination and transferred to the SEM preparation room up to 2 days prior to imaging. Shake inoculation of fresh leaf material was also performed in the SEM preparation room for short timescale experiments.

2.3.2 Growth Conditions for Fungal Cultures

All other fungal species used in this research were cultured under the conditions described below.

2.3.3 Media

Neurospora crassa, Aspergillus nidulans and *Botrytis cinerea* were maintained by regular sub-culturing on solid agar media (Oxoid Agar No. 3, Unipath Ltd., Basingstoke, Hampshire, UK). An agar strength of 2% w/v was used because it provided a firm gel which encouraged hyphae to grow upon the surface. This was more suitable for imaging. Agar media was prepared in 1 L flasks, autoclaved for 15 min at 121°C, allowed to cool to about 50°C and

poured into 8.5 cm diameter polystyrene Petri dishes (Disposables Media Ltd. UK). Petri dishes were stored at room temperature to prevent condensation and used within 2 weeks. Liquid media (for dilution of dyes and application of inhibitors) was prepared according to the same recipe but without agar, sterilised and divided into 10 ml vials and stored at 5°C.

Complete Medium

Malt extract agar (MEA) was used for culturing *A. nidulans* and *N. crassa* (Table 2.2). Liquid malt extract medium was prepared according to Table 2.2, but without agar.

Table 2.2 Malt extract agar.

Ingredient	Quantity
Malt extract (Fluka, UK)	20g
Agar	20g
Purified water	1.0 litre

Culture Conditions

Cultures of *A. nidulans* were grown at 30°C in darkness. *Neurospora crassa* and *Bot. cinerea* were grown at 25°C in darkness.

Storage of Fungal Material

Neurospora and *Aspergillus* strains were cultured on agar slants, consisting of universal glass tubes filled with 10 ml agar media, allowed to set at a 45° angle, and incubated with caps loosely fastened to allow adequate gas exchange. *Neurospora* cultures were incubated for 5-7 days at 25°C, and *Aspergillus* cultures were incubated for 5-7 days at 30°C, until significant sporulation had occurred. Spores were used to inoculate Petri dishes and slants, and stored at 4°C for up to 4 weeks, after which spores were transferred to fresh agar slants.

Silica Gel for Long-term Storage of Spores

For long-term storage, *N. crassa* and *A. nidulans* spores were preserved on silica gel (as described by Smith and Onions, 1983; Davis and de Serres, 1970). Silica gel (1-3 mm particle size) was sterilised at 180°C for 1.5 h and after cooling used to half fill sterile 20 ml universal glass vials sealed with polypropylene screw caps. The vials were temporarily closed and put on ice. 2 ml of sterile 7% w/v non-fat dried milk (Marvel, UK) was added, and stirred with a glass rod to form a suspension of spores. 0.5 ml of spore suspension was added

to each vial containing silica gel, closed and shaken vigorously until the spores appeared to be evenly distributed. Vials were immediately returned to ice to dissipate the heat released by wetting the silica gel. Vials were kept sealed at room temperature and cultures were recovered by shaking out a few crystals into fresh agar slant tubes.

2.4 Treatments

2.4.1 Droplet Application

Various droplet generators can be used to simulate field-sprayed droplets. These include track sprayers, piezo-electric applicators, micro-sprayers and Potter towers. In this study, comparisons were made between radio-labelled and non-labelled fungicide. Consequently, hand held micro-droplet applicator (for radiolabelled fungicide) and an automatic droplet applicator (for non radioactive material) were used (Fig 2.1). 0.2 μl droplets were applied because they are the smallest droplet sizes generated by these syringe systems.

Non-radioactive (cold) fungicide droplets were applied using a Burkhard PAX100 micro-droplet applicator (Burkhard, USA) to the abaxial surface of 2 week old wheat plants. Up to 6 droplets were applied to a 1 cm^2 region of the leaf.

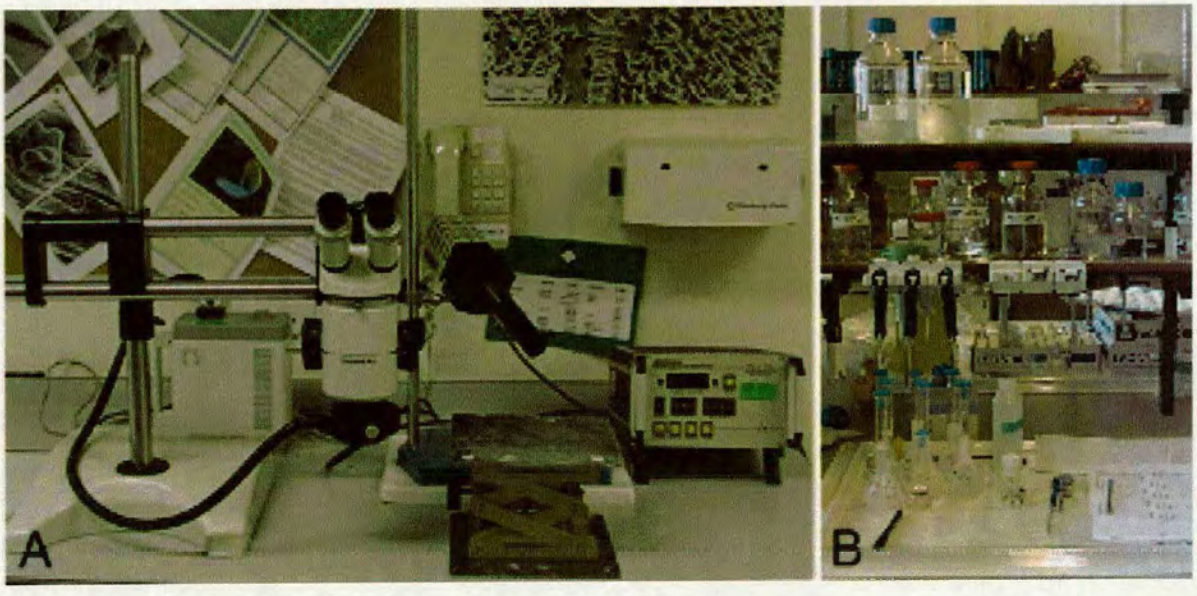

Figure 2.1: A: Burkhard PAX-100 microdroplet applicator and stereo microscope for application of non-radiolabelled fungicide. B: Bench in Biokinetics laboratory showing hand-held microdroplet applicator.

2.4.2 Wax Stripping

Leaf surface wax containing surface-bound radiolabelled fungicide was stripped from wheat using polyvinylsiloxane dental impression material (Cotene, UK). Leaves were pressed using a plant press (Syngenta, UK), freeze dried with a Modulo freeze drier (Edwards, UK) and then coated in a thin layer of adhesive (Spray mount, 3M, UK) and mounted on cardboard. Following this, leaves were gently removed with tweezers. Stripped leaves and leaf impressions were phosphorimaged in order to analyse azoxystrobin translocation. In order to qualitatively assess whether or not an adequate quantity of wax had been stripped from the leaf, fresh leaves were stripped and visualised using low temperature scanning electron microscopy (LT-SEM) (see section 2.6.2 for a full account of LT-SEM methodology). Quantity of wax remaining on the leaf surface was qualitatively assessed using these images.

2.4.3 Inhibitors

A variety of pharmaceutical agents have been identified which inhibit specific processes in the respiratory pathway of mitochondria. Furthermore, azoxystrobin has a recognised and specific target site on protein complex III of the mitochondrial respiratory pathway. Adjuvants are recognised to improve the uptake of certain compounds into some cells. The following inhibitors, fungicides and adjuvants were used in these experiments (Table 2.3).

Table 2.3 Inhibitors, fungicides and adjuvants.

Pharmaceutical agent	Type	Action	Supplier
FCCP	Inhibitor	Decoupler	Calbiochem, USA
Azoxystrobin	Fungicide	Respiratory inhibitor	Syngenta, UK
Amistar adjuvant	Adjuvant	Surfactant	Syngenta

2.5 Light Microscopy

Imaging of diluted formulations and droplets was carried out on a Leica DM RXE compound microscope fitted with a x40/0.75 numerical aperture (NA) plan semi dry objective (Leica, Germany). Fungi on leaves were imaged with a Leica M420 macroscope with an Apozoom 6:1 objective (Leica, Germany). Images were captured using a JVC KY-F55B CCD camera (JVC, Japan) and digitised with a Matrox Meteor 2 Colour Image Capture card (Matrox, UK) and stored on a Pentium PC (Intel, USA) running Leica LW500 and Lida software (Leica, Germany) under Microsoft Windows (Microsoft, USA).

2.5.1 Sample Preparation for Light Microscopy

0.1 ml and 0.2 μl droplets of formulation 1 (*Amistar* diluted in water) were applied to clean glass slides and imaged as they dried with a Leica DM RXE microscope (see above). Fungal specimens were examined *in situ* by excising a whole infected leaf sellotaped (Sellotape, UK) to a glass slide to inhibit movement. These were imaged with a Leica M420 macroscope (see above).

2.5.2 Image Processing

Images were stored in *.TIF format and processed using Leica Q Win image processing and analysis software (Leica, Germany) and further processed in Adobe PhotoShop 5.1 (Adobe, USA).

2.6 Scanning Electron Microscopy

Scanning electron microscopy is a method for high-resolution imaging of surfaces and uses electrons for imaging in a similar way to the use of visible light in conventional light microscopy. The advantages of SEM over light microscopy include greater magnification, flexibility in magnification (from 1 to 100 000 X magnification) and superior depth of field.

An incident electron beam is raster-scanned across the sample's surface and the resulting electrons emitted from the sample are collected to form an image of the surface. Images are typically, and in this study, obtained using secondary electrons, which give the greatest resolution of surface topographical features. Electron scattering, caused by the interaction between the electrons emitted from the sample and the incident beam, results in the emission of low-energy electrons from near the sample's surface. The orientation of surface features influences the number of electrons that reach the secondary electron detector. This causes variations in image contrast that represent the sample's surface topography.

2.6.1 Ambient Temperature Scanning Electron Microscopy

Ambient temperature scanning electron microscopy (AT-SEM) was done using a JEOL JSM6300 (JEOL, UK). Fresh excised leaf samples approximately 1 cm^2 in size were attached to 1 cm brass specimen stubs using double sided adhesive carbon tabs (Agar, UK). Samples were imaged with an accelerating voltage of 3.6 kV. Accelerating voltage represents a compromise between beam concentration and resolution. The relatively low accelerating

voltage selected for AT-SEM reflects the fact that fresh samples are less resilient to beam energy than cryo-preserved or chemically fixed samples. A working distance of 15, 25 or 45 mm was used, with an aperture diameter of 50 μm. Images were recorded at a resolution of 2K lines per image. Imaging of fresh material was kept to below 20 min to minimise vacuum collapse of samples.

2.6.2 Low Temperature Scanning Electron Microscopy

Many materials are sensitive to the vacuum conditions and high electron beam energy in the SEM. In many biological applications these are typically hydrated materials. Low temperature SEM provides a convenient method for the cryo-preservation of sensitive hydrated material without the need for chemical fixation. Furthermore, soft tissues can be freeze-fractured following cryo-preservation, enabling the exposure and visualisation of internal structures.

Low temperature scanning electron microscopy (LT-SEM) was carried out using a JEOL JSM6300 (JEOL, UK) equipped with a Cryotrans CT1500 (Oxford instruments, UK) (Fig 2.2). Excised leaf samples approximately 1 cm^2 in size were attached to 10 mm brass specimen stubs using a low temperature mounting medium (Miles Tissue Tek OCT, Miles, UK) and plunge cooled in liquid nitrogen prior to transfer to the cooled stage of the coating chamber attached to the SEM. Artefactual ice was removed in the column by sublimation (ice etching) at -92°C for up to 10 min before gold sputter coating in the argon chamber (pressure 0.1 mbar) at 500 V for 3 min. Samples were maintained between -150 and -165°C during coating and observation and imaged with an accelerating voltage of 4.9 kV, a working distance of either 15 or 25 mm and with an aperture size of 50 μm.

2.6.3 Image Processing

In both instances, digital images were collected on a Pentium PC running AnalySIS 3.0 software (Soft Imaging System, Germany). Images were automatically saved as *.TIF files which were processed using Adobe PhotoShop 5.1 (Adobe, USA).

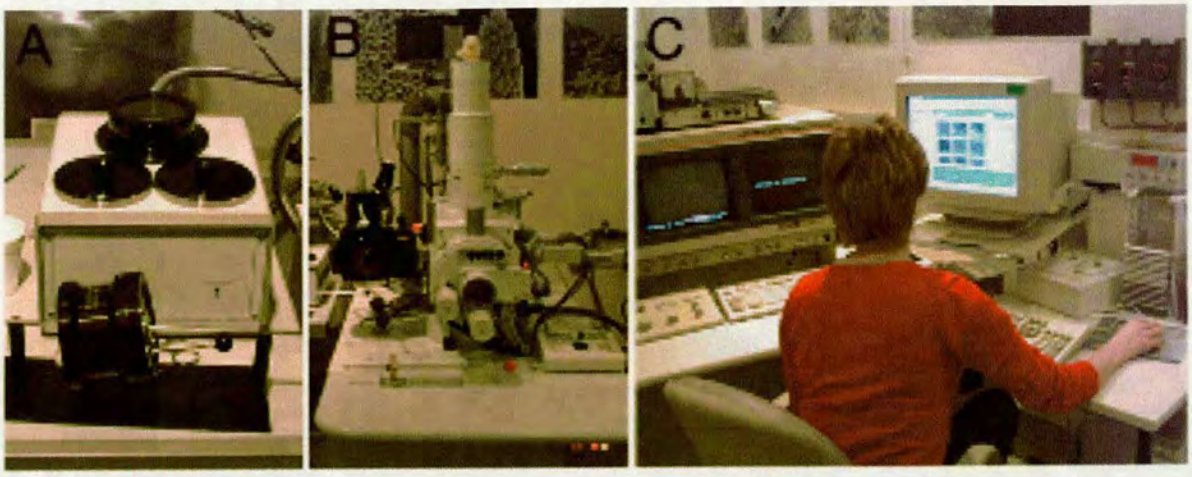

Figure 2.2: Scanning electron microscope system. A: device for specimen transfer and sub-cooling of liquid nitrogen, B: scanning electron microscope, C: PC for image acquisition.

2.7 Phosphorimaging

2.7.1 Radiolabelling Azoxystrobin

Formulation 5 (1250 ppm azoxystrobin, 1250 ppm *Amistar adjuvant*) was spiked with ^{14}C radiolabelled azoxystrobin to provide a count of approximately 100 discharges per second (dps). Single 0.2 μl droplets of radiolabelled fungicide were applied to wheat leaves using a hand held microdroplet applicator.

2.7.2 Image Plate

BAS III and BAS MS image plates (Fuji Film Co., Ltd, Japan) were used. The image plate is composed of three layers: a protective layer (10 μm); a photostimulable crystal layer (150 μm), and a polyester support layer (250 μm). The crystal layer consists of europium-doped barium fluorohalide compounds, where the europium acts as a luminescence centre which emits light from stored x-ray energy when photo-stimulated (see review by Goransson, 1995). Excised leaves treated with radiolabelled azoxystrobin were pressed and freeze-dried (Fig 2.3). This preserves the leaf, protects the image plate from moisture, ensures the radiolabelled fungicide is in close proximity to the image plate and ensures that no further movement of ^{14}C can occur within the plant tissue after the designated sample time.

Leaf material and polyvinylsiloxane impressions were mounted on cardboard using photograph adhesive (Nikon, UK), covered in photographic film (Nikon, UK) and placed face down against the imaging plate in a protective cassette. These cassettes were placed in a darkened lead safe for 3 days to minimise background radiation and allow adequate time for the image plate to develop without over-exposure.

2.7.3 Digitiser

A Bio-image analyser BAS1500 (Fuji Film co., Ltd, Japan) was used to analyse image plates. This system consists of an image reader, an image processor and an image plate eraser. Information stored on image plates is read using a helium neon (HeNe) laser (wavelength of 633 nm) which stimulates the crystal layer to emit light (photo-stimulated luminescence). The photo-stimulated light is converted into electric signals which are digitised (Fig 2.3). Image plates were loaded into the digitiser under darkened conditions. Following imaging, image plates were erased by exposing to high intensity lights for approximately 10 min. Images were saved on a PC running BAS image capture software (Fuji Film Co., Ltd, Japan) under Windows (Microsoft, USA).

2.7.4 Image Processing

Images from the phosphorimager were saved in Fuji's *.BAS format and analysed using TINA image analysis software (Fuji Film Co., Ltd, Japan). Images were exported in *.TIF format to Adobe Photoshop (Adobe, USA) for further processing.

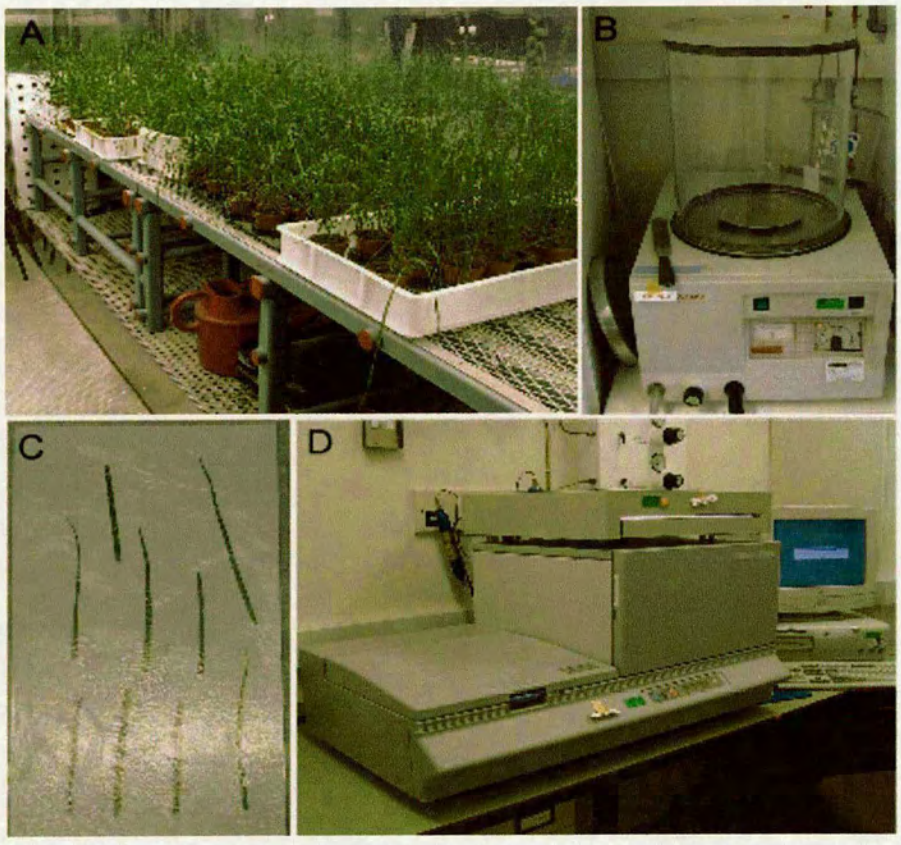

Figure 2.3: Equipment for phosphorimaging. A: Growth room, B: Freeze drier, C: freeze dried leaves mounted on card prior to image plate preparation, D: phosphorimager (comprising digitiser and PC for data acquisition.)

2.7.5 Combustion Analysis and Scintillation Counting

A common and precise method for obtaining quantitative data from radiolabelled specimens is sample combustion (oxidation) followed by liquid scintillation counting. When samples are combusted, the label from the ^{14}C-fungicide is liberated as $^{14}CO_2$. This is absorbed by a CO_2 trapping agent (Carbosorb, Packard, UK) mixed with the scintillant. The amount of radiolabel present in the sample can then be determined by scintillation counting. The scintillant contains two components; a solvent and a solute (or fluor). The beta particles produced as a result of isotope decay excite the solvent molecules which pass on their excitation energy to the solute by a collision process. The excited solute returns to ground state by the emission of light and the scintillation spectrometer counts the number of scintillations (photons released). This technique provides accurate information as to the quantity of radioactivity in the sample, but not its location or identity.

Although ^{14}C is not identified, only quantified, the time frame of these experiments coupled with azoxystrobin's high stability in and on plant tissue, it is reasonable to assume that any ^{14}C recorded was from radiolabelled azoxystrobin (Bartlett, personal communication). Hence the technique has been used here in conjunction with phosphorimaging to determine both the distribution and quantity of fungicide within the leaf tissue.

Leaves and wax-silicon impressions which had been phosporimaged were removed from their mounting card and combusted using an Oximate 387 oxidiser fitted with a robotic arm (Packard Bioscience, UK). Leaves were completely combusted, whereas polyvinylsiloxane partially combusted. This caused a potential 'loss' of radioactive material from the wax impressions which was not released during combustion. Background counts were taken, and droplets of radiolabelled fungicide were applied to paper and combusted and counted as controls. Because of the poor combustion of silicon impressions, the quantity of surface-bound fungicide was calculated from the dps value for control droplets minus the dps value for combusted leaf tissue.

Scintillation counting was performed using a Beckman 6000TA scintillation counter (Beckman, USA). Scintillation vials automatically filled by the Oximate 387 were counted and data were saved in ASCII text (*.TXT) format and imported into Kspread and XmGrace (GPL, running under SuSe 7.3) for statistical analysis.

2.8 Live-Cell Imaging

2.8.1 Sample Preparation

Live cell imaging was performed using filamentous fungi grown in culture only, as described previously. When the mycelium had grown 3-5 cm across the surface of the agar, peripheral portions of the colony, containing fast growing hyphae, were excised and transferred for imaging. During manipulation and preparation of samples, hyphal tips often stopped growing, but resumed growth within 2-10 min with the formation of one or two new tips. According to Robertson (1958), apical branching of hyphae is typical after treatments that arrest hyphal growth. Usually 10 min of recovery time was allowed before imaging. A block of agar approximately 20 mm^2 by 5 mm deep was cut from the edge of a colony grown in a Petri dish and inverted onto a droplet of liquid media (containing dye) upon a glass cover slip (Fig 2.4). A humid Petri dish chamber was sometimes placed above the slide for imaging over extended periods to reduce desiccation.

A variety of techniques for the study of filamentous fungi in culture have been described by Hickey (2001). It was concluded that the best compromise between image quality, cell viability and access to sample for experimental procedures was the 'inverted agar block' technique. Table 2.4 summarises the advantages and disadvantages of this approach.

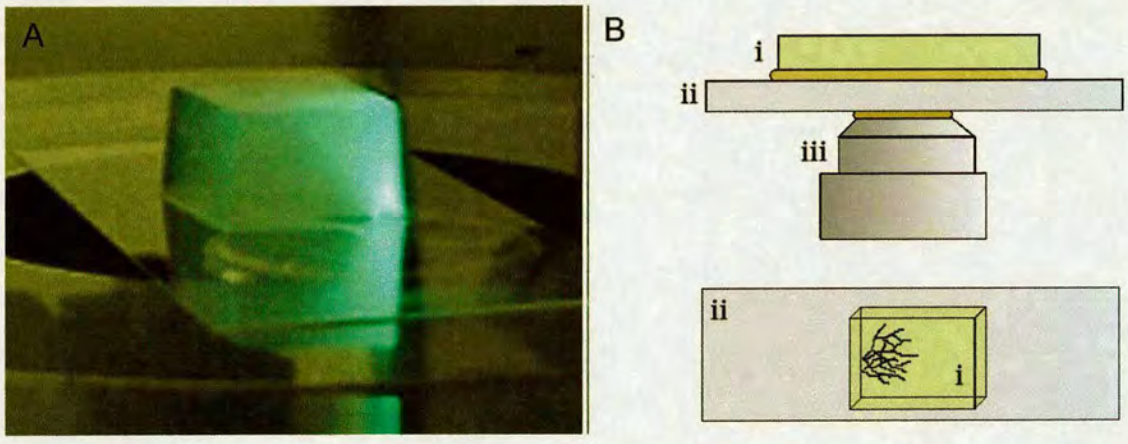

Figure 2.4: (A) photograph of inverted agar block under microscope, (B) cartoon of sample showing view of sample preparation. Above, side view: i = agar block; ii = cover slip, iii = objective lens. Below, top view: i = agar block, ii = cover slip. The mycelium is located between the agar block and the cover slip (adapted from Hickey, 2001).

Table 2.4 Advantages and disadvantages of inverted agar block technique (adapted from Hickey, 2001).

Advantages	Disadvantages
Good gas exchange	Dyes may leach into or bind to agar
Culture is moist	Difficult to wash or restain sample
3-6 h imaging time possible	Agar blocks must be kept moist
Hyphae grow between agar and glass	Reduced quality of brightfield images

2.8.2 Loading of Cell-Permeant Dyes

Most of the dyes used in this research have limited solubility in aqueous solutions and were therefore dissolved in organic solvents before dilution into the medium. In all cases the concentration of solvents (DMSO and EtOH) was kept below 0.2% in the final loading medium. Dyes used in these experiments are shown in Table 2.5.

Table 2.5 Summary of fluorescent dyes used (data from Molecular Probes Inc).

Dye	Selectivity	Exc. line	Em. max	Conc. (μM)	MW
FM 1-43	Membranes	514 nm	626 nm	25	512
FM 4-64	Membranes	514 nm	734 nm	25	608
Mitotracker Green	Mitochondria	488 nm	516 nm	10	672
Rhodamine 123	Mitochondria	514 nm	529 nm	5-50	381
DASPMI	Mitochondria	488 nm	585 nm	5	366

Abbreviations: Conc, concentration; Exc, excitation; Em, emission; MW,molecular weight

2.8.3 Introduction of Inhibitors and Fungicides to Samples

Inhibitors and fungicides were applied in dilution to cells preloaded with vital fluorescent probes. This was done by drawing off extraneous media (to reduce further dilution of the applied inhibitor) with tissue paper and placing the tip of a loaded Gilson pipette as close as possible to the region of mycelium being imaged. The application of compounds in liquid causes fungal hyphae to shift slightly out of focus, the occurrence of which was used as a precise indication of the time of application.

2.8.4 Confocal Laser Scanning Microscopy

Cells were imaged using confocal laser scanning microscopy (CLSM) to generate images of superior resolution and contrast than those obtained with a conventional light microscope. The confocal microscope uses an aperture (pinhole) in front of the photomultiplier tube (PMT) that rejects out-of-focus blur and enables optical sectioning (see review by Czymmek et al. 1994). Confocal microscopy was performed using either a Bio-Rad MRC600 or Bio-Rad Radiance 2000 system.

Bio-Rad MRC600

A Bio-Rad MRC600 system equipped with a 25 mW argon ion laser and mounted on a Nikon Diaphot TMD inverted microscope with epifluorescence equipment (all supplied by Bio-Rad Microscience, Hemel Hempstead, UK) was used (Fig 2.5).

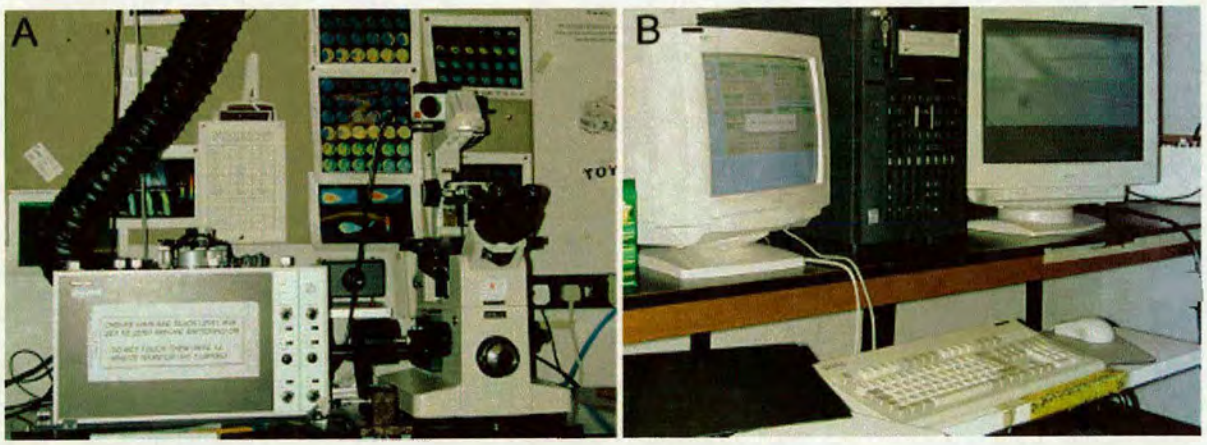

Figure 2.5: (A) BioRad MRC600 CLSM attached to a Nikon Diaphot inverted microscope. (B) Dell Poweredge PC for image acquisition and storage.

The laser power used was 1 or 3% of full intensity. Images were captured and stored on a Dell Poweredge 2300 computer (Pentium 3 500MHz; 256 mb RAM; 18 Gb hard disc) containing a Series 5 framestore, running COMOS (version 7; supplied by Bio-Rad). The laser beam could be regulated via neutral density filters to 1, 3 or 10% of full intensity. The MRC600 was equipped with two photomultipliers, PMT1 (Channel 1) and PMT2 (Channel 2) for fluorescence imaging. Table 2.6 gives an overview of the filter sets used (all supplied by Bio-Rad).

Table 2.6 Table of MRC600 filters used in this study.

Filter set	Exc. filter	Dichroic	Em. filter
Standard BHS	488/10nm BF	510nm LP	515nm LP
Standard GHS	514/10nm BF	540nm LP	550nm LP

Abbreviations: Exc. = excitation, Em. = emission, Dichroic = dichroic mirror, BHS = blue excitation filter set, GHS = green excitation filter set, BF = barrier filter, LP = longpass filter.

Settings for CLSM are a compromise between image quality and a need to minimise stress to cells (Parton and Read, 1999; Pawley, 1995). Table 2.7 lists the conditions on the Bio-Rad MRC 600 employed throughout the study. Cell health was assessed in terms of growth, cytoplasmic streaming and appearance under the microscope. The Bio-Rad MRC 600 offered the possibility of improving the temporal resolution by reducing the box size in vertical orientation. This leads to a decrease in the number of lines necessary to scan one frame. When possible, the hyphae were orientated horizontally relative to the frame width and could be imaged in a half to a quarter of the time used for scanning a full frame. The time taken to collect 1 full size image was approximately 3 s with the setting F1. By decreasing the box size to a quarter, one could theoretically obtain an image in just over 1 s. Because of problems with dye photobleaching and phototoxic effects, laser scanning of individual hyphae was kept to a minimum. Generally this initially required approximately 3 s of rapid scanning (using the F4 scan setting which takes 0.25 s to scan a full image frame) to obtain a median section through the cell, and then 1-2 slow scans using the F1 setting (3 s per full image) to produce the final image.

Table 2.7 Settings used for Bio-Rad MRC 600 confocal microscope.

Variable	Setting
Laser power	1-3% mW Argon ion laser
Scan speed	3s/512 lines
PMT gain settings	Dyes 40-70%; GFP 50-80%
PMT black level	To yield dark intensity of 10
Objectives	x40 dry (NA 0.95); x60 oil (NA 1.4)
Confocal aperture	circa 30% open
Electronic zoom	1 to 4

Bio-Rad Radiance 2000

A BioRad Radiance 2000 system equipped with a 40 mW argon ion laser and 1.5 mW HeNe laser and mounted on a Nikon TE2000 inverted microscope with epifluorescence equipment (all supplied by BioRad MicroScience, Hemel Hempstead, UK) was used (Fig 2.6). The laser power used was between 0.5 and 5% of full intensity. Images were captured and stored on a Dell Optiplex GX240 (Pentium 4 800MHz, 1 Gb RAM, 7 Gb SCSI hard disk) containing Unibrain framestore card running LaserSharp 2000 software (supplied by BioRad). The Radiance was equipped with 2 PMTs for fluorescence intensity imaging. PMT 1 was used to collect fluorescence from excitation using the argon ion laser, PMT 2 was used to collect fluorescence from HeNe excitation. Typical filter settings are shown in Table 2.8.

Table 2.8 Table of Radiance filters used in this study.

Channel	Em. filter	Dichroic
PMT1	HQ450/80 nm	DC500 nm LP
PMT2	HQ515/30 nm	DC560 nm LP

Abbreviations: Exc. = excitation, Em. = emission, Dichroic = dichroic mirror, HQ = high quality barrier filter, LP = longpass filter.

The Radiance system conferred several advantages over the MRC600 in terms of detector sensitivity, improved flexibility in acquisition software and improved Nikon optics. However, compromises also had to be made between image quality and the need to minimise stress to cells. Consequently, hyphae were generally oriented horizontally and temporal resolution was increased by reducing the number of lines that had to be scanned vertically. Due to improved flexibility from the LaserSharp 2000 software, a wide variety of settings could be used that minimised cell perturbation and improved image quality. Typically, hyphae were located using a 256 x 256 box size and a scan speed of 500 lines/s. Imaging was done at approximately 512 x 100 or 1024 x 200 resolution using a x60 water (1.4 NA) Nikon objective. Electronic zoom of up to 4 x was used, with a pinhole size of 1.2 to 1.8 mm.

2.8.5 Image Processing

Files were saved directly from both Bio-Rad confocal microscopes in Bio-Rad's *.PIC format. The Bio-Rad *.PIC files contain extra data with important information (time and date, objective used, zoom factor and distance between z-sections).

Images were viewed using the freeware software, Confocal Assistant version 4.02. In both cases images were exported in *.TIF format and exported to Adobe photoshop 5.1 (Adobe, USA) for further processing. Three dimensional intensity graphs were prepared using Soft-Work 3.2.3 software (Applied Precision Inc., USA).

2.8.6 Two Photon Laser Scanning Microscopy

Two photon laser scanning microscopy (TPLSM) conferred a number of potential benefits over CLSM including; reduction in sample photobleaching; reduced phototoxicity, and the ability to image deeper into thick tissue than was possible with CLSM. A technical overview of TPLSM is provided in Chapter 7 (section 7.1.3).

Two photon excitation was performed with a Mira tunable titanium sapphire laser (ti:sapph) coupled to a Verdi V8 diode pumped laser providing a tunable wavelength from approximately 700 - 980 nm, less than 200 fs pulse width and approximately 1.4 W peak power (supplied by Coherent, Scotland). Fluorescence detection and image acquisition was carried out using a BioRad Radiance 2000 (Fig 2.6) equipped with non-descanned detectors and a signal enhancing lens (BioRad, UK). For two photon microscopy, the confocal aperture is redundant and was therefore fully opened.

In the present study, TPLSM was critically assessed for its suitability for live-cell imaging of fungal cells. Consequently, a more detailed account of the methods used are provided in Chapter 7.

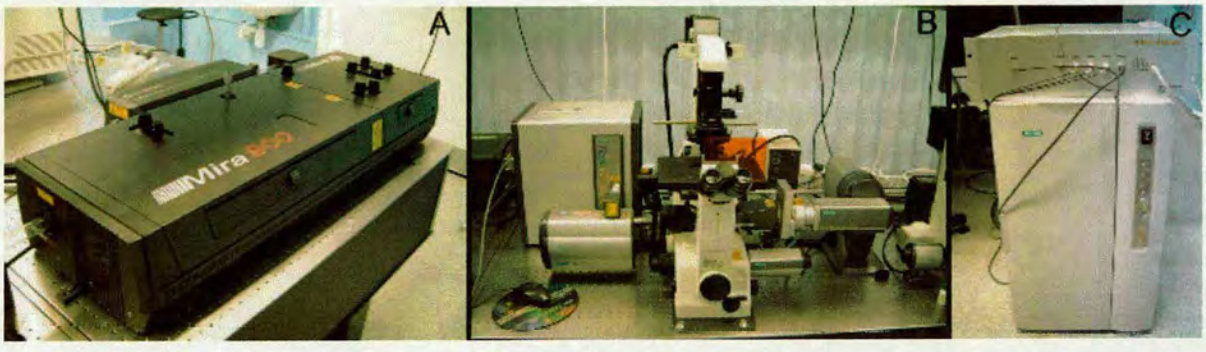

Figure 2.6: (A) Tunable pulsed laser for two photon excitation, (B) BioRad Radiance 2000 CLSM equipped with direct detectors and a signal enhancing lens to improve light capture and (C) Nikon LIMO fluorescence lifetime imaging unit pictured on top of the BioRad control unit.

2.8.7 Fluorescence Lifetime Imaging Microscopy

The optical sectioning capability and improved contrast reported for CLSM and TPLSM over conventional fluorescence microscopy make these instruments the ideal choice for fluorescence imaging of biological samples. However, the fluorescence of organic molecules is not only characterised by the emission spectrum, but also a characteristic lifetime.

When a dye molecule enters an excited state it can return by the emission of a fluorescence photon, by converting the absorbed energy internally or by transferring the energy to its environment. If a large number of molecules are excited by a short laser pulse, the fluorescence decay function is single exponential. If no energy is transferred to the environment, the lifetime is 'natural fluorescence lifetime', which is constant for a given molecule and refraction index of the media. Typical fluorescence decay values for commonly used fluorophores in biological microscopy are in the order of nanoseconds. If energy is transferred to the environment, lifetime decreases. Often this is associated with changes to ion concentration, oxygen concentration or pH value.

In this study, fluorescence excitation was performed using the tunable ti:sapph laser previously described, and fluorescence intensity was optimised by intensity imaging using the BioRad Radiance (see previous section). For FLIM, the ti:sapph laser was also used to provide an excitation synchronisation trigger. Fluorescence lifetime imaging was performed using a Nikon LIMO fast acquisition FLIM system attached through the (unused) third PMT slot of the BioRad Radiance. Fluorescence decay was measured using 4 time windows and set for each fluorescent probe such that each window (after 1) recorded approximately half the intensity of the previous window. This gave a typical gate width of 1.5 - 2 ns. A 256 x 256 box size was used, and lifetime data was recorded from a single scan lasting approximately 1 s. Images were saved in Nikons *.INC or *.IND format and imported into EZLIMO2000 software (Nikon, Europe). This software automatically calculated fluorescence lifetime values. Images and lifetime graphs were exported in *.BMP format and rendered for printing using the Gimp (GPL running under SuSe 7.3).

2.9 Image Processing for this Report

Type setting in LaTex (GPL, under SuSe 7.3) required that images be saved in *.EPS format. This was done using the Gimp (GPL, under SuSe 7.3). Only contrast and brightness settings (necessary for printing) were altered. Vector drawing was done using XFig (GPL, under Suse 7.3) and rendered for printing as above.

Chapter 3

Azoxystrobin Droplet Deposition

It cannot be that axioms established by argumentation can suffice
for the discovery of new works, since the subtlety of nature is
greater many times over than the subtlety of argument.

Francis Bacon

3.1 Introduction and Aims

3.1.1 Introduction

The formulation of fungicides with certain adjuvants can have a profound effect on their biological efficacy. However, commercial azoxystrobin formulations are applied by high-pressure sprays in large volumes, whereas in the present study, single droplets were applied using micro-droplet applicators. Under these circumstances a variety of practical problems present themselves such as: lack of droplet detachment from the applicator needle tip; sedimentation of the formulation in the needle, and the abrasion of leaf surface waxes by the droplet or needle tip during application. Differences in uptake rate can be significant for pesticide droplets of different sizes (Hart, personal communication; Shu Hua Lui et al., 1996). Furthermore, differences between formulations are known to have a profound effect on uptake and activity of many commercially important fungicides (Holloway et al., 1992). This chapter is therefore concerned with the description and analysis of fungicide droplet and deposit characteristics such as wettability, spread and annulus formation. From this work, an appropriate azoxystrobin formulation was selected for the experiments described in Chapters 4 and 5.

3.1.2 Aims

Specifically, the aims of this section were to:

- qualitatively analyse droplet characteristics for several fungicide formulations on the basis of reproducibility, delivery of active ingredient and mechanical damage to the leaf surface through application
- select an appropriate formulation based on similarity to field applications and reproducibility under laboratory conditions for the research in chapters 4 and 5

3.2 Results

3.2.1 Overview of Results

A review of the process by which the solid content of suspensions is distributed on leaf surfaces was provided in section 1.5.4. Initially, the light microscope was used to study the drying characteristics of 0.2 μl droplets of *Amistar* applied at field rate to glass slides. The initial images obtained indicated that as the droplet dried, the active ingredient (azoxystrobin) and other components of the formulation (adjuvant and essential inert materials that stabilise the formulation in commercial storage and use) were redistributed, resulting in a deposit annulus containing the solid material around the edge of the original deposit. These images suggested that even large crystals of azoxystrobin present in the formulation (greater than 1 μm diameter) were redistributed to the deposit edge as the droplet dried.

Despite the ubiquitous use of hand-held and automated micro-droplet applicators in fungicide research, surprisingly little information is available in the public domain which relates to their appropriate use and potential practical problems such as sedimentation of solids in the needle and difficulty in applying liquids to the hydrophobic leaf surface. It is an important prerequisite to micro-scale studies that a reproducible volume of fungicide with a known concentration of active ingredient can be applied to the leaf surface without causing damage to surface waxes and epidermal cells.

A series of formulations were applied and analysed using the scanning electron microscope (SEM). First, several techniques were compared in order to develop the most appropriate system for examining fungicide deposits on the leaf surface. Following this, ambient temperature SEM (AT-SEM), which was considered the best compromise between ease of use and image quality, was used to compare the deposits from several formulation types. Important characteristics associated with each fungicide formulation including wettability (how well the formulation adheres to the leaf) and surface spread (to what extent the droplet spreads across the leaf surface) were qualitatively compared. Qualitative assessment was also made between surface damage (how much damage had been caused to the leaf surface during the application process) and settling of active ingredient i.e. variation between the quantity of active ingredient deposited on the leaf from different droplets.

3.2.2 Light Microscopy of Drying Deposits

Initially, particles within the fungicide droplet were uniformly dispersed (Fig 3.1). Azoxystrobin particles, which range from sub micron to approximately 5μm diameter, and inert materials were suspended in the droplet. After 1 min, the solid content of the droplet began to aggregate at the edge of the deposit (Fig 3.2) and this process was shown to continue (Figs 3.3 and 3.4) as more of the other formulants previously contained within the formulation sedimented out of the suspension and moved to the droplet periphery under the influence of capillary flow and convection currents. After 7 min, drying had virtually completed, which caused the previously solubilised material to fall out of solution (Fig 3.5). The contact line of the drying drop did not move, which caused liquid from the droplet interior to replenish liquid evaporating from the droplet edge. This resulted in a deposit in which most of the solid content and soluble components formed a rim, or annulus, which marked the outline of the original droplet (Fig 3.6).

Figure 3.1: 0.2 μl droplet immediately after application. Note that the particles were evenly dispersed throughout the droplet and that azoxystrobin particles were shown to vary in size from approximately 1 to 10 μm in size. Although clay particles, which were used as an anti-settling agent, were also present these could not be distinguished from the active ingredient in this image. Bar = 20 μm.

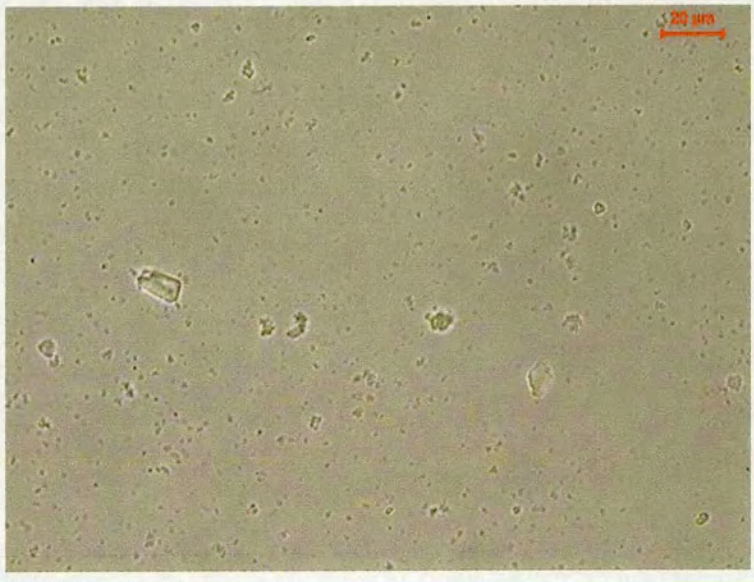

Figure 3.2: 0.2 μl: near the droplet edge, 1 min after application. After only 1 min the solid content of the droplet had begun to form aggregates within the droplet. Bar = 20 μm.

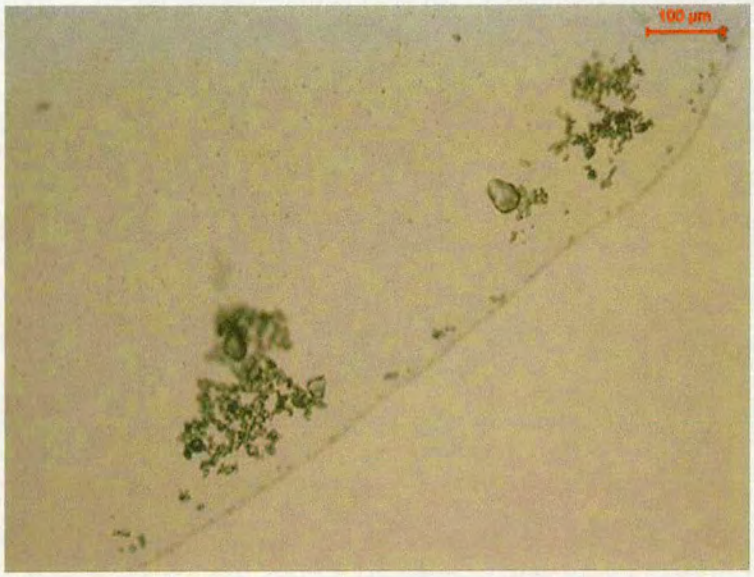

Figure 3.3: 0.2 μl: the droplet edge, 1 min after application. The solid material from the droplet continued to move to the periphery of the deposit. This process continued and suspended and poorly solubilised material formed a prominent annular ring around the final deposit. Bar = 100 μm.

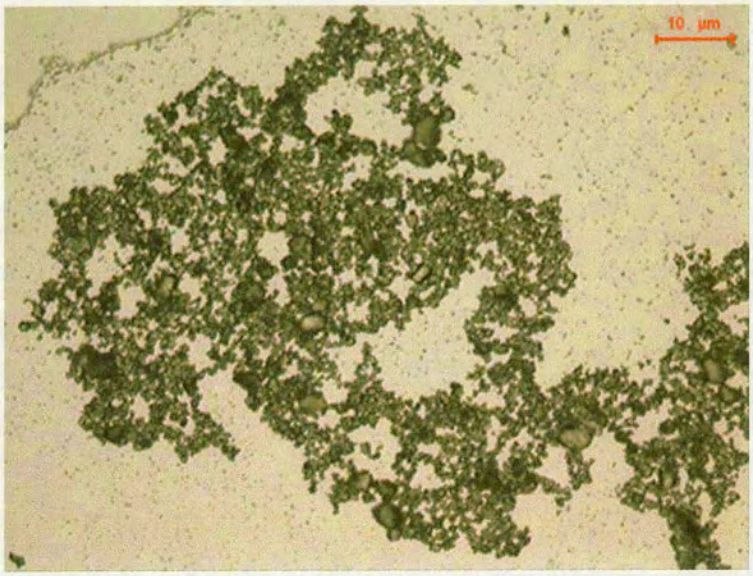

Figure 3.4: 0.2 μl droplet 4-5 min after application. Several minutes after application, large aggregates of the solid content of the formulation collected near the edge of the deposit. As the droplet dried, increasingly more particles settled out and moved to the edge of the deposit through the action of convection currents and capillary flow. Bar = 10 μm.

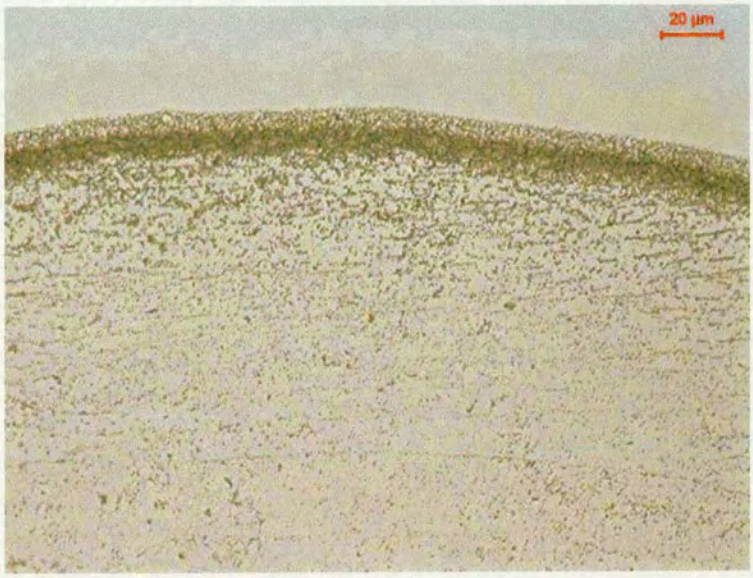

Figure 3.5: 0.2 μl droplet 7 min after application. By this time period nearly all of the material originally suspended or solubilised had collected at the deposit perimeter even though the droplet had not completely dried. Bar = 20 μm.

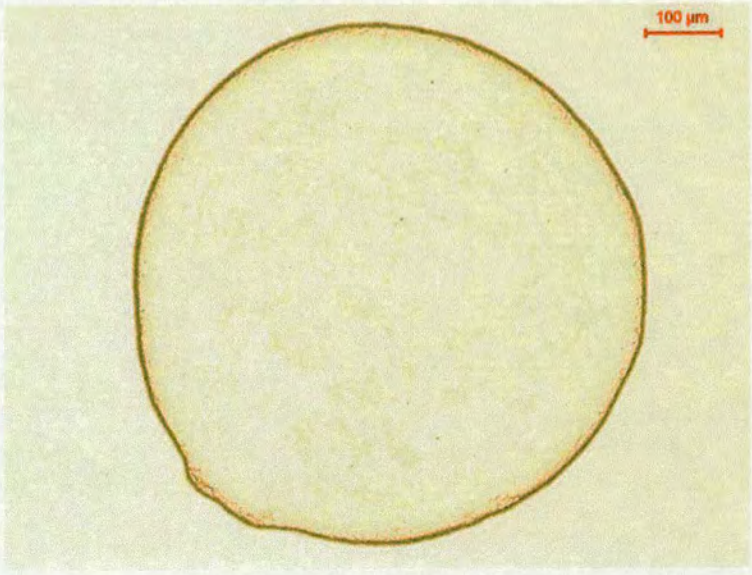

Figure 3.6: 0.2 μl droplet 14 min after application. The droplet had fully dried after 14 min. An annulus formed which delineated the original perimeter of the wet droplet. This annulus contained almost all of the active ingredient and anti-settling agent. From this image, it was not possible to ascertain how the adjuvant had dispersed. However, given its high solubility in water it was likely that some had been deposited behind the annulus. Bar = 100 μm.

3.2.3 Comparison of LT-SEM and AT-SEM Image Quality and Complexity

Scanning electron microscopy offers excellent resolution and good depth of field, and is therefore an appropriate and commonly used technique for imaging agrochemical deposits on leaf surfaces. However, although low temperature SEM confers a number of advantages over AT-SEM in terms of image quality and specimen stability, it is a time-consuming process. Before a comparison of azoxystrobin formulations or micro-arena of infection studies could be done, the advantages and disadvantages of AT-SEM and LT-SEM were assessed by comparing similar specimens. The results are described below and summarised in Table 3.1. This was an important prerequisite to this research because many samples had to be compared in a limited time period, necessitating the development of the quickest method which could provide images of acceptable quality. Although a variety of interesting features associated with the leaf deposit are apparent in these images, a full discussion of droplet deposition is provided later (section 3.2.4).

Specimen imaging using LT-SEM without gold coating the sample clearly resolved the fungicide deposits and leaf surface features of interest (Fig 3.7). The deposit annulus was also clearly defined. However, these images were unavoidably high in contrast and signal peaks often saturated the detector. Charging, whereby the electron beam charges certain parts of the sample and causes beam instability was also a serious problem, which increased with magnification. The benefit of not coating samples was an increase in speed of sample preparation (which is important for high throughput work) of approximately 20 min but this is far outweighed by the quality of the image that could be collected. Gold sputtering of the specimen (Fig 3.8) significantly reduced charging and secondary electron emission, and improved the tonal quality of the image which could be obtained. Imaging of gold-coated specimens with LT-SEM at appropriate magnification (Figs 3.9 and 3.10) could be performed for long time periods (several hours) with limited damage to the specimen.

Ambient temperature SEM dramatically increased the speed at which a sample could be prepared for imaging (approximately 10 min compared with approximately 45 min for LT-SEM) but is known to be problematic if the biological specimen is prone to desiccation and cell collapse in the vacuum of the SEM chamber (Jeffree and Read, 1991). However, high quality images which clearly resolved important features of the leaf and droplet at appropriate magnifications were routinely obtained under ambient conditions with no obvious tissue damage if imaging time was kept below 30 min (Figs 3.11 and 3.12).

Figure 3.7: Uncoated LT-SEM image of four *Amistar* deposits with added *Amistar adjuvant.* The annuli were clearly observed as white rings strongly contrasted against the dark background of the leaf. However, inconsistent secondary electron emission was a serious problem with these images, particularly at higher magnifications. Bar = 100μm.

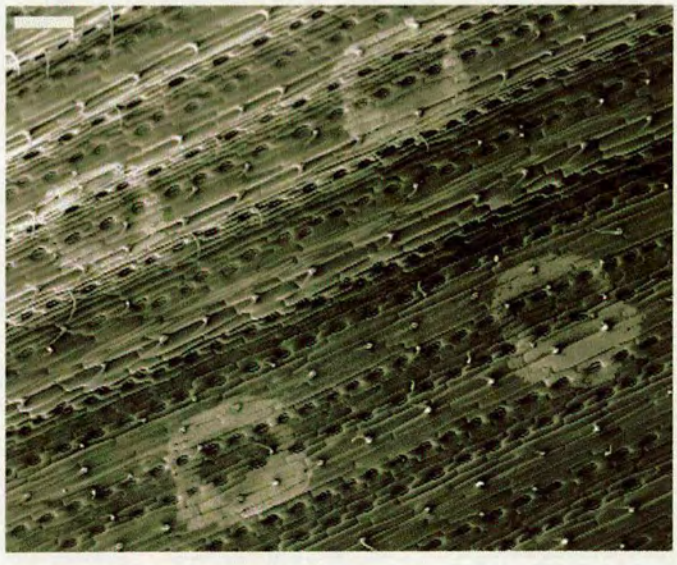

Figure 3.8: Gold-coated LT-SEM image of four *Amistar* deposits with added *Amistar adjuvant.* As with Fig 3.7, annuli and leaf surface structures were clearly resolved. Note that coating has dramatically improved the quality of the image by reducing saturation of the deposits and excessive contrast from inconsistent secondary electron emission. Bar = 100 μm.

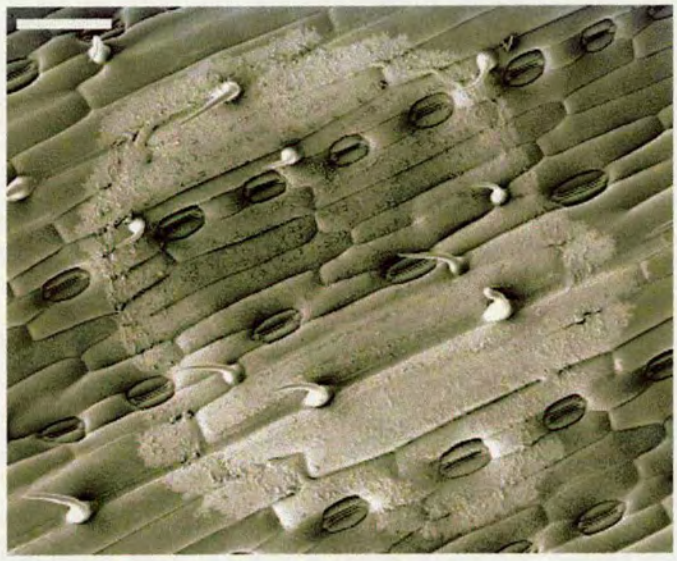

Figure 3.9: Gold-coated LT-SEM image of a single *Amistar* deposit. Coated specimens were more stable at higher magnifications than uncoated specimens. Note the annulus was clearly visible and contained most of the active ingredient and formulants. A lighter region of material was clearly shown which had advanced beyond the annulus proper. This was the advancing edge of the wetting agent, which had greater surface spread properties and crept further than the other solid components of the formulation. Bar = 100 μm.

Figure 3.10: Gold-coated LT-SEM image of edge of *Amistar* deposit. Images at high magnification could be recorded without damaging the specimen. Here, the deposit annulus is shown in more detail. Bar = 10 μm.

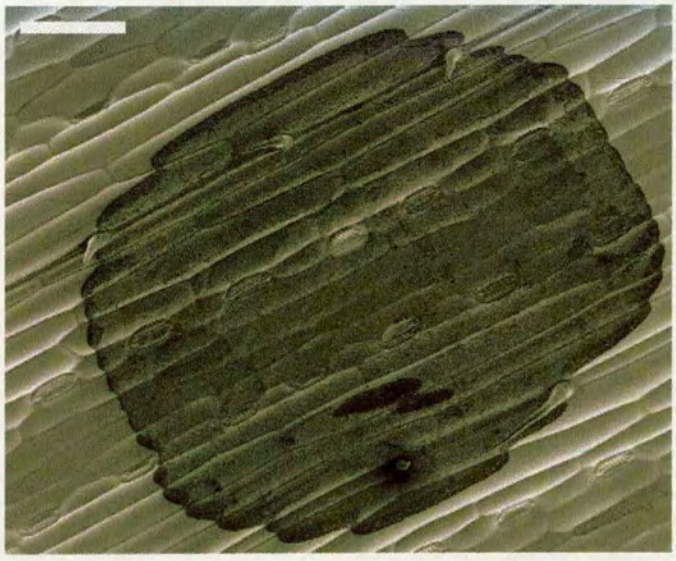

Figure 3.11: AT-SEM image of a single *Amistar* deposit. Specimen preparation for AT-SEM was considerably less time consuming than for LT-SEM. Given the high throughput of material necessary for this research, an efficient imaging system was attractive, but was required to provide data of acceptable quality. This AT-SEM image demonstrated that important surface features of both the leaf and deposit were well resolved by AT-SEM and no cellular collapse was induced as a consequence of desiccation. Bar = 100 μm.

Figure 3.12: AT-SEM image of edge of *Amistar* deposit. A potential problem with AT-SEM was specimen collapse by desiccation in the specimen chamber. This effect was often exacerbated at higher magnification. Generally, desiccation was not a problem if imaging time at high magnification was kept below 30 min. Bar = 10 μm.

The important advantages and disadvantages of the three imaging techniques described above are summarised in the following table.

Table 3.1 Comparison of ambient temperature and low temperature scanning electron microscopy of fungicide deposits.

Technique	Sample	Prep. time	Max. imaging time	Image quality	Damage
LT-SEM	Uncoated	about 30 min	over 1 h	Poor	None
LT-SEM	Gold-coated	over 45 min	over 1 h	Excellent	None
AT-SEM	Fresh	under 10 min	under 30 min	Very good	None

3.2.4 Comparison of Azoxystrobin Formulation Deposits

A variety of formulations of azoxystrobin were compared using AT-SEM. This was considered necessary to first understand more about the characteristics of fungicide droplets on the surface of cereal leaves as they dry, and secondly to develop a reproducible and realistic experimental system which could be employed for the fungicide-pathogen interaction studies presented in Chapters 4 and 5.

Although the formulations that caused least sedimentation and were easiest to apply to the cereal leaf surface were solvent based (given the hydrophobic nature of the leaf surface and the aqueous insolubility of the active ingredient), solvent-based fungicides are generally regarded to be more biologically effective than their water-based counterparts (Stock et al., 1998; Briggs and Bromilow, 1994). A 'good' formulation, then, is one that can be applied to the leaf surface reproducibly and without causing abrasion or damage, and which resembles spray-applied droplet deposits as closely as possible.

The most important variable affecting spray deposition levels downwind of the application are the droplet size spectrum of a spray application and the factors that affect this spectrum (Take, 1996). Droplet size has a profound impact on spray performance and drift (Hewitt et al., 1998). Consequently, nozzles and sprays are classified according to droplet size (Maynard et al., 1996; Doble et al., 1985). Agriculture spray droplets vary in size from as little as 5 μm volume mean diameter (VMD) for 'very fine' sprays, to 1000 μm and more for 'very coarse' sprays, with larger droplets drifting shorter distances than small ones (Table 3.2).

Table 3.2 ASTM/ASAE-572 standard nozzle sizes: comparison of droplet sizes produced by standard nozzles and potential for drift during application.

Classification	Symbol	VMD (μm)	Time to fall 10 ft	Drift in 3 mph wind
Very fine	VF	less than 100	66 min	3 miles
Fine	F	100-175	4.2 min	1100 ft
Medium	M	175-250	10 s	44 ft
Coarse	C	375-450	6 s	28 ft
Very coarse	VC	more than 450	2 s	8 ft

'Coarse' spray nozzle deposits have a VMD of approximately 250 μm and were calculated to contain 9.26 ng of active ingredient for a 1.25g/L application of *Amistar*. In this study, 0.2 μl droplets were applied. These have a VMD of 750 μm and are therefore 27 times the volume of droplets applied with a 'medium' sized nozzle (according to ASAE standard S-572 nozzle sizes).

In this study, *Amistar* droplets applied using a track sprayer varied dramatically in diameter, but were generally in the region of 100μm to 1000μm (Fig 3.13: courtesy of Jill Foundling, Syngenta). Therefore, although 0.2 μl droplets applied in this study had larger VMD than 'coarse' spray droplets, they were still within the range of droplet sizes produced by the track sprayer.

From figure 3.13, it is clear that most of the solid content from the droplet was located at the perimeter of each deposit, forming an annulus containing active ingredient and other formulants. The deposits were not completely circular, but instead formed less regular shapes on the leaf surface. This was probably because the droplets interacted with physical and chemical surface structures (such as epidermal cells, surface waxes, trichomes and stomata). Each droplet appeared to contain similar concentrations of solid material relative to size, and there was no apparent damage to the leaf caused by the application method (although it is worth noting that cereal leaf waxes are abraded in field conditions through contact with other plants, adverse weather conditions, and also insects, animals and machinery).

With this in mind, the following factors were considered when assessing 'experimental' formulations (see 2.1.2 for details of formulation composition) -

- physical properties: such as the amount of active ingredient contained in each droplet, droplet diameter and volume, deposit shape, and the range in size of azoxystrobin particles observed on the leaf
- chemical properties: such as what concentrations of adjuvant or solvent were added to the formulation
- practical considerations: such as whether the leaf surface was damaged during application

A field rate formulation of *Amistar* (formulation 1) could not be reproducibly applied to the leaf using the droplet applicator on the basis that the droplet being applied would not adhere to the leaf in favour of the needle tip without significantly perturbing surface waxes. Damage to surface wax is a potentially serious problem because it can alter the wettability and spread of the fungicide, and potentially alter the speed of uptake into the cuticle and epidermal cells and diffusion of fungicide through surface wax. Given that localised movement through epidermal cells, cuticle, and surface waxes was of primary interest to this research it was essential that these problems were addressed and overcome.

No data were recorded for formulation 1 on either the abaxial or adaxial surface of the leaf. An azoxystrobin suspension in water i.e. without solvents applied as 0.2 μl droplets would not detach from the column of liquid in the needle capillary.

Given the profoundly hydrophobic nature of the leaf surface, formulations with improved adhesional properties were developed. The first of these, formulation 2, contained active ingredient dispersed in water and a water miscible solvent (IPA). As anticipated, this formulation was found to adhere to the leaf in favour of the applicator needle, although some perturbation of surface wax occurred as a result of the droplet not being cleanly transferred to the leaf surface. Of greater concern was the observation that the droplet applicator did not deliver similar quantities of fungicide to the leaf surface (Fig 3.14) and dramatically varying quantities of fungicide were observed in different deposits.

An annulus did form from these droplets, but significantly more of the solid content of the formulation was dispersed within the deposit than was recorded for field spray and applicator applied droplets of formulation 1 (Fig 3.15). This was probably a consequence of using a water miscible solvent, which holds solids in solution for longer during the drying process, reducing the time available for the annulus to form. Further features of interest were the appearance of non-wetted stomata (Fig 3.16) and the active ingredient adhering to trichomes (Fig 3.17). Stomatal cavities and trichomes are recognised to provide a faster route for the uptake of some pesticides (and in the case of stoma, cuticular uptake can be bypassed completely). Stomata were generally wetted by spray-applied *Amistar*, and active ingredient was also shown to settle on trichomes.

Formulation 3 contained *Quadris* suspended in 25% IPA. This delivery system therefore benefitted from containing the antisettling agent used in *Amistar*, but used a water miscible solvent to improve wettability (by reduction in surface tension) in favour of *Amistar adjuvant*. A deposit annulus was formed, although a greater quantity of solid material was again deposited behind the annulus than was observed in field applications. The use of the anti-settling agent from *Quadris* did reduce the degree to which the fungicide settled in the needle and led to more uniform fungicide delivery, although some variation between deposits was still apparent (Figs 3.18 and 3.19).

Both formulation 2 and formulation 3 were considered unsuitable for the following reasons-

- an unknown and potentially very different concentration of fungicide was present in different deposits, leading to high variation of active ingredient concentration between samples
- the use of a water miscible solvent could increase uptake time relative to field application.
- a larger surface area is available for uptake (due to solid content being well dispersed throughout the deposit)

Anecdotal evidence suggested that single 0.2μl droplets of typical field rates of *Amistar* would be impossible to apply to the leaf without significantly damaging surface wax unless a thin film of water was applied to the leaf surface first, by blowing across the leaf surface immediately prior to application (C.A. Hart and A. Howell, personal communication).

However, a field rate formulation of *Amistar* (formulation 4) was applied as a benchmark and significant surface wax disruption and mechanical damage to the surface was observed (Figs 3.20 and 3.21). An important benefit of this formulation, however, was that no noticeable settling of the fungicide in the needle was observed, and the deposit was apparently identical to similarly sized droplets applied using high pressure spray machinery. The annulus was of particular interest because little or no fungicide was found to settle within the deposit, with most of the solid content being deposited in the annulus (Fig 3.22). Imaging at higher magnifications revealed that active ingredient, anti-settling agent and adjuvant were mostly deposited in the annulus. Particle size of active ingredient is estimated to vary from between approximately 0.01 and 5 μm diameter (Fig 3.23).

The problems outlined above were solved by the development of formulation 5, which contained the same concentration of active ingredient and anti-settling agent as the field applied formulation with the addition of extra *Amistar adjuvant*. The anticipated practical improvements to manual application with limited or no surface wax perturbation, while using the same compounds at similar or identical concentrations to field applied formulation, were observed. Not only was no wax perturbation observed, but the quantity of solid content delivered in different deposits was qualitatively indistinguishable (Fig 3.24). An interesting and distinct feature of this formulation was that *Amistar adjuvant* displayed significant surface creep beyond the annulus proper which was not observed in field-applied deposits (Fig 3.25).

The important differences between these formulations are shown in Table 3.3. It was clear that formulation 5 represented the best compromise between practical handling and application of fungicide while keeping as true as possible to field-sprayed applications.

Table 3.3 Comparison of formulations.

	Adjuvant	Reproducibility	Damage	Similarity to field
1	None	Impossible	Unknown	Unknown
2	Solvent	Very poor	Limited	Very dissimilar
3	Solvent/antisettler	Poor	Limited	Dissimilar
4	Adjuvant/antisettler	Good	Wax damage	Very similar
5	2x adjuvant/antisettler	Excellent	Limited	Similar

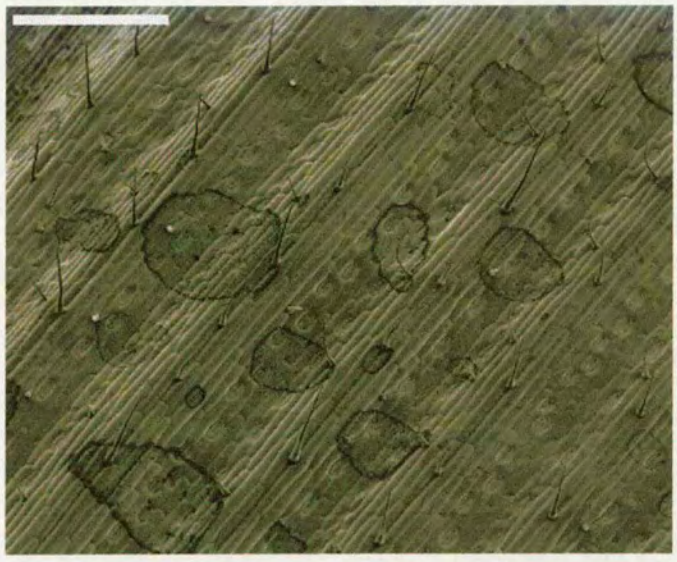

Figure 3.13: *Amistar* tank mix, field-sprayed. Experimental droplets were intended to resemble field conditions as closely as possible. Note that field spray deposits vary in size (between 100 μm and 1000 μm) and that no observable mechanical damage to the leaf was caused by the application process. Bar = 1 mm. Image courtesy of Jill Foundling, Syngenta.

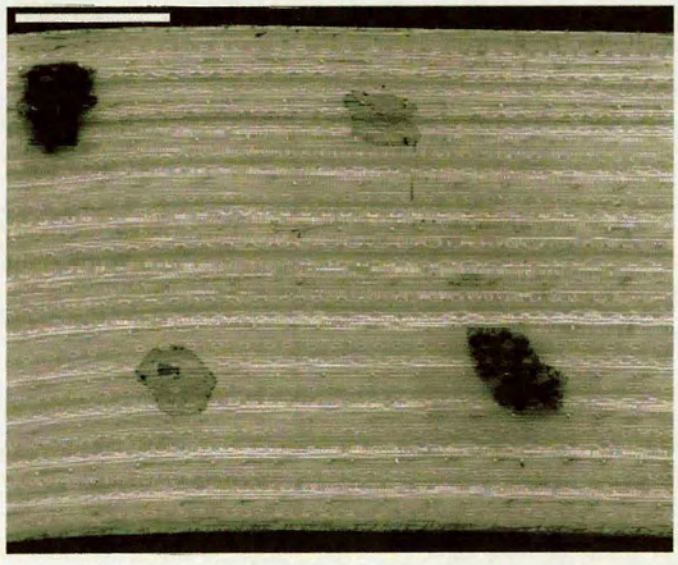

Figure 3.14: Abaxial leaf surface treated with formulation 2. Apparently no mechanical damage was caused to the leaf through the application process. The difference in contrast between the three droplets in the field of view demonstrate that different quantities of solid material from the formulation were deposited. This was probably a consequence of formulation ingredients settling in the applicator needle. Bar = 1 mm.

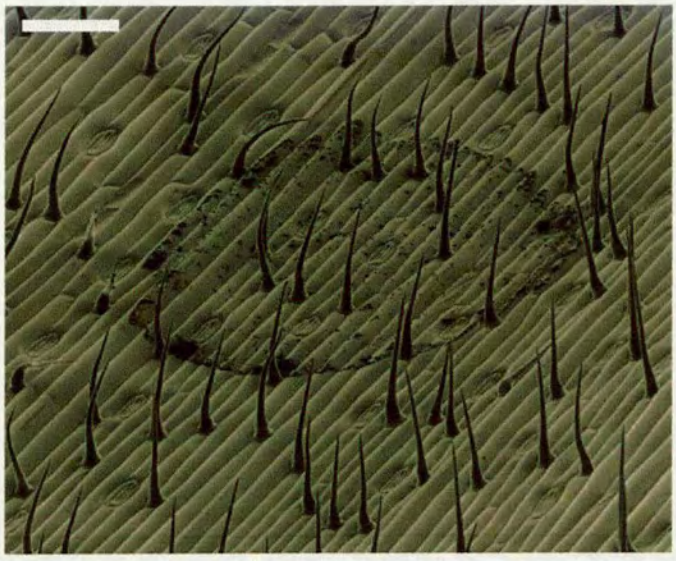

Figure 3.15: Abaxial leaf surface treated with formulation 2. At higher magnification the droplets dried in a roughly circular shape despite the topographical features of the leaf surface and surface wax chemistry. This was probably due to the effects of the solvent used in the formulation. Significant differences between the drying properties of these droplets with field applied *Amistar* suggested it was unsuitable for later experiments. Bar = 100 μm.

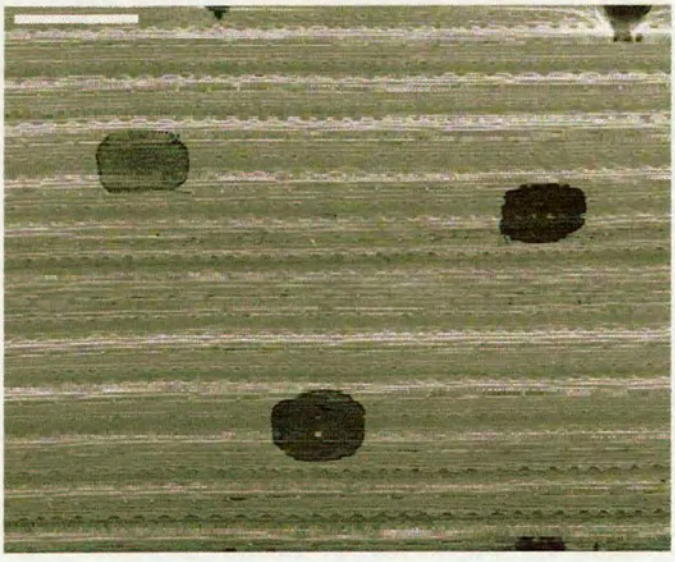

Figure 3.16: Abaxial leaf surface treated with formulation 3. The use of fine milled azoxystrobin in formulation with IPA was anticipated to decrease the rate of settling in the applicator needle. In fact the reverse was the case, and significantly more solid material was deposited in two of the three deposits. Bar = 1 mm.

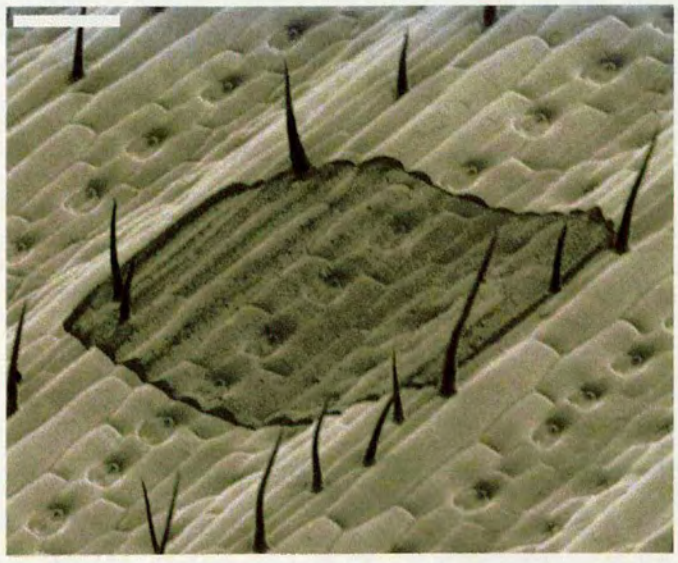

Figure 3.17: Abaxial leaf surface treated with formulation 3. Whereas spray applied *Amistar* deposits were irregularly shaped, which was indicative that leaf surface topography and waxes had affected the drying process, these droplets remained largely unaffected and dried in more regular shapes. A higher quantity of solid material settled within the deposit although the majority was still located in the annulus. Bar = 100 μm.

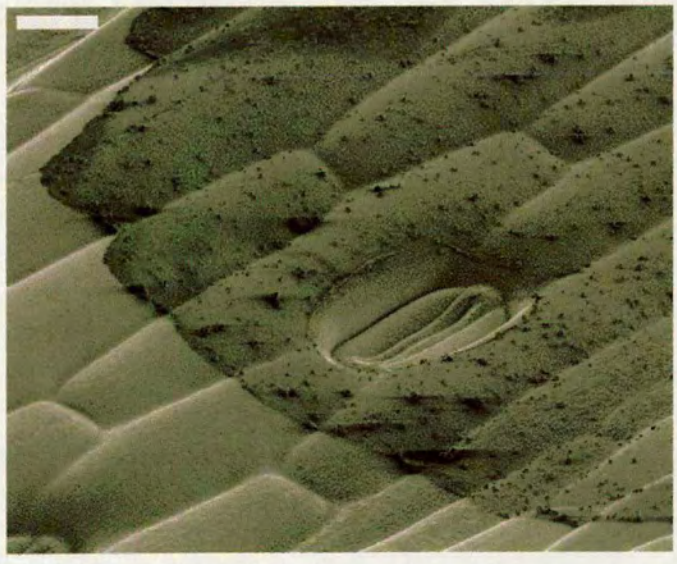

Figure 3.18: Abaxial leaf surface treated with formulation 3. Here a stomata remained non-wetted despite the application of fungicide formulated with a water miscible solvent. Azoxystrobin particles are distributed more uniformly throughout the whole deposit. On the one hand, the larger surface area available for uptake as a result of this may increase the uptake speed of the fungicide relative to field droplets. Alternatively, however, the lower surface concentration of adjuvant may decrease uptake rate. Bar = 10 μm.

Figure 3.19: Abaxial leaf surface treated with formulation 3. In this case azoxystrobin particles settled on a trichome. Adhesion to trichomes was not observed in fungicide formulations which did not contain IPA. Trichomes are generally recognised as providing a more efficient uptake path for some fungicides and further suggested that this formulation would not provide an appropriate replica of field conditions. Bar = 10 μm.

Figure 3.20: Abaxial leaf surface treated with formulation 4. Here, the extent to which hand-applied formulations with poor wetting agents could mechanically damage the leaf surface during application was observed. Wax was significantly disrupted during the application process. Given that wax provides an important barrier to liquids on the leaf surface, this could significantly increase uptake rate into epidermal cells and affect localised diffusion through surface wax. Bar = 1 mm.

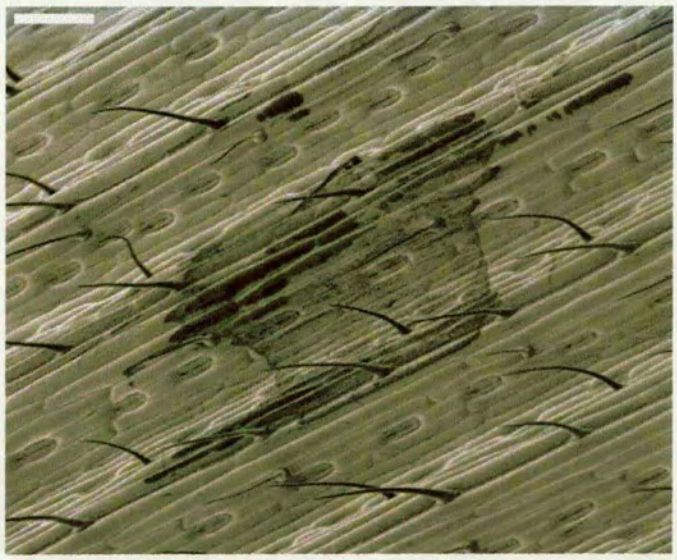

Figure 3.21: Abaxial leaf surface treated with formulation 4. Higher magnification images of the droplets shown in Fig 3.20 revealed the extent to which wax had been mechanically damaged during droplet application, in this case within and around the deposit. Bar = 100 μm.

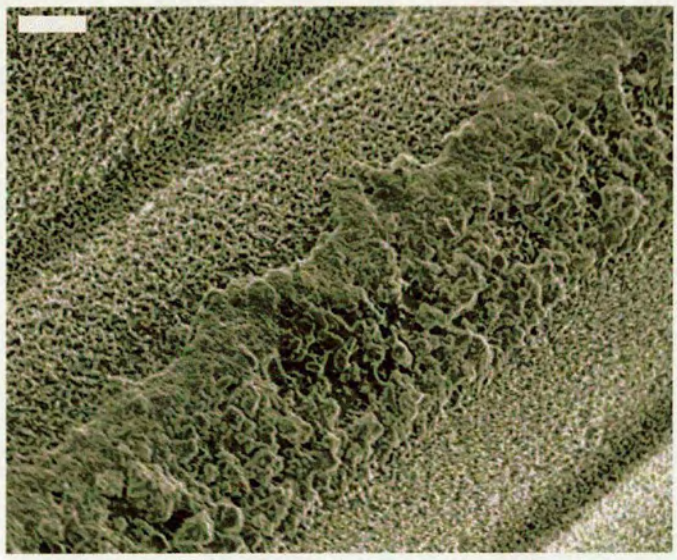

Figure 3.22: Abaxial leaf surface treated with formulation 4. This formulation is a chemical replica of the droplets in Fig 3.13. Azoxystrobin particles, adjuvant and the anti-settling agent were contained within the annulus. Note that no solid material from the droplet settled behind the annulus. Bar = 1 μm.

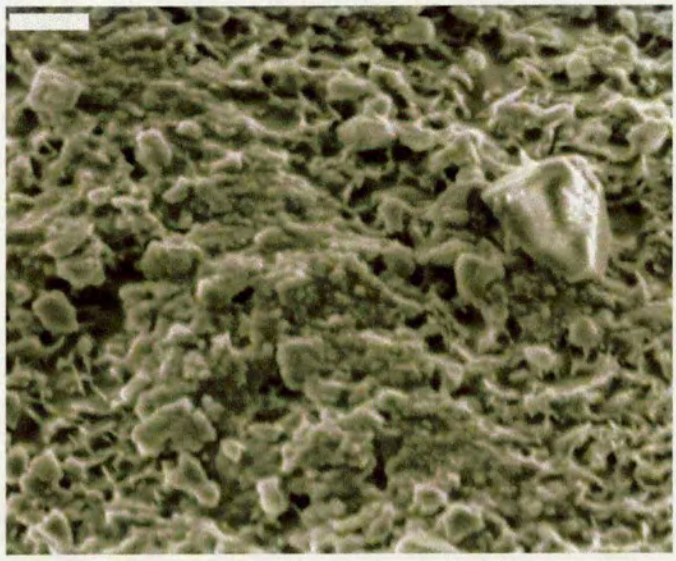

Figure 3.23: Abaxial leaf surface treated with formulation 4. Azoxystrobin particles within the annulus were visualised. Particles of active ingredient were estimated to vary from between sub-μm size to more than 2 μm in diameter. Bar = 1 μm.

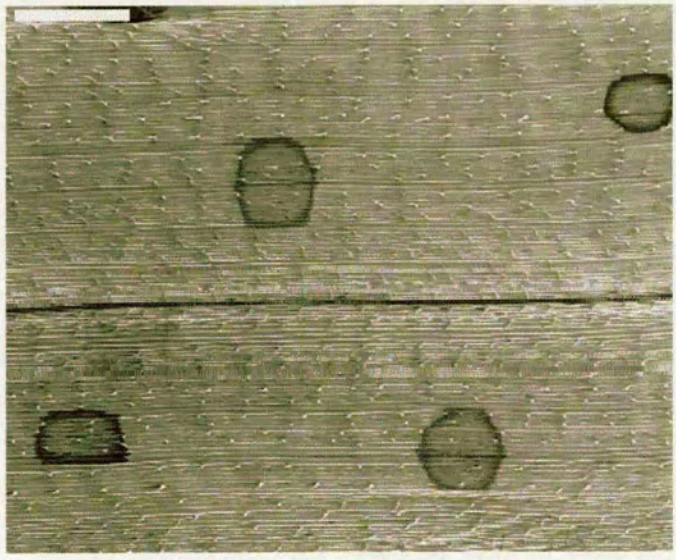

Figure 3.24: Abaxial leaf surface treated with formulation 5. No surface damage nor wax perturbation was apparent as a consequence of fungicide application. The droplets varied in shape and area although a prominent annulus had developed. Bar = 1 mm.

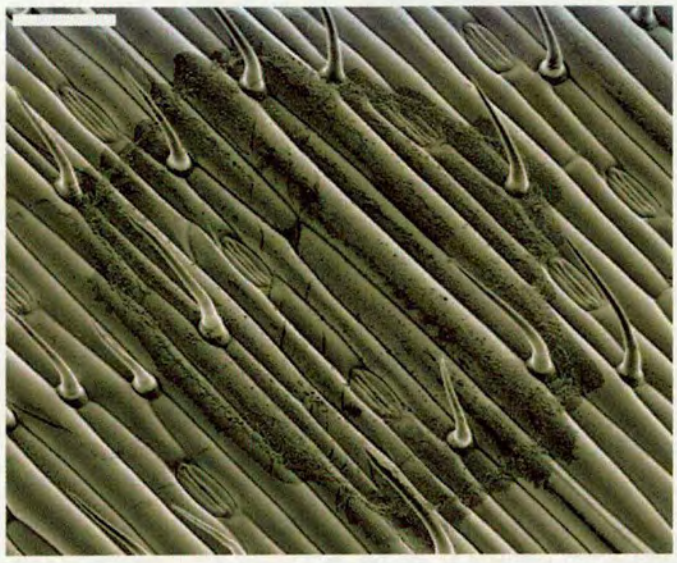

Figure 3.25: Abaxial leaf surface treated with formulation 5. Note that although most of the solid content was deposited in the annulus, areas containing solid components of the formulation were deposited along epidermal cells. A dark region was also observed extending beyond the particulate deposit perimeter. This was probably adjuvant which had been deposited beyond the annulus. The chemical and physical similarity between these deposits and the field applied droplets suggested that this formulation was an excellent laboratory replica because it was reproducible and did not cause obvious damage to the leaf surface or surface waxes. Bar = 100 μm.

Figure 3.26: Abaxial leaf surface treated with formulation 5. Here the surface creep of the wetting agent was shown in more detail as a darker region that extended several μm beyond the annulus. Bar = 1 μm.

3.3 Discussion

3.3.1 Mechanism of Annular Deposit Formation

The study of small-scale interactions between pathogens and fungicide deposits on cereal leaves requires that a consistent and reproducible volume of liquid containing similar concentrations of fungicide can be delivered by a droplet dispenser. Although the application of droplets to leaf surfaces may appear to be a trivial process, small differences in droplet volume, adjuvant, fungicide concentration and application technique may contribute to significant differences in the foliar distribution and uptake rate of the applied fungicide.

The initial aims of this research therefore concerned the delivery of single micro-droplets to cereal leaves with the aim of developing an application system that consistently delivered single droplets to the leaf surface which contained fungicide and adjuvant components which were similar to field-applied droplets, and that could be applied to the leaf in similar volumes to the high-pressure spray machinery used in agricultural applications.

The obvious alternatives to single droplet application, of using either a track sprayer or Potter tower to apply fungicide formulations, were not possible. The research programme for which droplets were used required the application of radiolabelled fungicides which could not be allowed to contaminate the track sprayer. The Potter tower, which was found to produce similar droplets to the track sprayer (data not shown), was located too remotely from the SEM preparation laboratory to be practical for short-time scale studies of fungicide/fungus interactions on the leaf surface.

Initially, 0.2 μl droplets of field-rate formulations were applied to glass slides to analyse the characteristics of particulate sedimentation throughout the drying process. From the data presented, a time-course of droplet drying was characterised in which homogeneously distributed particles were observed to aggregate within 1 min of application to the microscope slide. Within 5 min, significantly greater quantities of solid material were relocated to the periphery of the droplet. This process continued for a further 10 min, after which time the droplet had dried and the majority of active ingredient and anti-settling agent had relocated to the deposit perimeter and formed an annulus. *Amistar adjuvant* could not be resolved by the light microscope and may have been present throughout the deposit.

Such ring, or annular, deposits are commonplace wherever drops containing dispersed solids evaporate on a surface (Deegan et al., 1997) and the presented data is perhaps unsurprising. The formation of annular deposits is believed to be consistent regardless of the nature of the dispersed material, carrier liquid, or substrate. Recent experimental evidence suggests that the phenomenon is due to geometrical constraints; the free surface, constrained by an immobile contact line, forces fluid to the droplet perimeter to replace evaporated liquid (Deegan et al., 1997).

In the present study, it is interesting to note that even comparatively large particles (above 10 μm diameter) of azoxystrobin were redistributed to the deposit perimeter during the drying process, suggesting that almost all of the active ingredient within the fungicide formulation will be concentrated in the annulus, rather than homogeneously distributed throughout the deposit, regardless of particle size.

Although the processes governing deposit formation have received limited attention by the agrochemical community, a significant volume of research has been conducted into the effects of formulation chemistry on foliar distribution and uptake within the industry. The physical factors affecting droplet deposition are, however, of inherent interest to certain industries, such as those involved in the development of surface coatings applied as liquids, and the deposition of inks during printing (Ball, 1997). Research by authors in these fields has led to the present understanding of droplet deposition described here and in section 1.5.4 (Deegan et al., 1997; TAPPI, 1996; Picknett and Bexton, 1976).

3.3.2 SEM Techniques in the Study of Pesticide Deposits

Although the application of fungicide droplets to glass slides demonstrated that *Amistar* deposit formation was consistent with the annular deposition of other solutes in solvents applied to a variety of substrates, it is well known that leaf surface micro-roughness and surface chemistry can profoundly affect droplet deposition on leaves (Hart and Young, 1987; Juniper and Jeffree; 1983). Prior to an investigation into differences between formulation type and droplet deposition, SEM techniques were necessarily developed to enable the imaging of such samples and take advantage of the improved spatial resolution and depth of field conferred by SEM over light microscopy.

Since the commercial introduction of the SEM in the 1960s, a wide range of applications in the plant and agrichemical sciences have taken advantage of the capacity of the instrument to visualise complex surface topographies with improved depth of field (approximately 300 times better than can be obtained with light microscopy) and the large range of magnifications available (Jeffree and Read, 1991). Low temperature SEM has often been the technique of choice for the examination of botanical specimens and agrochemical deposits (e.g. Wettstein-Knowles, 1997; Jeffree and Read, 1991; Hart and Young, 1987; Baker and Holloway, 1971). The popularity of LT-SEM can be attributed to the improved specimen immobilisation and stabilisation times achieved by cryofixation compared with chemical fixation (Read, 1991), and considerable improvements in specimen viability during imaging compared with AT-SEM (Jeffree and Read, 1991).

Scanning electron microscopy is typically performed at low pressure to avoid the absorption, scattering and spreading of the electron beam by gases. At ambient temperature and low pressure, volatile components of plant specimens (most notably water) are quickly lost through evaporation, which causes specimen collapse and dimensional changes in the specimen (Jeffree and Read, 1991). Nevertheless, high quality images of botanical specimens under ambient conditions have been obtained by some authors (e.g. Krulik, 1980; Robards, 1978; Pease et al., 1966). Furthermore, the interactions between pesticide spray droplets and leaf surfaces have been successfully studied in a variety of crop plants under ambient conditions following gold sputter coating (Baker et al., 1983).

In the present study, a high throughput of material was necessary due to time constraints. Specimen preparation for LT-SEM was approximately 45 min or longer. The time required for specimen preparation for AT-SEM was typically 10 min or less, and was therefore attractive because a high throughput of material was possible while the inherent advantages of SEM imaging could still be exploited. Initially, non-coated cryopreserved specimens were observed, and were found to suffer from inconsistent secondary electron emission which caused signal flare. Despite the improvement in specimen preparation time (approximately 30 min), image quality was sufficiently poor to render this approach unacceptable. Sputter coating of these samples significantly improved image quality but led to an unacceptable increase in sample preparation time.

Ambient temperature SEM represented the most appropriate compromise between sample preparation time and image quality. From the data presented, it was apparent that high quality images of fresh, non-coated samples could be collected which clearly resolved all of the surface features of interest without causing specimen collapse, provided that imaging time was reduced. For LT-SEM, imaging on the cold stage of the SEM was possible for extended periods (several hours). Conversely, for AT-SEM specimen collapse occurred between 30 and 45 min of imaging. Rates of specimen collapse increased at higher magnification. However, image acquisition for a given sample could be achieved within 10 min, and very high magnifications were unnecessary. Consequently, AT-SEM was used in preference to LT-SEM or light microscopy.

3.3.3 Mechanical Damage and Deposit Consistency

Deposits from several formulation types were compared using AT-SEM. The selection of an appropriate fungicide formulation was of primary importance, based not only on the physical properties of the deposit, but also the chemical properties of the formulation. Several aspects of droplet delivery were of interest, namely: whether active ingredient could be applied in consistent volumes to the leaf surface; whether mechanical damage occurred, whether deposit size was consistent with field deposits, and whether chemical composition was similar to agrochemical spray composition. It is possible that small differences in any of these could have wide ranging implications for uptake and fungicide efficacy. The reasons for this are discussed below.

Initially, attempts were made to apply droplets to wheat leaves of azoxystrobin suspended in water at typical active ingredient field rate. These droplets would not adhere to the profoundly hydrophobic surface of the leaf, necessitating the development of a formulation that could be successfully applied to the leaf surface. An increase in the dose of agrochemical received by the target plant could lead to an overall increase in uptake (Stock and Holloway, 1993). Therefore, formulations applied in the present study were imaged and consistency of droplet deposition was qualitatively assessed. Because differences in applied dose could affect uptake, formulations in which inconsistent volumes of fungicide were deposited, were deemed inappropriate.

ISO-propylalcohol, which is a water miscible solvent and would therefore be predicted to reduce droplet surface tension and improve wettability, was used in formulation 2 and formulation 3. From the data presented, these formulations could be applied to the leaf surface without causing damage to epicuticular wax. However, consecutive droplets produced by the applicator needle of both formulation 2 (azoxytrobin/IPA) and formulation 3 (*Quadris*/IPA) produced deposits with significantly different quantities of fungicide, and were considered too dissimilar to spray-applied droplet deposits.

In this study, field rate droplets of *Amistar* could only be applied to the leaf surface if epicuticular wax was mechanically abraded by the needle tip. Epicutical wax in terrestrial plants serves the purpose of controlling water loss when stomata are closed. The cuticle also reduces the loss of inorganic and organic solutes from the interior tissue by the leaching impact of rain (Riederer and Schreiber, 1999). It follows then, that the abrasion of hydrophobic surface waxes will improve leaf surface wettability by fungicide formulations. However, by their very nature, the physical and chemical properties of the cuticle and epicuticular wax also determine the uptake of foliar applied pesticide solutions (Reiderer and Schonherr, 1999; Geyer and Schonherr, 1989).

Furthermore, some studies have shown surfactant adjuvants in pesticide formulations that dissolve or disrupt epicuticular waxes have increased uptake rates compared to those that did not (Stock and Holloway, 1993). In the present study, the use of field-rate *Amistar* was considered unacceptable. Although the physicochemical properties of the formulation were necessarily identical to field-applied droplets, the physical consequences to the leaf surface of the application process could significantly affect the subsequent uptake and activity of the formulation.

The generally held view that surfactants increase cuticular wettability and, hence, permeability to agrochemcials by dissolving or disrupting the covering of wax on cuticle surfaces, has recently been called into question. It had been proposed that wax molecules could be removed in solution by solubilisation with the surfactant after absorption through the cuticle (Cox, 1989). However, subsequent attempts to confirm surfactant-induced damage by SEM have failed to detect any dramatic changes in wax morphology or distribution, even after a surfactant has physically penetrated the wax layer (Noga et al., 1991). Indeed, studies of spray droplets and deposits on leaf surfaces using SEM typically show residual active ingredient and surfactant covering intact epicuticular wax (e.g. Hart and Young, 1987).

Although increasing the effective contact area of a deposit would be expected to increase the magnitude of diffusion of a solute through the cuticle, experiments using applications of single droplets have demonstrated that there is no general correlation between the efficiency of surfactant-induced uptake and the apparent contact area of the corresponding droplet (Schonherr and Riederer, 1991).

In the present study, deposits formed by all successfully applied formulations were in the region of 750 μm diameter. These deposits fell within the ASAE range of 'very coarse' droplets (see Table 3.2) and, because evidence exists that droplet area has no significant impact on uptake rate, were considered to be acceptable for subsequent experiments.

From the data presented, droplet deposits of formulation 5 were observed to cause no epicutical wax abrasion, deposited consistent quantities of fungicide from consecutively applied droplets, and were within the VMD range of track-sprayed droplet deposits. The application of this formulation required a two fold increase in concentration of the surfactant *Amistar adjuvant*. Surfactants are important components of fungicides, and have been found to enable decreases in the dose of active ingredients without sacrificing biological activity (Kirkwood, 1993).

The mechanisms by which foliar uptake of pesticides can be promoted by non-ionic surfactants is still poorly understood, but they may affect spray coverage, droplet retention or the physical state of the residue on the crop surface (Riederer and Schonherr, 1990; De Ruiter et al., 1988). Furthermore, they may function by altering solubility relationships within the cuticle, and possibly increase uptake rates of active ingredients (which penetrate cuticles poorly) by co-penetration with surfactant (which penetrates cuticles rapidly)(Kirkwood, 1993; Holloway and Stock, 1990; Silcox and Holloway, 1989; McCall, 1988). Work with herbicides has demonstrated that the uptake rates of hydrophobic active ingredients were optimally increased by the addition of alcohol-based surfactants (Holloway and Stock, 1989).

In the present study, three formulation options were available -

- use formulation 4, which was chemically identical to field-applied droplets but caused signifcAnt damage to epicutical wax
- use formulation 5, which was chemically similar to field-applied droplets but contained higher concentrations of the same surfactant and did not cause damage to epicuticular wax
- develop a formulation which combined IPA and *Amistar adjuvant* to improve wettability

The most prudent choice of formulation was considered to be formulation 5. Although uptake rates may be slightly improved by using an increased concentration of surfactant, *Amistar adjuvant* is recognised as being relatively inert (D.W. Bartlett and C.A. Hart, personal communication). Formulation 5 was therefore expected to most closely simulate field-applied droplets.

It should be stressed that, due to time constraints and practical limitations, no attempt was made in the present study to quantify the uptake rates of azoxystrobin with different adjuvants, or compare uptake rates through damaged and non-damaged leaves. Single droplet studies are regularly performed by agrochemical companies to study a variety of phenomena. The potential problems associated with such an approach are poorly represented in the literature and are certainly worthy of future research.

Chapter 4

Azoxystrobin Micro-Biokinetics

> Scientific truth should be presented in different forms, and should be regarded as equally scientific whether it appears in the robust form and the vivid colouration of a physical illustration, or in the tenuity and paleness of a symbolic expression.
> James Clerk Maxwell

4.1 Introduction and Aims

4.1.1 Introduction

The infection micro-arena was envisaged as a region of the leaf approximately 1 mm^3 in which the first interactions between azoxystrobin and its target pathogen occur. Generally, studies of pathogen/fungicide/host interactions are conducted on a far larger scale in which fungicide activity is measured in terms of percentage leaf area affected or number of plants in a crop which survive. Although these studies provide insight into, for example, basic fungicide efficacy, appropriate application rates for fungicides and effectiveness of adjuvants, they provide no direct information regarding how the fungicide interacts with the pathogen on the leaf surface at the single droplet/single cell or colony level. Furthermore, despite extensive research into host/pathogen interactions and disease resistance mechanisms (see reviews by Knogge, 1996 and Hammond-Kossack and Jones, 1996), micro-scale studies of pathogen/pesticide interactions have received limited attention. Two commercially important pathogens of wheat were selected for these micro-scale experiments. *Puccinia recondita*, which causes brown rust on wheat, and *Blumeria graminis*, which causes powdery mildew infection, are responsible for devastating crop losses throughout the world and were therefore of interest in this study.

4.1.2 Aims

Specifically, the aims of this section were to -

- develop appropriate imaging techniques using the scanning electron microscope for the study of fungicide control of *Puccinia recondita* and *Blumeria graminis*
- analyse the curative activity of deposits from single droplets of azoxystrobin on wheat leaves infected with *P. recondita* over short time periods (less than 3 h)
- analyse the curative activity of deposits from single droplets of azoxystrobin on wheat leaves infected with *B. graminis* over short time periods (less than 24 h)
- analyse the preventative activity of deposits from single droplets of azoxystrobin on wheat leaves infected with *B. graminis* over short time periods (less than 7 h)

4.2 Results

4.2.1 Overview of Results

In Chapter 3, descriptive microscopy of azoxystrobin formulation deposits was carried out and an azoxystrobin formulation appropriate to the experiments described below was developed. In this chapter, SEM was used experimentally to analyse the short time-scale contact and translocational activity of this azoxystrobin formulation on colonies of *P. recondita* and *B. graminis in planta.*

Initially, a variety of SEM techniques were considered in order to develop an appropriate imaging system for the course of these experiments. Wheat leaves and both pathogens were observed *in planta* to gain familiarity with the organism and to determine an appropriate assay for fungicide activity. Despite the application of high doses of azoxystrobin to established *P. recondita* colonies, no effect was apparent over short time periods (1-5 h). Treatment of younger colonies was a practical impossibility due to the difficulties in locating the significantly fewer numbers of sub-epidermal hyphae. Therefore, detailed analysis of the preventative and curative activity of azoxystrobin was done using *B. graminis* only. However, LT-SEM techniques were successfully employed in the imaging of *P. recondita* on the leaf surface and in sub-epidermal leaf compartments.

Comparisons were made between the LT-SEM techniques necessarily developed for the study of *P. recondita* and AT-SEM techniques which were used in Chapter 3. Ambient temperature SEM at relatively low magnifications provided good spatial resolution and excellent depth of field. By using AT-SEM in favour of LT-SEM, much higher throughput of material was possible and was therefore developed to image fresh *B. graminis* samples on wheat.

Following the development of appropriate imaging techniques, curative activity was followed in *B. graminis* colonies on the surface of wheat over 1 h to 1 day time periods. An important area of interest to this research was the relative speed of azoxystrobin translocation through different leaf tissues at the micro-scale level. Despite analysis of efficacy over short distances in *B. graminis*, no definite conclusions could be drawn as to how far the translocational effect recorded was a result of movement of fungicide through plant epidermal cells, as opposed to movement through hyphal compartments. In order to gain a clearer understanding of leaf-specific translocation, inhibition of germination studies were conducted. The obvious benefit of this approach was that spores do not have hyphal compartments through which azoxystrobin can translocate.

A time course of fungal development of *B. graminis* was carried out from 30 min to 36 h on whole wheat leaves in the absence of azoxystrobin. These were compared with the development of germinating spores in the micro-arena - i.e. the localised region on the leaf comprising the fungicide deposit and the fungal spores. Germination rates and fungal development were then analysed over a 1-7 h time period. Application of formulation 5 (1.25g azoxystrobin per L; pseudo-field rate) showed very high preventative activity and the increasing zone of fungicidal activity as a result of translocation through foliar compartments was measured. Data tables and descriptive statistics related to the research presented in this chapter are provided in Appendix 10.1.

4.2.2 Wheat Leaf Structures Imaged with LT-SEM

Before commencing a study of infected tissue, it was first necessary to identify important structures of the leaf in order to establish normal tissue from infected tissue. Observations from the imaging of surface and internal structures of healthy wheat plants are shown in Figs 4.1 (epidermis), 4.2 (surface wax) and 4.3 (lateral fracture). Relatively low magnification images of the leaf surface clearly resolved important structures on the leaf such as trichomes, piliferous cells, silica cells and stomata. Higher magnification images of the same leaf resolved surface wax structures. The location and composition of trichomes, stomata and surface waxes can play an important role in the foliar uptake of fungicides into the leaf.

Following freeze fracture, internal structures of the leaf such as substomatal cavities and mesophyll cells were readily identifiable. Cross sections of the epidermis and cuticle were identified. These, along with epicuticular wax, represent a significant barrier to the absorption of leaf applied fungicides (Staubert, 1993).

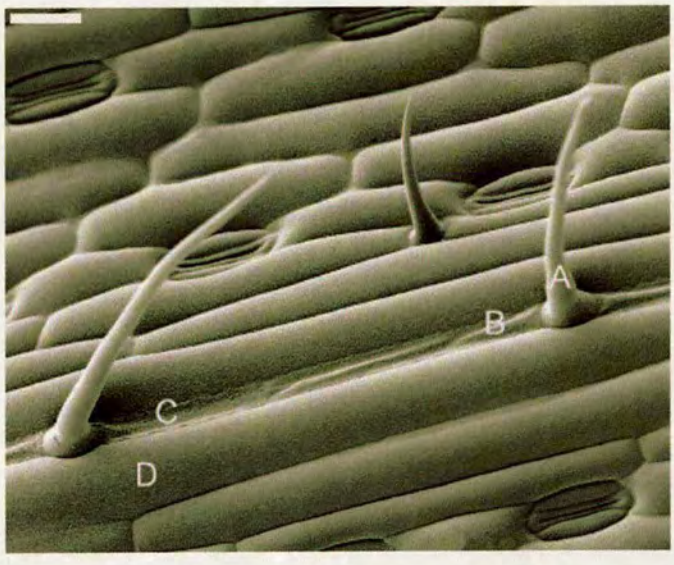

Figure 4.1: LT-SEM image of the surface of a non-infected control leaf (abaxial surface) at relatively low magnification. Note the prominent surface features of the leaf surface including prickle hairs (A), piliferous cells (B), silica cells (C) and epidermal cells (D). Stomata are abundant and comprise subsidiary cells (E) and guard cells (F), which surround the opening of the stoma. Bar = 10 μm.

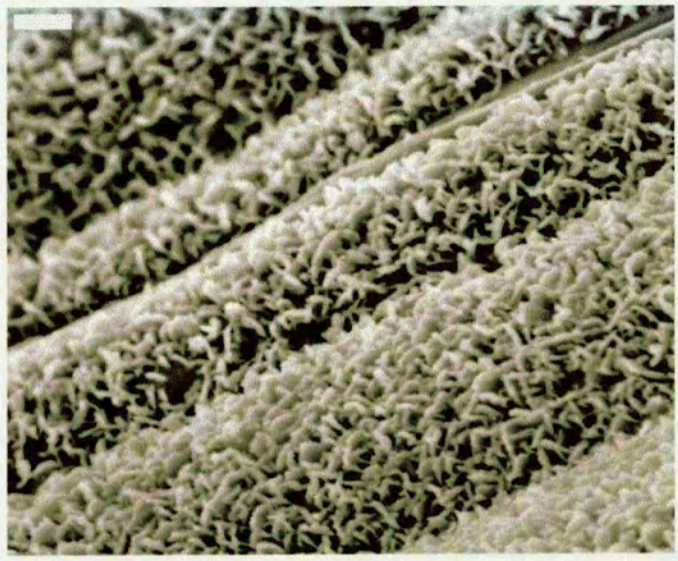

Figure 4.2: LT-SEM of the same leaf at higher magnification showed that wheat leaves were covered in a layer of crystalline epicuticular waxes. These wax structures provide the leaf with a profoundly hydrophobic surface, not only through their chemical composition but also because their micro-morphology traps air and prevents wetting. Bar = 1 μm.

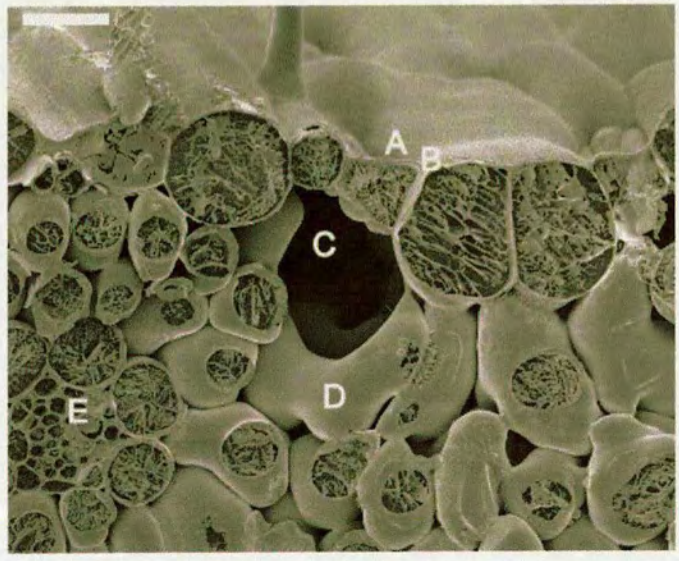

Figure 4.3: LT-SEM of an etched, partially freeze-dried lateral cross-section of a non-infected wheat leaf. Note the prominent structural features resolved, including the cuticle (A) and location of epidermis (the epidermis is not resolved) (B), sub stomatal cavity or air space (C), mesophyll cell (D), and vascular bundle (E). Bar = 10 μm.

4.2.3 *Puccinia recondita* Infected Tissue Imaged with LT-SEM

In order to observe the internal structures of wheat infected with *P. recondita*, freeze-fracturing of infected tissue was necessary. Images obtained from freeze fractured samples showed that cryo-preservation in liquid nitrogen of sub-epidermal hyphae was excellent, with no observed collapse of internal plant or fungal cells. Natural collapse of spores erupting through the leaf did occur, although this may have resulted from the transfer of infected plants from the growth room to the SEM laboratory, rather than as a consequence of the cryo-preservation process. Successful curative application of azoxystrobin to *P. recondita* has been shown to result in hyphal collapse and was considered an appropriate assay for fungicide efficacy (Hart, 1995). These data were therefore collected as a control for comparison with treated samples.

Longitudinal fracturing of the leaf (i.e. fracturing along the leaf, from tip to base) provided a larger area for imaging and gave a cleaner fracture than lateral fracturing. Careful sample preparation enabled images of *P. recondita* infection on the leaf surface and in internal structures to be collected from the same sample (Figs 4.4 and 4.5). This was significant because it enabled the successful location and measurement of the deposit on the leaf surface relative to internal fungal structures. Sub-epidermal hyphae were successfully imaged with limited damage from etching and no collapse of fungal tissue was observed (Fig 4.6)

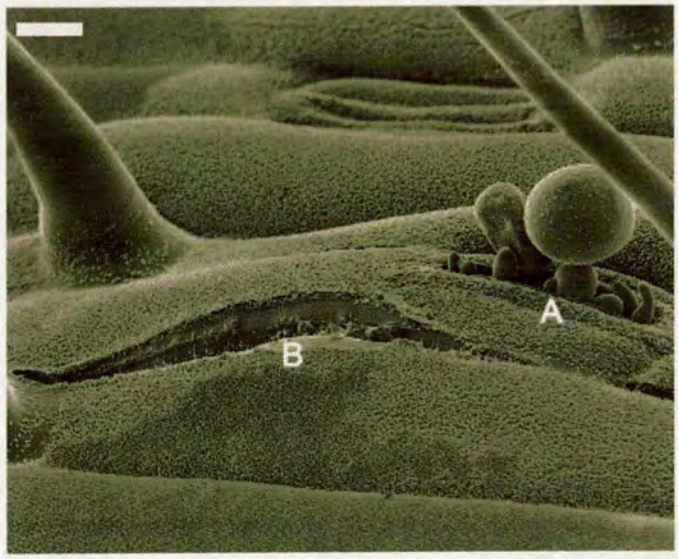

Figure 4.4: Gold coated, etched LT-SEM image of *P. recondita* spores which had erupted through the stoma (A). Damage to the surface of the leaf (B) was probably due to mechanical pressure from spores within the host, rather than sample preparation. Bar = 10 μm.

Figure 4.5: Freeze-fracture of the same sample. Careful preparation and fracture enabled sub-epidermal tissue and surface tissue to be imaged in the same sample, in this case uredosomes were observed in the process of rupturing the leaf. Bar = 10 μm.

Figure 4.6: Freeze-fracture of infected tissue. Sub-epidermal hyphae were clearly resolved and found to occupy most of the intracellular spaces between plant cells. Little or no tissue collapse had resulted from the transport or preparation procedure. Unlike pustules, this fungal tissue was protected from the atmosphere during transport from the growth room to the SEM laboratory and probably accounted for the improvement in sample turgidity.
Bar = 10 μm.

4.2.4 Investigation into the Curative Activity of Azoxystrobin on *Puccinia recondita*

Curative activity of 1.25g/L azoxystrobin (pseudo-field rate) and double the concentration of active ingredient (2.5g/l) was investigated on wheat at a comparatively late stage of infection, similar to the leaves shown in the previous section. No significant curative activity was observed at field rate or twice field rate after 1 h and 3 h (Fig 4.7: 1.25g/L after 1h, Fig 4.8: 2.5g/L after 3h). These data were interesting because they suggest established *P. recondita* colonies have a high level of tolerance to azoxystrobin in the short term. Work in the same laboratory (Hart, 1995; Hart, unpublished) offered compelling evidence that after 24 h sub-epidermal *P. recondita* hyphae had collapsed, probably as a consequence of contact with azoxystrobin. However, these observations were from sprayed samples rather than samples treated with individual droplets. The data described above stimulated a necessary evolution in approach because no activity was observed within the time period of interest.

Figure 4.7: Freeze-fracture of infected tissue treated with 1.25 g/L of azoxystrobin after 1 h. No difference was observed between the morphology of treated hyphae compared with untreated hyphae imaged previously. The criterion for fungicidal activity was hyphal collapse; none was observed. Bar = 10 μm.

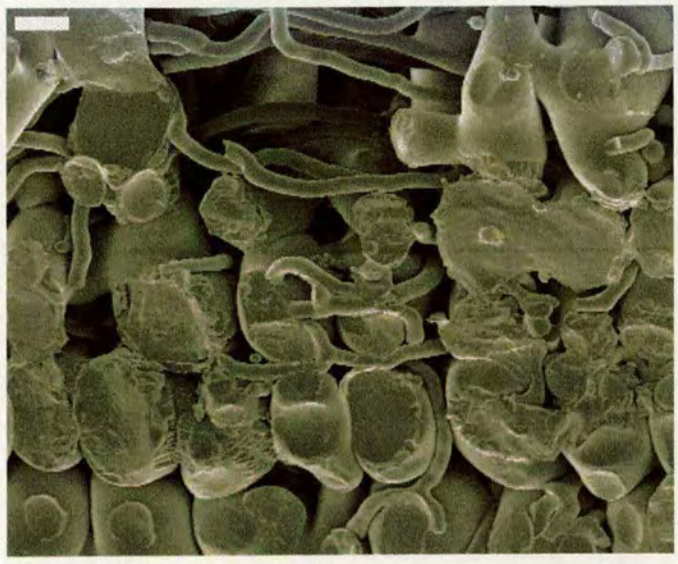

Figure 4.8: Freeze-fracture of infected tissue treated with 2.5 g/L of azoxystrobin after 3 h exposure. Despite doubling the application rate and increasing exposure time no difference was observed between treated and untreated samples. Bar = 10 μm.

4.2.5 Investigation into the Curative and Preventative Activity of Azoxystrobin on *Blumeria graminis*

Because of the high levels of tolerance to azoxystrobin observed using *P. recondita* over the short time periods of interest to this research, a similar approach was taken with *B. graminis*. The principle benefit of this system was that it was not prone to desiccation on the leaf surface and could therefore be imaged at less advanced stages in the infection cycle. Furthermore, because the hyphae of interest were on the surface of the leaf, it was comparatively easy to measure their distance from the treatment deposit (in fact, both deposit and pathogen could be observed in the same field of view).

Initially, a time course of *B. graminis* infection was performed using LT-SEM and AT-SEM to demonstrate that cryo-preservation was unnecessary for SEM of *B. graminis*. This also served as an important control for the comparison of turgidity on non-treated and treated hyphae and spores. Following this, a 1-24 h time course of curative activity and a 1-7 h time course of preventative activity on *B. graminis* hyphae and spores respectively was performed. Potent curative and preventative control of *B. graminis* by azoxystrobin was observed over short time periods.

4.2.6 Ambient Temperature SEM and LT-SEM of Wheat Infected with *Blumeria graminis*

A time course of *B. graminis* was done using both LT-SEM (Figs 4.9 (less than 3 h), 4.10 (9-12 h) and 4.11 (about 36 h)) and AT-SEM (Figs 4.12 (less than 3 h), 4.13 (9-12 h) and 4.14 (about 72 h)). This enabled the critical assessment of LT-SEM and AT-SEM for the imaging of certain fresh plant and fungal materials. It also provided two important controls. These were: 1. a baseline of germination rate (for analysis of preventative activity of azoxystrobin) and; 2. a baseline for rate of hyphal collapse (for analysis of curative activity of azoxystrobin). Low temperature SEM and AT-SEM imaging of *B. graminis* revealed that LT-SEM confers advantages in both spatial resolution and protection from tissue collapse over long imaging periods. However, it is important to note that both the higher degree of spatial resolution achieved by LT-SEM and improved sample viability were unnecessary for these experiments. Indeed, no collapse of fungal tissue was observed using AT-SEM if imaging time was kept to below 30 min and spatial resolution was more than adequate to distinguish features of interest in the sample. This allowed a relatively high throughput of material using AT-SEM which could not have been achieved using LT-SEM.

Figure 4.9: Gold-coated LT-SEM image of wheat leaf surface showing recently germinated *B. graminis* spore 3 h after inoculation. The spore is covered in wax secreted by the spore and a primary germ tube is visible. Bar = 1 μm.

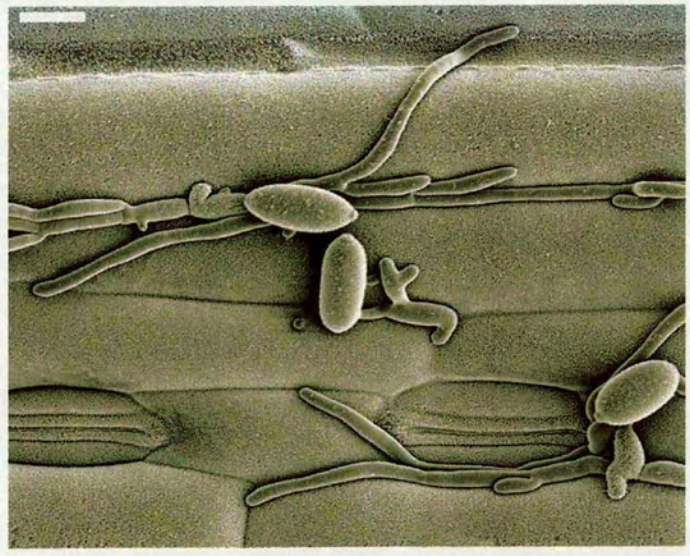

Figure 4.10: Gold-coated LT-SEM image of the wheat leaf surface showing hyphal extension from *B. graminis* spores 9-12 h after infection. Note the hyphae have extended within the contours of epidermal cells. Bar = 10 μm.

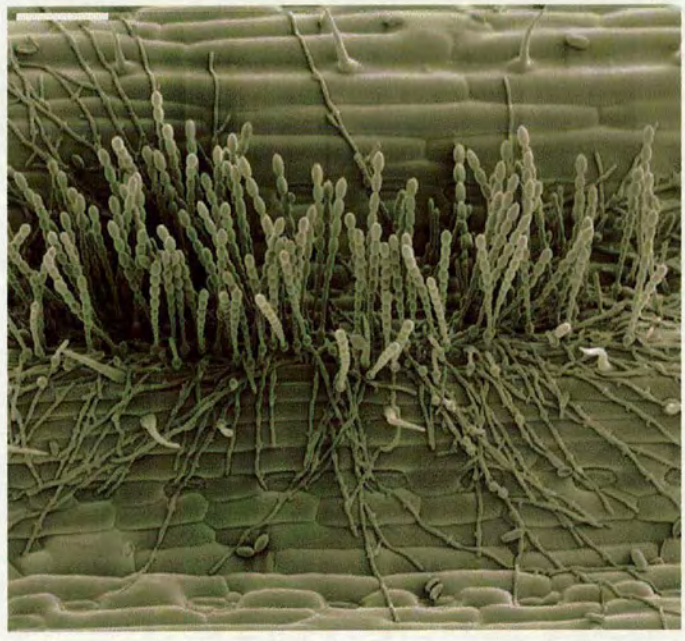

Figure 4.11: Gold-coated LT-SEM image of the wheat leaf surface 72 h after infection showed sporulating *B. graminis* colonies. Under natural conditions, spores from these conidia would be dispersed onto leaves of the same plant or different plants in a crop and spread infection. The life-cycle (germination through to sporulation) has taken approximately 3 days. Bar = 100 μm.

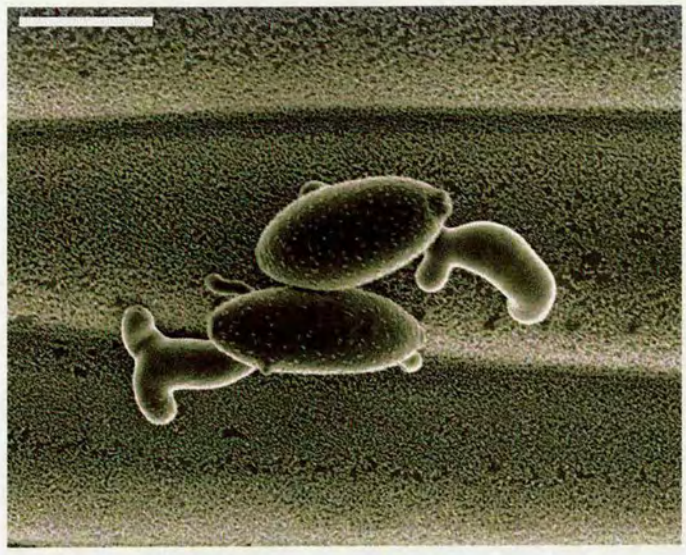

Figure 4.12: Uncoated fresh sample imaged with AT-SEM. The same time-course described in the previous 3 images was repeated using fresh, uncoated samples. Here, spore germination 3 h after inoculation was observed. Imaging at higher magnification than this often resulted in collapse of the fungal tissue. Note, however, that at this magnification spore surface wax was resolved, as were relevant surface features. Bar = 10 μm.

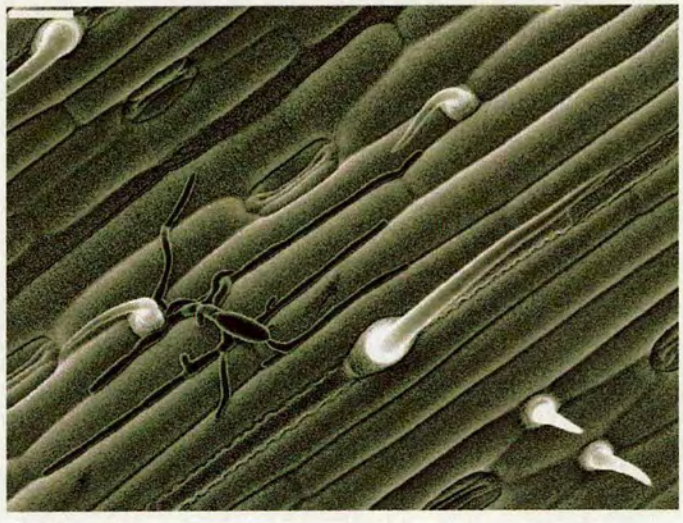

Figure 4.13: Uncoated fresh sample imaged with AT-SEM. Hyphal extension of *B. graminis* 9-12 h after infection. A general criticism levelled at the imaging of uncoated material is a loss of resolution due to a decrease in contrast. In these specimens this criticism would appear unfounded; excellent tonal range was observed and leaf and fungal structures were easily identified including silica cells, trichomes, hyphae and stomata. Bar = 10 μm.

Figure 4.14: Uncoated fresh sample imaged with AT-SEM showing sporulation of *B. graminis* 72 h after infection. Images of comparable quality to LT-SEM were taken at low power for all 3 stages of the *B. graminis* life-cycle previously described. On the basis of these data, AT-SEM was used in preference to LT-SEM in order to increase the number of repetitions for subsequent experiments. Bar = 100 μm.

4.2.7 Curative Activity of Azoxystrobin on *Blumeria graminis*

Curative activity against *B. graminis* using field rate applications (formulation 5) of azoxystrobin were analysed over time periods ranging from 1-24 h. Leaves inoculated with *B. graminis* 15-18 h previously were treated with a single droplet of azoxystrobin (1.25g/L). Fungicidal activity was measured as a percentage of collapsed fungal tissue. It was hypothesised that the observed zone of fungicidal control would increase over time as azoxystrobin diffused through epidermal cells and surface waxes and translocated through leaf xylem.

Unlike *P. recondita*, fungicidal activity (i.e. hyphal collapse) was observed after 1 h (Fig 4.15). All hyphae and spores within the deposit had collapsed, possibly as a result of wetting from the adjuvant rather than fungicidal activity *per se*. Fungicidal control was observed beyond the perimeter of the deposit at distances of 150 μm basipetally and laterally, and 200 μm acropetally. This distance increased after 7 h (Fig 4.16) to 250 μm basipetally to the deposit perimeter, and 400 μm acropetally to the deposit. This effect was consistent and reproducible. This result was very interesting because it demonstrated that levels of fungicidal activity could be measured over very short time periods and at the microscopic level.

It is accepted that azoxystrobin moves through the apoplast and cell walls only, and not through phloem. The direction of movement, therefore, has always been demonstrated to be in an acropetal direction. This view is the result of experiments which made exclusive use of phosphorimaging and combustion analysis of radiolabelled azoxystrobin over time periods spanning several days. The application of SEM to the analysis of fungicide activity and translocation properties offers the opportunity to explore translocation phenomena at considerably greater spatial resolution. With this in mind, a longer time course was run in which 18 h old infected plants were treated with a single droplet of azoxystrobin and imaged 24 h after treatment (Figs 4.17 and 4.18). Fungicidal activity was observed at a distance of 7 mm basipetally to the deposit and up to 5 cm in an acropetal direction corresponding with the tip of the leaf.

These data were potentially very significant. For the first time, azoxystrobin's short-term activity was measured and significant basipetal activity was observed. However, it was difficult to establish to what extent these translocational properties were due to movement of azoxystrobin through leaf tissue as opposed to movement through hyphal compartments in the mycelium. This led to a final evolution of the experimental approach in which preventative activity was measured by analysing data collected from germinating *B. graminis* spores (less than 1 h after inoculation) rather than from established colonies.

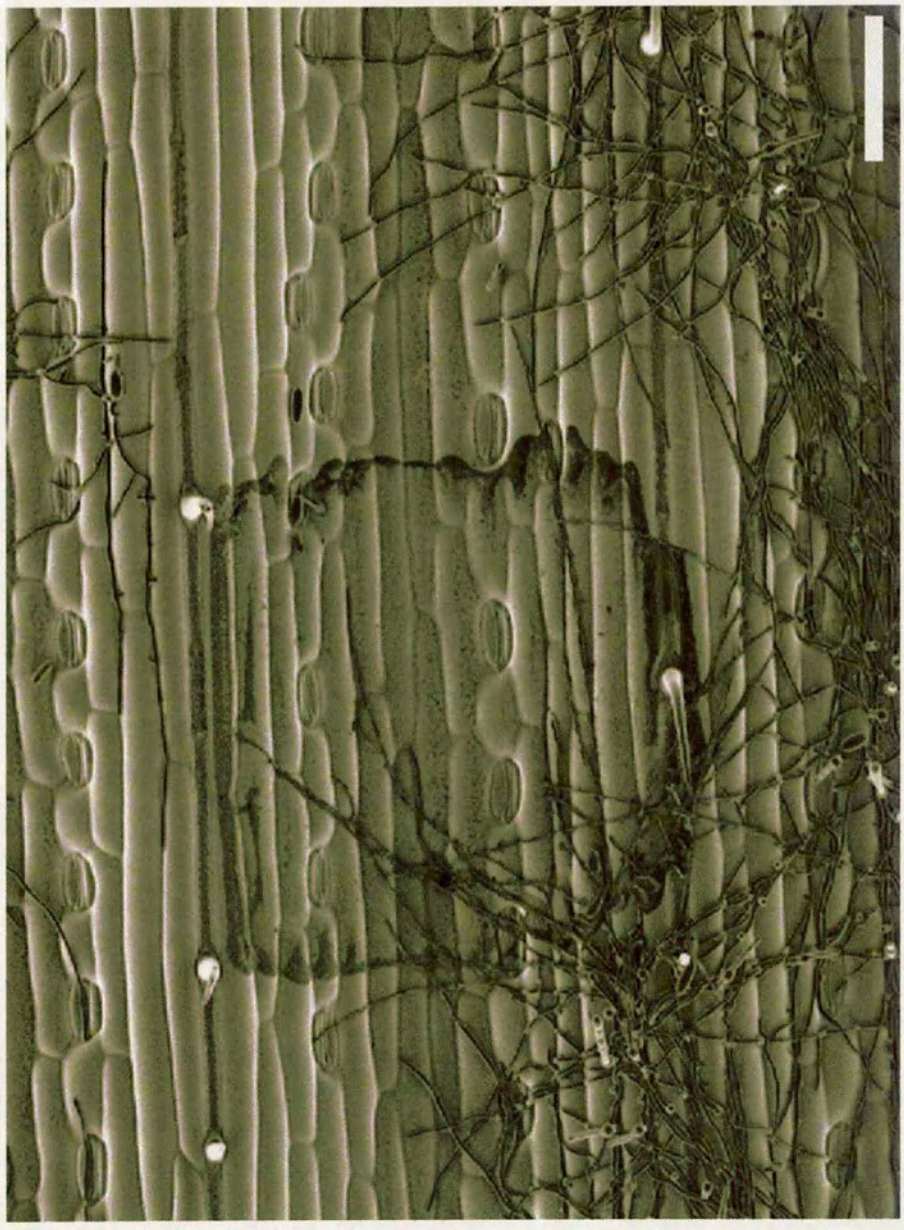

Figure 4.15: AT-SEM image of *B. graminis* mycelium 1 h after treatment with 1.25g/L azoxystrobin. Regions of the mycelium upon which the fungicide droplet was placed were all found to have collapsed, and evidence of mycelial collapse up to 200 μm acropetally beyond the deposit was observed. Spores collapsed at greater distances from the deposit than was the case for mycelium. Bar = 100 μm.

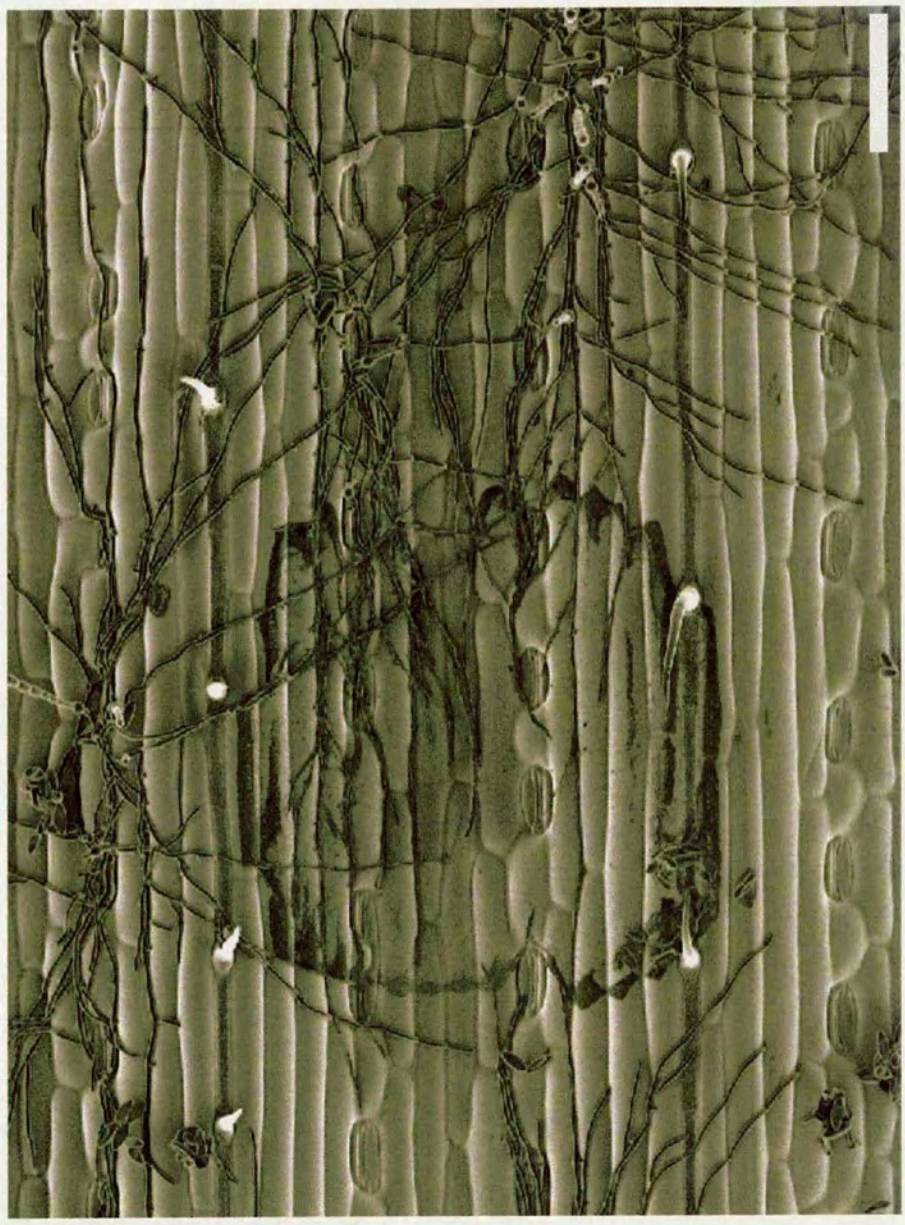

Figure 4.16: AT-SEM image of *B. graminis* mycelium 7 h after treatment with 1.25g/L azoxystrobin. As before, regions of the mycelium upon which the fungicide droplet was placed were all found to have collapsed. Mycelial collapse beyond the deposit was observed at greater distances (up to 400 μm acropetally) than after 1 h. Spores had collapsed at greater distances from the deposit than was the case for mycelium and at greater distances than was observed after 1h. Bar = 100 μm.

Figure 4.17: AT-SEM image of *B. graminis* mycelium 24 h after treatment with 1.25g/L azoxystrobin. Unexpected basipetal activity was observed after 7 h (Fig 4.25) at distances of 250 μm. After 24 h this distance had increased to 7 mm. The deposit (see *) exhibited fungicidal activity 7 mm basipetally in a straight line and up to 5 mm behind the deposit generally. Bar = 1 mm.

Figure 4.18: Higher magnification AT-SEM image of *B. graminis* mycelium lying basipetally to the deposit, 24 h after treatment with 1.25g/L azoxystrobin. Given that azoxystrobin is not phloem mobile and has no vapour phase, this movement can only be accounted for by diffusion through surface wax and/or diffusion through epidermal cells. These concepts were considered in greater detail in the following section. Bar = 1 mm.

4.2.8 Preventative Activity of Azoxystrobin on *Blumeria graminis*

It was estimated from SEM images in section 4.2.6 that 97% of *B. graminis* spores had either remained turgid or had germinated on the leaf surface after 30 min. In this series of experiments, a single 0.2 μl droplet of azoxystrobin (formulation 5) was applied to wheat and subsequently inoculated with *B. graminis* 0, 1, 3, 5 or 7 h after treatment. Spore collapse was considered an appropriate assay for fungicidal activity and was calculated against this germination rate.

Although formulation 5 contained additional adjuvant, this was not thought to exhibit fungicidal activity *per se*. This was tested by applying 100 g/L of adjuvant to the leaf (formulation 6) and inoculating with *B. graminis* spores. Spores were left for 1 h prior to imaging. Although spores landing within the deposit did not germinate, spores landing within several μm did germinate (Figs 4.19 and 4.20).

This technique was performed using formulation 5. After 0 h (NB, 0 h refers to time after treatment plus approximately 30 min to allow the droplet to dry) spores landing on or within the deposit had collapsed (Fig 4.21), but spores landing several μm beyond the deposit were still turgid (Fig 4.22). After only 1 h, spores that had landed within a 150 μm zone around the entire deposit had collapsed (Figs 4.23 and 4.24). The lateral zone of inhibition remained relatively static at 150 μm after 3 h and 5 h. A significant increase in biological activity was, however, observed longitudinally. After 3 h, spores that had landed within a 200 μm region basipetally to the deposit and 250 μm acropetally to the deposit had collapsed (Figs 4.25, 4.26 and 4.27). This trend continued; after 5 h spores landing within a 350 μm region basipetally to the deposit had collapsed and spores landing 550 μm acropetally to the deposit had collapsed (Figs 4.28, 4.29 and 4.30). After 7 h, the basipetal zone of inhibition remained at 350 μm to the deposit whereas the acropetal zone of inhibition had extended to 700 μm beyond the perimeter of the deposit (Fig 4.31). These data are graphed in Fig 4.32.

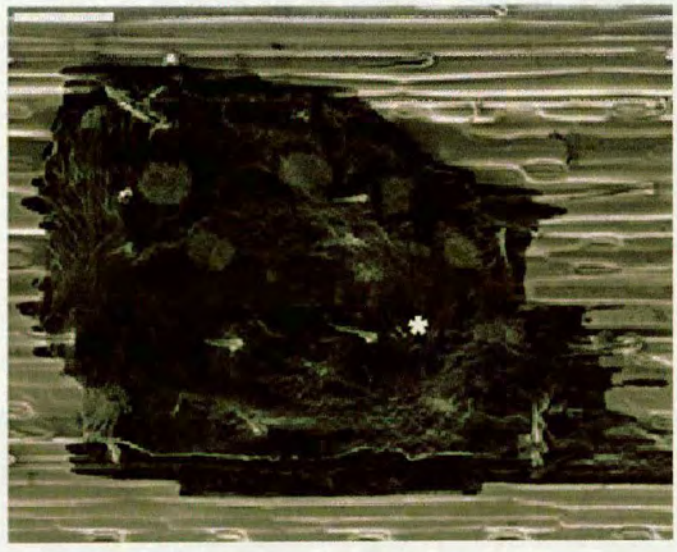

Figure 4.19: AT-SEM of fresh sample treated with 100 g/L of *Amistar adjuvant* and inoculated with *B. graminis* spores 2 h after treatment. After 1 h, spores that had landed within the deposit had collapsed (see *). From this image and Fig 4.27 it was clear that although direct contact with the deposit did inhibit spore germination, spores landing very close to the deposit (less than 10 μm) were still viable. This suggested that translocation of *Amistar adjuvant* and its potential fungicidal activity would not influence spore germination in this study. Bar = 100 μm.

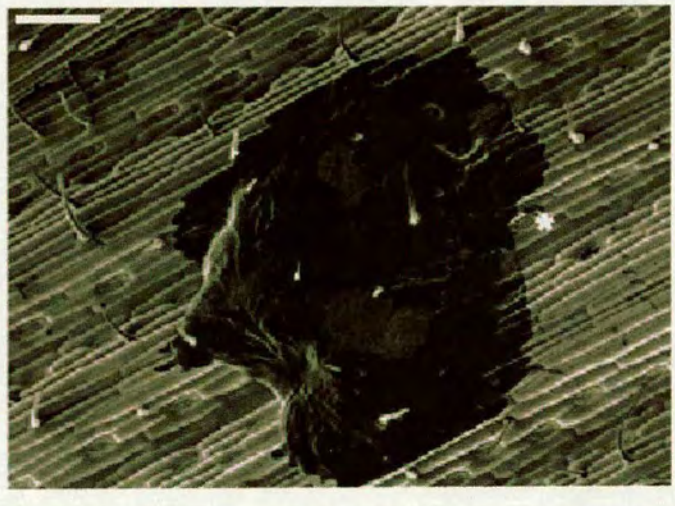

Figure 4.20: AT-SEM image of fresh sample treated with 100 g/L *Amistar adjuvant* and inoculated with *B. graminis* spores 2 h after treatment. After 1 h, spores that had landed within 10 μm of the dry deposit were turgid and had germinated (see *). Bar = 100 μm.

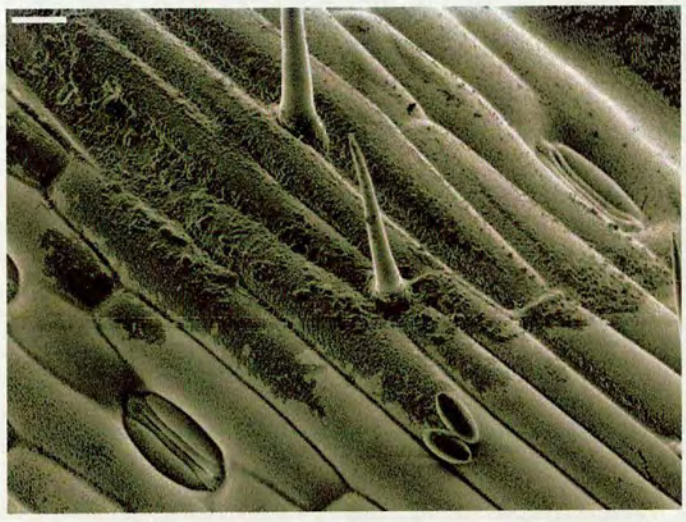

Figure 4.21: AT-SEM of fresh sample treated with formulation 5 and inoculated with *B. graminis* spores within 30 min of application and imaged immediately. Spores that had landed within several μm of the deposit (spores shown acropetally to the deposit in this image) had not collapsed. Note the period of time from inoculation to imaging was not long enough for germination to begin. Bar = 10 μm.

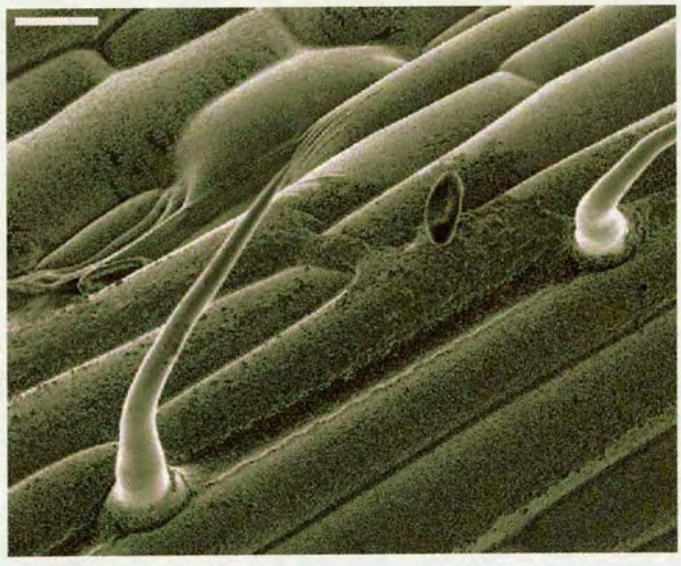

Figure 4.22: AT-SEM of fresh sample treated with formulation 5 and inoculated with *B. graminis* spores 1 h after application and imaged immediately. Spores that landed directly on the deposit annulus had collapsed (in this image the spores landed on the deposit perimeter, basipetally to the centre of the deposit). Bar = 10 μ.

Figure 4.23: AT-SEM of fresh sample treated with formulation 5 and inoculated with *B. graminis* spores 1 h after application and imaged immediately. Here, spores landing basipetally to the deposit collapsed at a distance of approximately 100 μm from the droplet perimeter. After 1 h, spores were found to have collapsed up to 150 μm around the entire deposit. Bar = 100 μm.

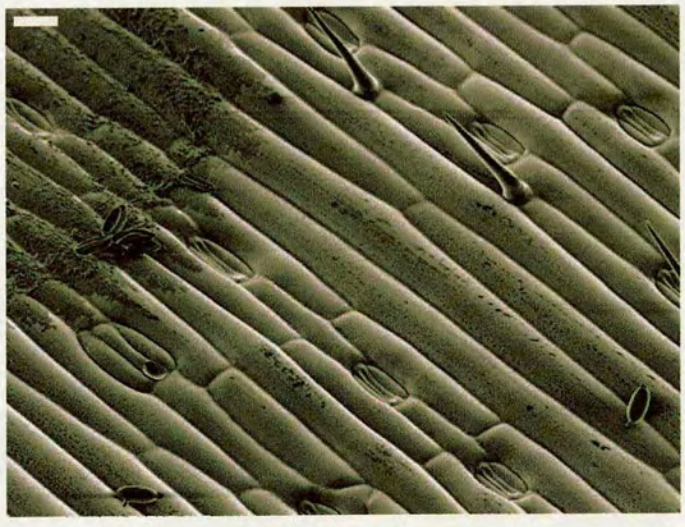

Figure 4.24: AT-SEM of fresh sample treated with formulation 5 and inoculated with *B. graminis* spores 1 h after application and imaged immediately. Here, spores that had landed acropetally to the deposit collapsed at a distance of approximately 120 μm from the annulus. Spores that had landed 150 μm acropetally to the deposit germinated. A cluster of 6 spores that landed on the deposit had collapsed. Bar = 10 μm.

Figure 4.25: AT-SEM of fresh sample treated with formulation 5 and inoculated with *B. graminis* spores 3 h after application and imaged immediately. Here, spores that had landed acropetally to the deposit collapsed at a distance of approximately 270 μm from the annulus. Spores that landed within 300 μm acropetally to the deposit germinated. Bar = 100 μm.

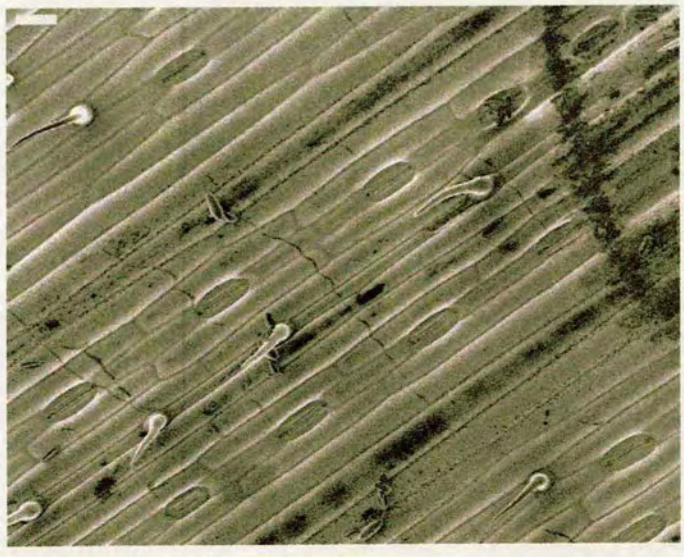

Figure 4.26: AT-SEM of fresh sample treated with formulation 5 and inoculated with *B. graminis* spores 3 h after application and imaged immediately. Here, spores that landed basipetally to the deposit collapsed at a distance of approximately 170 μm from the annulus. Spores that landed within 200 μm basipetally to the deposit collapsed. In this image, several spores that landed beyond 200 μm acropetally to the deposit germinated. Bar = 10 μm.

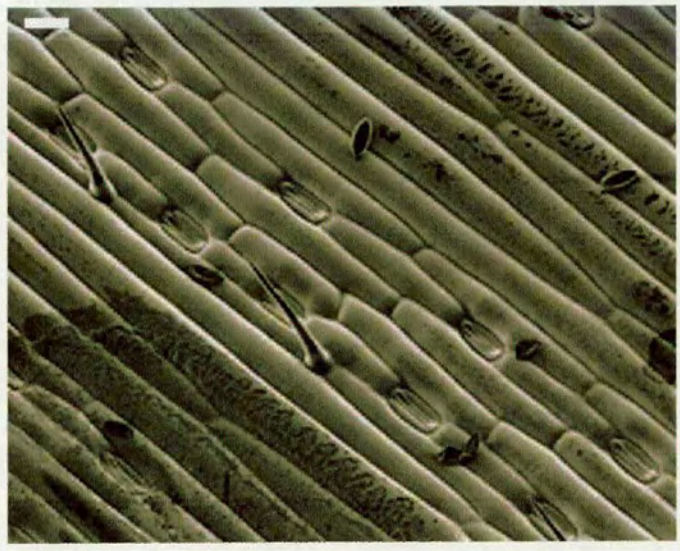

Figure 4.27: AT-SEM of fresh sample treated with formulation 5 and inoculated with *B. graminis* spores 3 h after application and imaged immediately. Here, spores that landed laterally to the deposit collapsed at a distance of approximately 100 μm from the annulus. Spores that landed within 150 μm laterally to the deposit collapsed. In this image, several spores that landed beyond 150 μm laterally to the deposit germinated. Bar = 10 μm.

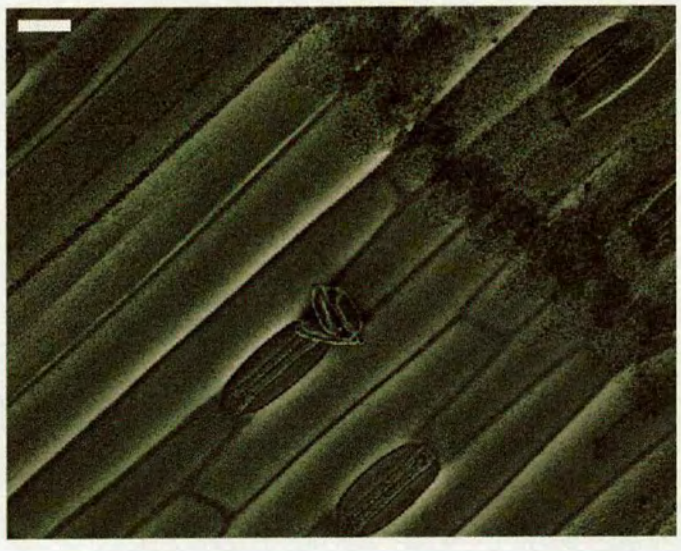

Figure 4.28: AT-SEM of fresh sample treated with formulation 5 and inoculated with *B. graminis* spores 5 h after application and imaged immediately. Here, spores that landed basipetally to the deposit collapsed at a distance of approximately 300 μm from the annulus. Spores that landed within 350 μm basipetally to the deposit collapsed. Bar = 10 μm.

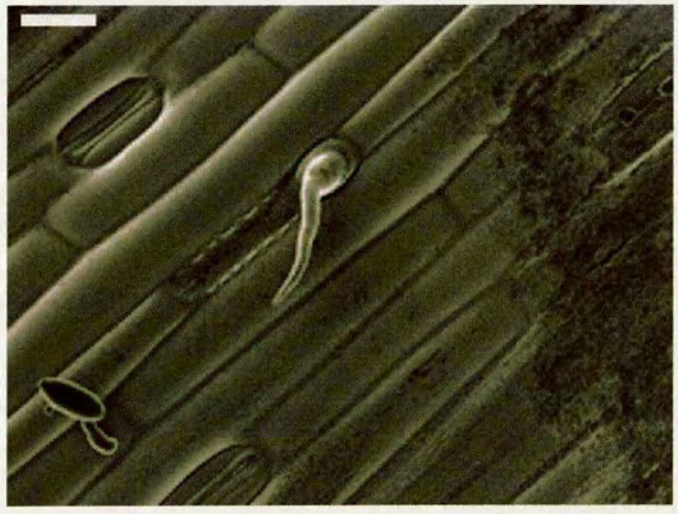

Figure 4.29: AT-SEM of fresh sample treated with formulation 5 and inoculated with *B. graminis* spores 5 h after application and imaged immediately. Here, spores landing basipetally to the deposit have collapsed at a distance of approximately 300 μm from the annulus. Spores that landed within 350 μm basipetally to the deposit were found to have collapsed. Bar = 10 μm.

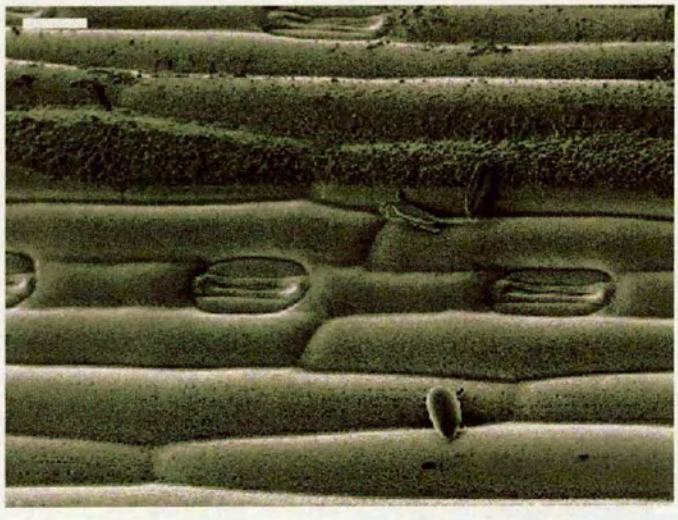

Figure 4.30: AT-SEM of fresh sample treated with formulation 5 and inoculated with *B. graminis* spores 5 h after application and imaged immediately. Here, spores that landed laterally to the deposit collapsed at a distance of approximately 150 μm from the annulus. Bar = 10 μm.

Figure 4.31: AT-SEM of fresh sample treated with formulation 5 and inoculated with *B. graminis* spores 7 h after application and imaged immediately. Here, spores that landed basipetally to the deposit collapsed at a distance of approximately 300 μm from the annulus. Spores that landed within 350 μm basipetally to the deposit collapsed. Spores that landed up to 130 μm laterally to the deposit also collapsed. Bar = 100 μm.

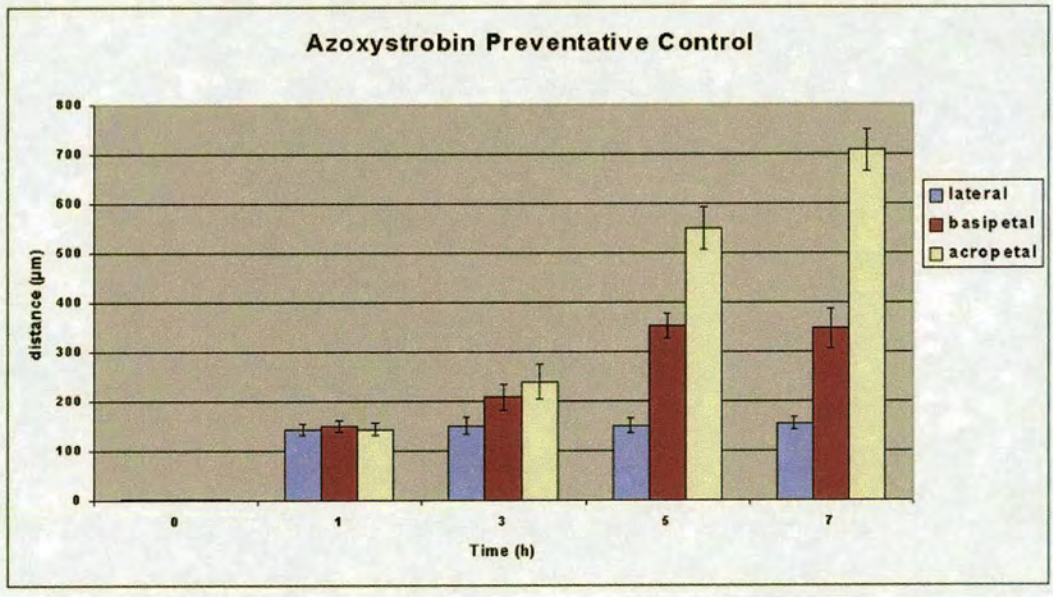

Figure 4.32: Graph showing extent of curative activity of azoxystrobin (formulation 5) on *B. graminis* in lateral, basipetal and acropetal directions.

4.3 Discussion

4.3.1 Curative Activity of Azoxystrobin on *Puccinia Recondita*

Low temperature SEM has commonly been performed to image frozen-hydrated fungal material and fungus-plant interactions on a wide variety of fungal species and hosts, including *Puccinia striiformis, Phytophthora infestans, Aspergillus niger* and *Blumeria graminis* (Read, 1992; Mendgen et al., 1992; Nicholson et al., 1988). The internal structures of tissues, cells and organelles can be exposed by freeze-fracturing following cryopreservation.

In the present study, wheat leaves infected with *P. recondita* were imaged at a late stage in the infection cycle (i.e. sporulation). Cryo-preservation, freeze-fracturing, sputter coating and ice-etching provided an excellent sample for LT-SEM imaging, and images were recorded which were of comparable quality to those achieved by other authors working with rust fungi (e.g. Mendgen et al., 1992). Some spores which had broken through the leaf epidermis were observed to have collapsed. However, cell collapse is a natural, reversible phenomena in many fungal spores (Beckett et al., 1984) and was probably not caused by the specimen preparation technique employed.

Studies have been conducted into the curative activity of some strobilurins using the LT-SEM. Hyphal collapse was observed using the LT-SEM in mycelium of *Plasmopora viticola* and *Uncinula necator* following treatment with the strobilurin fungicides azoxystrobin and kresoxim-methyl, respectively (Godwin et al., 1997; Leinhos et al., 1997). From the data presented, no mycelial collapse was observed in sub-cuticular hyphae of *P. recondita* after 1 h or 3 h following application of field-rate and double field-rate doses of azoxystrobin.

There are two obvious reasons for this result, either *P. recondita* at such a late stage of infection was tolerant to azoxystrobin, or the applied fungicide had not reached the target pathogen. The latter is the least likely explanation. In this study, techniques were developed that enabled the imaging of both the leaf surface (where the fungicide deposit was located) and the internal structures of the specimen. Consequently, the deposit was located and mycelium lying close to this deposit were then imaged.

Although work by Hart (1995) did demonstrate curative activity of azoxsytrobin on *P. recondita*, several important differences existed. First, azoxystrobin was applied using a track sprayer, therefore a far greater volume of fungicide was applied to the leaf surface compared with the present study. Secondly, leaves were treated at a much earlier stage in the infection cycle. Thirdly, specimens were cryo-preserved and imaged 24 h after treatment.

The combination of applying greater volumes of fungicide to less established colonies, and allowing a longer time period for the fungicide to exhibit biological activity, probably accounted for the differences in mycelial collapse observed between these studies.

All of the commercialised strobilurins, including azoxystrobin, have been demonstrated to have a broad spectrum of fungicidal activity. However, strobilurins vary in their levels of activity against different plant diseases, and not all of them give high levels of control against fungi from all the major groups of pathogenic fungi (Bartlett et al., 2002). For example, kresoxim-methyl and trifloxystrobin give only poor to moderate control of a number of Basidiomycete diseases including wheat and barley brown rusts (Institut des Cereals et des Fourrages, 2001). Conversely, azoxystrobin has good efficacy on the wheat and barley brown rusts (Bartlett et al., 2002).

Studies with azoxystrobin, trifloxystrobin and pyraclostrobin have demonstrated that spore germination and zoosopore motility are stages of fungal development that are particularly sensitive to strobilurins. This can be explained by their biochemical mode of action, with the consequence that they are particularly effective against these highly energy-demanding stages of fungal development (Stierl et al., 2000; Godwin et al., 1997; Leinhos et al., 1997; Godwin et al., 1994). Although both curative and eradicant activity have been demonstrated, azoxystrobin is considerably more effective when applied prior to, or at an early stage of infection (Godwin et al., 1999).

The biochemical mode of action of azoxystrobin, and the associated implications for application timing, are in contrast to some other groups of fungicides, including the triazoles, which inhibit ergosterol biosynthesis. Triazoles are generally ineffective against fungi during the germination and early germ-tube growth stages, because fungal pathogens obtain a supply of ergosterol from reserves within the spore (Hanssler and Kuck, 1998). However, these compounds are more effective at late stages in the infection cycle when endogenous levels of sterols have been depleted (Baldwin, 1995).

It is therefore unsurprising that azoxystrobin showed no curative activity against *P. recondita* at the late stage of the infection cycle investigated. However, the primary objective of the present research was to identify localised fungicidal tranlsocation, over several hours at the single droplet level using azoxystrobin. Consequently, fungicide-induced mycelial collapse of *P. recondita* was not explored further. It would be interesting to repeat the experiments described over longer time periods and using a track-sprayer to apply azoxystrobin, in order to gain a clearer understanding of how mycelium of *P. recondita* are affected by azoxystrobin.

Furthermore, given azoxystrobin's apparently poor curative activity on established colonies of *P. recondita*, it would perhaps be beneficial to repeat the described experiments using a range of fungicidal active ingredients, including sterol biosynthesis inhibitors, to discover whether alternative fungicidal compounds demonstrate improved curative activity under these conditions.

4.3.2 Comparison of AT-SEM and LT-SEM techniques in the Study of *Blumeria Graminis*

From the results discussed in the previous section, it was clear that curative activity of azoxytrobin on established *P. recondita* colonies could not be followed over the short time periods of interest at the single droplet level. Curative activity of azoxystrobin is reported to be superior against rust infections as opposed to mildew, however, curative control has been observed on established colonies of *B. graminis* within 7 h of treatment (Godwin et al., 1994). Under the experimental conditions used in the present study, it was possible to observe *B. graminis* using SEM at an earlier stage of infection than was possible with *P. recondita*, which was anticipated to improve observed biological activity.

Imaging of *P. recondita* necessitated the use of LT-SEM because the mycelium was susceptible to collapse and imaging required the exposure of internal plant tissue by freeze fracturing. Conversely, *B. graminis* was found to be particularly resilient to the desiccating effects of AT-SEM, and the mycelial mat could be imaged on the leaf surface. Consequently, AT-SEM was used to image *B. graminis* in the present study.

Development of *B. graminis* was followed from germination through to sporulation using LT-SEM and AT-SEM. Comparable images were achieved using both techniques. Within 3 h, the primary germ tube had developed and often the appressorial germ tube was also observed. Some authors have placed the development of primary and appressorial germ tubes at between 30 min and 2 h after inoculation (Carver et al., 1995). After approximately 12 h, several runner hyphae had developed, and were observed generally following the anticlinal junction between host cells. Similar results were observed by other authors (Carver et al., 1995; Kunoh et al., 1988) at between 36 h and 48 h post infection.

Touch sensing has been reported in some fungi (e.g. *Puccinia hordeii*), perpendicular to the orientation of host epidermal cells (Read et al., 1992). Evidence also exists that appressoria formation in some species is dependent on topographical signals from the host surface (Collins and Read, 1997). In the present study, runner hyphae were observed growing in the anticlinal junction between epidermal cells, parallel to the orientation of these cells. No attempts were made to identify the reasons for this orientation, although it is possible that surface topographical features and touch sensing by hyphae, or that the anticlinal junction simply offers the path of least resistance for growth, are responsible for this.

After approximately 72 h, sporulation had occurred. Other authors have examined sporulation in mildew after 7 days (Carver et al., 1995), although it is not clear whether sporulation had commenced prior to this time. From the data presented here, it is clear that AT-SEM did not cause the collapse of either the mycelial mat or conidia of *B. graminis* and images of appropriate quality could be collected to observe surface-lying colonies of *B. graminis* without the need for cryo-preservation. This enabled a higher throughput of samples during the course of this research.

4.3.3 Curative Activity of Azoxystrobin on *Blumeria graminis*

From the data presented, azoxystrobin demonstrated good curative activity within 7 h of application, which supported the results of other authors (Godwin et al., 1994). Of particular interest was the observation that hyphal collapse occurred at marginally greater distances acropetally to the deposit, compared to basipetally and laterally, after 1 h. Furthermore, this distance increased after 7 h in all directions, with the greatest increase (control at 400 μm) acropetally to the deposit. These distances were very small, and complications arise in interpreting these data because it was not clear how much of this movement was due to translocation through plant tissue and how much may have been due to fungicide redistribution through the mycelium.

Fungal hyphae grow continuously by division of a tip cell. This results in an extensive mycelium, of which the tip cell is the most distal part. Growth of this cell requires continuous synthesis of cell wall, as well as migration of cytoplasm and organelles. Cell division also produces sub-apical cells which, in contrast to the tip cell, grow only by branching. The result is an extensive, branched mycelium (Shepherd et al., 1993).

Transport of nutrients takes place through the mycelium, and is likely to have both symplastic and apoplastic components (Cairney, 1992). Symplastic transport occurs along hyphae by diffusion, cytoplasmic streaming, and osmotically generated mass flow through the fungal cytoplasm. In Basidiomycetes, continuous symplastic flow is dependent on transport through septal pores exclusively in the cytoplasmic compartment (Jennings, 1989; Thompson et al., 1987). Work involving fluorescent probes has demonstrated that the redistribution of fluorescent material is independent of both the rate and direction of cytoplasmic streaming (Shepherd et al., 1993b).

It seems likely, therefore, that fungicides can be redistributed through the fungal mycelium by a process of diffusion through the cytoplasm, in much the same way that some nutrients are. In the present study, the redistribution of azoxystrobin through plant tissue was of primary interest, particularly localised movement through epicuticular wax and epidermal cells. Although it is interesting to note that the observed zone of fungicidal control may be increased by a process of redistribution within the mycelium, it questions the assumption that hyphal collapse in regions of the mycelium distal from the fungicide deposit had occurred as a consequence of localised movement through the plant. Furthermore, it is possible that established colonies, in which a large mycelial mat is already established, are more resistant to fungicides (particularly strobilurins) than younger colonies or germinating spores.

Of considerable interest was the observation that a significant basipetal zone of control was present after 24 h. Treatment of established colonies, which were imaged after 24 h of fungicide droplet application, revealed mycelial collapse at distances of up to 7 mm from a single droplet deposit. Uptake of azoxystrobin is recognised to be a gradual process, with approximately 25% of applied material being absorbed into the leaf within 24 h of application (Bartlett et al., 2002). However, translocation of azoxystrobin is in the xylem only, with studies showing that 8% of the active ingredient entering leaves had moved above the point of uptake within 8 days of application (Godwin et al., 1999). Azoxystrobin is not phloem mobile nor redistributed by air, but does display translaminar movement (Bartlett et al., 2002).

From the presented data, it would appear that significant redistribution of azoxystrobin has occurred within 24 h, which has had a profound anti-fungal effect on established colonies of *B. graminis*. However, it was still unclear whether this was a consequence of diffusion through epicuticular wax, redistribution through epidermal cells, diffusion through cells within the mycelial mat, or a combination of all three.

4.3.4 Preventative Activity of Azoxystrobin on *Blumeria graminis*

Preventative control of *B. graminis* from single fungicide droplets was observed over a 7 h time course. The two obvious benefits of this approach were that germinating spores had only developed small germ tubes which almost completely removed the potential for fungicide relocation through fungal cells, and that preventative control is recognised to be more potent than curative control (Godwin et al., 1994). From the data presented, excellent preventative activity was observed. Spores which were applied to treated leaves and imaged immediately only collapsed if they had made direct contact with the fungicide droplet deposit. After 1 h, a 150 μm zone of inhibition was observed which surrounded the entire deposit. This zone increased over time, with the greatest increase observed acropetally (700 μm after 7 h). Basipetal and lateral movement had also increased, but to a lesser extent.

Interestingly, this zone of control was greater than was observed after 7 h in established colonies. It might have been anticipated that this zone would decrease because fungicide would be unable to diffuse through fungal cells. However, established colonies are more resilient to anti-fungal agents, and therefore it is possible that the fungicide was diffusing through the mycelial mat, but that spores were more susceptible to lower doses of fungicide than hyphae, and that this accounted for the increase in zone of biological activity observed. In the present study, no attempt was made to analyse the movement of antifungal agents through the mycelial mat, although this would undoubtedly prove a fascinating topic for further research.

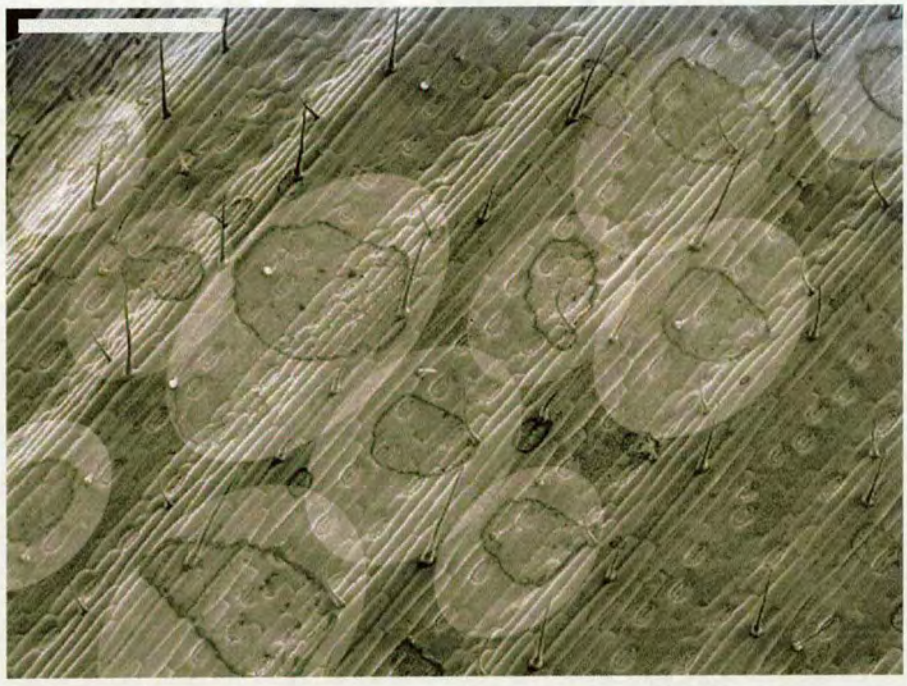

Figure 4.33: AT-SEM of spray applied droplets of *Amistar* applied to wheat. The zones of spore inhibition have been superimposed onto the image (shown as white ellipses) to demonstrate that after only 7 h a significant area of the leaf would already exhibit potent preventative activity against *B. graminis*. Bar = 1 mm.

From the data presented, it was concluded that azoxystrobin is a potent inhibitor of spore germination at field application rates and that activity and control from single deposits could increase over very short time periods. Because the distance to which the zone of activity was found to increase was not uniform around the deposit, it is likely that different processes are responsible for movement in different planes. Least control was observed laterally to the deposit, a greater extent of control was observed basipetally to the deposit, and most control was observed acropetally to the deposit.

Although the distances of biological activity reported were relatively small (generally in the order of several hundred μm), it is possible that even over short time periods the translocation of some strobilurins could prove significant, as demonstrated in Fig 4.33. A virtual zone, delineating the extent of biological control of fungicide on the leaf surface after 7 h for a spray-application is shown, based on the results presented in this chapter. This image suggests that near total preventative control against *B. graminis* could be achieved only a few hours after treatment.

Chapter 5

Measuring Azoxystrobin Uptake and Translocation in Wheat

The great tragedy of science - the slaying
of a beautiful hypothesis by an ugly fact.
T. H. Huxley (1893) Collected Essays

5.1 Introduction and Aims

5.1.1 Introduction

Phosphorimaging, in conjunction with combustion analysis and scintillation counting, provides a method for qualitatively analysing the movement of radiolabel in leaf tissue (phosphorimaging) and a precise method for calculating the quantity of radiolabel in a given volume of tissue (combustion analysis and scintillation counting). These techniques were therefore employed to analyse the true extent of fungicide movement, following application with ^{14}C azoxystrobin, with a view to comparing actual translocation with the zone of inhibition identified in Chapter 4. Azoxystrobin is metabolised very slowly. Due to the short time-scale of these studies recorded radiolabel was certainly due to the presence of azoxystrobin.

Although the movement of azoxystrobin over 3 day and longer time periods has been well characterised (Bartlett, 2002; Godwin et al., 1999) relatively little is known about the short timescale (less than 24 h) movement of small (i.e. field deposit size) quantities of fungicide. The possible relevance of these translocation events to rates of and timing of fungicide application have been somewhat overlooked in the past.

In the previous chapter, a zone of inhibition of spore germination was identified and its increasing area of effect was analysed over time. Although it was possible to identify the advancing edge of fungicidal control through leaf tissue and surface wax at increasing distances from the droplet deposit, it was not possible to discern whether this represented the true extent of fungicide translocation. The following experiments were therefore designed with a view to resolving this question.

5.1.2 Aims

Specifically, the aims of this section were to:

- analyse movement of azoxystrobin in whole leaves over short time periods by phosphorimaging
- analyse movement of azoxystrobin over a 24 h time period in leaf surface waxes and leaf tissue by wax stripping and phosphorimaging
- quantitatively analyse azoxystrobin uptake into leaf tissue over 24 h through combustion analysis of wax stripped leaves

5.2 Results

5.2.1 Overview of Results

In chapter 4, an assay for fungicide activity on the surface of wheat was developed using *Blumeria graminis* in conjunction with AT-SEM. Good control was observed, as was an increasing zone of control which suggested azoxystrobin quickly diffused through surface structures and translocated through xylem vessels. Phosphorimaging of radiolabelled fungicide over the same time period provided a convenient method for imaging how far the fungicide had physically moved from the deposit (as opposed to how far it exerted control).

First, a 7 h time course of fungicide movement on normal wheat leaves was done. Plants from which these leaves had been excised were kept under identical conditions to those used for AT-SEM work. The same general trend was observed, although the fungicide was shown to have travelled further than the region at which it was biologically active against *B. graminis*.

The possibility that this was because fungicide was not available for uptake into fungi on the leaf surface was examined by stripping surface wax from treated leaves. Low temperature SEM showed that a high percentage of surface wax was removed in the process. Results were compared over a 24 h time course and showed that although most of the fungicide was still present in waxes on the leaf surface and therefore available for uptake, a significant quantity of translocated fungicide resided in sub-surface tissue. This was presumably unavailable for uptake into fungal cells and may explain the difference between zone of biological activity compared with zone of physical movement.

Finally, quantitative analysis of the relative concentration of surface and sub-surface fungicide was performed over a 1-24 h time course to provide an approximation of how quickly azoxystrobin was absorbed into epidermal and sub-epidermal cells. Uptake was approximately linear over 24 h after which time about 9% of applied azoxystrobin had entered the leaf. These results, particularly when considered in conjunction with the results described in Chapter 4, demonstrate that localised movement could have a profound effect on short-term surface cover of the leaf. Data tables and descriptive statistics related to the research presented in this chapter are provided in Appendix 10.2.

5.2.2 Phosphorimaging of Radiolabelled Azoxystrobin over 7 h

Leaves were treated with radiolabelled fungicide and left for 1, 3, 5 or 7 h before being excised, pressed and freeze dried, developed and imaged. The phosphorimager successfully resolved the deposit annulus, and an increasing zone of fungicide was observed as time progressed (Fig 5.1). The phosphorimaging system has a maximum resolution of 100 μm, and the deposit was recorded at approximately 750 μm in diameter. Movement is defined as fungicide imaged beyond the deposit perimeter and an error margin due to resolution was taken into account.

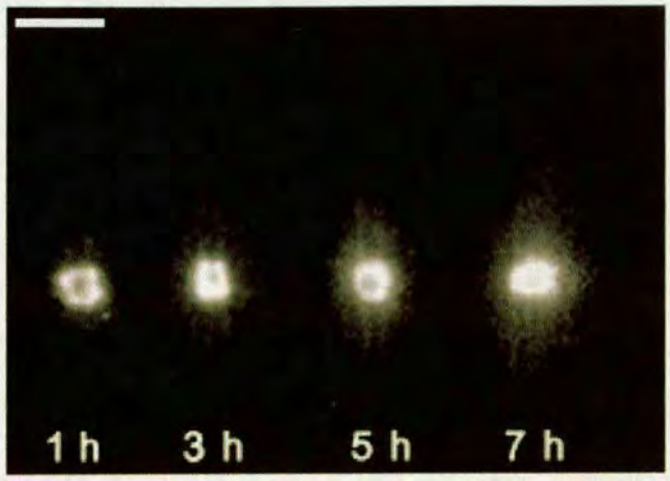

Figure 5.1: Phosphorimages showing whole excised wheat leaves labelled with 0.2 μl of azoxystrobin (formulation 5) over a 1-7 h time period. The brightest regions correlate with the greatest concentrations of fungicide. Note that the deposit annulus was resolved (visible as an intense bright ring with a dark centre). It was clear from these images that the fungicide translocated most in an acropetal direction and, to a lesser extent, basipetally and laterally. Bar = 1 mm.

After 1 h, azoxystrobin had extended laterally up to 600 μm from the perimeter of the deposit. Basipetal movement was measured at 1200 μm from the deposit edge, and acropetally at 1700 μm. After 3 h fungicide movement had increased in all directions, with lateral movement measured at 1700 μm. Longitudinal movement was greater, with basipetal movement placed at 2300 μm and acropetal movement at 3300 μm. After 5 h and 7 h lateral movement had not increased, and was also measured at 1700 μm in both cases. Basipetal movement had also remained static at 3000 μm. Acropetal movement had continued to increase however; after 5 h movement was measured at 4700 μm, after 7 h this figure had risen to 11500 μm. These results are graphed in Fig 5.2 (longitudinal movement) and Fig 5.3 (lateral movement).

The figures calculated for fungicide movement, particularly acropetal movement, are far in excess of the figures suggested by the bioassay studies (section 4.2.9, previous chapter). Variation between study groups could have accounted in part for this difference, or the result may have been because fungicide had diffused into internal tissue but had not yet diffused back out onto the leaf in sufficient quantity to inhibit germination or cause hyphal collapse. To explore this possibility a second time course was done (this time at up to 24 h) using whole excised and wax stripped leaves.

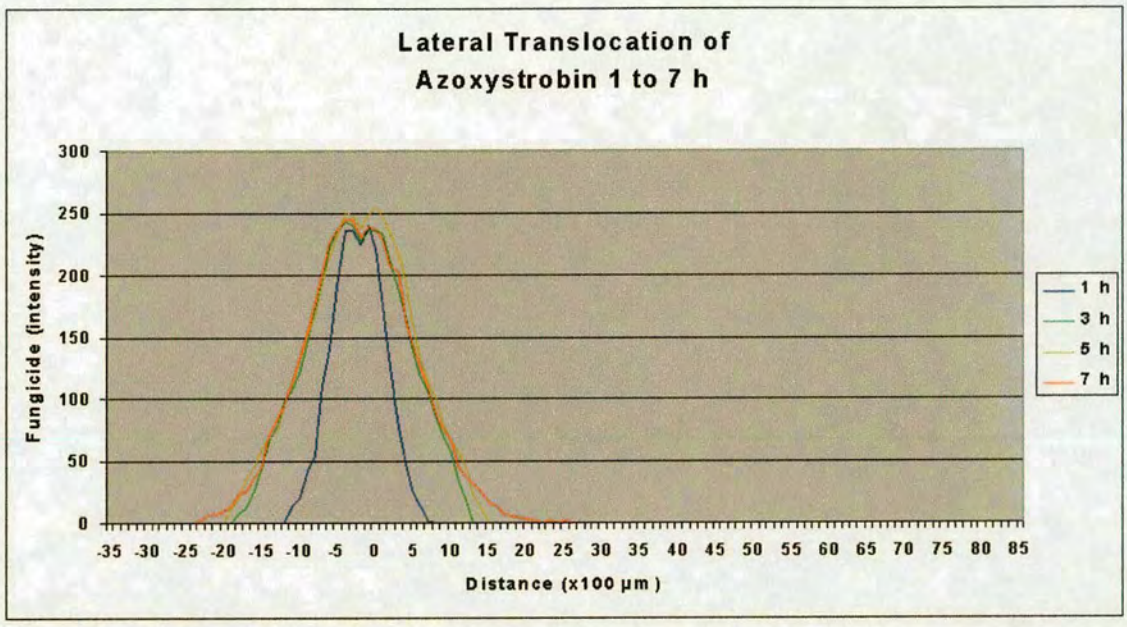

Figure 5.2: Graph showing longitudinal translocation (acropetal and basipetal) for 1-7 h time course for whole excised wheat leaves treated with 0.2 μl of azoxystrobin (formulation 5). '0' on the X axis represents the centre of the deposit, positive numbers relate to movement acropetally to the deposit, negative numbers relate to basipetal movement.

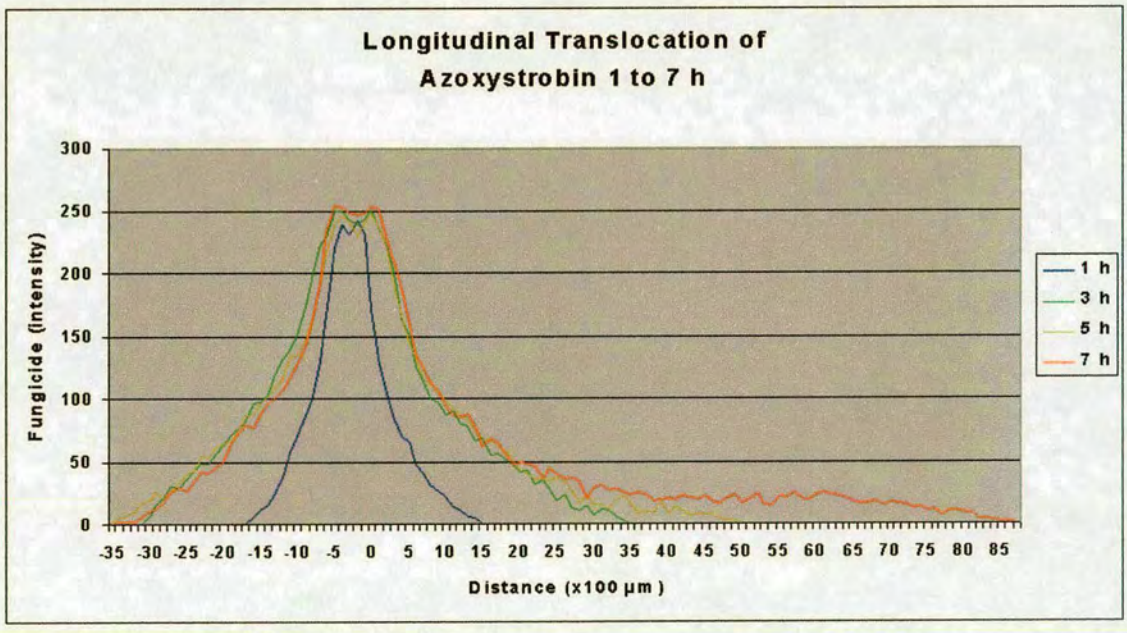

Figure 5.3: Graph showing lateral translocation for 1-7 h time course for whole excised wheat leaves treated with 0.2 μl of azoxystrobin (formulation 5).

5.2.3 Low Temperature SEM of Wax Stripped Leaves

In the previous section, it was shown that azoxystrobin had translocated considerably further than the region of biological control observed in Chapter 4 (section 4.2). To test whether this was due to unavailability of fungicide - i.e. the fungicide not being present on the leaf surface, quantitative analysis of the amount of fungicide present in leaf surface wax and in plant tissue was done using phosphorimaging and combustion analysis and scintillation counting.

Prior to the measurement of translocation of radiolabelled fungicide, the amount of wax removed from leaves using polyvinylsiloxane was estimated by comparison of non-stripped and wax-stripped leaves using LT-SEM. Epicuticular wax continuously covers all surface lying structures on wheat leaves (Fig 5.4 and 5.5). For a fungicide with no vapour phase activity (such as azoxystrobin) the fungicide must be present on the leaf surface or within surface waxes to exert biological control over surface bound pathogens. Polyvinylsiloxane was shown to partially remove surface wax and it was estimated that in excess of 80% of surface wax was reproducibly removed by this process. Levels of wax stripping were similar regardless of the presence of different leaf surface structures (such as stomata and trichomes). Less wax is removed at the periphery of the polyvinylsiloxane deposit, necessitating complete coverage of the leaf before stripping. An impression of the leaf surface is made by the polyvinylsiloxane which will reveal the crystalline structure of the wax if it is heated until the wax melts (C.E. Jeffree, personal communication). This suggested that wax is not dissolved in the process, which makes the technique preferable to acetate stripping.

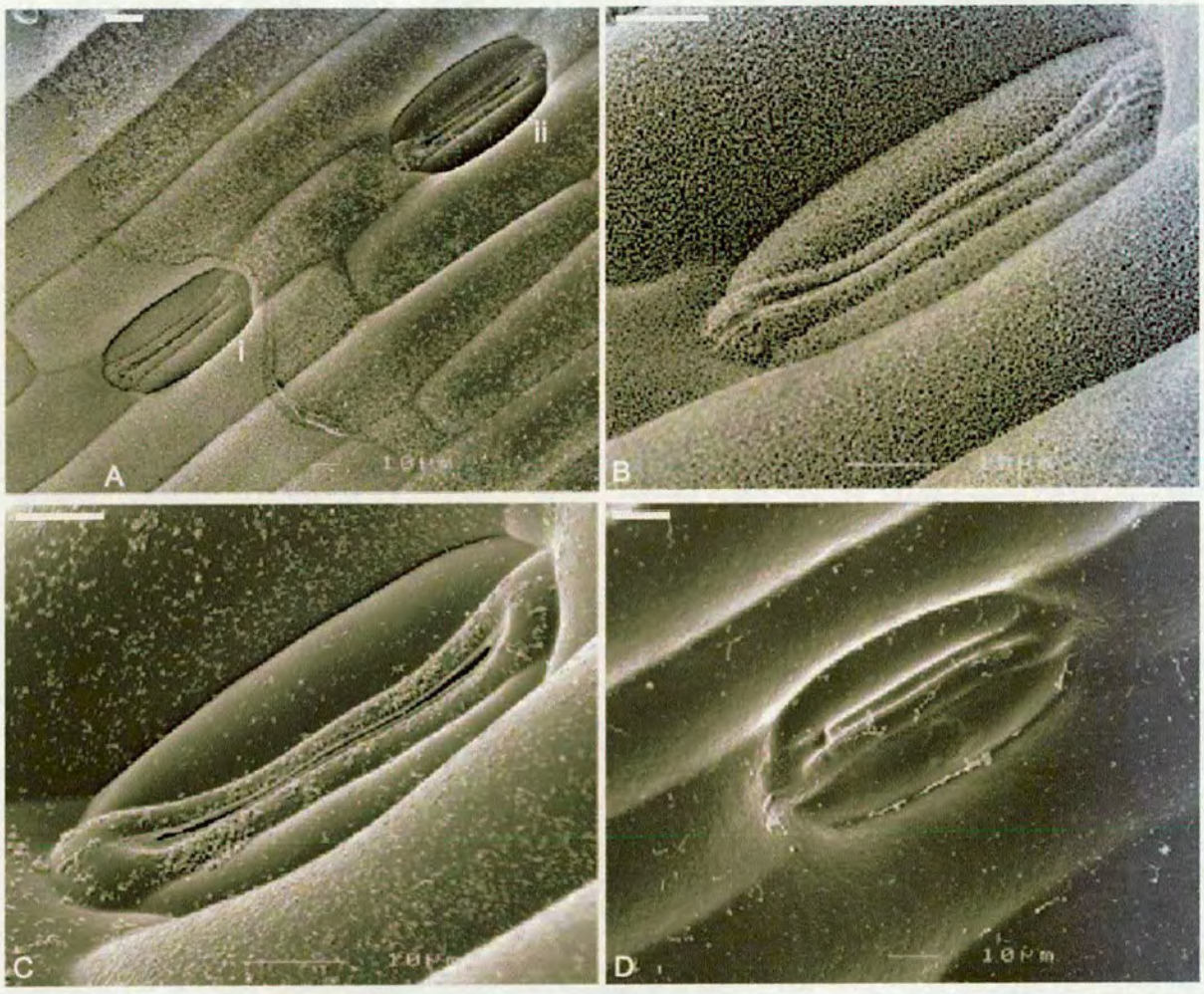

Figure 5.4: Four LT-SEM images of stomata on the abaxial surface of excised wheat leaves. A: (i) non-stripped part of the leaf showing intact surface wax and (ii) wax-stripped region of leaf. B: Higher magnification image of non-stripped stomata showing that the surface of the stomata and surrounding tissue is covered by a continuous layer of surface wax. C: Higher magnification image of of wax stripped stomata - it was estimated that approximately 80% of wax had been removed. D: image showing the impression of a stomata left in the polyvinyl siloxane after the stripping process. Bar = 10 μm.

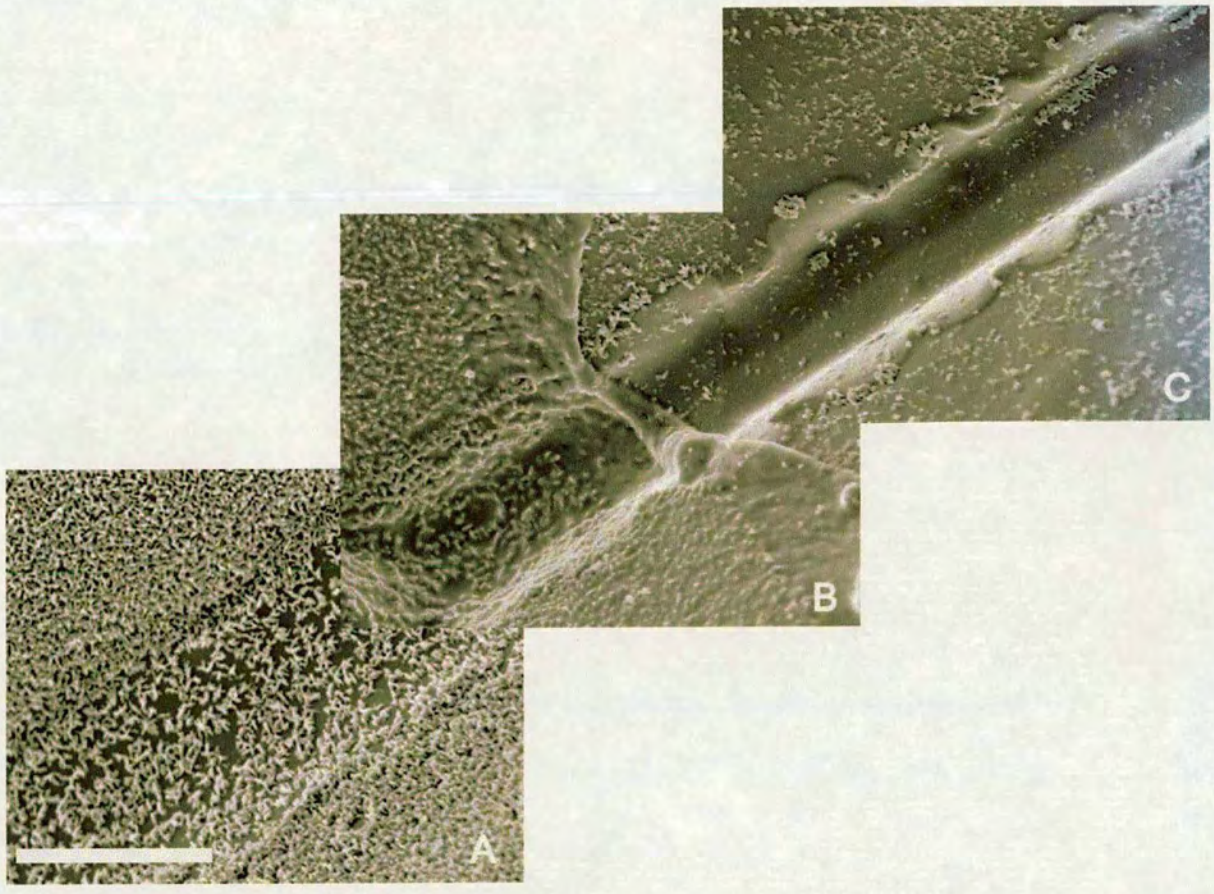

Figure 5.5: Montage of 3 LT-SEM images of neighbouring regions of the leaf surface. A: non-stripped region. B: edge of polyvinylsiloxane stripping. C: wax-stripped region. Again, it was estimated that at least 80% of wax was removed in this process. In this case a silica cell was wax-stripped. Leaf surface structures were found not to interfere with the quantity of wax removed. Bar = 10 μm.

5.2.4 Phosphorimaging of Normal and Wax Stripped Leaves

Excised wheat leaves were stripped of wax and the polyvinylsiloxane impressions and wax-stripped leaves were phosphorimaged (Fig 5.6). The stripped leaf and wax impression images were compared and redistribution of the fungicide was analysed for both sets.

Longitudinal and lateral movement was similar to section 5.2.2 (1-7 h) over the initial part of the time course. After 12 h, acropetal movement increased at an increasing rate, which suggested that azoxystrobin was freely moving in xylem vessels by this time. Comparison with the polyvinylsiloxane impression revealed that this trend was replicated for azoxystrobin present on the leaf surface, but was present on the surface at significantly shorter distances from the deposit as observed for whole leaves. A comparison was made of the area of leaf covered in whole and stripped leaves. These data are shown in Fig 5.7.

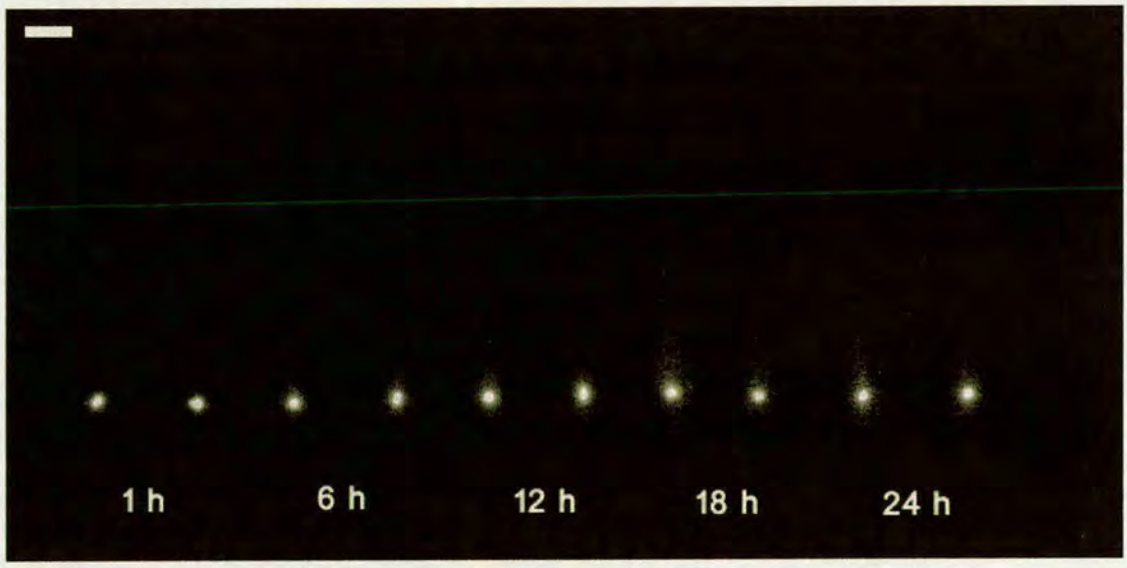

Figure 5.6: Phosphorimages showing 1-24 h time course of radiolabelled azoxystrobin (formulation 5) translocation. These images showed that over the first hour fungicide travelled further through surface wax than in leaf tissue. Thereafter, azoxystrobin translocation through the leaf tissue exceeded translocation through wax. The difference between leaf tissue and wax translocation continued to increase throughout the duration of the time course. Phosphorimages of the stripped leaf are shown on the left for each time point, phosporimages of polyvinlysiloxane impressions are shown on the right. Bar = 1 mm.

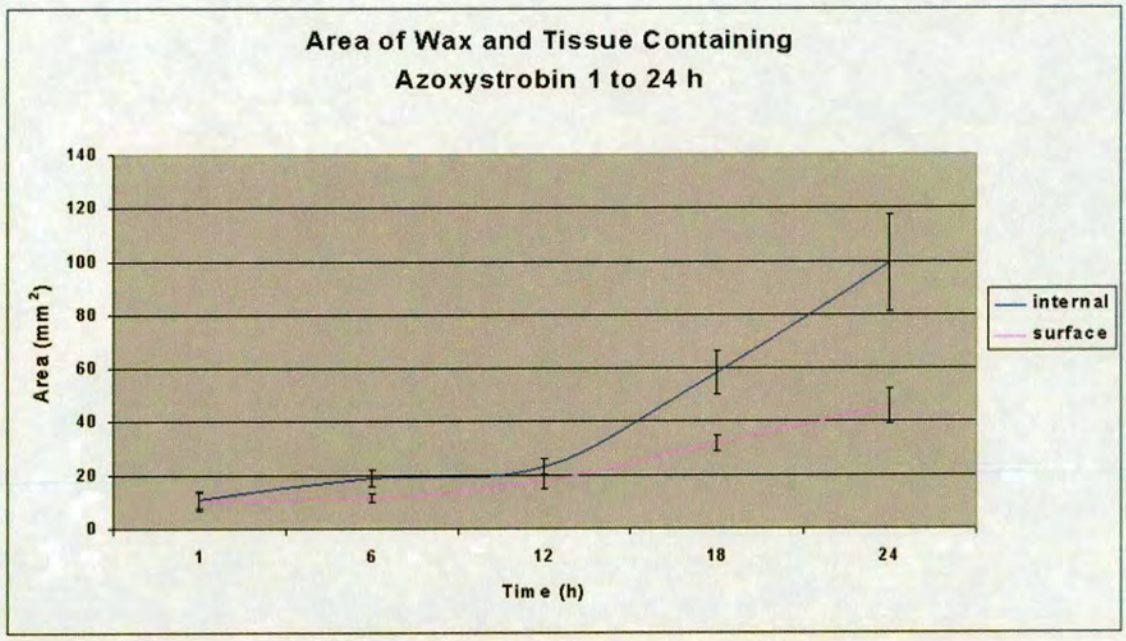

Figure 5.7: Graph showing area of leaf surface and leaf tissue containing azoxystrobin over a 1-24 h time course following application of a single 0.2 μl droplet of azoxystrobin (formulation 5).

5.2.5 Combustion Analysis and Scintillation Counting of Wax Stripped Leaves

Combustion analysis and scintillation counting, whereby radioactively labelled material is burned and the subsequently released $^{14}CO_2$ is measured, provides a means to quantitatively analyse the amount of radiolabelled axozystrobin in a selected region of the leaf. By comparing the amount of fungicide in the leaf and in the wax, uptake rates of fungicide into the leaf can be estimated. Unfortunately, polyvinylsiloxane burns poorly leaving most of the radiolabel trapped within the non-burned residue. To overcome this, a 0.2 μl droplet of radiolabelled azoxystrobin was burned and counted. This represented the amount of applied fungicide. Counts from the wax stripped leaves (which burn completely) were subtracted from this control. The difference gives a good indication of the amount left on the leaf surface. These data are shown in Fig 5.8.

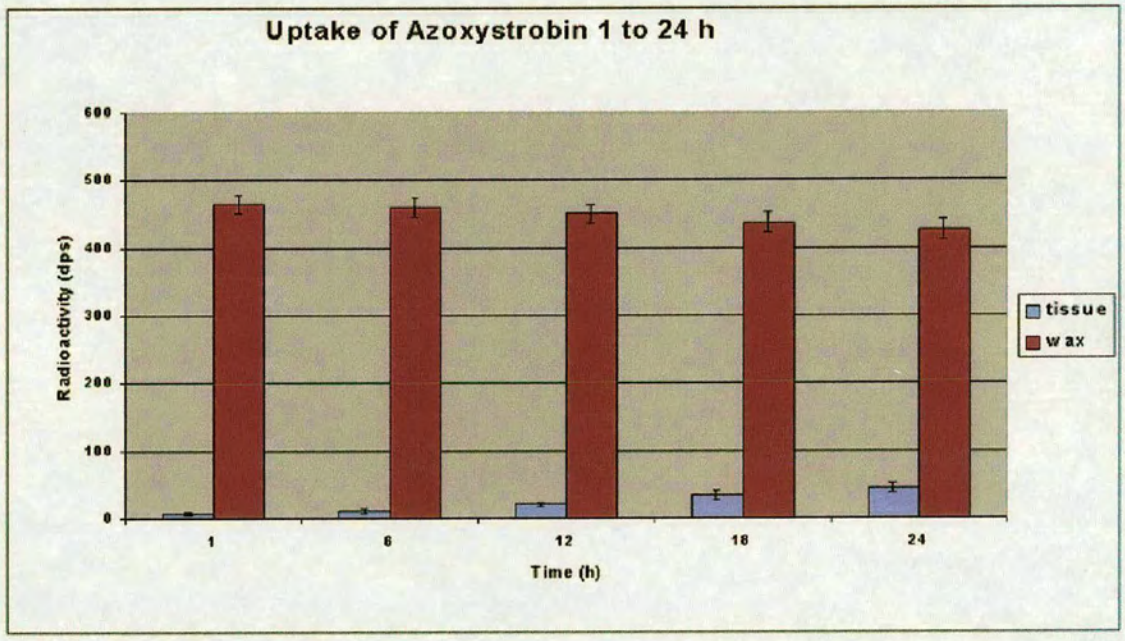

Figure 5.8: Graph showing uptake rate of azoxystrobin into wheat leaves over 24 h time period following application of a single 0.2 μl droplet of azoxystrobin (formulation 5).

5.3 Discussion

5.3.1 Redistribution of Azoxystrobin over 7 h

In Chapter 6, a zone of curative and preventative activity from axozystrobin was shown to increase over time. However, it was not possible to properly measure the uptake rate of azoxystrobin into the leaf, or its redistribution on the leaf surface, from these experiments. In the present chapter, azoxystrobin uptake into wheat leaves was measured using radiolabelled fungicide in conjunction with phosphorimaging, combustion analysis and scintillation counting techniques to further understand the redistribution of azoxystrobin over short time periods, and provide and explanation for the observations made in Chapter 4. Then benefit of this approach, was that uptake of azoxystrobin could be quantitatively measured, and the spatial location of azoxystrobin within the leaf and on the leaf surface could be visualised.

The various strobilurins that have been commercially released have different physicochemical properties that confer a wide range of biokinetic behaviours. Uptake of azoxystrobin into the cells of the leaf following surface application has been quantified in a broad range of crops in the field and under commercial conditions and has, unsurprisingly, been shown to depend on formulation type, additives, mixtures with other products the type and condition of the crop, and environmental factors (Bartlett et al., 2002).

Uptake of azoxystrobin is recognised to be a gradual process, with typically between 10-25% of applied azoxystrobin absorbed into the leaf after 24 h depending on formulation and the condition of the leaf (Bartlett et al., 2002; Bartlett, personal communication). Azoxystrobin is also xylem systemic, with studies showing 8% of the active ingredient entering the plant leaf had moved above the point of uptake within 8 days of application.

In the present study, uptake of azoxystrobin was initially analysed over 7 h in whole leaves. These results showed that azoxystrobin had relocated considerably greater distances after 1, 3, 5 or 7 h than was observed for its biological control. The observed rate of translocation for azoxystrobin was interesting in itself. Although the uptake and translocation of many pesticides, including azoxystrobin, has been extensively studied, they are generally not conducted over such short time periods or for single droplet deposits. In the present study, azoxystrobin was shown to translocate significant distances from the droplet deposit over very short time periods. Furthermore, the redistribution of azoxystrobin was not uniform around the deposit. Acropetal movement was considerable greater than basipetal movement, and basipetal movement was greater than lateral movement.

Of considerable interest, was the observation that translocation of radiolabelled fungicide was far in excess of the observed increased zone of biological activity reported in Chapter 4. The reasons for this were not clear, although two obvious possibilities existed. The first was that azoxystrobin was present on the leaf surface at too low a dose to effectively inhibit spore germination of *B. graminis*. The second, was that azoxystrobin may have translocated great distances from the deposit, but was not available on the leaf surface for uptake by and inhibition of fungal spores.

5.3.2 Uptake, Translocation and Redistribution of Azoxystrobin after 24 h

To further analyse azoxystrobin uptake, and understand this discrepancy, wax stripping techniques were employed to enable comparison of the quantity and location of azoxystrobin on the leaf surface and within the leaf. These experiments also used single droplets, and were conducted over an extended (24 h) time period. Phosphorimages of complete leaves, wax stripped leaves, and polyvinlysiloxane impressions (containing surface wax and surface-bound fungicide) were compared. From these data, it was concluded that although approximately 9% of applied axoystrobin had entered the leaf within 24 h, it was only present on the leaf surface at far smaller distances from the droplet deposit than azoxystrobin within the leaf. Furthermore, axoystrobin that had entered the leaf had only been redistributed acropetally to the droplet deposit.

These data strongly suggested that over the first 1 - 10 h after application, azoxystrobin rapidly spread short distances through surface wax and epidermal cells. Phosphorimaging of stripped leaves and polyvinlysiloxane containing surface wax showed that most movement was acropetal to the deposit, basipetal movement was marginally less, and lateral movement was least. This is consistent with the hypothesis that early movement of azoxystrobin is through wax and epidermal cells, and the relatively shorter distances traversed laterally by azoxystrobin is due to the fact that epidermal cells are not as wide as they are long.

After 5 h, lateral movement was observed to increase at an increasing rate in stripped leaves, whereas azoxystrobin within the polyvinylsiloxane impression remained static. This suggested that azoxystrobin had entered xylem and was beginning to translocate acropetally in the direction of transpiration.

However, the fact that no azoxystrobin was observed on the leaf surface at these increased distances suggested that although azoxystrobin may have crossed the cuticle into the xylem, it had not passed back through the cuticle onto the leaf surface.

This observation is consistent with the relatively small zone of inhibition observed in Chapter 4: although azoxystrobin had moved significantly greater distances within the leaf than was represented by its biological activity, it was not present on the leaf surface at that time and would therefore be unable to inhibit surface-lying spores or mycelium of *B. graminis*. This conclusion was further supported by the observation that surface-bound azoxystrobin in polyvinylsiloxane impressions had relocate a similar distance after 24 h to the basipetal curative activity observed for azoxystrobin on *B. graminis* after 24 h.

Uptake studies of azoxystrobin have generally concentrated on extended time-course studies from 1 - 8 days, and have identified azoxystrobin's movement as being primarily through xylem. Little attention has been paid to the localised movement of azoxystrobin prior to its entry and translocation via xylem. In the present study, the uptake rates for azoxystrobin and the time scale observed for entry into the xylem are similar to those reported by other authors (e.g. Godwin et al., 1999). Of particular interest, however, is the observation in Chapter 4 and the present chapter, that localised movement from single droplets would account for significant initial coverage of the leaf if fungicide is administered by spray application.

Early, test, compounds of azoxystrobin had a solubility in water of as little as 0.03 ppm. The physical properties of these strobilurins prevented them from being redistributed through the plant because they were too lipophilic to be mobile in plant tissue. The requirement for mobility within the plant led to the development of azoxystrobin, although it is still relatively lipophilic and water solubility is approximately 6 ppm (Clough et al., 1994). These physical properties would account for its slow rate of uptake.

A model, consistent with the variations in the extent of biological activity observed acropetally, basipetally and laterally to the deposit in Chapter 4 and those measured over 1 to 7 h in the current chapter, is shown in Fig 5.9. In this, azoxystrobin is anticipated to diffuse through surface wax, epidermal cells and xylem, but not though phloem (hence the limited basipetal movement). For this to be the case, one would anticipate most movement to occur acropetally over time, as the fungicide diffuses through surface waxes and enters epidermal cells and xylem tissue, and is moved longitudinally up the leaf.

A lesser degree of movement would be anticipated basipetally because azoxystrobin is not phloem mobile; fungicide would still be anticipated to diffuse through surface waxes and move through epidermal cells. Finally, only limited movement would be anticipated laterally. It would be assumed that this would also take place through surface wax and epidermal cell diffusion, however because epidermal cells are long and thin, running longitudinally along the leaf surface, the rate of lateral movement through epidermal cells would be less than for basipetal and acropetal diffusion.

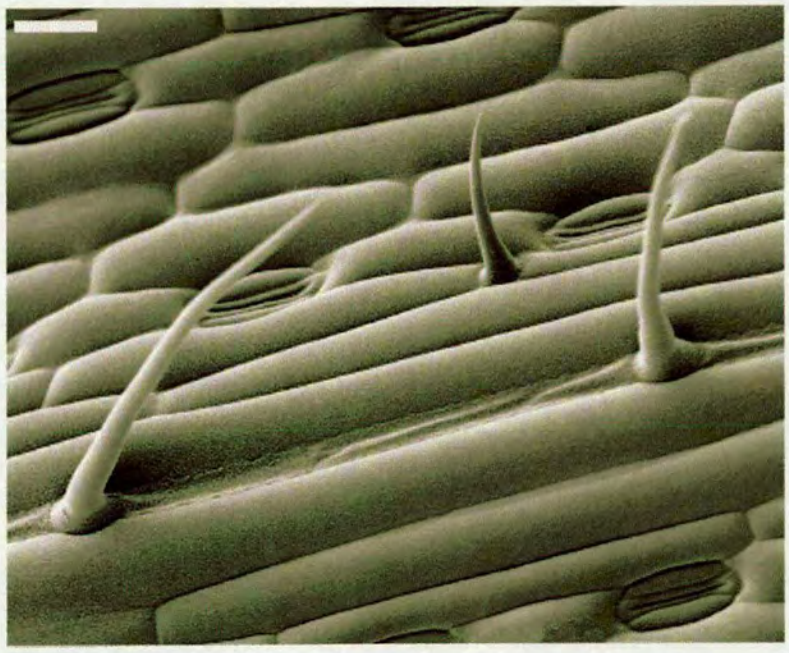

Figure 5.9: SEM image of the surface of a wheat leaf, showing the orientation and dimensions of epidermal cells. Epidermal cells are long and thin, and are orientated longitudinally to the leaf. Initial surface wax diffusion, similar in all directions from the fungicide droplet deposit, would account for the limited zone of control observed after 1 h. Diffusion through epidermal cells would account for the increase in basipetal and lateral activity. Due to the orientation of epidermal cells, it would be the case that fungicide entering, for example, two epidermal cells in a lateral direction would move approximately 20 μm, whereas fungicide which had diffused longitudinally through two epidermal cells could cover a distance in excess of 100 μm. The increased zone of inhibition observed acropetally can be accounted for by additional xylem motility, although it is likely that wax diffusion and movement through epidermal cells will also continue over time, at least until the droplet has dried.

Chapter 6

Live-Cell Imaging of Mitochondrial Spatial Location, Morphology and Physiology in Fungal Hyphae

Nearly every man who develops an idea works it up to the point where it looks impossible, and then he gets discouraged. That is not the point to get discouraged.
Thomas Edison

6.1 Introduction and Aims

6.1.1 Introduction

In Chapter 3, azoxystrobin formulations were developed to enable the application of doses of fungicide formulation similar to those applied under field conditions. In Chapter 4, the most suitable formulation was variously applied to wheat leaves inoculated with *Puccinia recondita* and *Blumeria graminis* to visualise micro-scale interactions between fungicide and fungus on the host surface. In Chapter 5, phosphorimaging and combustion analysis experiments were performed to further analyse micro-scale activity and translocation events associated with azoxystrobin. This series of experiments demonstrated that droplets approximating field rate could be applied to the surface of wheat leaves without causing damage, that low doses of azoxystrobin exhibited profound preventative and curative activity on *B. graminis* and that azoxystrobin translocated significant distances through wheat over very short time periods and the zone of observed biological activity increased within this time frame.

Given that many modern fungicides, including azoxystrobin, have sites of activity on the mitochondrial respiratory pathway it is perhaps surprising that relatively little is known about their uptake into fungal cells or their effect on mitochondrial or cellular viability following uptake. The use of fluorescent probes in conjuction with confocal laser scanning microscopy (CLSM) offers not only a powerful tool for the study of mitochondrial morphology, spatial organisation and physiology, but also the opportunity to improve our understanding of the potential uptake mechanisms of fungicides and their effect on intracellular organelles.

The dynamic morphology and organisation of mitochondria in living hyphae of filamentous fungi has received limited attention from the scientific community. Although video-enhanced microscopy of many different organelles has been done (e.g. Lopez-Franco and Bracker, 1996; Lopez-Franco et al, 1995; Lopez-Franco et al., 1994) selective staining of specific organelles was not visualised. This can be obtained by using fluorescent probes and recombinant fluorescent proteins. Some work has been done on a variety of cellular processes including endocytosis (Read and Hickey, 2001; Fischer-Parton et al., 2000) and hyphal fusion (Hickey et al., 2002; Glass et al., 2001) Investigative microscopy into mitochondrial biology has been performed using fixed specimens, often at the ultra-structural level, but few studies have explored mitochondrial organisation and dynamics in living fungal hyphae.

Confocal microscopy combined with the use of vital dyes or recombinant fluorescent proteins allows a potentially non-invasive technique for the study of living hyphae and enables the collection of time lapse sequences and 3-D sectioning at high temporal and spatial resolution. A number of mitochondrion-selective probes are available which exhibit changes in optical and fluorescence activity upon accumulation in the energised mitochondrial system. Examples include DASPMI, safranine O, nonylacridine orange, Rhodamine 123, and JC-1 (Cossarizza and Salvioli, 2000; Diaz et al, 1999; Salvioli et al, 1997; Duchen and Biscoe, 1992).

Furthermore, fluorescent probes have been developed which selectively target mitochondria but binding and fluorescence are not conditional upon the energised state. Examples include Mitotracker Green and Mitotracker Red (Bowser et al, 1999). In addition to these, the styryl dyes FM4-64 and FM1-43 are found to stain mitochondria in fungal cells following prolonged exposure to the dye (Fischer-Parton et al., 2000). The successful targeting of GFP to the mitochondria of *Aspergillus nidulans* (by fusion of GFP to the SUAPRGA1 mitochondrial protein) provides a further opportunity to examine mitochondria *in vivo* without the requirement of an external factor (other than blue or green light), which allows cells to be imaged with minimal perturbation (Brackhage, 2000; Fernando-Abaolos et al, 1998).

6.1.2 Aims

Specifically, the aims of this section were to -

- compare a variety of mitochondrion-selective fluorescent probes for the study of mitochondria in filamentous fungi on the basis of selectivity, phototoxicity, photobleaching and dynamic range
- study the spatial organisation and morphology of mitochondria in apical and sub-apical cells of filamentous fungi
- analyse the relative membrane potential of mitochondria in apical and sub-apical cells of filamentous fungi with the potentiometric marker Rhodamine 123
- develop an assay for mitochondrial activity in *A. nidulans* and the plant pathogen *Botrytis cinerea*, and study the dynamics of mitochondrial inhibition and cell death following treatment with azoxystrobin or FCCP

6.2 Results

6.2.1 Overview of Results

A diverse range of fluorescent probes are commercially available for the study of mitochondria. The selectivity of these dyes to the target organelle can vary dramatically, as can their cytotoxic and phototoxic effects. Although many of these dyes have been extensively visualised in animal cells, their characteristics may differ when applied to filamentous fungi. With these potentially significant practical issues in mind several vital dyes, including Rhodamine 123, DASPMI, FM 1-43, FM 4-64 and Mitotracker Green were critically assessed for the study of filamentous fungi *in vivo*. Mitochondrion-targeted GFP in *A. nidulans* was also assessed.

From this research, the most suitable dyes were used to label mitochondria in living cells of *A. nidulans, N. crassa* and *Bot. cinerea*. The spatial location of mitochondria, a comparison of the volume of apical regions of hyphae occupied by mitochondria, and variations in mitochondrial activity were analysed through time-course imaging and the collection of 3-D (x,y,z) data sets.

Applications of the mitochondrial inhibitor FCCP and the fungicide azoxystrobin were found to cause changes in the spatial location and morphology of mitochondria. The potentiometric marker Rhodamine 123 was used to develop an assay for mitochondrial activity. Cells labelled with Rhodamine 123 were treated with azoxystrobin and a time course of fungicide uptake and associated mitochondrial dysfunction and cell death was performed. Cessation of growth and significant reductions in mitochondrial membrane potential were found to occur less than 1 min after application, strongly supporting the hypothesis that azoxystrobin's primary route of uptake into fungal cells is by diffusion.

6.2.2 Comparison of Mitochondrion-Selective Probes

Characteristics of the mitochondrion-selective probes DASPMI, Rhodamine 123, Mitotracker Greeen, FM1-43. FM4-64, and mitochondrion-targeted GFP were compared in *A. nidulans*. Of these, FM4-64 and FM1-43 are styryl dyes commonly used to label endocytic events, Mitotracker Green and GFP are probes whose fluorescence is not dependent on the electrochemical gradient across the mitochondrial membrane, and DASPMI and Rhodamine 123 are potentiometric markers whose fluorescence intensity is directly related to mitochondrial membrane potential.

Unfortunate consequences of CLSM are that the fluorescent probes used to label the specimen suffer from photobleaching (whereby dye fluorescence decreases following laser excitation) and the cell suffers from phototoxic effects (whereby a combination of laser scanning in conjunction with a cytotoxic dye adversely affects the specimen). Consequently, although all 6 probes were found to label mitochondria in *A. nidulans* (Fig 6.1), some were more suitable than others. Suitability of probes for the study of fungal mitochondria were selected on the basis of 1. photobleaching, 2. phototoxicity, 3. length of time required to label mitochondria, 4. dye-selectivity, 5. cytoplasmic staining, 6. level of fluorescence in media and 7. dynamic range (which was of particular interest for the potentiometric dyes DASPMI and Rhodamine 123).

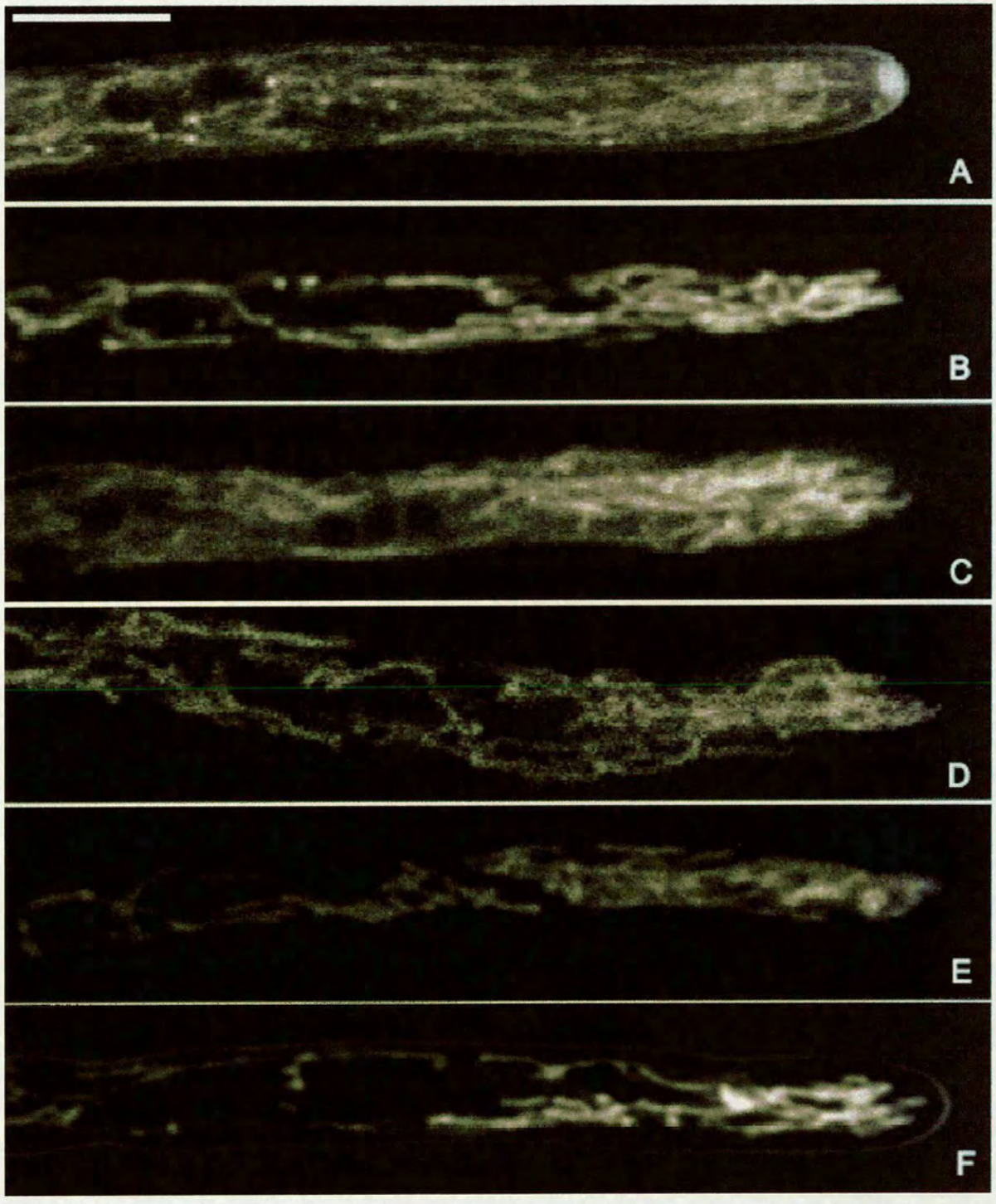

Figure 6.1: Comparison of staining in *A. nidulans* with (A) FM4-64, (B) FM1-43, (C) Mitotracker Green, (D) GFP, (E) DASPMI and (F) Rhodamine 123. Although all 6 probes were found to label mitochondria, differences in selectivity and levels of photobleaching and phototoxicity were observed between dyes. Bar = 10 μm

Staining Characteristics of the Styryl Dyes FM4-64 and FM1-43

Cell membranes provide a convenient vehicle for the loading of live and fixed cells with lipophilic dyes. Cells can generally tolerate high concentrations of lipophilic dyes and lateral diffusion of these dyes through the endomembrane network and vesicular transport through organelles can lead to staining of the membranes throughout the entire cell, even if the dye is applied locally. Consequently, lipophilic dyes have been used extensively in live cell research to label cells (Ribchester et al., 1994), organelles (Ledley et al., 1992) liposomes, (Perin et al., 1989) and lipoproteins (Barack et al., 1989) in a wide variety of studies.

Of the lipophilic dyes commercially available, FM4-64 and FM1-43 are relatively easy to use because they bind rapidly to the plasma membrane and their fluorescence is strongly enhanced upon binding. Both FM4-64 and FM1-43 have long Stokes shifts (250 nm for FM 4-64, 150 nm for FM 1-43) and can be excited with the 514 nm line of the argon ion laser (Molecular Probes, 2003; Betz et al., 1996). Recent work by Hickey (2001) and Fisher-Parton et al. (2000) on endocytic events in filamentous fungi reported mitochondrial staining with both dyes in a variety of species, including *A. nidulans, Bot. cinerea, N. crassa, P. recondita, Sclerotinia sclerotiorum* and *Phycomyces blakesleeanus*. In this study, both dyes were used to label mitochondria in *A. nidulans* and compared with other mitochondrion-selective markers for their suitability in live-cell imaging of fungal mitochondria.

FM4-64 is typically used to label endocytic events in cells. Studies of dye internalisation into *N. crassa* cells at low temperature (Fischer-Parton et al., 2000) and in the presence of the metabolic inhibitor sodium azide (Hickey, 2001) have shown that FM4-64 is unable to diffuse freely across the plasma membrane. However, after approximately 30 min, FM4-64 was observed to stain mitochondria under normal conditions. In this study, cells were left for more than 45 min before imaging to maximise labelling of mitochondria. The plasma membrane was brightly stained, diffuse background staining of the cytoplasm was observed and mitochondria could be distinguished. Repeated laser scanning (1% laser power, 514 Argon ion, 60x 1.4 NA, zoom 4, F1 scan speed) for 60s resulted in an approximately 60% reduction in fluorescence signal from photobleaching (Fig 6.8).

FM4-64 was relatively non-selective for mitochondria and intense background staining of the plasma membrane and spitzenkorper was observed. Background from cytoplasmic staining (possibly due to the labelling of sub-resolution vesicles) was high. Phototoxic effects were not obvious, with mitochondria remaining tubular in shape, their spatial location unaltered and growth rate remaining constant throughout the time course of repetitive scanning.

FM1-43 has been used to label endocytic events in yeast (Vida and Emr, 1995) and filamentous fungi (Fischer-Parton et al., 2000). Mitochondria were found to be much more intensely stained with FM1-43 than FM4-64 (Fisher-Parton et al., 2001). In this study, FM1-43 was found to label mitochondria relatively quickly (after approximately 20 min) and less non-selective staining was observed than with FM 4-64. The plasma membrane became brightly stained within 2 min of dye application but fluorescence intensity relative to mitochondrial fluorescence decreased after approximately 10 min. The spitzenkorper was generally not observed with the low dye concentrations used in this study (higher concentrations of dye enabled the visualisation of the spitzenkorper, but such high dye concentrations were unnecessary for the visualisation of mitochondria and were therefore avoided to reduce toxicity).

FM1-43 was relatively resistant to the potentially deleterious effects of repetitive laser scanning. Photobleaching was low and fluorescence intensity decreased by 30% after 60 s repetitive scanning (Fig 6.8). No phototoxic effects were observed and growth rate remained unaltered and mitochondria retained their tubular shape and location within the hyphal tip. Mitochondrial staining was far more selective than was observed for FM4-64, with no background signal from cytoplasmic staining (Fig 6.3).

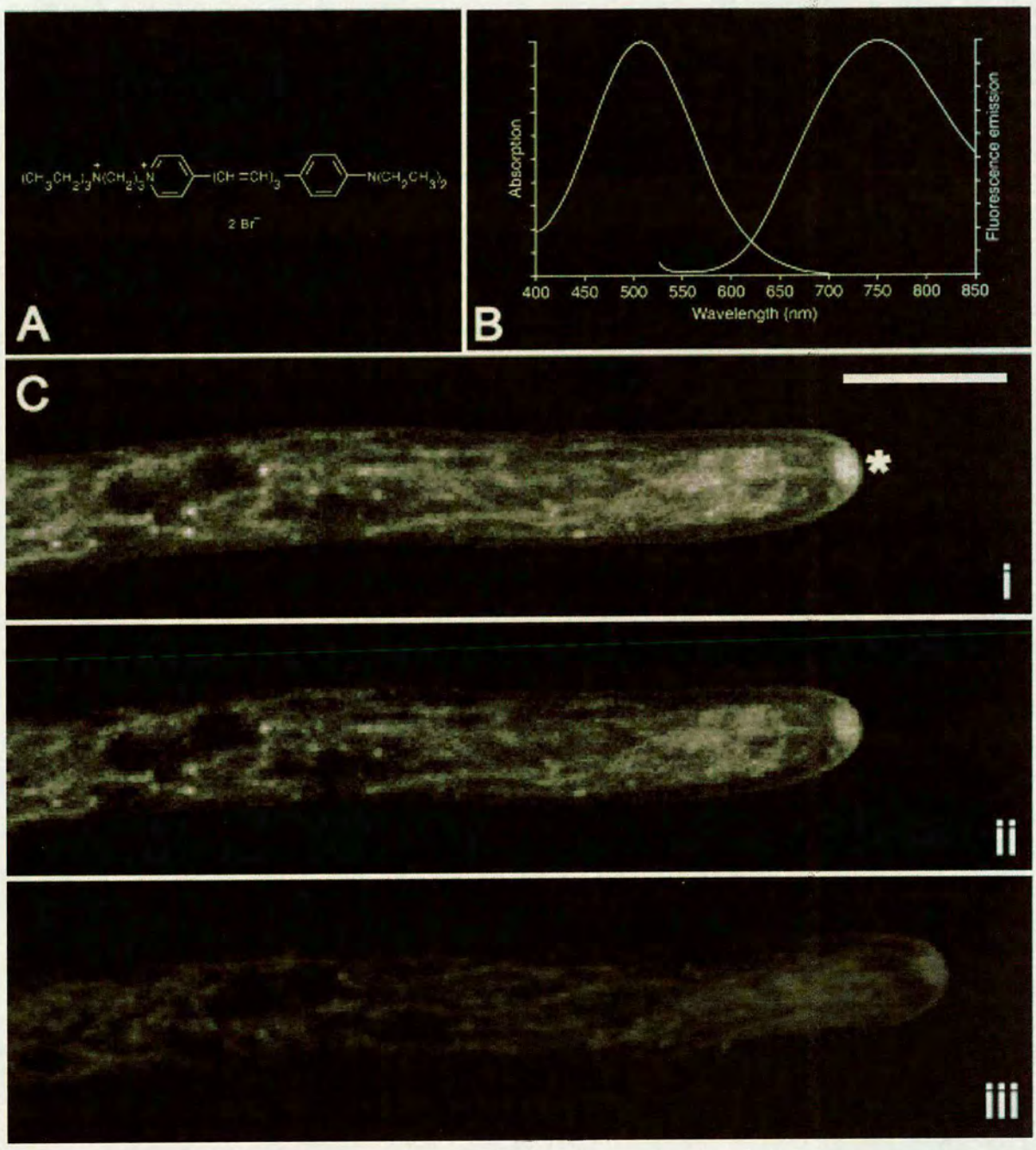

Figure 6.2: Staining characteristics of FM 4-64 over a 60 s time course of repeated scanning. A) Molecular structure of FM 4-64 (molecular weight = 608), B) Emission and excitation maxima, C) Time series of repeated scanning i) 0 s, ii) 30 s, iii) 60 s. Note that mitochondria were labelled but there was a high level of background fluorescence and staining of other cell structures (e.g. * = spitzenkorper). Phototoxic effects were limited but photobleaching was observed (A and B, adapted from Molecular Probes, 2003) Bar = 10 μm.

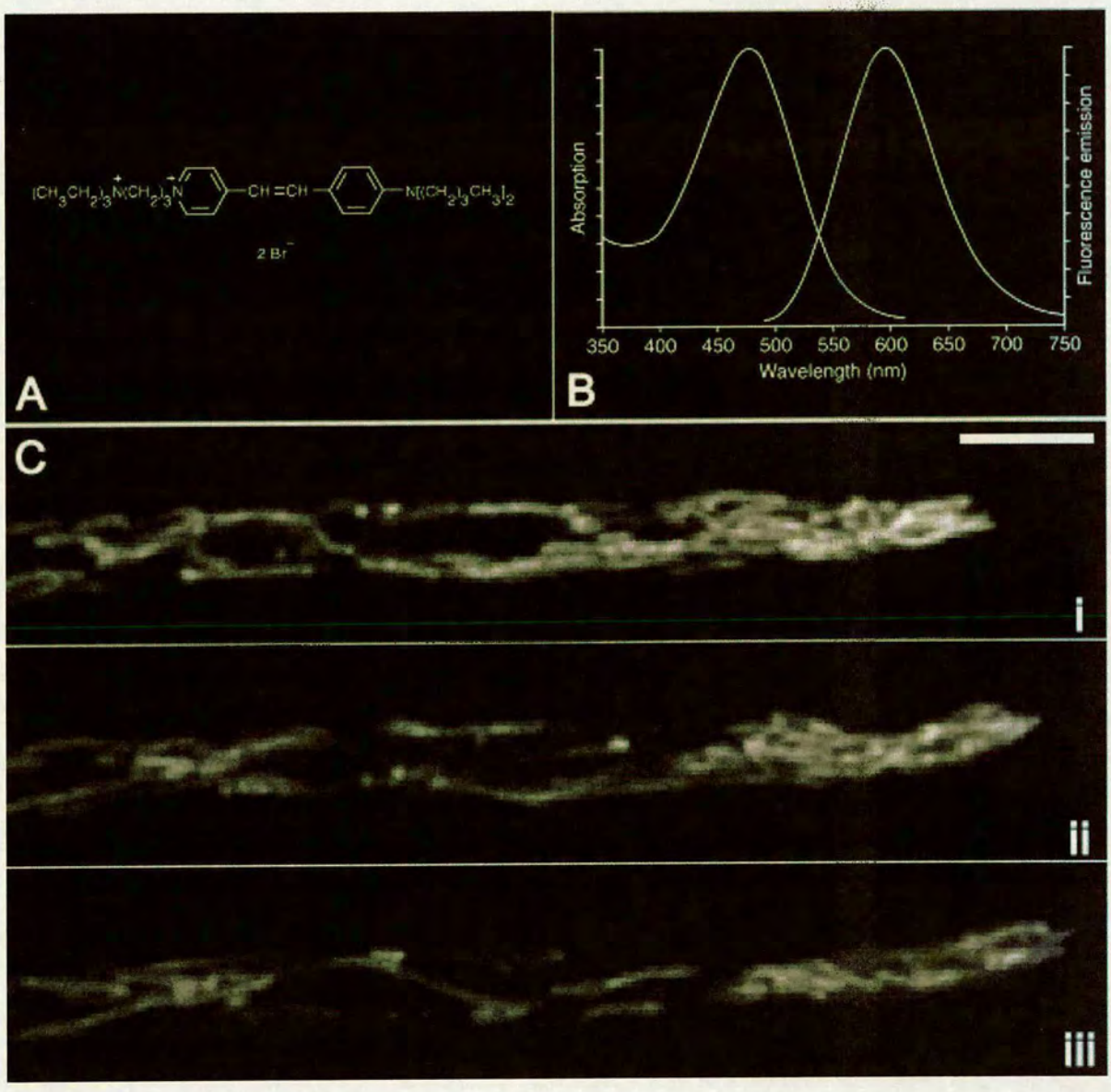

Figure 6.3: Staining characteristics of FM1-43 over a 60 s time course of repeated scanning. A) Molecular structure of FM1-43 (molecular weight = 611), B) Emission and excitation maxima, C) Time series of repeated scanning i) 0 s, ii) 30 s, iii) 60 s. Note that mitochondria were intensely labelled and non-selective labelling was minimal. Photobleaching and phototoxic effects were limited (A and B adapted from Molecular Probes, 2003).
Bar = 10 μm.

Staining Characteristics of the Non-Potentiometric Probes Mitotracker Green and GFP

MitoTracker probes are cell-permeant mitochondrion-selective dyes that passively diffuse across the plasma membrane and accumulate in active mitochondria. Seven Mitotracker probes are commercially available from Molecular Probes Inc., that differ in their spectral characteristics, oxidation state and fixability. The uptake of most mitochondrion-selective dyes is dependent on the mitochondrial membrane potential. MitoTracker Green is a possible exception and was therefore selected for this study.

Green Fluorescent protein was originally cloned from the jellyfish *Aequoria victoria* by Prasher (1992). The vast majority of studies involving GFP have been performed in yeast (Cormack, 1998). The first successful expression of GFP in filamentous fungi was by Spellig (1996) in *Ustilago maydis*, followed soon after by expression in *A. nidulans* (Fernandez-Abalos et al., 1998; Suelmann et al., 1997). Since then, GFP has been expressed in at least 16 different fungal species (Lorang et al., 2001). The GFP protein is very stable *in vivo* and expression has been observed in whole organisms, cell populations, individual cells, and organelles (Cormack, 1998; Ward, 1998; Cubitt et al., 1995). Green fluorescent protein has been successfully targeted to mitochondria in *A. nidulans* (Brakhage, 2000).

Green fluorescent protein can be excited at 395 nm or 475 nm and emits light at a maximum of 508 nm. In this study, excitation was with the 488 nm Argon ion laser line. Green fluorescent protein was of particular interest because its fluorescence in mitochondria is unrelated to the potentiometric gradient across the mitochondrial membrane. This provided an opportunity to visualise mitochondria without recording variations in fluorescence intensity between mitochondria, unlike most other dyes.

Mitotracker Green was assessed in this study because it is apparently highly selective to mitochondria and is not potentiometric (Molecular Probes, 2003) compared to other available probes. In comparison with the other dyes, except FM1-43, there was less plasma membrane staining. Mitochondria were intensely stained after approximately 1 min, even at the low doses used. Relatively high background staining, possibly as a consequence of the dye associating with other small components of the cell, was observed with only FM4-64 displaying greater non-selective fluorescence. Differences in fluorescence intensity were observed between mitochondria and apical mitochondria fluoresced more strongly than those more than 30 μm behind the tip, which suggested that apical mitochondria took up more dye, or that the dye was potentiometric.

Mitotracker Green was extremely susceptible to the effects of photobleaching and a 70% decrease in fluorescence intensity was recorded after 60 s repetitive scanning (Fig 6.8). The dye was also more phototoxic than others tested, with the exception of DASPMI. Growth rate decreased by approximately 50% following repetitive scanning, and mitochondrial morphology and spatial location was affected. Mitochondria had become spherical and may have fragmented. Furthermore, mitochondria retracted from the tip and apparently dispersed following repeated scanning (Fig 6.4).

The use of mitochondrion-targeted GFP provided an opportunity to study mitochondria using CLSM without the need to apply potentially toxic dyes. Fluorescence intensity was lower than could be achieved with fluorescent dyes but still yielded a strong enough signal for imaging, and some background fluorescence was observed. This suggested that GFP was not perfectly targeted to the mitochondria. Variations in intensity were observed between hyphae within the same colony. Mitochondria at the hyphal tip gave a slightly lower signal than those 5 μm and further behind the tip. GFP was, however, particularly unaffected by photobleaching and fluorescence intensity dropped by only 25% following repeated scanning (Fig 6.8). Furthermore, there were no obvious phototoxic effects; growth rate remained constant, and mitochondrial morphology and spatial location were unaffected (Fig 6.5).

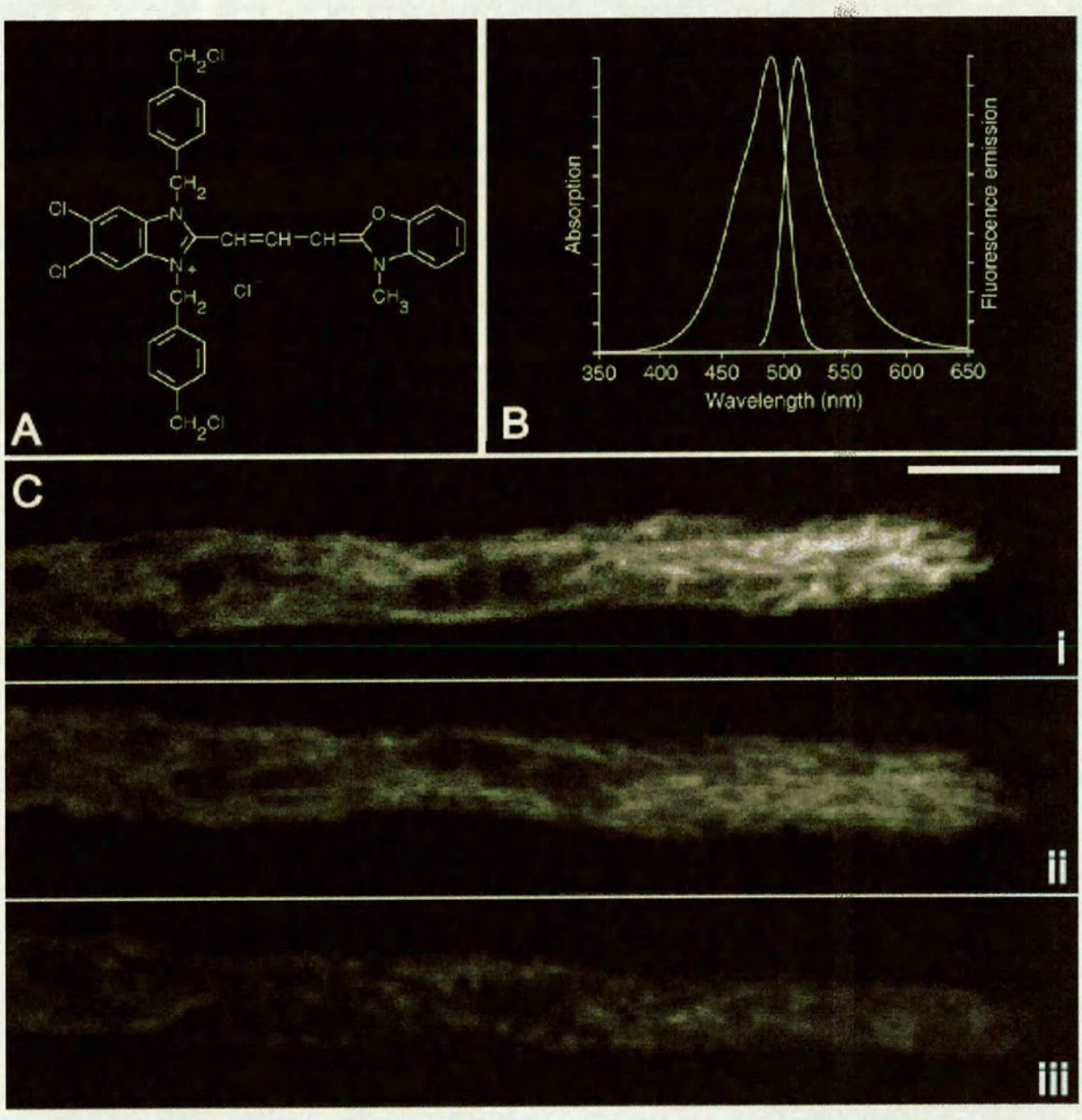

Figure 6.4: Staining characteristics of Mitotracker Green over a 60 s time course of repeated scanning. A) Molecular structure of Mitotracker Green (molecular weight = 672), B) Emission and excitation maxima, C) Time series of repeated scanning i) 0 s, ii) 30 s, iii) 60 s. Note that only mitochondria were intensely labelled but a high degree of background staining was observed. Phototoxic effects and photobleaching were severe (A and B, adapted from Molecular Probes, 2003) Bar = 10 μm.

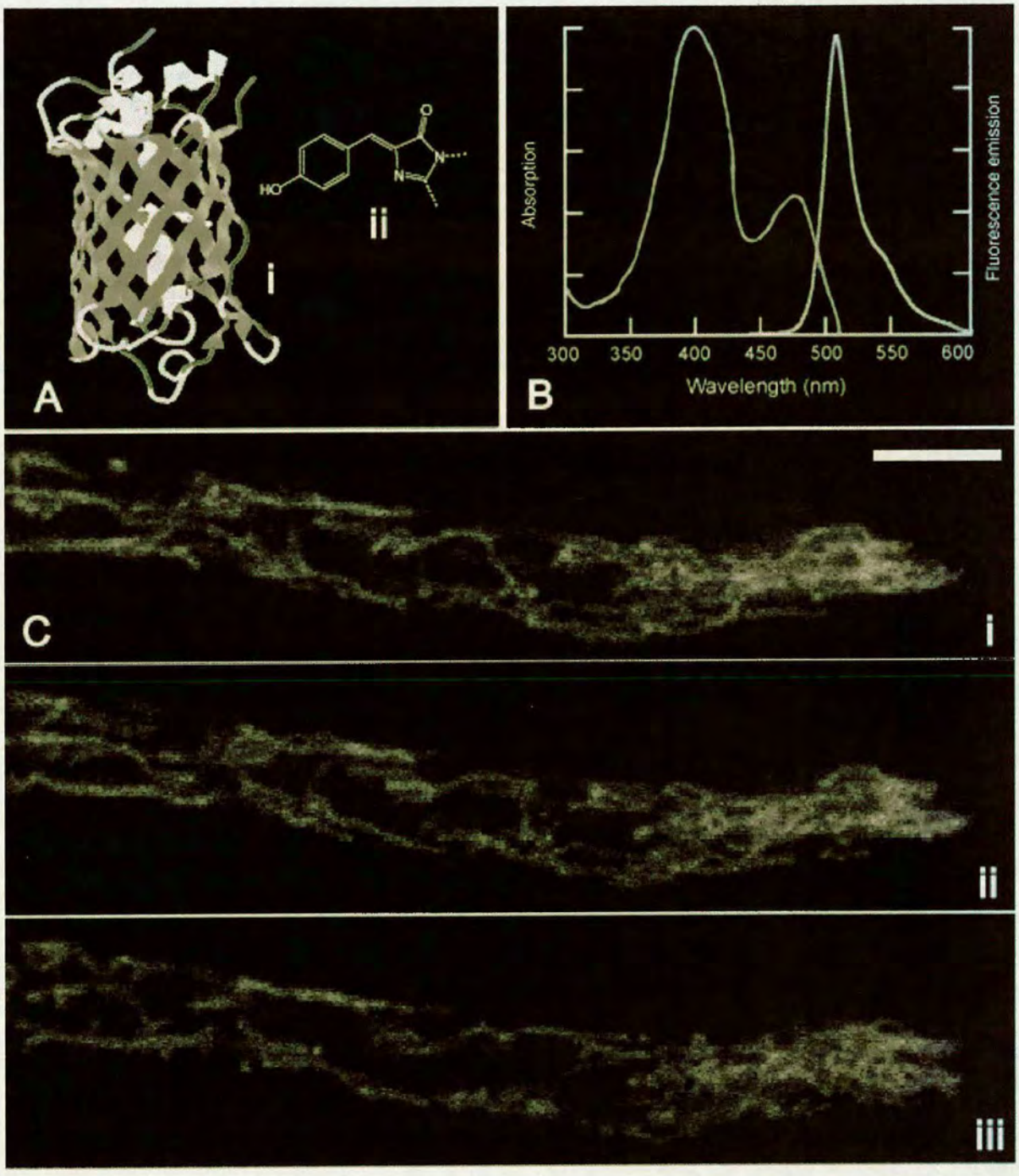

Figure 6.5: Fluorescence characteristics of mitochondrion-targeted GFP in *A. nidulans* over a 60 s time course of repeated scanning. A) GFP is a 27 kDa protein (i) with a 395 nm or 475 nm excitable fluorophore (ii), B) Emission and excitation maxima, C) Time series of repeated scanning i) 0 s, ii) 30 s, iii) 60 s. Note that mitochondria fluorescence was intense but no fluorescence was recorded from other cell structures. Some limited background fluorescence was observed. Phototoxic effects were not observed and photobleaching was limited (A and B, adapted from Subramaniam et al., 2003). Bar = 10 μm..

Staining Characteristics of the Potentiometric Markers Rhodamine 123 and DASPMI

Rhodamine 123 is a cell-permeant, cationic, fluorescent dye that is readily sequestered by active mitochondria without inducing cytotoxic effects. It is rapidly taken up by diffusion and has been shown to label mitochondria within several minutes (Lan Bo Chen, 1990; Wiseman et al., 1985). Conversely, DASPMI is a styryl dye and takes up to 30 min to label mitochondria according to some authors (Berecter-Hahn, 1990). Unlike the lipophilic rhodamine and carbocyanine dyes, rhodamine 123 and DASPMI are considerably more selective towards mitochondria and do not, for example, stain the endoplasmic reticulum (McConnell, 1990).

Rhodamine 123 and DASPMI have been used in a wide variety of animal cell applications with many different cell types, including the visualisation of presynaptic nerve terminals (Yoshikami and Okun, 1984), live bacteria (Kaprelyants and Kell, 1992), plants (Petit, 1992) and human spermatozoa (Auger et al., 1993). Both Rhodamine 123 and DASPMI are potentiometric markers, in that their fluorescence intensity is directly linked to the electrochemical gradient across the mitochondrial membrane. These properties have enabled the study of such events as apoptosis (Duchen and Biscoe, 1992), mitochondrial transmembrane potential and other membrane-related activities (Duchen et al., 1990).

As well as analysing relative mitochondrial activity in fungal cells, one of the primary interests of the present study was to analyse the effect of azoxystrobin on mitochondrial morphology. This included analysis of mitochondrial activity following uptake of azoxystrobin, and the mode of uptake for low doses of the fungicide. These potentiometric markers were therefore of interest because they provided the opportunity to analyse changes in mitcohondrial electrochemical gradient following application of mitochondrial inhibitors. To improve the validity of these experiments it was particularly important to understand the levels of cyto- and photo-toxicity following dye application and laser irradiation, in order to distinguish the potentially deleterious effects of imaging as opposed to the fungicidal effects of azoxystrobin.

Rhodamine 123 was found to label fungal mitochondria within several minutes. Mitochondrial fluorescence was intense at relatively low doses and the plasma membrane was labelled, but not intensely. Background fluorescence, from dye in the medium, was more obvious for Rhodamine 123 than the other probes tested. Non-selective labelling of other cellular components was not observed.

No phototoxic effects were observed from Rhodamine 123, with mitochondria remaining tubular and spatial location within the hyphal compartment unaltered. Growth rate was unaffected and photobleaching was recorded at 25% after 60 s scanning. Rhodamine 123 was an excellent label for mitochondrial activity and fluorescence intensity of mitochondria at the tip was 70% brighter than mitochondria 30 μm behind the tip. Furthermore, Rhodamine 123 still retained excellent dynamic range after photobleaching (Figs 6.6 and 6.8). On the basis of these results it was considered an appropriate marker for mitochondrial activity.

Like Rhodamine 123, DASPMI is also marketed as a mitochondrion-selective potentiometric marker. Mitochondria were labelled within 20 min of dye application and the plasma membrane was also labelled. Background fluorescence was not observed and the dye was highly selective to mitochondria although plasma membrane staining was more intense compared to Rhodamine 123. Phototoxic effects were observed, however, and mitochondria were found to become spherical and receded from the hyphal tip after 60 s scanning.

Photobleaching caused a 50% reduction in fluorescence intensity. Dynamic range, prior to photobleaching was good, and fluorescence intensity of mitochondria at the tip was 35% higher than mitochondria 30 μm behind the tip. Dynamic range was not as good in DASPMI compared with Rhodamine 123, and decreased drastically after photo-bleaching. Furthermore, growth rate decreased throughout the time course of scanning and growth had stopped entirely after 60 s (Figs 6.7 and 6.8). Although DASPMI was still considered an appropriate dye for imaging the morphology and spatial arrangement of mitochondria under controlled imaging conditions, the decreases in dynamic range following photobleaching and cellular and mitochondrial toxicity following repeated scanning made it unsuitable for time courses of fungicide uptake.

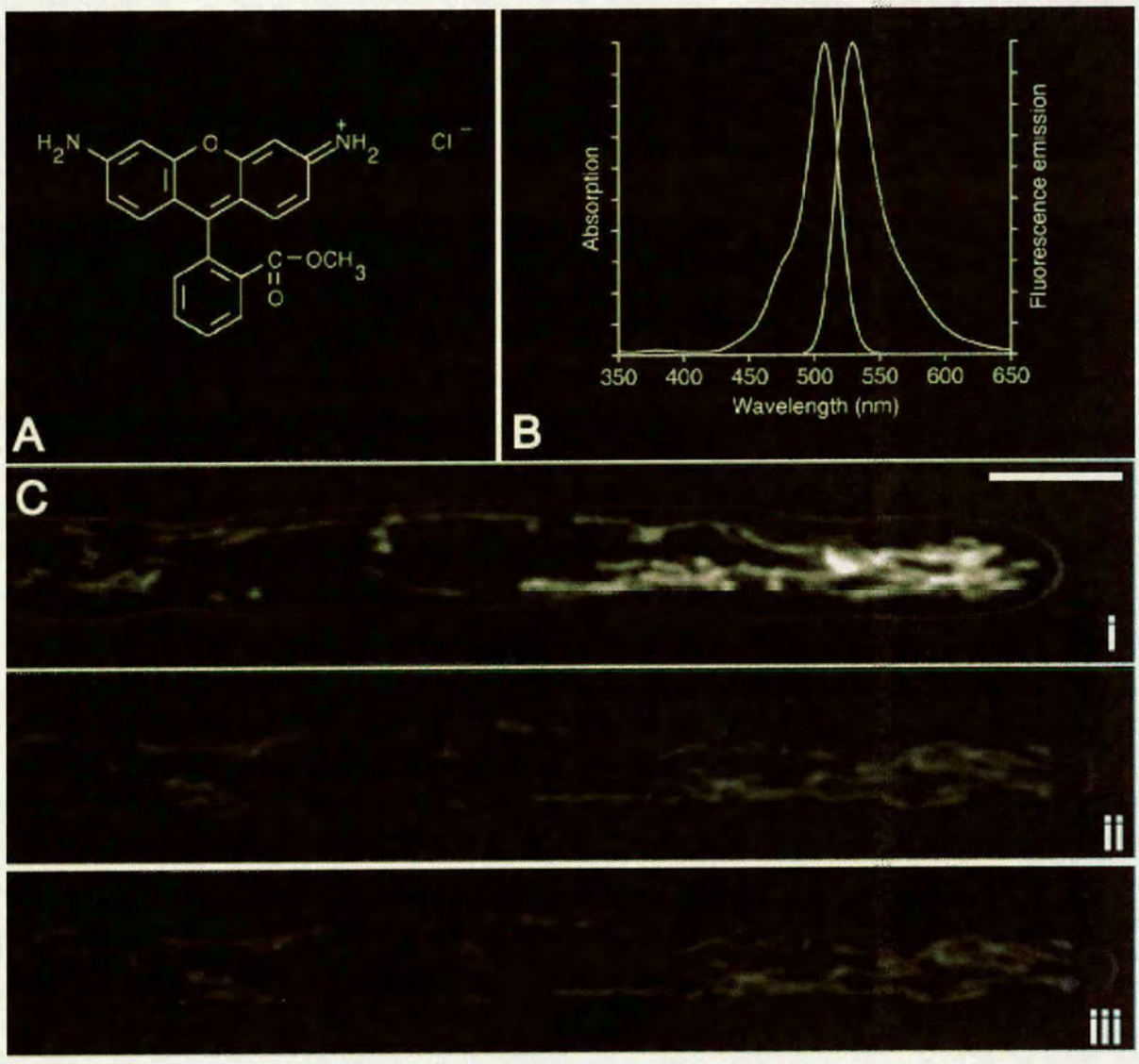

Figure 6.6: Staining characteristics of Rhodamine 123 over a 60 s time course of repeated scanning. A) Molecular structure of Rhodamine 123 (molecular weight = 381), B) Emission and excitation maxima, C) Time series of repeated scanning i) 0 s, ii) 30 s, iii) 60 s. Note that mitochondria are intensely labelled and there is a high variation in relative intensities of mitochondria located at the tip compared with those further behind the tip. Background fluorescence from dye in the media was observed and the plasma membrane was labelled, although less than in other dyes used. Phototoxic effects were not observed and limited photobleaching was observed (A adapted from Lan Bo Chen, 1989; B adapted from Molecular Probes, 2003). Bar = 10 μm.

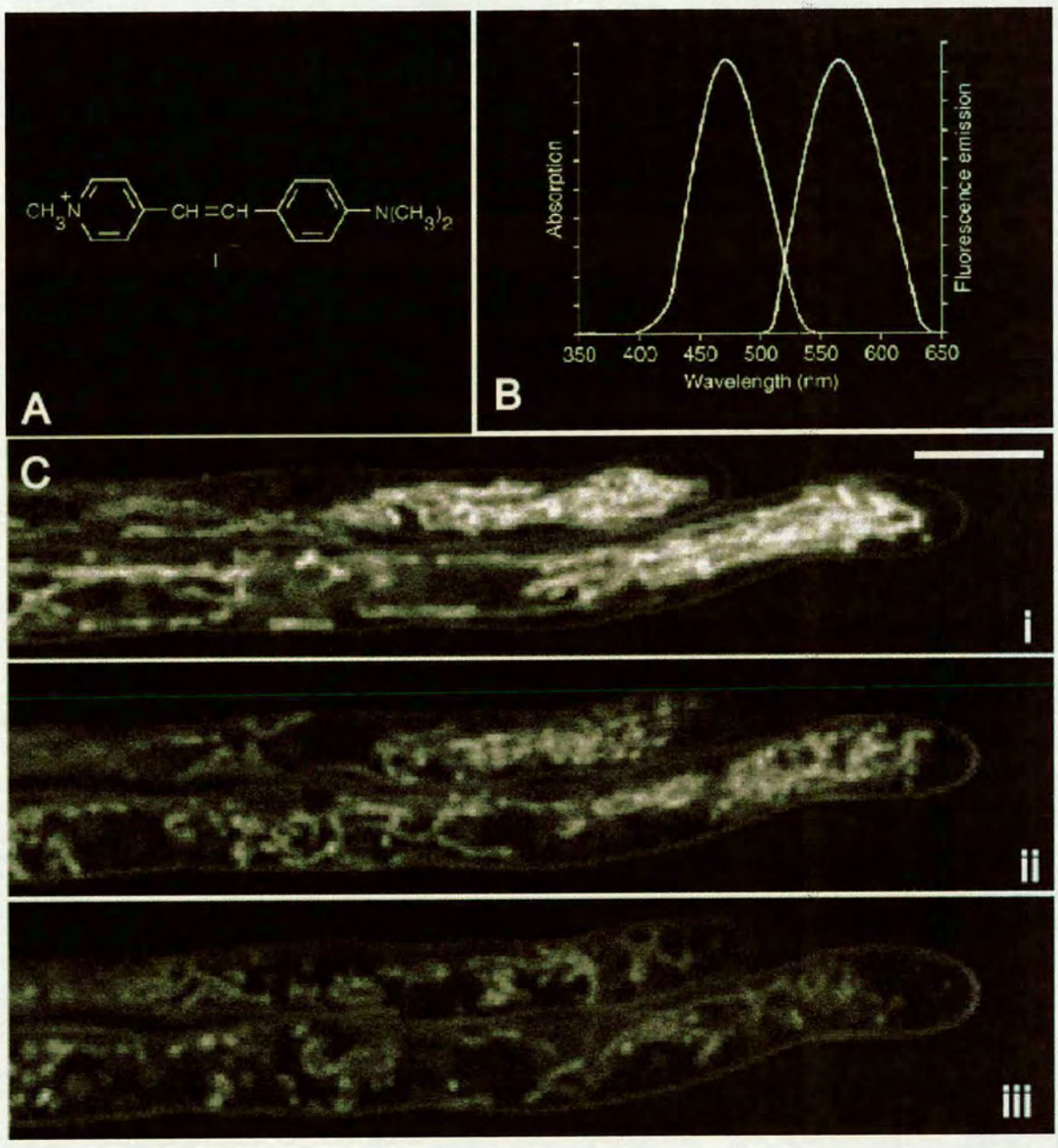

Figure 6.7: Staining characteristics of DASPMI over a 60 s time course of repeated scanning. A) Molecular structure of DASPMI (molecular weight = 366), B) Emission and excitation maxima, C) Time series of repeated scanning i) 0 s, ii) 30 s, iii) 60 s. Note that mitochondria were intensely labelled and the plasma membrane was intensely labelled also. Background fluorescence was low and staining of other cell structures was not observed. Phototoxic effects were severe - mitochondria became spherical and receded from the hyphal tip - and photobleaching was significant (A adapted from Molecular Probes, 2003; B adapted from BioRad, 2003). Bar = 10 μm.

Comparison of Dynamic Range of Mitochondrion-Selective Probes Following Photobleaching

All 6 probes were compared for photobleaching following 60 s repetitive scanning. Intensity of mitochondrial fluorescence along a 100 μm transect from the tip was measured. These data gave a clear indication of whether or not the probes tested were potentiometric, to what extent they photobleached and, in the case of those probes that were potentiometric, how dynamic range was affected following photobleaching. FM4-64 and GFP were the only probes in which mitochondrial fluorescence was generally uniform along the whole cell. In the case of GFP, fluorescence at the tip was slightly lower than for the rest of the cell.

Mitotracker Green, whose fluorescence is described as independent of mitochondrial electrochemical gradient (Molecular Probes, 2003) was found to cause much higher fluorescence intensity in mitochondria at the hyphal tip. It also photobleached rapidly and dynamic range was drastically reduced following photobleaching. FM1-43 fluorescence was slightly higher in mitochondria at the tip compared with those behind the tip. Rate of photobleaching was low for FM1-43 compared with other probes except GFP. Rhodamine 123 showed excellent dynamic range and fluorescence of mitochondria at the tip was considerably more intense than in sub-apical mitochondria. Photobleaching was observed but limited and dynamic range was good after photobleaching. DASPMI had a lower dynamic range than Rhodamine 123 and was photobleached more rapidly and to a greater extent. Furthermore, its dynamic range significantly decreased after photobleaching, although this may be because the dye was toxic and had caused a decrease in mitochondrial membrane gradient (Fig 6.8).

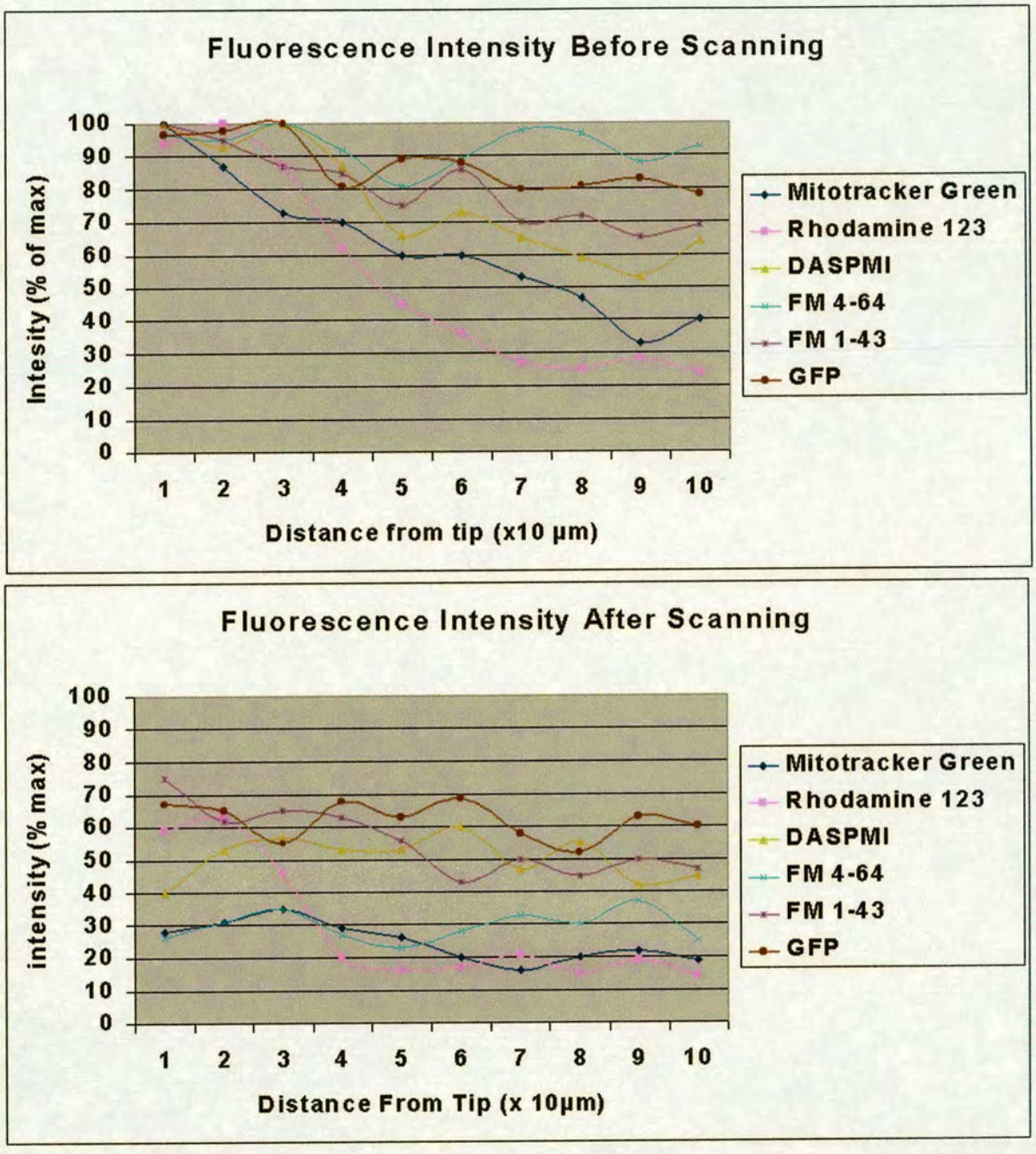

Figure 6.8: Graphs showing fluorescence intensity of all 6 probes along a median transect down the lengths of growing hyphae before repeated scanning (top) and after 60 s repeated scanning (bottom). Note the uniformity in fluorescence along the transect prior to scanning for GFP and FM4-64 and the relative dynamic ranges of the remaining dyes with the highest dynamic range recorded for Rhodamine 123. After 60 s repeated scanning the fluorescence intensity in all 6 dyes was reduced. Note that photobleaching was low in FM1-43 and GFP , and that a high dynamic range was recorded in Rhodamine 123 after photobleaching.

6.2.3 Morphology and Spatial Location of Mitochondria in Filamentous Fungi

Following the comparison of fluorescent probes available for the live-cell imaging of mitochondria in filamentous fungi, it was concluded that the potentiometric markers Rhodamine 123 and DASPMI, and the fluorescent probes FM 1-43 and mitochondrion-targeted GFP were the most suitable for imaging fungal mitochondria. Here, the spatial location, morphology and dynamics of mitochondria were analysed in *A. nidulans, N. crassa* and *Bot. cinerea.*

In *A.nidulans*, very long mitochondria, measuring over 20 μm in length, were observed at the hyphal tip (Fig 6.9a). Mitochondria were most densely arranged at the hyphal tip and were estimated to occupy approximately 95% of the median section of the cell up to a distance of 40 μm behind the tip. Mitochondria in these regions were generally longer and more tubular than sub-apical mitochondria, which had a more spherical appearance (Fig 6.9b). Apical mitochondria generally ranged in length from 3-10 μm, whereas sub-apical mitochondria were generally shorter with lengths of between 0.5-4 μm.

The spatial location and morphology of mitochondria observed in *A.nidulans* were similar in *N.crassa* and *Bot. cinerea.* In *N. crassa*, mitochondria were densely located at the hyphal tip (Fig 6.10a, insert) and were densely arranged up to 100 μm behind the tip. Sub-apically, mitochondria were more sparsely located and much shrter mitochondria predominated (Fig 6.10a). In *Bot. cinerea*, a 60 μm region at the hyphal tip was observed to be densely packed with mitochondria. Sub-apical cells were again observed to contain fewer mitochondria than the hyphal tip (Fig 6.10b), although these were generally longer in appearance than was observed in *A. nidulans* and *N. crassa.*

Mitochondria were generally arranged longitudinally within cells and were highly motile. Time-lapse imaging of hyphal tips revealed that mitochondria usually moved in the direction of growth at a similar rate to tip elongation. Less frequently, mitochondria were observed to relocate more quickly than the rate of elongation, commonly in the direction of growth (Fig 6.11). Mitochondria were also observed moving freely through septal pores in the direction of cytoplasmic streaming (Fig 6.12).

In all 3 species, mitochondria were absent from the very apex of the hyphal tip. Comparisons of cells of *N. crassa* and *A .nidulans* labelled with FM4-64 (which labels the endocytic pathway) and FM 1-43 (which labels the plasma membrane and mitochondrial membrane) suggested that this region of the cell was occupied by the apical vesicle cluster (or spitzenkorper) and that mitochondria were unable to penetrate the space it occupied (Figs 6.13 and 6.14).

Furthermore, negatively stained regions of the apical cell located behind the hyphal tip (at distances of 50, 60 and 100 μm in *A. nidulans, Bot. cinerea* and *N. crassa* respectively) were observed. Comparison of *N. crassa* cells labelled with DASPMI or DASPMI and nuclear-targeted GFP suggested that these negatively stained regions corresponded with the location of nuclei within the apical cell. The spatial orientation of mitochondria around these negatively stained regions demonstrated that mitochondria were highly plastic and capable of bending around other organelles (data not shown).

Work by Hickey (2001) demonstrated that branch formation in some filamentous fungi occurred when a spitzenkorper formed beneath the plasma membrane in a sub-apical region of the hypha. Under these circumstances, this region of the plasma membrane bulged, and a new branch formed. In this study, the movement of mitochondria into new branches was observed in *N. crassa* cells labelled with Rhodamine 123. During branch formation, the plasma membrane swelled and a new tip formed sub-apically to the existing tip. After approximately 25 s, this new tip reached a length of 5 μm before mitochondria entered the new branch (Fig 6.15).

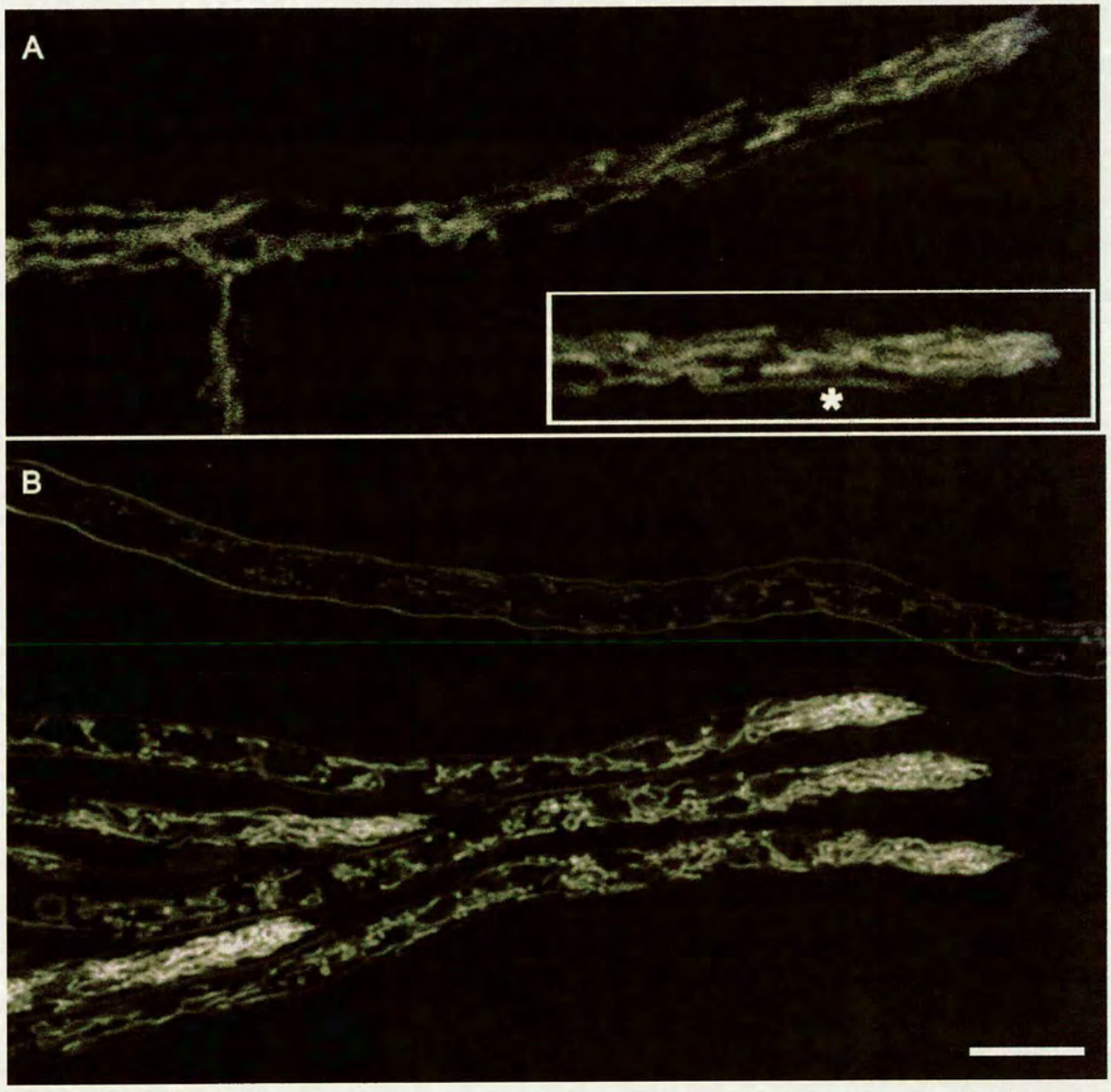

Figure 6.9: (A) Hyphal tip of *A. nidulans* labelled with mitochondrion-targeted GFP. Note that mitochondria were most densely packed in the apical region of the hyphal tip. These mitochondria were generally much longer than sub-apical mitochondria, reaching lengths of above 20 μm (insert, see *). (B) Image of 5 hyphal tips of *A. nidulans* labelled with DASPMI, which were growing near a subapical cell. Note the dense arrangement of mitochondria in the tips compared with the sub-apical cell, and that higher numbers of spherical mitochondria are present in the sub-apical cell. Bar = 10 μm.

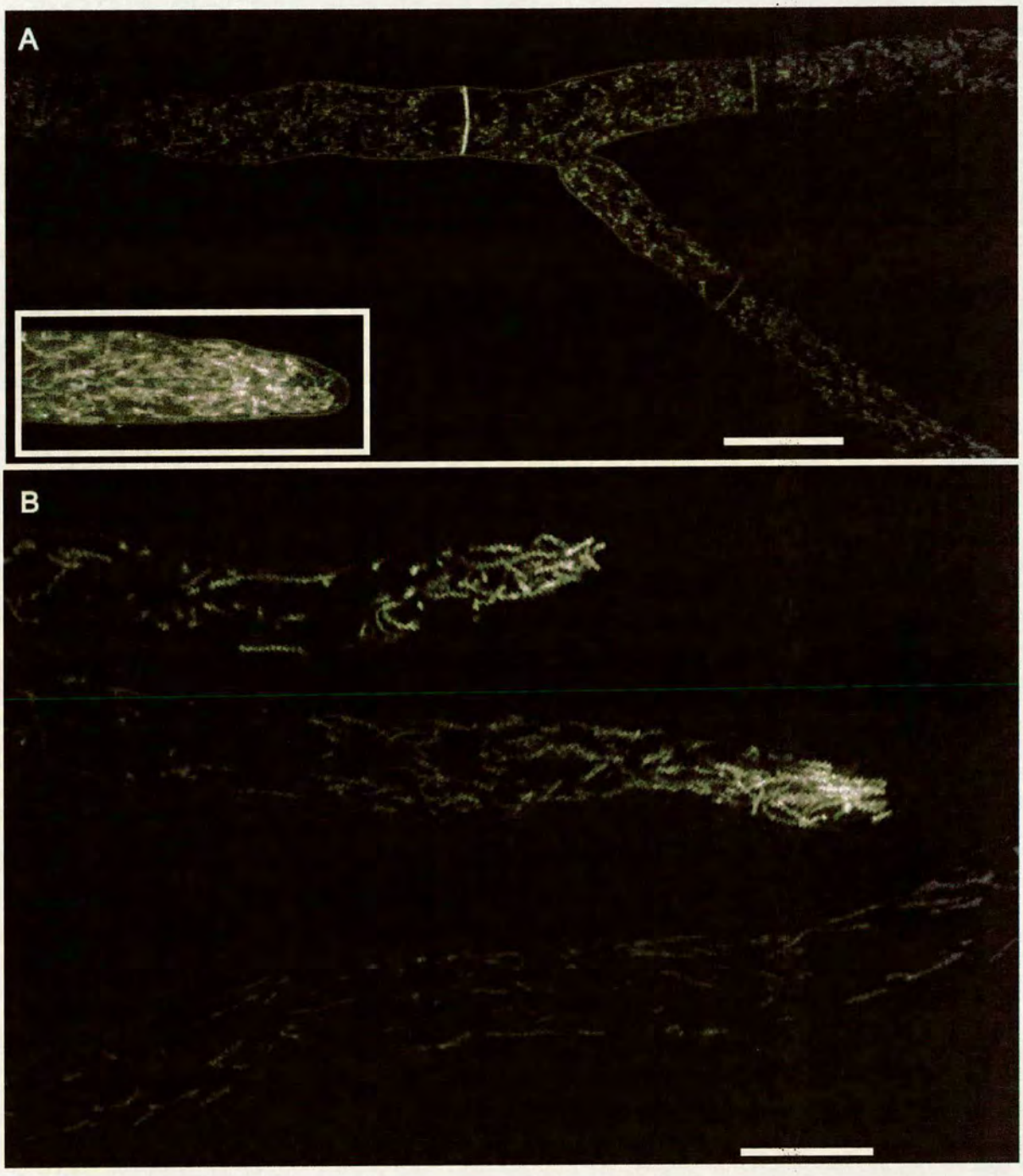

Figure 6.10: (A) Hyphal tip (insert) and sub-apical cells (main picture) of *N. crassa*. Note that mitochondria were more densely arranged in the apical region of the cell (i.e. the tip) compared with the sub-apical cell. In *N. crassa*, sub-apically located mitochondria were shorter than the elongated, tubular mitochondria of hyphal tips. (B) Image of 2 hyphal tips of *Bot. cinerea* which were growing next to a sub-apical cell. Again, note the dense spatial arrangement of mitochondria in the most apical regions of the tip compared with the sub-apical cell. As with *N. crassa* and *A. nidulans* sub-apical mitochondria are much shorter than apical ones. Bars = 10 μm.

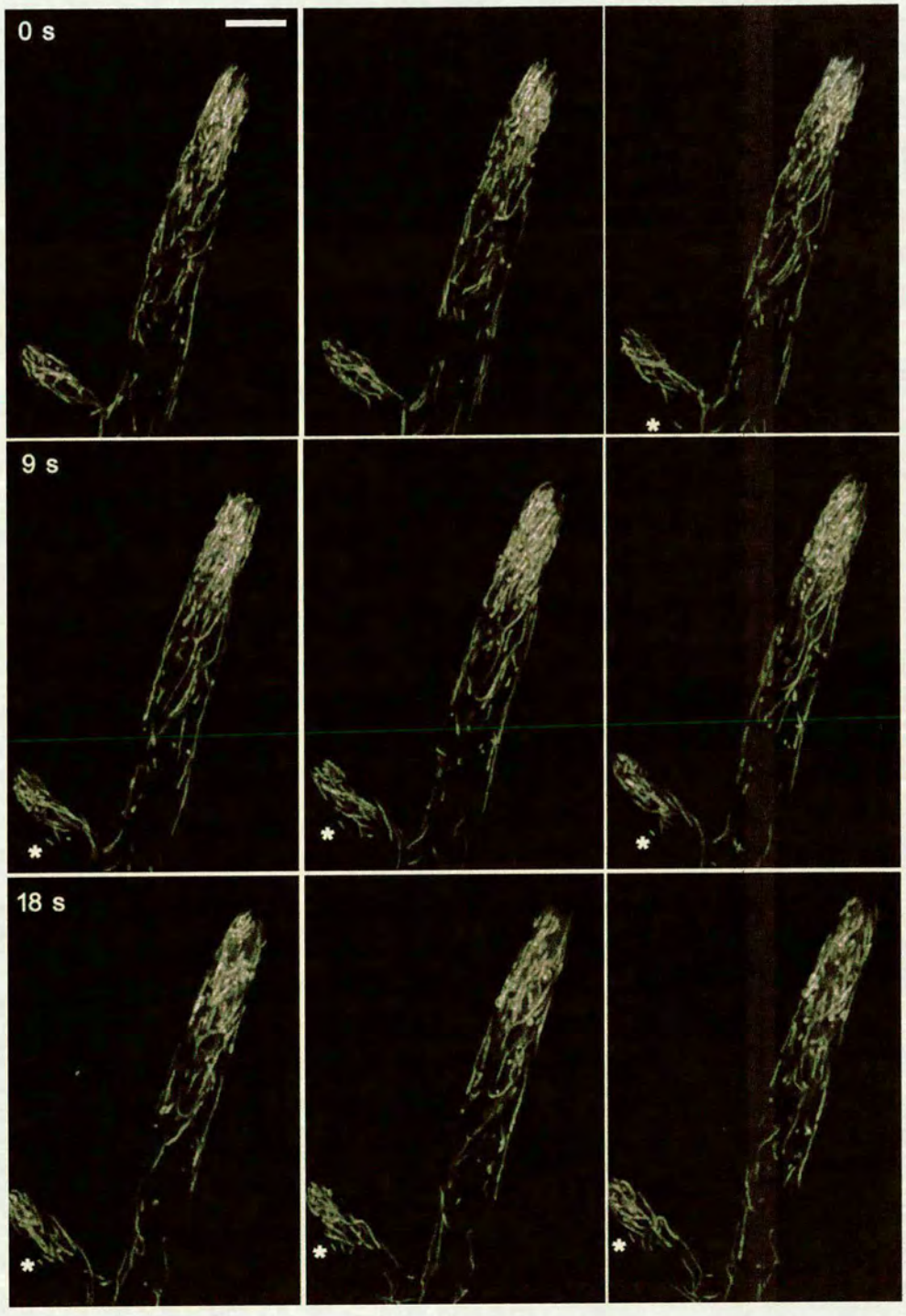

Figure 6.11: Time course of tip elongation in a branched apical cell of *Bot. cinerea* labelled with Rhodamine 123. Mitochondria were generally longitudinally arranged within cells and maintained a position within the cell consistent with the rate of elongation (i.e. they 'kept up' with the growing tip). Occasionally, mitochondria were observed moving towards the tip at a rate far in excess of the rate of tip growth (see *). Bar = 10 μm.

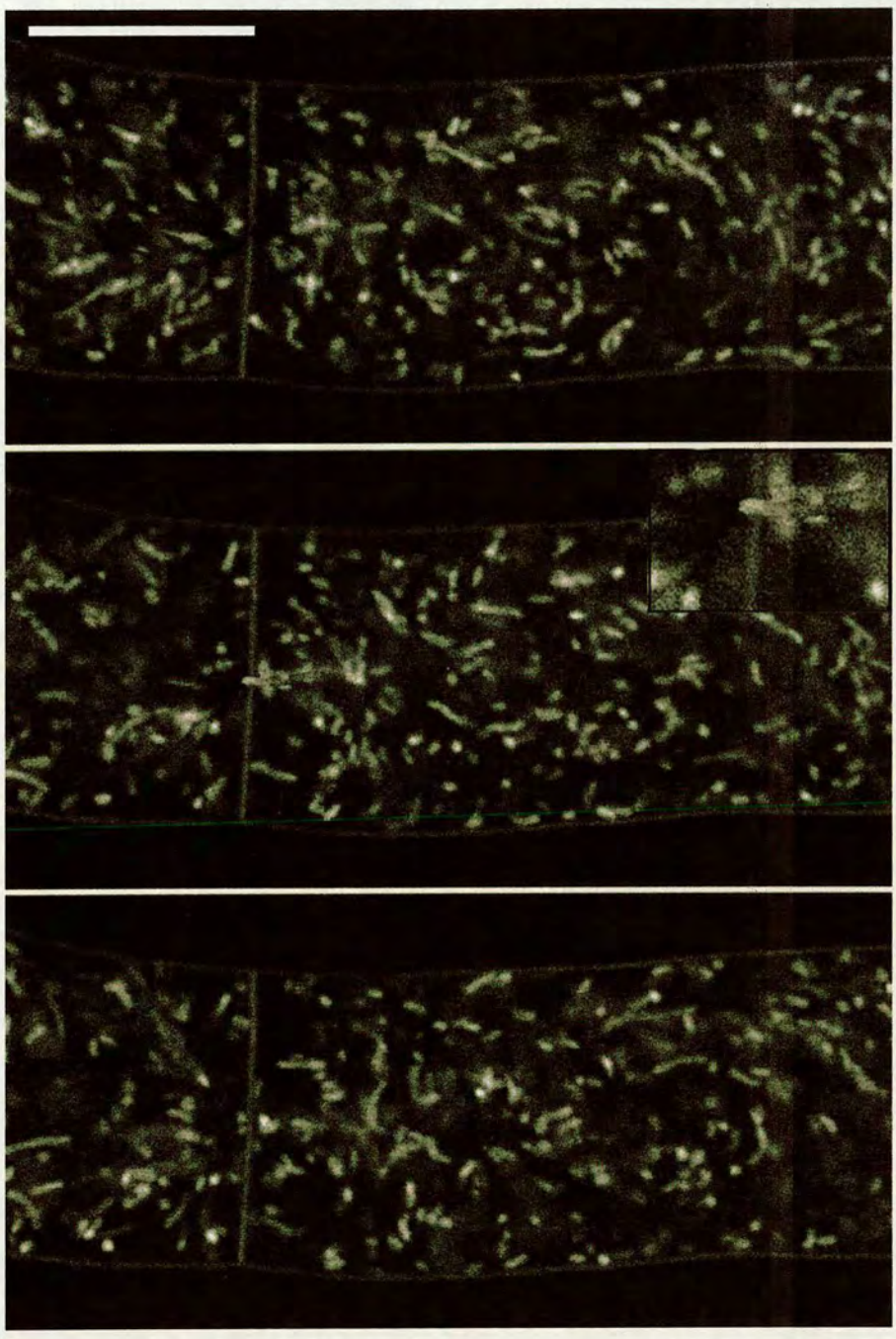

Figure 6.12: Time course of cytoplasmic streaming through a septal pore in *N. crassa* labelled with DASPMI. Septal pores provide a portal for the movement of cellular components through the cell. Cytoplasmic streaming in filamentous fungi is in the direction of elongation. In this series of images, mitochondria were observed moving through septal pores (see insert) in the direction, and at the rate of, cytoplasmic streaming. Mitochondria were observed to be not only highly plastic organelles but also highly motile ones. The rate of movement observed for mitochondria traversing septal pores was therefore greater than the typical rate of movement of tip-bound mitochondria (which moved at the rate of tip elongation). Bar = 5 μm.

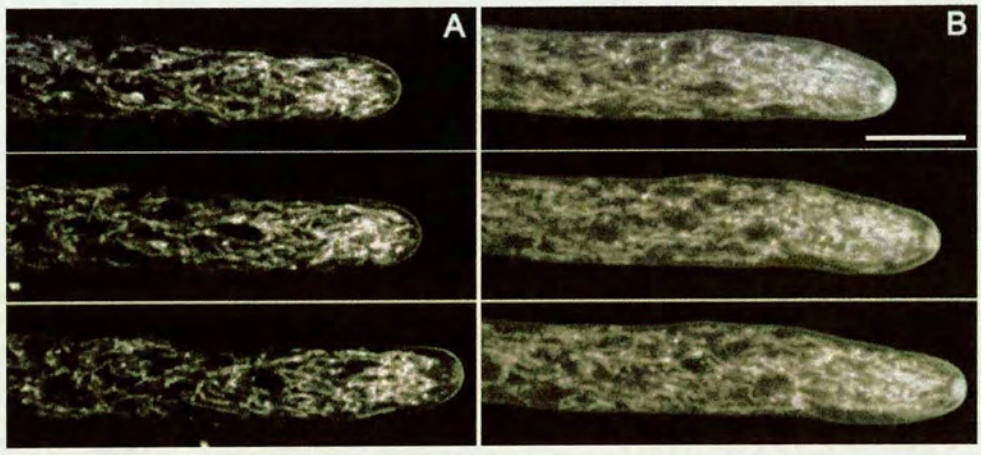

Figure 6.13: Time course showing a comparison of hyphal tips of *N. crassa* labelled with (A) FM1-43 and (B) FM4-64. Note that in hyphae labelled with FM1-43, mitochondria were absent from the very tip of the cell. In hyphae labelled with FM4-64 this region of the cell corresponded with the area occupied by the apical vesicle cluster of the spitzenkorper, and suggested that mitochondria were unable to penetrate this region. Bar = 10 μm.

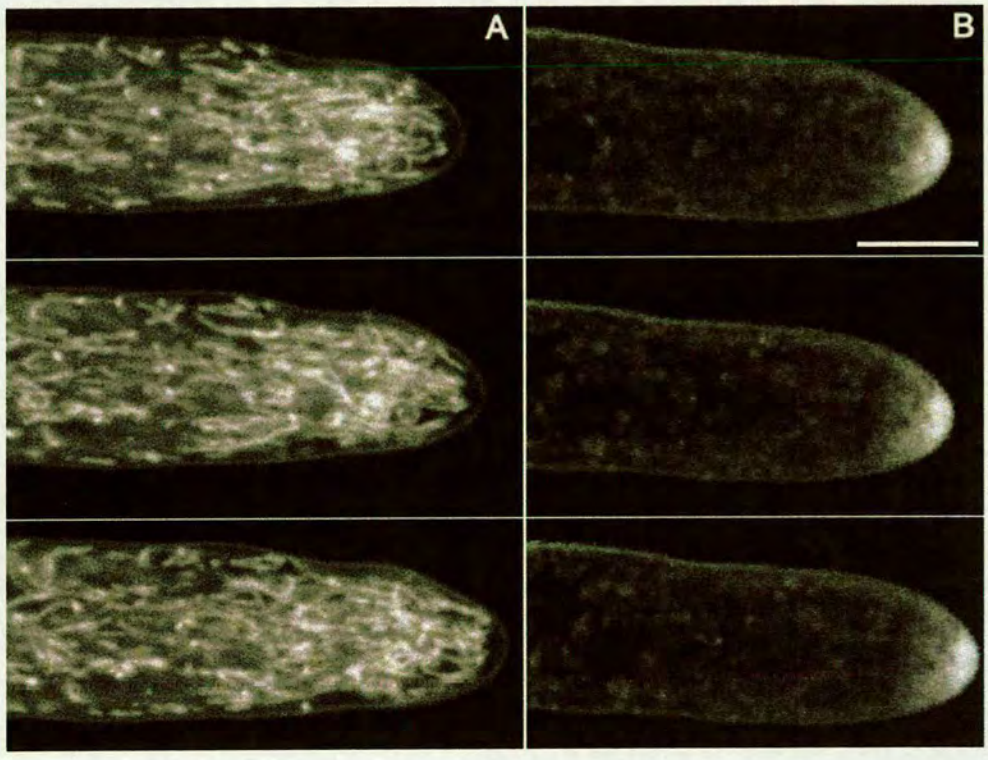

Figure 6.14: Time course showing a comparison of hyphal tips of *N. crassa* labelled with (A) FM 1-43 and (B) FM 4-64. These cells were similar to *A. nidulans* (data not shown), in that the most distal region of the hyphal tip, containing the apical vesicle cluster, was not penetrated by mitochondria. Bar = 10 μm.

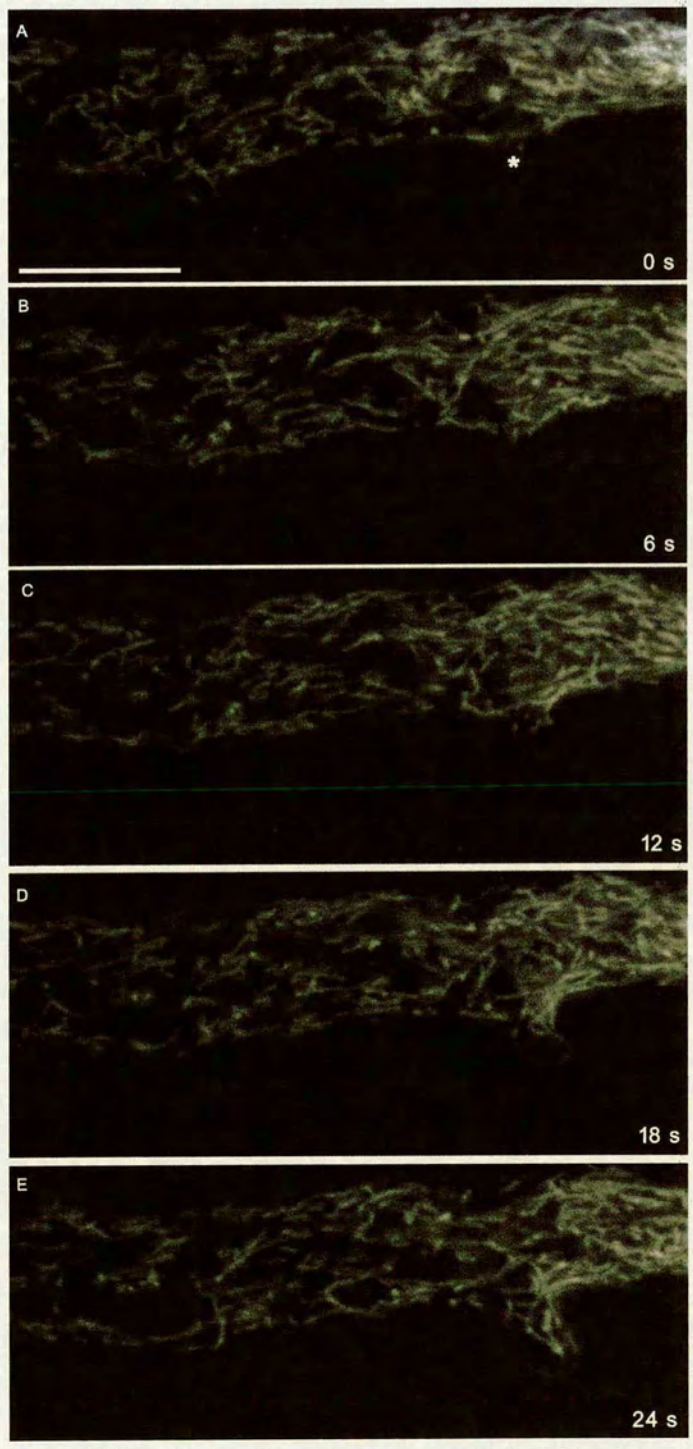

Figure 6.15: Series of 5 images from a time course of branch formation in *N. crassa* labelled with Rhodamine 123, approximately 100 μm behind the hyphal tip. (A) a new branch began to form (see *) and grew to a length of approximately 5 μm (B and C) before mitochondria from the existing cell entered the new branch (D and E). Bar = 10 μm.

6.2.4 Physiology and Activity of Mitochondria in Filamentous Fungi

The potentiometric marker, Rhodamine 123, was used to label mitochondria in cells of *N.crassa, A. nidulans* and *Bot. cinerea.* The primary aim of this study was to compare relative mitochondrial membrane potentials in different regions of the apical cell. Although differences in activity between various cell types have been measured in animal cells using Rhodamine 123 (e.g. Duchen et al, 1992), similar differences between mitochondrial membrane potential in fungi have not been reported.

In all 3 species, mitochondrial membrane potential (measured by differences in fluorescence intensity from Rhodamine 123) was found to be greatest in the apical region of the hyphal tip, coinciding with the region of the cell containing the most densely arranged mitochondria. Intensity measurements for this region (covering an area of 80 μm length multiplied by the width of the cell) were compared with a region of identical area 300 μm behind the tip.

The greatest differences in activity were observed in *A. nidulans* and *Bot. cinerea*, with apical mitochondria fluorescence intensity recorded as over 80% more intense than mitochondria in the sub-apical region (Figs 6.16 and 6.17). In *N. crassa*, mitochondria at the tip were substantially more active than those in the sub-apical region, although maximum fluorescence in the sub-apical region was approximately 60% of the tip region (Fig 6.18). A comparison was made in *A. nidulans* between fluorescence from Rhodamine 123 labelling and fluorescence from GFP-targeted to mitochondria. In cells expressing GFP, mitochondrial fluorescence intensity was generally uniform along the length of the cell (Fig 6.19), suggesting that differences recorded using Rhodamine 123 were a consequence of differences in membrane electro-chemical gradient (as opposed to differences in fluorescence intensity through shifts in focus along the length of the cell).

These data suggested that not only were mitochondria most densely located in the hyphal tip in filamentous fungi, but these mitochondria also exhibited the highest electro-chemical gradients across their membranes, which suggested they were also producing the highest quantities of ATP.

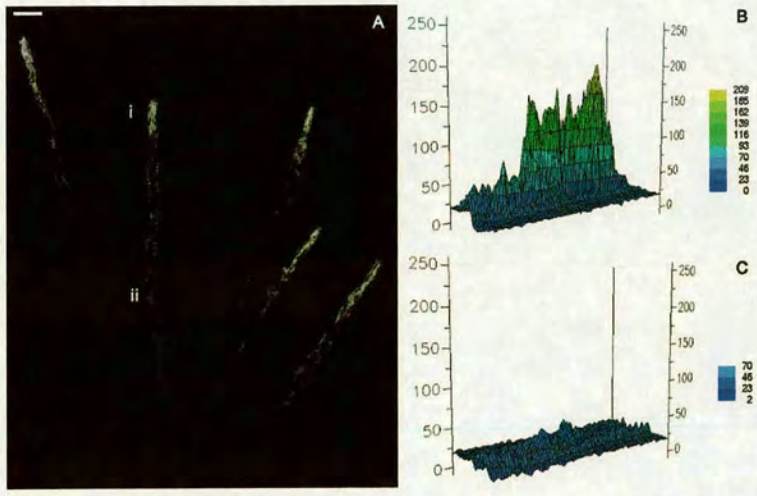

Figure 6.16: (A) Apical cell of *A. nidulans* labelled with Rhodamine 123. Mitochondrial fluorescence intensity was plotted in an apical and sub-apical region of the cell (regions i and ii) and plotted in 3-D graphs (B, apical region and (C) sub-apical region). Intensity, and therefore mitochondrial activity, was highest in the apical region. Fluorescence intensity was approximately 80% greater in the apical region compared with the sub-apical region. Bar = 10 μm.

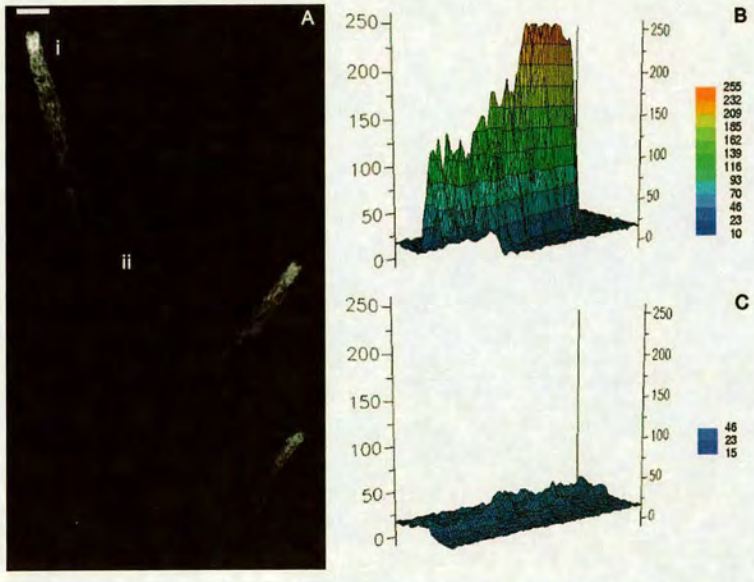

Figure 6.17: (A) Apical cell of *Bot. cinerea* labelled with Rhodamine 123. As before, mitochondrial fluorescence intensity was plotted in an apical and sub-apical region of the cell (regions i and ii) and plotted in 3-D graphs (B, apical region and (C) sub-apical region). Fluorescence intensity was approximately 80% greater in the apical region compared with the sub-apical region, which indicated that mitochondria in this region of the cell were most active. Bar = 10 μm.

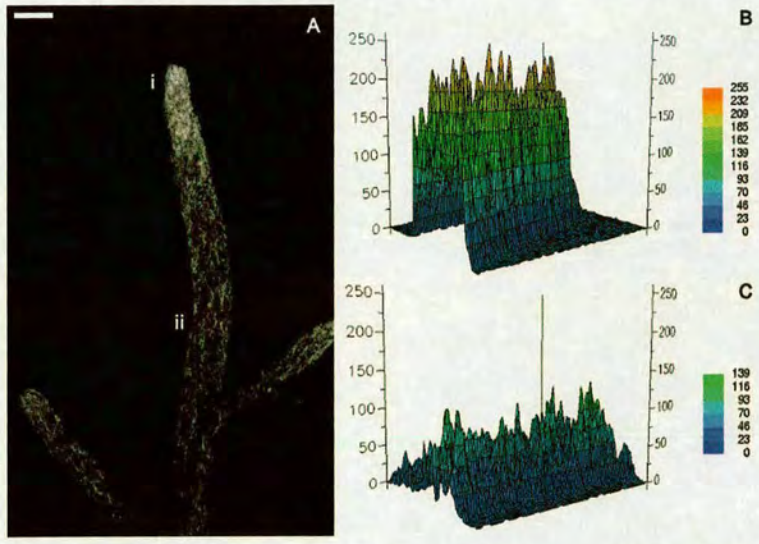

Figure 6.18: (A) Apical cell of *N. crassa* labelled with Rhodamine 123. As before, mitochondrial fluorescence intensity was plotted in an apical and sub-apical region of the cell (regions i and ii) and plotted in 3-D graphs (B, apical region and (C) sub-apical region). Fluorescence intensity was approximately 60% greater in the apical region compared with the sub-apical region, indicating that mitochondria in this region were most active. Bar = 10 μm.

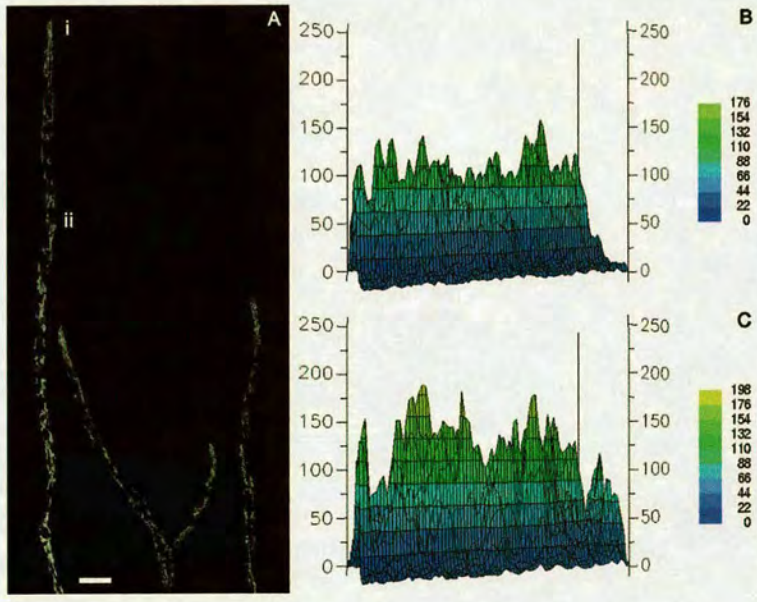

Figure 6.19: (A) Apical cell of *A. nidulans* labelled with mitochondrion-targeted GFP. Variations in fluorescence intensity can result from cells growing in and out of the plane of focus. However, 3-D graphs plotted from apical (B) and sub-apical (C) regions (regions i and ii in A) of the cell showed uniform intensity along the apical cell. This supported the assertion that differences in intensity reported in Figs 6.17 to 6.19 were due to differences in mitochondrial activity. Bar = 10 μm.

6.2.5 Morphological and Spatial Location of Mitochondria Following Treatment with FCCP and Azoxystrobin

Applications of a variety of mitochondrial inhibitors have been shown to cause changes to membrane potential in the mitochondria of a variety of different cell types (Duchen et al., 1992). In this study, changes to the morphology, spatial organisation and activity of mitochondria following treatment with azoxystrobin were of primary interest. Initially, time courses of mitochondrial dysfunction and cell death were followed in apical cells of *N. crassa* after treatment with FCCP. Following this, sequences in the fatal disruption of mitochondria in *A.nidulans* and the plant pathogen *Bot. cinerea* were investigated after treatment with low doses of azoxystrobin.

Neuropsora crassa cells, labelled with FM 1-43, were treated with a 100 μM concentration of FCCP in an osmotically balanced malt extract solution. Such high concentrations of FCCP generally caused cells to burst once irradiated with laser light (Fig 6.20a). Lower concentration solutions (50 μM) resulted in the swift and fatal disruption of cellular processes, although imaging after several minutes revealed simply that cell growth had stopped and mitochondria had probably fragmented (Fig 6.20b). A time course of FCCP treatment showed that the morphological characteristics of tip bound mitochondria were immediately affected (within 10 s), changing from tubular shaped structures into rounded structures. After 30 s, most mitochondria had fragmented. At this time point, cell growth completely and irreversibly ceased. Between 30 s and 60 s, mitochondria continued to fragment, such that any further morphological or spatial differences could not be detected because of the background fluorescence from dye which had leaked into the cytoplasm from damaged mitochondria (Fig 6.20c).

Cultured cells of *A. nidulans* and *Bot. cinerea* were treated with low doses (less than 6 ppm) of azoxystrobin in an osmotically balanced solution. Initially, cells of *A. nidulans* labelled with FM 1-43 were observed 5 min after treatment (Fig 6.21). In these cells, growth had stopped and mitochondrial location and morphology were significantly different to non-treated cells. Mitochondria were more spherical in appearance and had retracted from the hyphal tip. Furthermore, mitochondria were less densely arranged than in healthy cells, either as a consequence of fragmentation or, more likely, dispersal.

A time course of treatment with a lower dose of azoxystrobin (less than 0.6 ppm) was followed in *Bot. cinerea* labelled with Rhodamine 123 to analyse rate of uptake, changes to morphology and spatial location of mitochondria within the hyphal tip, and to analyse differences in mitochondrial activity after treatment. Growth rate was immediately affected (within 10 s of treatment) and completely stopped within 50 s of application. Within this time period, mitochondria became more spherical, less densely arranged and retracted slightly (approximately 10 μm) from the tip of the cell (Fig 6.22). These data demonstrated that azoxystrobin was exerting a biological effect on fungal cells approximately 10 s after application and strongly suggested that diffusion was the primary pathway for uptake under these conditions.

Decreases in mitochondrial activity were also observed within this time frame. Between 20 and 25 s, fluorescence intensity decreased in the tip region by approximately 10%, and by approximately 5% in a region of the cell 100 μm behind the tip. Within 50 s of treatment, fluorescence intensity at the tip had reduced by approximately 75%, and fluorescence intensity in the sub-apical region had decreased by approximately 65% (Fig 6.23). Comparison of the time course of decreases in growth rate and mitochondrial activity suggested that growth rate decreased approximately 7 s prior to decreases in fluorescence intensity (Fig 6.24). These results were consistent and reproducible (see Appendix 10.3), single data sets are presented below for ease of interpretation.

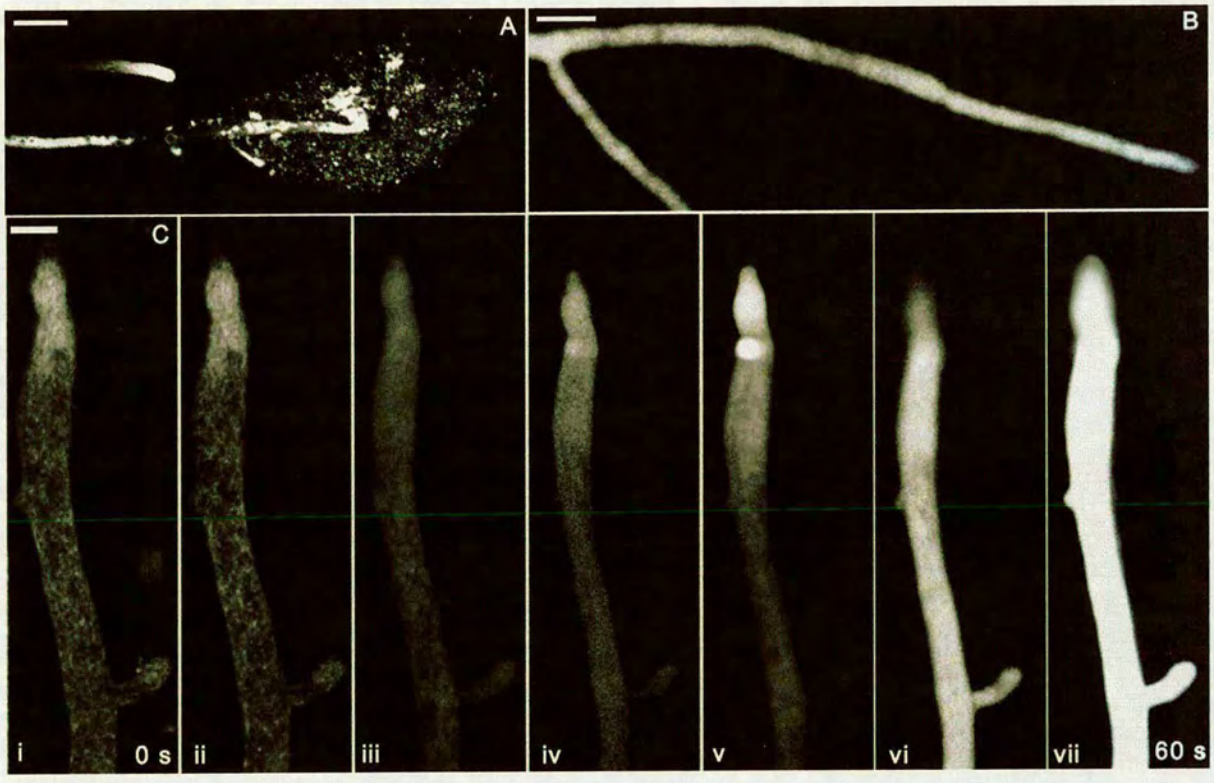

Figure 6.20: (A) Apical cells of *N. crassa* treated with a 100 μM concentration of FCCP burst upon contact with the inhibitor. Lower concentrations of FCCP (50 μM) caused a cessation of growth and mitochondria to fragment (B). (C) A time course of uptake of FCCP (50 μM concentration) revealed that FCCP caused mitochondria to become more spherical and fragment within 10 s of treatment (i and ii). Within 30 s, growth had stopped and most mitochondria had fragmented (iii and iv). Within 60 s, any remaining mitochondria had also fragmented which caused dye to leak into the cytoplasm. Bars = 10 μm.

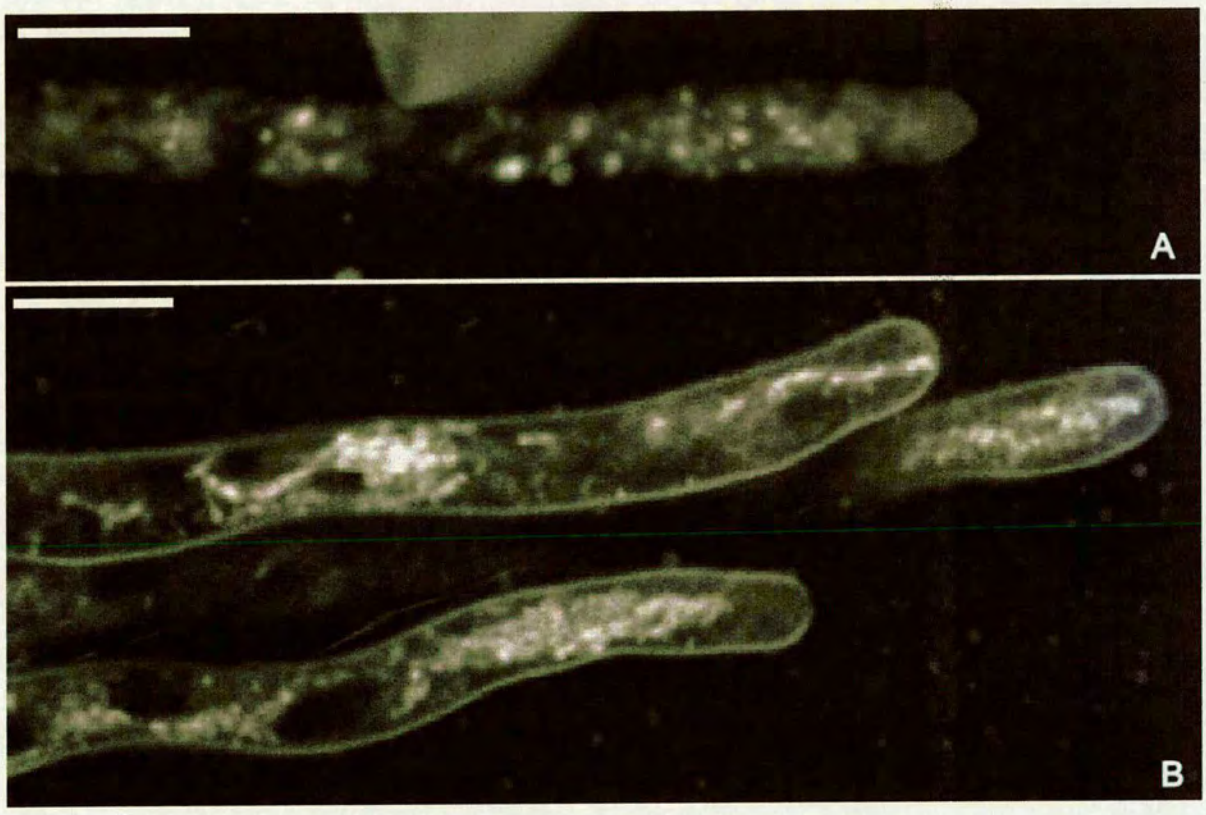

Figure 6.21: Apical cells of *A. nidulans* labelled with FM 1-43 and imaged 5 min after treatment with azoxystrobin (6 ppm). (A) 3-D projection of treated cell. Note that mitochondria had become more spherical, and a decrease in fluorescence was observed at the tip, consistent with dispersal or fragmentation of mitochondria. (B) Image of 3 neighbouring apical cells of *A. nidulans* 5 min after treatment. Mitochondria were generally observed to retract from the tip, become less densely arranged and become less elongated in their morphology. In both cases (A and B) growth had irreversibly stopped. Bars = 10 μm.

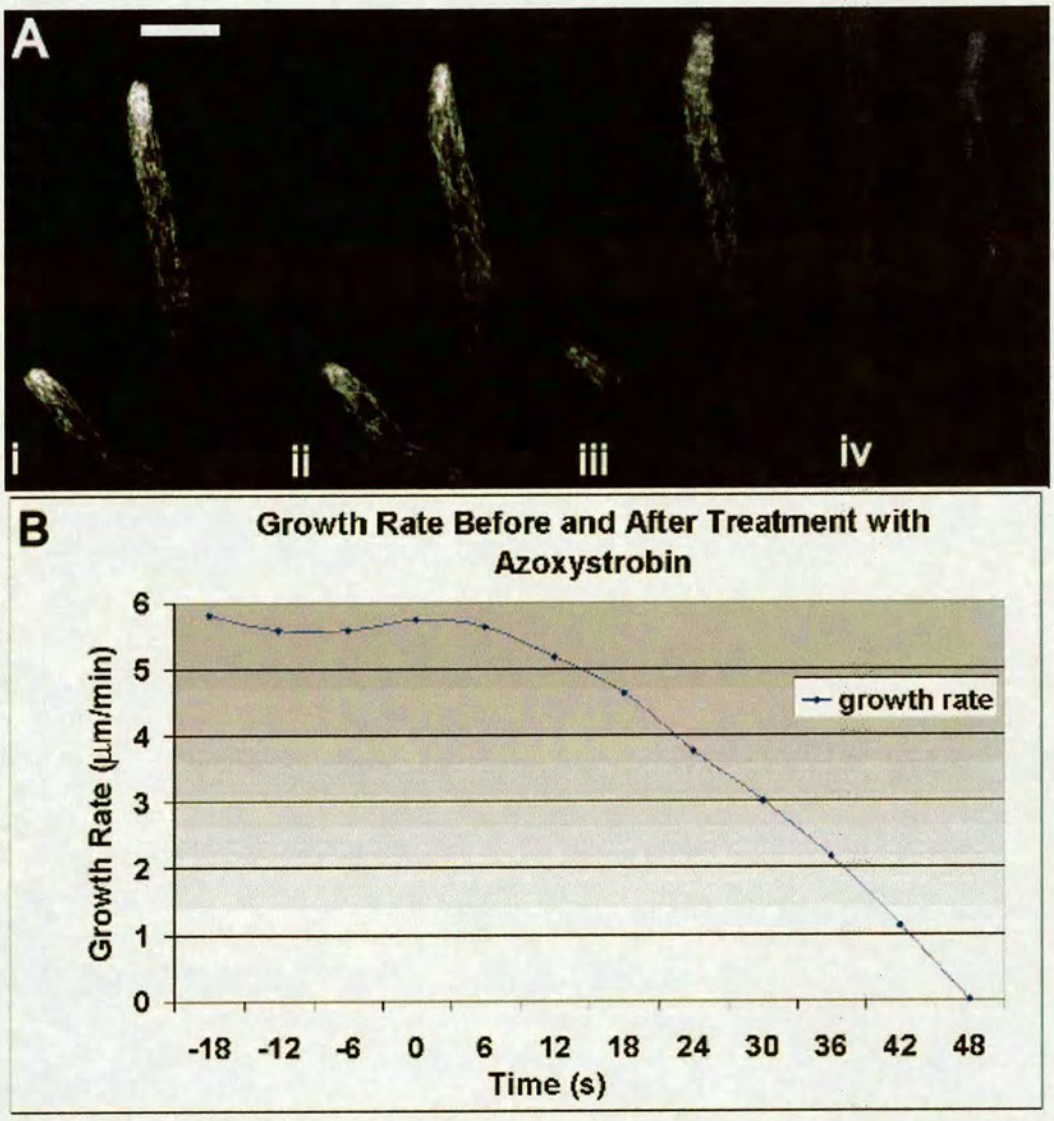

Figure 6.22: (A) Series of images following a time course of azoxystrobin uptake (less than 0.6 ppm) in apical cells of *Bot. cinerea* labelled with Rhodamine 123. Prior to treatment, mitochondria were densely located within the hyphal tip and were generally elongate in appearance (i). Within 15 s, the area of densely packed mitochondria at the tip had decreased in size (ii). Within 30 s, significant differences to the morphology and spatial arrangement of mitochondria were observed, with a marked increase in the number of spherical, compared to elongate, mitochondria and a slight retraction of mitochondria from the tip of the cell (iii). Within 45 s, mitochondria had begun to disperse from, or fragment, in the hyphal tip (iv). (B) These changes in morphology and spatial location coincided with a decrease in growth rate. Prior to treatment, growth rate was measured at 6 μm/min. Growth rate began to slow to 5 μm/min within 15 s of treatment and continued to decrease for a further 35 s before stopping completely. Bar = 10 μm.

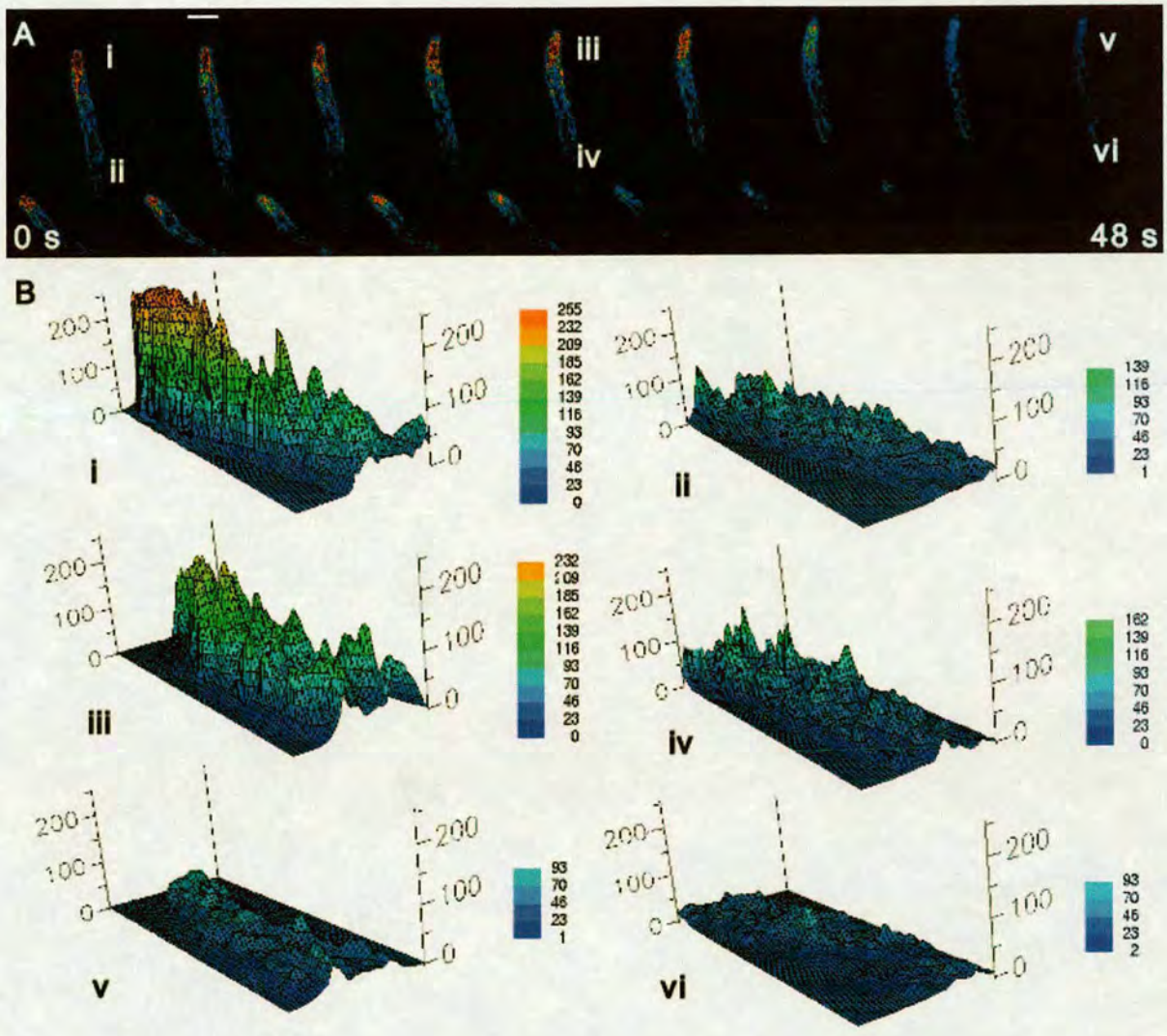

Figure 6.23: (A) Series of pseudo-coloured images showing changes in fluorescence intensity in mitochondria of *Bot. cinerea* over a 48 s time course following treatment with azoxystrobin. A series of 3-D graphs of fluorescence intensity were plotted to measure mitochondrial activity in an apical and sub-apical region of the hyphae throughout the course of uptake. (B) 0 s after treatment (i and ii, representing regions Ai and Aii), fluorescence intensity was greatest at the apical tip (maximum pixel intensity value 255 compared with 130 in the sub-apical region). Within 25 s of application (iii and iv, representing regions Aiii and Aiv), fluorescence intensity had decreased by 10% in the apical region and 5% in the sub apical region. Within 48 s of application (v and vi, representing regions Av and Avi), fluorescence intensity had decreased by 75% in the apical region and 65% in the sub-apical region, which indicated that mitochondrial activity had been significantly compromised by azoxystrobin. The time-scale for changes to mitochondrial activity followed a similar time-scale to the changes in morphology, spatial location and growth rate previously described (Fig 6.22). Bar = 10 μm.

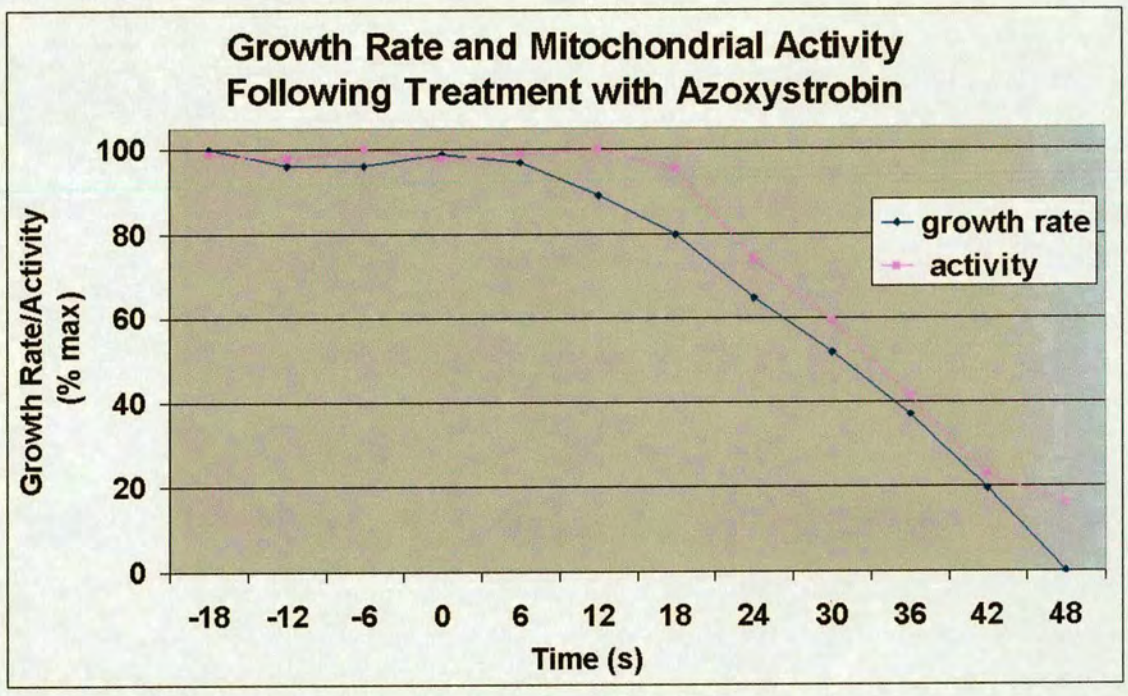

Figure 6.24: Graph showing the time-scale of decreases in mitochondrial activity superimposed over the time-scale of decreases in growth rate (as percentage of maximum). Decrease in growth rate occurred approximately 6 s after application of azoxystrobin and decreased at an approximately linear rate for the following 40 s. Measured decreases in mitochondrial activity succeeded decreases in growth rate by approximately 7 s. Decreases in fluorescence were also approximately linear over time until approximately 42s and levelled off at 48 s. Within 48 s, growth rate had completely stopped, and mitochondrial activity had decreased to its minimum recorded value. It would be expected that mitochondrial activity would decrease first, causing a decrease in available cellular energy from ATP, followed by a decrease in growth rate. In fact, the opposite was observed; possible explanations for this anomaly are discussed later.

6.3 Discussion

6.3.1 Comparison of Mitochondrion-Selective Probes

Careful selection of a fluorescent dye is a necessary prerequisite to the successful imaging of cells with the confocal microscope. Over the past 25 years, since the first confocal microscopes became commercially available, a variety of new dyes have been developed specifically for confocal imaging. However, the majority of applications involve animal cells, and the characteristics of some dyes are significantly different when applied to filamentous fungi. There is no guarantee that a dye which has been successfully applied to the imaging of mitochondria in, for example, mammalian cells, will be appropriate for the imaging of mitochondria in filamentous fungi. Consequently, the staining characteristics and physiological effects of a variety of commonly used mitochondrion-selective probes were compared in *A. nidulans* prior to the study of mitochondrion morphology, physiology and inhibition.

It was particularly interesting to note that styryl dye FM1-43 was an excellent stain for mitochondria in *A. nidulans*, whereas it has been used most commonly to label endocytic events in animal cells. The successful targeting of GFP to cellular components of some filamentous fungi, including mitochondria in *A. nidulans*, avoids many of the problems associated with dye application (especially toxicity, non-selective staining). In the present study, however, the production of GFP-transformants was not possible. Consequently, *A. nidulans* was the only transformant containing mitochondrion-targeted GFP available for imaging. Comparison of photobleaching rates, levels of phototoxicity and the dynamic range of potentiometric probes (before and after photobleaching) led to the selection of FM1-43 and DASPMI for the study of mitochondrial morphology and spatial location in three species of filamentous fungi. The potentiometric probe, Rhodamine 123, was the least toxic and produced the highest dynamic range, ands was therefore selected for the analysis of mitochondrial membrane potential.

6.3.2 Mitochondrial Morphology and Dynamics

Mitochondria have been shown to display an amazing plasticity of form and distribution (Yaffe, 1996). Although their internal structural organisation is highly conserved, the external shape of mitochondria is variable. In addition to the classic kidney-shaped organelles observed in electron micrographs, mitochondria are frequently found as reticulated networks. These networks are extremely dynamic in growing cells, with tubular sections dividing in half, branching and fusing to create a fluid tubular web (Bereiter-Hahn and Voth, 1994).

In differentiated mammalian cells, such as cardiac muscle or kidney tubules, mitochondria are often localised to specific cytoplasmic regions rather than randomly distributed (Porter and Bonneville, 1973). Further studies involving *Drosophila melanogaster* have confirmed that some alterations in mitochondria are developmentally programmed, with characteristic mitochondrial migrations or morphological changes occurring at key stages in cellular differentiation (Fuller, 1993; Mignotte et al., 1989).

In the present study, a variety of morphological differences were observed between mitochondria located in different cellular regions. Mitochondria in the apical region of the cell were typically elongate and tubular, and closely resembled bacteria. Although, differences in the number of mitochondria were observed between species, the same patterns of morphology and spatial organisation were similar; the greatest volume of mitochondria were located at the tip and these were generally larger than sub-apical mitochondria. These results support the observations of Fischer-Parton et al (2000) and Hickey (2001), who observed shorter, less densely arranged mitochondria in sub-apical cells compared with apical cells, in a variety of filamentous fungi.

Fungal cells grow by apical extension only, and growth is likely to require high levels of cellular energy from ATP. *Neurospora crassa* was the largest and fastest growing fungus studied, and was found to have the greatest number of mitochondria at the tip. Conversely, *A. nidulans* was the slowest growing and smallest fungus in the study, and contained fewer mitochondria. Given that mitochondria play a vital role in the production of cellular energy (Markham, 1995), it seems likely that the high energy requirements associated with growth have led not only to the increased number of mitochondria located in the tip region, but also accounts for the greatest number being present in faster growing species.

Microscopic studies performed nearly 80 years ago supported early suggestions that mitochondria were related to bacteria (Altmann, 1925). However, mitochondria lack flagella, cilia or other structures associated with bacterial motility. In the present study, mitochondria were observed to be highly motile and typically moved in the direction of growth. Although it is possible that cytoplasmic streaming controls the movement of mitochondria in fungi, the spatial location of mitochondria observed in different regions of the tip, and their movement into new branches, suggests that spatial organisation cannot be accounted for by cytoplasmic streaming alone, for this would probably lead to a more random spatial organisation than was observed.

Microscopic studies of the cytoskeleton has revealed colocalisation of mitochondria with certain cytoskeletal components. In particular, many studies have documented colocalisation of mitochondria with microtubules in diverse cell types including mammalian neurons, sperm cells, cultured fibroblasts and the yeast *Saccharomyces pombe* (Baummann and Murphy, 1995; Couchman and Ress, 1982; Heggeness et al., 1978). Live-cell fluorescence microscopy of *N. crassa* revealed mitochondria tracking along microtubules. Further studies in animal cells have identified the role of the microtubule-based motor proteins kinesin and cytoplasmic dynein in binding and transporting mitochondria along microtubules (Nangaku, 1994).

Actin and tubulin are the major cytoskeletal proteins found in fungi, although others have been reported (Roberson, 1992; Hoang-Van and Turin, 1987; Watts et al., 1985). The highest concentrations of actin in filamentous fungi were observed in areas of cell growth and differentiation, namely; hyphal apices, septal walls sites of sub-apical branching (Roberson, 1992; Tiburzy et al., 1990; Salo et al., 1989). Although a complex actin cytoskeleton has been identified in *Sclerotium rolfsii* (Roberson, 1992), the role of actin in mitochondrial movement is not clear. In *Saccharomyces cerivisiae*, a fraction of mitochondria colocalised with actin cables (Drubin et al., 1993). However, mutations that caused total loss of actin cables did not affect mitochondrial transport (Goodson et al., 1996; Simon and Swayne, 1995).

Recent work by Hickey (2001) in mutant cells of *N. crassa* which lacked kinesin, revealed that mitochondria were not present at the hyphal tip. These results suggested that kinesin plays a major role in the organisation of mitochondria within cells of filamentous fungi. Research using mouse cells has demonstrated that kinesin-bound mitochondria were motile along microtubules *in vitro* (Nangaku, 1994).

Although no attempts were made in the present study to identify the mechanisms affecting the mechanical organisation and movement of mitochondria in filamentous fungi, these results supported the view that a complex cytoskeleton within fungal cells is responsible for the organisation of mitochondria. For example, during branch formation, the new tip was observed to elongate to approximately 5 μm prior to the entry of mitochondria. This series of events suggests a level of organisation that requires the assembly of a microtubule network. The study of the cytoskeleton in filamentous fungi is ongoing, and would certainly benefit from further live-cell studies which take advantage of the resolving power of the confocal microscope.

6.3.3 Mitochondrial Physiology

The mitochondrial electron transport chain develops and maintains potential across the inner mitochondrial membrane of the order of -150 to -200 mV by expulsion of protons from the matrix. This provides the energy which drives the diffusion of protons back into through the proton channel of the F_1-F_0 ATP synthase, promoting ATP synthesis. Rhodamine 123 is a fluorescent probe which accumulates within mitochondrial membranes, and fluorescence signal positively correlates with mitochondrial membrane potential. It has been widely used in a variety of studies involving animal cells to compare relative membrane potential between mitochondria in a variety of cell types, and to analyse apoptosis and the effects of oxygen, calcium and other chemicals on membrane potential (Duchen, 1999; Duchen and Biscoe, 1992; Biscoe and Duchen, 1990; Mills and Jobis, 1972).

The popularity of Rhodamine 123 in animal cell studies has waned somewhat since the commercial availability of an alternative potentiometric dye, JC-1. The advantage of JC-1 over Rhodamine 123 (and other potentiometric probes), is that it changes colour reversibly from red to green as membrane potential increases (Cossarizza and Salvioli, 2000). In the present study, JC-1 labelled mitochondria poorly and formed aggregates in the plasma membrane or cell wall and appeared to be unable to successfully penetrate cells of filamentous fungi (data not shown). Authors working on plant mitochondria have also reported problems with labelling mitochondria using JC-1 (M. Fricker, personal communication) and it seems likely that cell wall may provide a barrier to dye penetration into plant and fungal cells which is not present in animal cells. Consequently, mitochondrial membrane potential was analysed using Rhodamine 123 in the present study.

In all three species studied, a striking difference was observed in the fluorescence signal from Rhodamine 123 between apical and sub-apical bound mitochondria. Because Rhodamine 123 fluorescence increases in mitochondria with higher membrane potential, it is reasonable to conclude that mitochondria in the tip regions of filamentous fungi are producing the greatest levels of ATP. Work on animal cells has demonstrated that the relationship between Rhodamine 123 fluorescence and mitochondrial membrane potential in isolated mitochondria is linear (Emaus et al., 1986). In the present study, Rhodamine 123 fluorescence intensity from labelled mitochondria was measured in apical and sub-apical regions of *A. nidulans, N. crassa* and *Bot. cinerea.* These results suggest that mitochondrial membrane potential was 80% higher in apical regions of *A. nidulans* and *Bot. cinerea* compared with sub-apical regions. In *N. crassa* mitochondrial membrane potential was 60% greater at the tip compared with membrane potential in a sub-apical region of the same cell.

Differences have been reported for mitochondrial membrane potentials using Rhodamine 123 in a variety of mammalian cells. Although increased membrane potential is recognised to drive ATP synthesis, exact quantities of ATP synthesised by differently charged mitochondria remains unknown. However, cells recognised as requiring the most energy, namely cardiac cells and hepatic cells, were found to have the most mitcohondria, and these possessed the highest membrane potentials (Devin et al., 1998; Bullough et al., 1989; Amchenkova et al., 1988). From the present study, it was particularly interesting to note that membrane potential varied significantly between mitochondria in different regions of the same cell. Furthermore, it is likely that the tip region, where cell growth exclusively occurs, is the most energy demanding. Not only were mitochondria in these regions observed to possess mitochondria with the greatest membrane potentials, but they were also the site of the greatest number of mitochondria. Furthermore, apical mitochondria were typically larger than those located in sub-apical regions.

6.3.4 Mitochondrial Inhibition

It is clear from the data presented above, that mitochondria in the apical cells of filamentous fungi are responsible for producing significant quantities of ATP, necessary for driving cell growth through elongation of the hyphal tip. Given that mitochondria play such a crucial role in the life of the cell, it is not surprising to find that mitochondrial dysfunction plays a crucial role in cell death. In the present study, FCCP and azoxystrobin, both recognised inhibitors of mitochondrial respiration, were applied to cells of *N. crassa, A. nidulans* and *Bot. cinerea* and a time course of cell death was followed.

Work on mammalian cells has demonstrated that acute mitochondrial dysfunction causes catastrophic energy failure in cells ands results in necrotic cell death, for example during ischaemia or anoxia (Duchen, 1999). Furthermore, subtle forms of mitochondrial dysfunction are believed to be responsible for certain neuro-degenerative disorders such as Parkinson's disease (Schapira et al., 1998) and motoneuron diseases (Kong and Xu, 1998). Mitochondrial dysfunction is also recognised to cause disruption and cell death in filamentous fungi, and has therefore been exploited as a potential site of activity for some fungicides, including the strobilurins (Bartlett et al., 2002; Deacon, 1995).

Relatively high concentrations of FCCP cause *N. crassa* cells to burst, possibly as a consequence of osmotic shock. Lower concentrations of FCCP caused mitochondria to change their morphology from elongate, tubular structures to spherical ones. This change in mitochondrial morphology was similar to the phototoxic effects observed in mitochondria labelled with DASPMI, although it occurred over a much faster time period. Following this, mitochondria fragmented and released dye into the cytoplasm.

Treatment of *A. nidulans* with relatively low doses of azoxystrobin also caused mitochondria to become more spherical and they often retracted from the hyphal tip and formed aggregates. Lower numbers of mitochondria were observed after treatment, and it is likely that these had burst. Some authors, working on animal cells, have reported that mitochondria swell upon the depolarisation of the potentiometric gradient across the inner mitochondrial membrane. This occurs when respiration is inhibited (Duchen, 1993). Given that FCCP and azoxystrobin both inhibit mitochondrial respiration, it seems likely that changes to mitochodrial morphology and mitochondrial fragmentation is a consequence of swelling following membrane depolarisation.

The observation that mitochondria retract from the hyphal tip and form aggregates following exposure to azoxystrobin may also be linked to changes in the availability of cellular ATP. Mitochondrial organisation within the fungal cell is probably controlled by the cystoskeleton, most likely through the binding of mitochondria to microtubules by the motor protein kinesin. Kinesin binds microtubules and transduces chemical energy into mechanical work as ATP is hydrolysed, to power polarised movement along microtubules (in this case, in the direction of the tip). It stands to reason, that if cellular ATP levels decrease as a consequence of mitochondrial dysfunction following treatment with a respiratory inhibitor, kinesin will no longer have an energy source available to maintain the position of mitochondria within the cell. Alternatively, morphological changes to mitochondria caused by membrane depolarisation and swelling, may lead to the disassociation of mitochondria from the microtubule network. These two possibilities are not mutually exclusive.

Treatment of *Bot. cinerea* with a low dose of azoxystrobin caused irreversible cell death within 50 s of treatment. Within 6 s, growth rate began to decrease and growth had stopped completely within 48 s. Decreases in membrane potential, measured using Rhodamine 123, began 13 s after treatment. Within 48 s, membrane potential in the apical region had decreased by 75%, and by 65% in the sub-apical region.

Although residual Rhodamine 123 fluorescence was observed, this was probably a consequence of background fluorescence from the dye, rather than the result of a lower potentiometric gradient across the mitochondrial membrane. The speed of uptake and activity strongly suggests that azoxystrobin enters fungal cells by diffusion. Given that azoxystrobin is a profoundly hydrophobic molecule of low molecular weight, it would be anticipated to diffuse freely through lipid membranes, and these results are unsurprising.

It was interesting to note that cell growth was affected 7 s before the mitochondrial membrane depolarised. A likely series of events might be as follows; a) azoxystrobin reaches target site, b) respiration is inhibited and membrane potential decreases, c) ATP production ceases, and d) cell growth stops as ATP is used up. However, the observed results do not fit this hypothesis and two possibilities exist. The first is that Rhodamine 123 fluorescence is saturated, and thus decreases in membrane potential are not immediately apparent. Although slight saturation of Rhodamine 123 was sometimes observed, this is an unlikely explanation because decreases in membrane potential in the sub-apical region (which was not saturated) followed the same time course as membrane potential in the apical region. Furthermore, when membrane potential did decrease, it did so very rapidly in both the apical and sub-apical mitcohondrial membranes. This suggests that 13 s after treatment mitochondrial membrane potential was suddenly and catastrophically affected. An alternative explanation is provided below.

Mitochondrial ATP synthesis is coupled to respiration through a chemiosmotic mechanism. Oxidation of substrate by the respiratory chain develops a proton electrochemical gradient. This provides the energy that drives proton flux through the F_1-F_0 ATP synthase, which includes a proton translocator as an integral part of the enzyme complex. Proton flux thus drives ATP synthesis. The potential contributes to the equilibrium state of the ATP synthase. As the equilibrium shifts, for example on depolarisation of the inner mitcohondrial membrane, by an alternative route for proton influx that bypasses ATP synthase, so the activity will reverse. Consequently, ATP synthase hydrolyses ATP and extrudes protons, leading to the maintenance of membrane potential until ATP is entirely consumed. Therefore, mitochondria can act as ATP consumers as well as producers (Ducehen et al., 1993). ATP synthase can therefore be viewed simply as an ATPase, which acts as a synthase by virtue of the mitochondrial membrane potential. When the inner membrane depolarises, the enzyme activity reverts to ATPase activity and consumes ATP and pumps out protons.

Removal of substrate (either carbon or oxygen) or exposure to inhibitors of respiration leads to the cessation of respiration, the process that maintains membrane potential. It may seem counter-intuitive that mitochondria could provide a primary mechanism of ATP depletion and may precipitate cell death when its function is compromised. However, this activity has been ascribed to the relative independence of mitochondria, possibly as a consequence of their prokaryotic origins: it is useful for mitochondria to consume ATP and conserve membrane potential because this prevents mitochondria from swelling. Clearly this is not in the interests of the cell, and many cells express an inhibitory protein, IF1, which inhibits ATP consumption by mitochondria (Walker, 1994). It is unclear whether this protein exists in filamentous fungi. The consumption of ATP by mitochondria, however, may account for the observation that decreases in growth rate precede depolarisation of the mitochondrial membrane.

Chapter 7

Live-Cell Two Photon Laser Scanning and Fluorescence Lifetime Imaging Microscopy of Filamentous Fungi

The definition of insanity is a man who does the
same thing twenty times, expecting different results.
Attributed to Benjamin Franklin

7.1 Introduction and Aims

7.1.1 Introduction

In the previous chapter fluorescence intensity images were acquired in order to analyse the biology of mitochondria in living filamentous fungal cells. Although intensity data acquired with the confocal microscope provided information regarding the spatial organisation and physiology of mitochondria, a variety of practical problems had to be overcome. These included:

- selecting appropriate mitochondrial markers and optimising imaging protocol to avoid photo- and cyto- toxicity.
- using the most selective markers (i.e. probes that labelled as few cellular components other than mitochondria as possible)

Two techniques that are of increasing interest in live cell imaging are two photon scanning microscopy (TPLSM) and fluorescence lifetime imaging microscopy (FLIM). The potential benefits conferred by these techniques over single photon confocal laser scanning microscopy (CLSM) acquisition are potential decreases in phototoxicity and photobleaching (TPLSM) and the acquisition of lifetime data which remains constant regardless of photobleaching and varies depending on the biophysical environment of the probe (FLIM).

The possibility therefore exists that photo- and cyto- toxicity can be reduced enabling extended (longer time course) or increased (slower scan speed) acquisition times. Cellular components of interest can be distinguished from other regions (inevitably stained by non-selective fluorescent probes) if the local environments are sufficiently distinct to elicit a difference in probe lifetime. The theoretical and practical implications of both techniques are discussed below.

7.1.2 Aims

Given the enormous potential TPLSM and FLIM offer for improvements in resolution and discrimination in live cell imaging of filamentous fungi, a series of experiments were designed to critically assess their usefulness in this regard. The aims of this research were to:

- compare TPLSM and CLSM of several organelle markers to critically assess the usefulness of TPLSM to live cell imaging of filamentous fungi
- compare live cell imaging of mitochondrial probes using TPLSM and CLSM
- optimise 2 photon excitation of several probes to enable acquisition of lifetime data
- compare the lifetimes of several fluorescent probes in cells of *Neurospora crassa*
- distinguish between 2 probes with similar emission spectra within the same cell on the basis of lifetime
- compare the lifetimes of the mitochondrial marker DASPMI in the mitochondria and plasma membrane of living *N. crassa* cells

7.2 Overview of Technology

7.2.1 Two Photon Scanning Microscopy

Molecular excitation by two-photon absorption confers several advantages over single-photon excitation and as a consequence holds great promise for vital imaging of biological systems using laser scanning microscopy. Fluorescence microscopy is frequently limited in its sensitivity and spatial resolution by background due to out of focus fluorescence. Two-photon excitation avoids this background fluorescence by virtue of its non-linear optical absorption characteristics, which almost completely limit the excitation to the high-intensity region at the focal point of the excitation laser. Since excitation of background fluorescence is avoided, no confocal spatial filter is necessary and, theoretically, TPLSM offers all the advantages of single-photon CLSM plus the absence of out of focus photobleaching and photodamage.

7.2.2 Principles of 2 Photon Excitation

Two-photon excitation refers to the simultaneous absorption of 2 photons of longer, but not necessarily identical, wavelengths that combine their energies to produce the molecular excitation of a fluor that would otherwise require a single photon with a shorter wavelength (Fig 7.1). The transition probability for simultaneous two-photon absorption depends on the square of the instantaneous light intensity. Consequently, very short pulses (typically 100 femtoseconds at 100MHz) are used to increase the average two-photon absorption probability for constant average incident power. The use of such short pulses is also of absolute importance in live cell imaging in order to permit image acquisition over reasonable time periods while using power levels that can be tolerated by biological systems.

Most of the properties that make TPLSM useful for fluorescence microscopy derive from the quadratic dependence (i.e. non-linear) of the excitation probability on the excitation light intensity. That is, in a focused excitation beam the excitation probability beyond the focal region falls off with the fourth power of the distance along the optical axis (z-direction). The obvious advantage is that only a limited region of the excited tissue is excited by the pulsed laser. As a result, out of focus bleaching and photodamage, and alignment through a detection pinhole (as is the case with confocal microscopy) is unnecessary because this spatial filter can be removed entirely. Conversely, with single-photon excitation, the entire sample is excited through the z-axis along the entire path of the laser beam and continuous photobleaching and photodamage can be caused in the specimen above and below the region of interest, even though they are not being imaged (Fig 7.2).

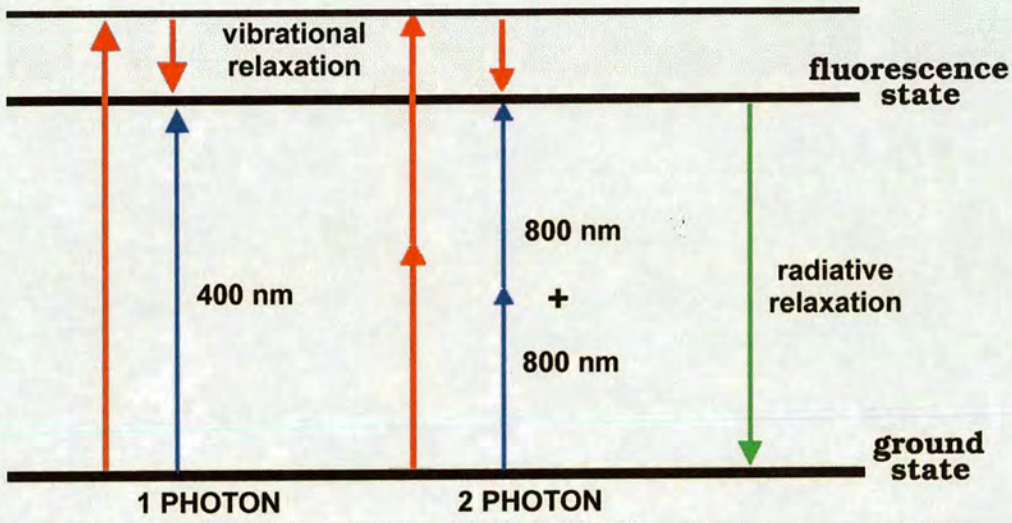

Figure 7.1: Principle of single photon and 2 photon excitation for CLSM and TPLSM respectively. Two photon excitation requires 2 photons of light of twice the wavelength as 1 photon continuous wave light to elicit the same excitation of the fluorophore from ground to fluorescence state. Relaxation events (caused, for example, by resonance energy transfer) reduce the energy level slightly, the remaining energy is released as fluorescence when the fluor returns to ground state. The wavelength of fluorescence emitted is identical following excitation with both the 400 nm single photon and 800 nm 2 photon laser.

The fact that only the region of the sample that the laser is focused on is being excited provides an alternative detection strategy for TPLSM. Furthermore, the longer wavelengths used are generally able to penetrate deeper into tissue than the shorter wavelengths used in single-photon excited confocal microscopy. Because the excitation light is already focused at the point of excitation, the confocal aperture is removed. Because all of the emitted light is in focus any light returning from the sample can be detected with no loss of spatial resolution. This can have a profound impact on the collection of light scattered by the sample, whereas in confocal microscopy this light would be blocked by the confocal aperture. In TPLSM any light returning from the sample is of value, is not blocked by an aperture, and can provide significant improvements. These modifications to detection and the potential improvements over CLSM are shown in Fig 7.3.

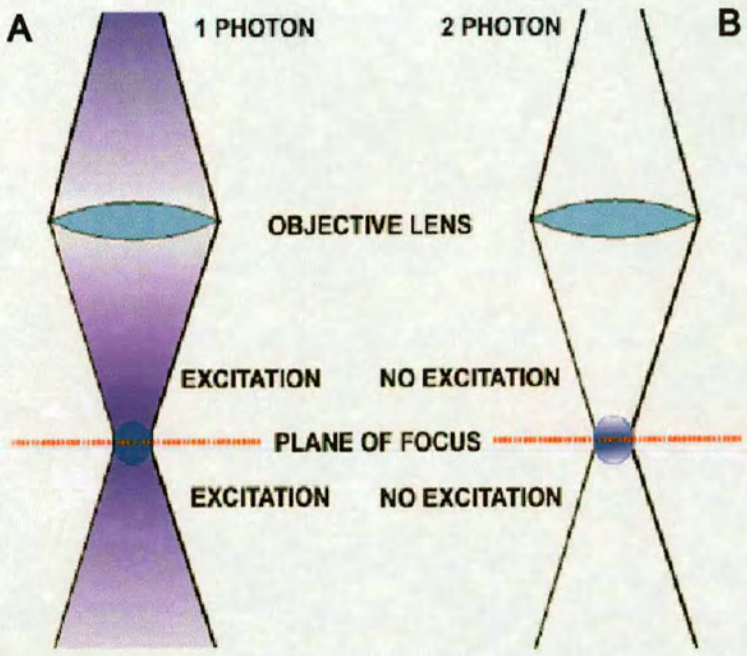

Figure 7.2: Comparison of laser irradiation of the sample in CLSM (A) and TPLSM (B). The area of irradiation is shown in purple. For single photon excitation a region above and below the plane of focus is constantly irradiated, whereas for 2 photon excitation only the region of focus is irradiated.

Two photon microscopy has been used in a number of live cell applications including the measurement of free calcium concentrations in motile cells (Williams et al., 1993) and cardiac myocytes (Piston and Webb, 1991), NADH concentrations as an indicator of cellular energetics (Piston et al., 1994), and to map the distribution of ligand-gated ion channels (Denk, 1994; Denk, 1993). Two photon microscopy of living filamentous fungi is, however, poorly represented in the literature. Given that plant pathogenic fungi are generally capable of invasion deep into host tissue, the advantages of TPLSM over CLSM (particularly increased penetration and the improvements in collection of scattered light) could provide a new opportunity to examine pathogen/host interactions in non-sectioned, living biological specimens.

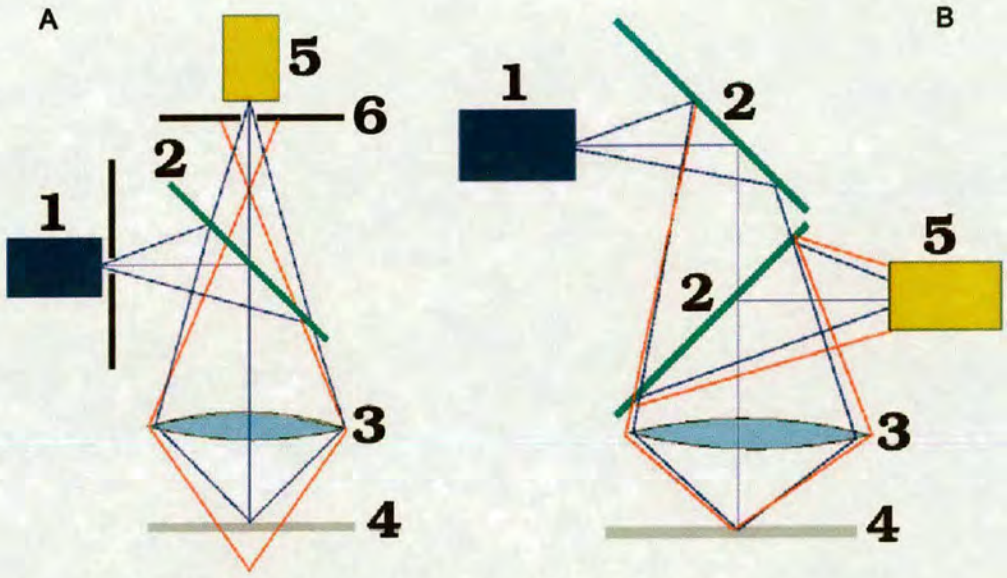

Figure 7.3: Comparison of light paths in CLSM (A) and TPLSM (B). Because all of the light for TPLSM is in focus the confocal aperture is removed. Detectors are placed closer to the sample to increase collection of the fluorescent light emitted. 1: laser (single photon continuous wave for CLSM, 2 photon pulsed infrared laser for TPLSM), 2: dichroic mirror, 3: objective lens, 4: sample, 5: photomultiplier tube, 6: confocal aperture (for CLSM only). In focus light is represented by blue lines, scattered (or out of focus) light is represented by red lines. Note that for TPLSM scattered light is still useful because it originates from the focal point of the sample.

7.2.3 Fluorescence Lifetime Imaging Microscopy

A variety of fluorescent probes are used in cell imaging applications to analyse organelle dynamics, the location of proteins and other cellular processes. Imaging of fluorescence intensity has generally not provided information about the biophysical environment of the organelle, protein or molecule that has been labelled, with few exceptions. Fluorescence lifetime imaging microscopy is an emerging technique that, in addition to position and intensity, also provides information regarding the average time a fluorophore remains in an excited state following excitation. Fluorescence decay has already provided information concerning the biophysical environment of a number of probes including GFP (Suhling et al., 2001), calcium markers (Szmacinski et al., 1994; Lakowicz et al., 1992), PH sensors (Hai-Jui Lin et al., 1998) and others. A distinct advantage lifetime imaging confers over intensity imaging is that the absolute lifetime is independent of probe concentration, photobleaching, light scattering and excitation intensity (Hermann et al., 1997).

Fluorescence lifetime imaging can be implemented in wide field (WF) as well as laser scanning microscopy (LSM). Several techniques are currently employed for the measurement of lifetime on bulk samples and can be divided into frequency-domain-based methods and time-domain-based methods (such as time-correlated single-photon counting or TCSPC). Of the two, time-domain-based methods are proving the more popular, and the most common method for lifetime measurement is TCSPC. In this case, fluorescent molecules are excited using a brief pulse of light after which the single photon emission is recorded. Typically a trigger pulse is synchronised with the excitation light source and starts a time-to-amplitude converter (TAC). The fluorescence emitted by the sample is detected by a photomultiplier tube (PMT), sent through a discriminator and used to stop the TAC. The output from the TAC is proportional to the time difference between the start and stop pulses. An analogue to digital converter (ADC) digitises the signal which is sent to a histogramming memory location. The process is repeated numerous times and a histogram of the fluorescence decay curve is constructed (Fig 7.4).

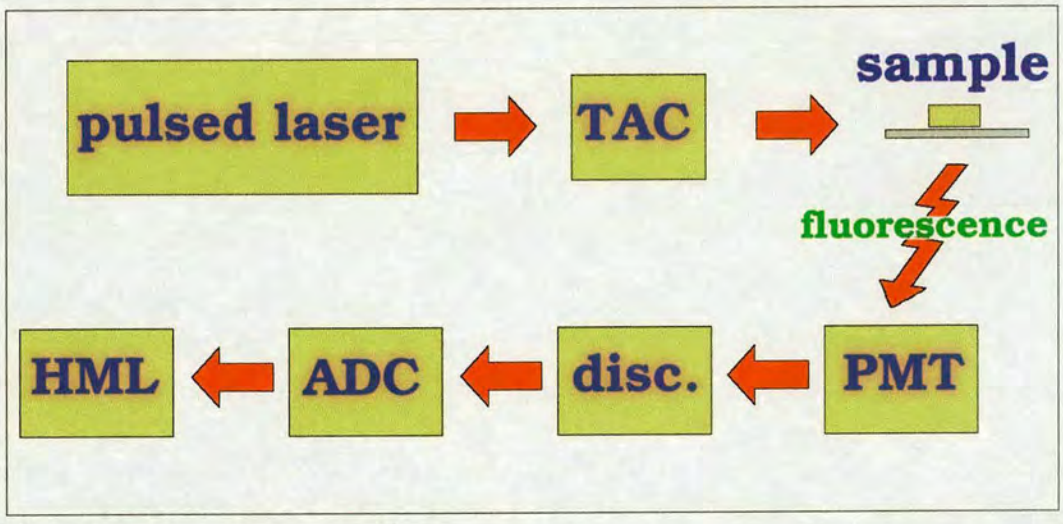

Figure 7.4: Cartoon showing a typical setup for FLIM. Excitation is done using a pulsed infrared (IR) laser, this pulse is synchronised with a time-to-amplitude converter (TAC), sample fluorescence is captured with the photomultiplier tube (PMT) and sent through a discriminator (disc.) which stops the TAC. The output is digitised using an analogue to digital converter (ADC) and the digitised signal is stored in the histogramming memory location (HML).

Data acquisition time can be significantly improved if pulsed excitation is employed in combination with time-gated detection techniques. Here, one or more detectors are used that can either be rapidly switched on and off, or that can have their output digitally analysed in several separate time windows following each pulse.

Several benefits make FLIM a potentially valuable technique in conjunction with, or instead of, LSM. These include:

- discriminating between different fluorophores with similar or overlapping emission spectra, providing their lifetimes are sufficiently different; e.g. FITC and chlorophyll auto-fluorescence have been successfully separated on the basis of lifetime in the algae *Gymnodinium nagasakience* (Draaijer et al., 1995).

- quantifying concentrations of molecules or ions within cells. Differences in lifetime of fluorescent probes and fluorescent proteins as a result of binding with specific ions (e.g. calcium) or other proteins provides a means to quantitatively assess the concentration of these molecular species in living cells (e.g. Lakowicz et al., 1992; Draaijer, 1995).

- discriminating between different cellular regions based on lifetime differences of probes in dissimilar biophysical environments (Suhling et al., 2001; Murata et al., 2000)

7.3 Results

7.3.1 Overview of Results

In Chapter 6, a variety of fluorescent probes were used to explore mitochondrial morphology, spatial location and physiology in living fungal cells. The effects of the mitcohondrial inhibitors FCCP and azoxystrobin were also investigated. Several limitations associated with imaging using CLSM presented themselves, including: differentiating between fluorescence emission from dyes with similar emission spectra when they were used to label the same cell; differentiating between regions of interest and non-selectively labelled regions within the cell (in this case mitochondria and plasma membrane), and developing imaging techniques to minimise the deleterious effects of photobleaching and phototoxicity.

Two photon LSM offers the opportunity to tune the excitation source laser to a specific wavelength anywhere in the region of approximately 720 to 980 nm, which would be anticipated to improve fluorescence from fluorophores and therefore enable a reduction in the laser power required and/or a reduction in the concentration of dye required for effective labelling. Furthermore, because two photon excitation delivers a non-continuous beam of smaller volume, photobleaching of out of focus regions of the cell and potential decreases in the level of light that reach the sample would be anticipated to reduce photodamage.

Initially, TPLSM was performed on living cells of *Neurospora crassa* to assess the usable tuning range of the laser (using the continuous wave equivalents of UV excitation and 475 nm excitation). Long excitation wavelengths were found to be particularly damaging to cells expressing GFP-targeted to nuclei. Shorter excitation wavelengths were found to improve cell viability. Following this, TPLSM was assessed for the imaging of Rhodamine 123. Again, long wavelengths were found to significantly damage cells, whereas shorter wavelengths were no more damaging than was observed using CLSM (described in Chapter 6). Two photon excitation of Rhodamine 123, DASPMI, GFP-targeted to mitochondria and FM1-43 was achieved.

No improvements in cell viability were observed for TPLSM compared with CLSM. Furthermore, TPLSM offered no improvement in resolution. However, images of comparable quality to CLSM were acquired, and excitation wavelengths and acquisition protocols were optimised for the live-cell imaging of filamentous fungi with TPLSM.

Techniques employed for TPLSM were utilised for FLIM of filamentous fungi. Unlike with fluorescence intensity imaging, fluorescence lifetime remains unaltered despite shifts in focus and dye photobleaching. Fluorescence lifetime does, however, vary as a consequence of local environment and many fluorescent probes have a characteristic lifetime. Fluorescence lifetime imaging microscopy was therefore assessed for its usefulness in the study of fungal mitochondria and as a potential technique to further study the effects of fungicides and inhibitors on fungal cells.

Initially, a lifetime standard for GFP (fluorescent beads labelled with GFP) was imaged. The lifetime measurements acquired were similar to those recorded for *N. crassa* cells with nuclear-targeted GFP. Following this, lifetime measurements were recorded for the mitochondrio selective probe Rhodamine 123. Because FLIM provides a unique opportunity to distinguish between probes based on their lifetime characteristics as opposed to their emission wavelengths, cells labelled with both GFP and DASPMI were imaged. It was possible to distinguish between both dyes in the same cell based on differences in their fluorescence lifetimes.

Fluorescence lifetime is variable depending on the local environment of the dye. Consequently, lifetime imaging of DASPMI was performed in an attempt to distinguish between membranes with high electro-chemical gradients and membranes with low or no membrane potential. Spatial resolution is much reduced for FLIM compared to CSLM or TPLSM. However, mitochondrial membranes and the plasma membrane could be distinguished in the same cell on the basis of differences in fluorescence lifetime between regions of the cell.

7.3.2 Live-Cell TPLSM of Filamentous Fungi

Irradiation of cells with UV light can be very damaging to live cells. Furthermore, UV lasers are relatively expensive (approximately 30,000 GBP) and produce a lot of heat which can place an inhibitively high load on laboratory air conditioning or must be removed by a dedicated water cooling system. Consequently, the possibility of exciting UV dyes at less damaging longer wavelengths (e.g. 730 nm for TPLSM compared with 370 nm for CLSM) without the need to purchase a specific laser, is an attractive proposition. Although two photon lasers are currently more expensive than continuous wave lasers typically employed for fluorescence imaging (in excess of 100,000 GBP), excitation across a spectrum from 720 nm to above 960 nm is theoretically possible and could negate the requirement for a host of wavelength-specific continuous wave lasers.

Initially, the UV-excited probe Calcafluor was excited using a pulsed laser tuned to 730 nm (Fig 7.5a). Strong fluorescence intensity was observed in cell walls of spores and hyphae of *N. crassa*. The ti:sapph laser used in this study could be tuned, with the use of a pumped oscillator, to wavelengths in excess of 1.3 μm. However, water absorption of light above 950 nm required the laser cavity to be purged with nitrogen, and wavelengths above 1 μm require the fitting of specialised optics. Consequently, the longest wavelength used was 950 nm. Excitation of FM 4-64, which typically requires a 514 nm argon-ion laser for continuous wave excitation, in *N. crassa* was successfully achieved at this wavelength (Fig 7.5b).

Excitation of nuclear-targeted GFP in *N. crassa* at 950 nm caused cells to burst after 12 s of imaging (Figs 7.6). Reducing the laser wavelength to 880 nm conferred no improvement (Fig 7.7) but a further reduction to 810 nm was found to be less damaging and enabled extended imaging time-courses to be performed (in excess of 5 min at 6 s intervals). However, fluorescence signal from cells was low despite increasing the laser power and fine-tuning the excitation wavelength. Increases in signal were therefore only possible by increasing the gain on the photomultiplier tubes, which caused a decrease in signal to noise ratio and led to the collection of images with increased background noise (Fig 7.8).

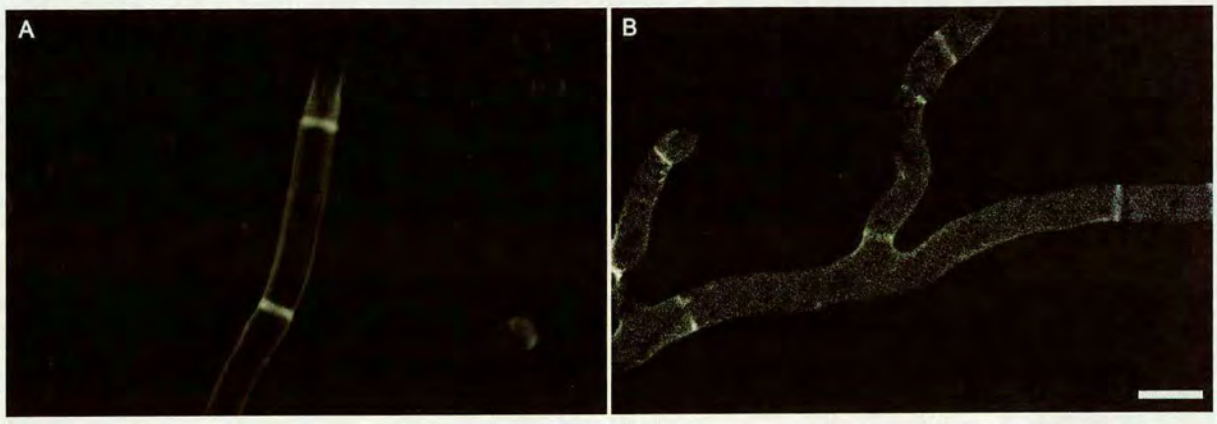

Figure 7.5: Dye excitation at both ends of the standard tuning range of the Ti:sapph laser was possible. (A) Excitation of the UV-excited dye Calcafluor was possible with the two photon laser tuned to 730 nm. Irradiation with a 370 nm UV laser causes significant damage to live cells, which may be avoided with the longer wavelengths used by two photon lasers. (B) At the furthest end of the standard tuning range, 950 nm, excitation of FM 4-64 was possible. Imaging of FM 4-64 using CLSM typically required a 514 nm argon-ion laser. These images indicate that a single, tunable two photon laser can excite dyes that would otherwise require a variety of wavelength-specific continuous wave lasers. Bar = 10 μm

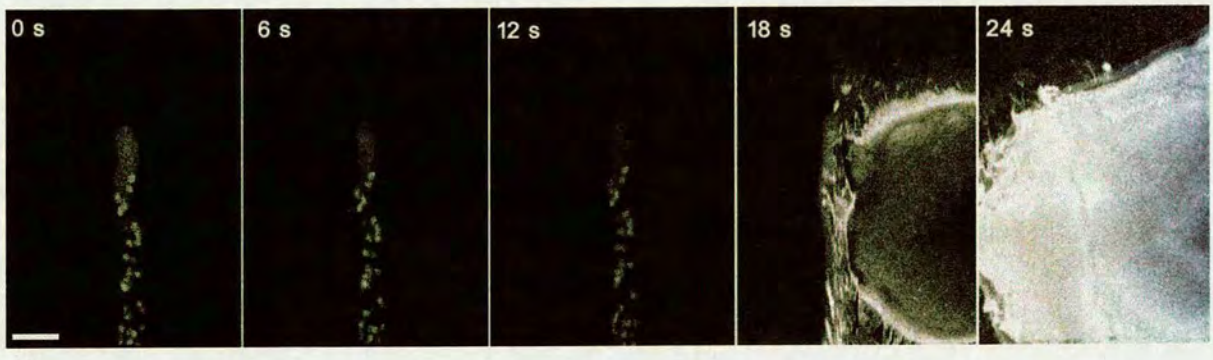

Figure 7.6: Excitation of probes at long wavelengths in cells of *N. crassa* caused a high degree of damage to cells through specimen heating. In this case, cells expressing nuclear-targeted GFP were observed to burst after 3 scans at 6 s intervals. Background noise was higher than observed using CLSM, probably due to saturation of the fluor. Therefore, fluorescence signal could only be improved by increasing amplifier gain of the photomultiplier tubes, which decreased the signal to noise ratio. Bar = 10 μm

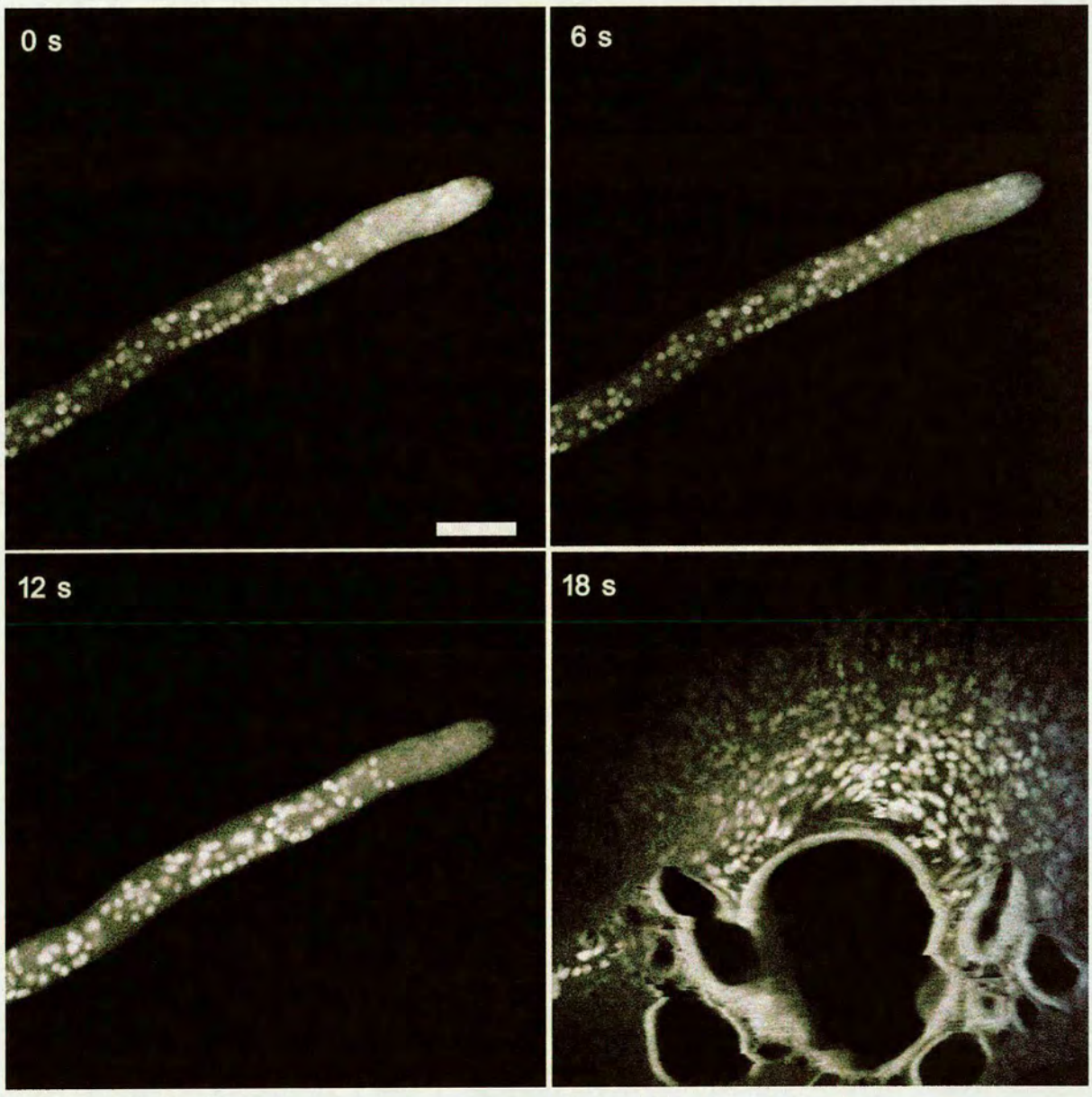

Figure 7.7: Despite reducing the wavelength of the pulsed laser to 880 nm, no improvement in cell viability was observed. In this case, an image was acquired at exactly the same time the cell burst and nuclei were visible exiting the cell and entering the medium immediately surrounding the burst tip. Bar = 10 μm

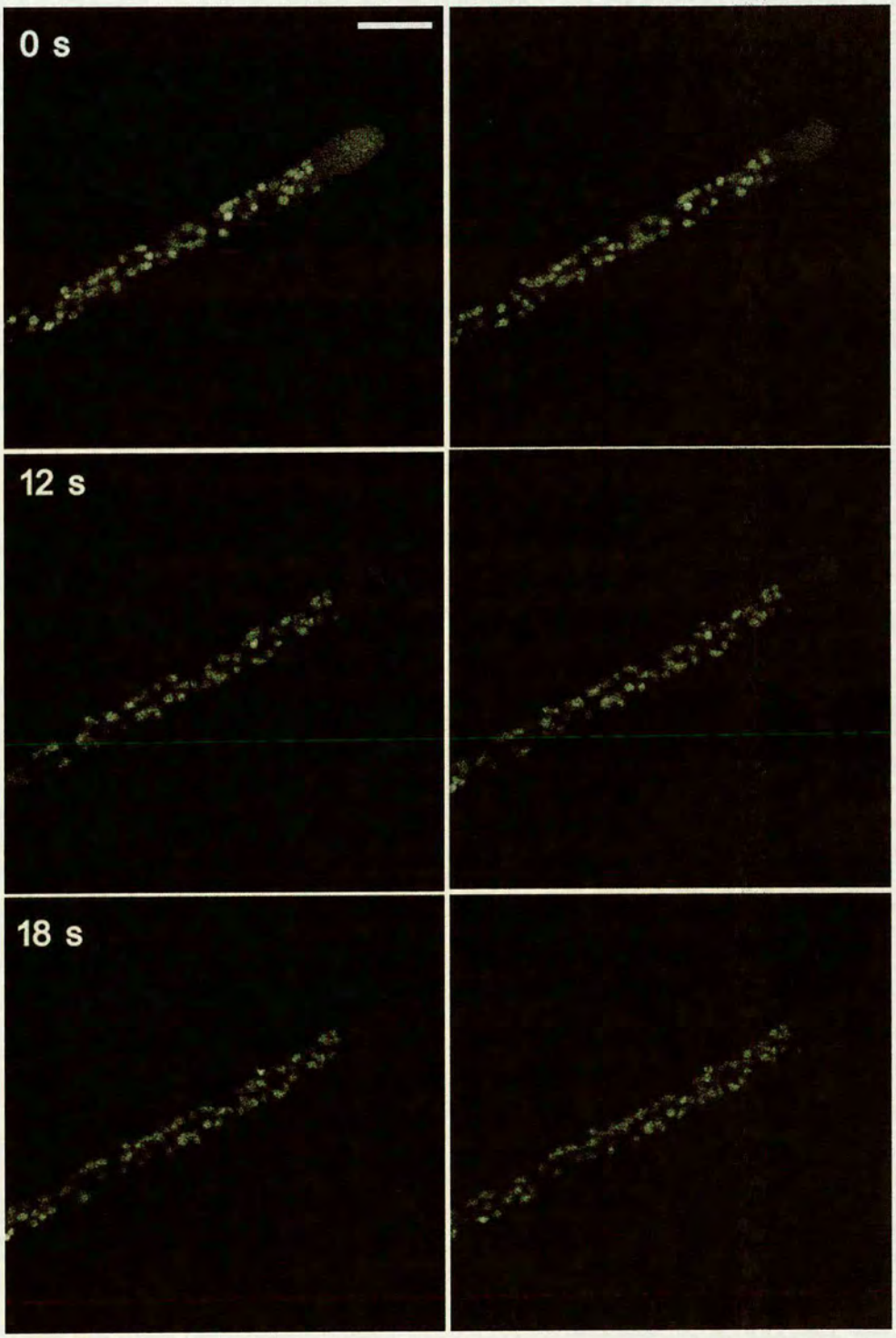

Figure 7.8: A further reduction of wavelength, in this case to 810 nm, improved cell viability dramatically. A time-course of acquisition was possible for more than 5 min at 6 s intervals and growth rate was similar to that recorded using the 488 nm laser for CLSM.
Bar = 10 μm

Of primary interest to this research was TPLSM of fungal mitochondria in living fungal cells. Excitation of Rhodamine 123 was performed at a series of wavelengths. Rhodamine 123 is typically excited at 488 nm using CLSM. Although excitation cross-spectra for fluorescence probes can vary significantly for one photon and two photon excitation, the dye was initially excited at 900 nm, which coincided with a shoulder on the one photon excitation cross-spectra (of 450 nm). The consequences of 900 nm excitation to *N. crassa* cells were similarly catastrophic to those recorded in GFP-labelled cells. The cell burst within 16 s of imaging at 4 s intervals (Fig 7.9). The wavelength was reduced to 830 nm, which led to improved cell viability. However, cell morphology was altered after 12 s (3 scans at 4 s intervals) and hyphal tips narrowed indicating that hyphae were stressed (Fig 7.10). Growth rate was unaffected. Further reduction of the wavelength, to 780 nm, enabled the acquisition of high quality images without causing cell stress. Hyphae did not narrow as they had done at 830 nm excitation, fluorescence intensity and signal to noise ratio were also high. The dye's dynamic range was also preserved and photobleaching was not observed (Fig 7.11).

Following this, several other mitochondrion-selective probes of interest were imaged using TPLSM (Fig 7.12). Excitation of DASPMI in cells of *N. crassa* was optimal at 840 nm, although the hyphal tip was observed to narrow after 16 s (4 scans at 4 s intervals). Mitochondrion-targeted GFP was successfully excited at 820 nm. Fluorescence intensity was lower than continuous wave excitation with the 488 nm laser, but no photodamage was observed after 36 s (9 scans at 4 s intervals). Excitation of FM1-43 in *N. crassa* was only possible at extended wavelengths (950 nm). After 20 s (5 scans at 4 s intervals) mitochondria began to retract from the tip and apical branching commenced. Apical branching is symptomatic of hyphal stress, and growth rate was reduced shortly after irradiation commenced.

Two photon LSM offers a theoretical improvement in resolution when imaging deep into tissue, because the longer wavelengths provided by the pumped ti:sapph laser are able to penetrate further than shorter wavelengths form continuous wave lasers. The theoretical maximum resolution for both techniques is comparable. Hyphal tips of *N. crassa* labelled with Rhodamine 123 were imaged at a resolution of 1024 lines, electronic zoom 4 with a 100x objective (1.4 NA) using CLSM (488 nm argon-ion) and TPLSM (780 nm pulsed ti:sapph). Although the images obtained were similar in terms of resolution, after 5 s continuous scanning, imaging with TPLSM had begun to photobleach the dye and stress the cell (the cell began to narrow at the tip). These effects were not observed for CLSM (Fig 7.13).

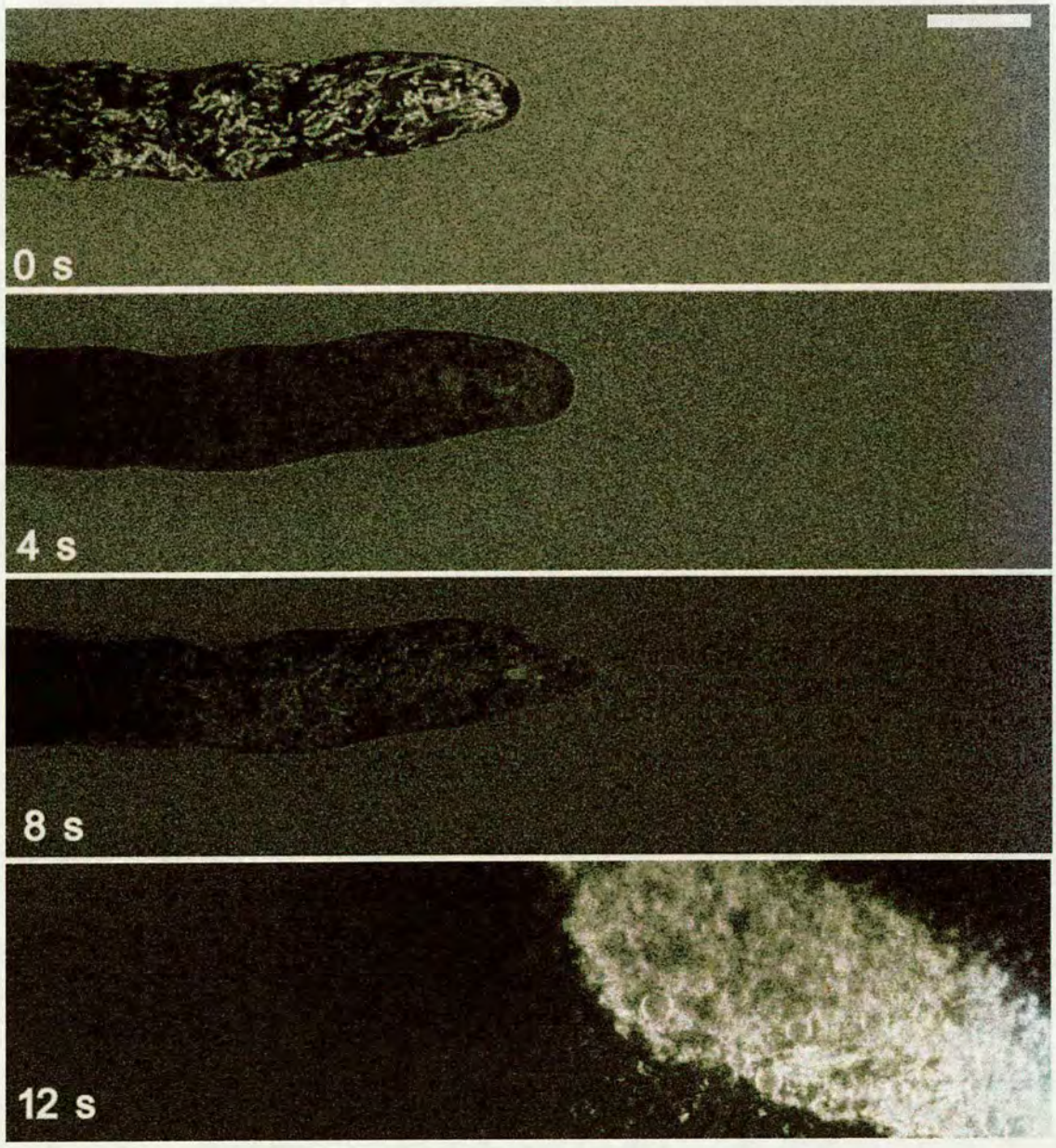

Figure 7.9: Excitation of Rhodamine 123 at 900 nm caused *N. crassa* cells to burst within 12 s of imaging (4 scans at 4 s intervals). Similar effects were observed in *N. crassa* cells expressing nuclear-targeted GFP. Long wavelengths, in the near infrared, appeared to have a significantly damaging effect on fungal cells. This was most likely a consequence of the sample being heated by the infrared beam, causing the cytoplasm to boil and the cell to burst. Bar = 10 μm

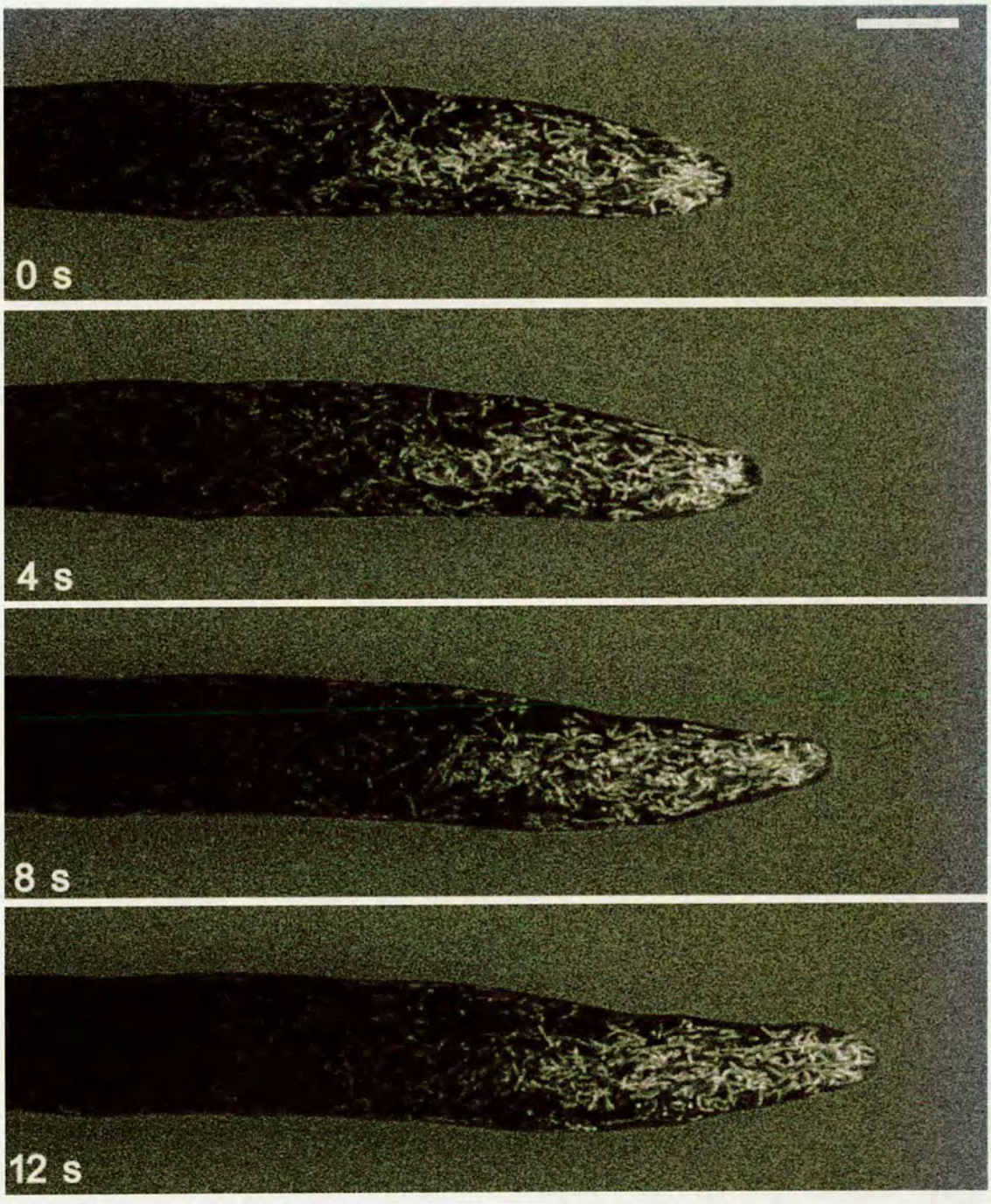

Figure 7.10: Reduction of the excitation wavelength from 900 nm to 830 nm improved cell viability dramatically. However, although growth rate was unaffected during this time period (12s, 4 scans at 4 s intervals), the hyphal tips were observed to narrow, which is symptomatic of stress. Live-cell imaging studies of organelle dynamics or the inhibitive effects of pharmaceutical and fungicidal agents would be difficult to interpret in cells which were displaying signs of stress. Bar = 10 μm

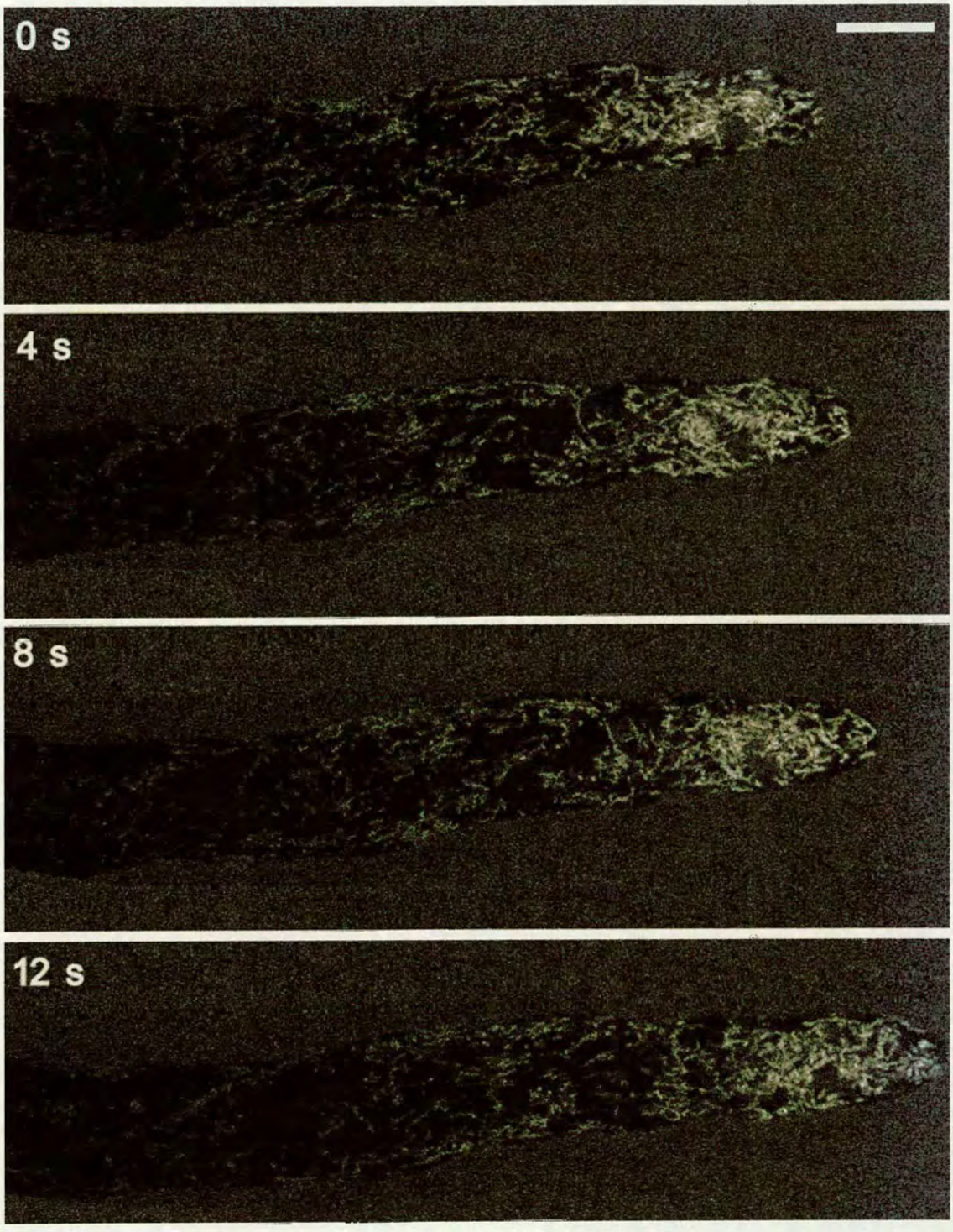

Figure 7.11: Further reduction of the excitation wavelength to 780 nm enabled extended imaging time-courses to be performed with no observable photodamage. Growth rate remained constant and similar to those observed in CLSM and neither phototoxic effects nor dye photobleaching were observed. Note that, as with CLSM, a gradient of intensity from the tip to the sub-apical region of the hyphal cell was present indicating variations in mitochondrial activity along the hypha. Bar = 10 μm

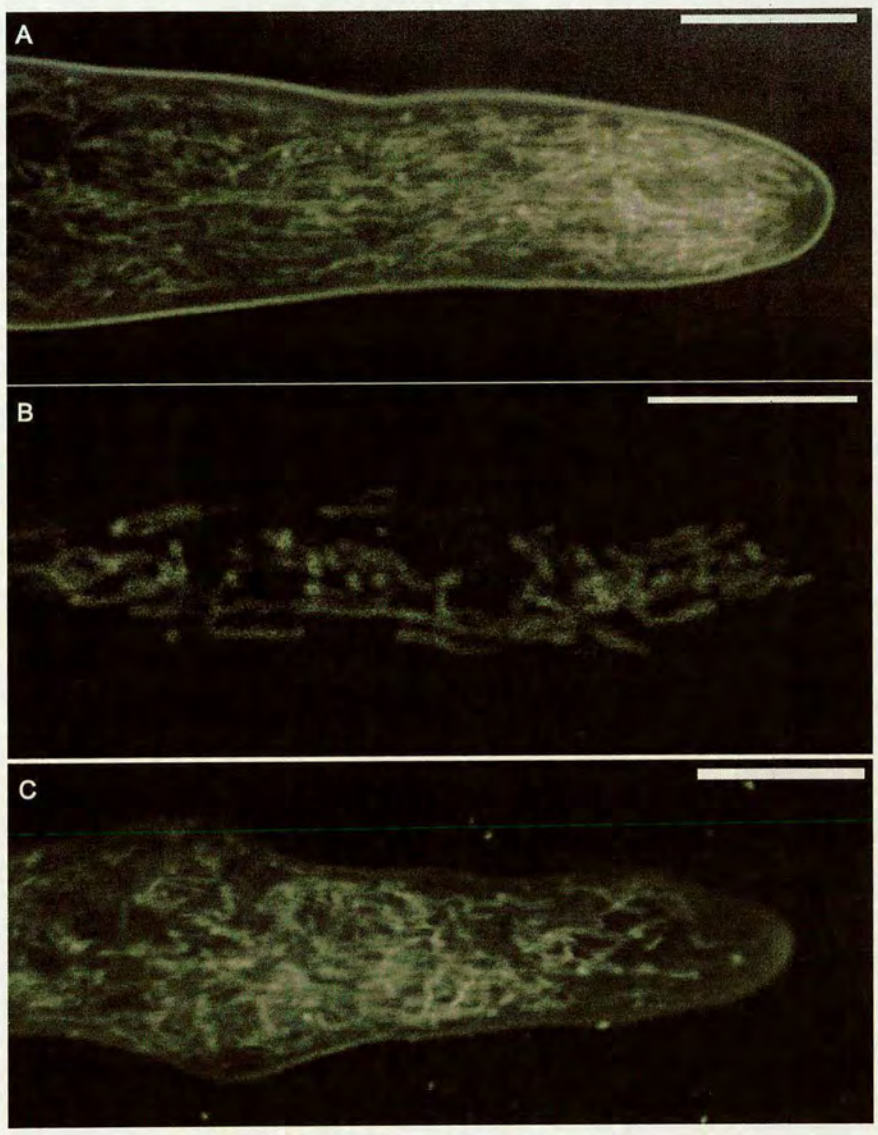

Figure 7.12: TPLSM was performed on a further 3 mitochondrion-selective probes which were successfully imaged using CLSM, described in Chapter 6. (A) *Neurospora crassa* cells labelled with DASPMI showed signs of stress after 12 s (4 scans at 4 s intervals), with the hyphal tip narrowing. This was consistent with the results obtained for Rhodamine 123. However, the extended wavelength was necessary for optimal excitation of the dye. (B) Mitochondrion-targeted GFP was imaged in *A. nidulans* at 820 nm. Fluorescence intensity was relatively low, but no deleterious effects from the imaging process were observed. (C) Excitation of FM1-43 in *N. crassa* cells required a longer wavelength than was necessary for excitation of the other mitochondrion-selective probes imaged (950 nm). Although fluorescence intensity was relatively high, mitochondria were observed to retract from the tip and apical-branching had commenced after only 20 s (5 scans at 5 s intervals). Based on previous observation, it is surprising that these cells did not burst, which suggested FM1-43 may have been less phototoxic than certain other probes. Bars = 10 μm

Figure 7.13: Comparison of resolution of (A) CLSM (488 nm argon ion) and (B) TPLSM (780 nm ti:sapph) at 1040 line resolution, electronic zoom 4 with a 100x (1.4 NA) objective in hyphal tips of *N. crassa* labelled with Rhodamine 123. Resolving power is similar for both techniques, but note that (B) TPLSM caused the dye to photobleach more rapidly than (A) CLSM, and the hyphal tip had narrowed. Bar = 10 μm

7.3.3 Live-Cell FLIM of Filamentous Fungi at High Temporal Resolution

From the previous section, TPLSM appeared to offer no significant benefits over CLSM for the imaging of living fungal hyphae under the experimental conditions used. However, the recent commercial availability of two photon FLIM presented the opportunity to collect lifetime data from live cells, as opposed to intensity data as recorded in Chapter 6 and in the previous section. An obvious prerequisite for two photon FLIM is the excitation of dyes with a time-synchronised 2 photon irradiating beam. Furthermore, to achieve high temporal resolution a strong signal is of high importance, to enable a single fast scan of the region of interest.

Current hardware limitations (associated with the coupling of BioRad and Nikon hardware) imposed a maximum capture resolution of 256 x 256 pixels. Furthermore, because light collection and infrared transmission through high magnification objectives (e.g. 100x) is less than for lower magnification objectives (e.g. 40x) further constraints were placed on magnification and spatial resolution. Assessment of a range of objectives, laser powers and wavelengths was performed prior to the collection of the following lifetime images. However, in every case the maximum laser power that the cell could survive for over 5 s was used, in conjunction with a 40 x water immersion objective (1.2 NA), 256 x 256 box size and identical dye concentrations to those for CLSM and TPLSM. In each case, the sample was scanned once.

Initially, a lifetime standard was imaged, consisting of a slide of 5 μm beads intensely labelled with GFP which had a known lifetime of 2.2 ns. Two photon excitation was performed at 820 nm. Despite a relatively low photon count (less than 100 photons), a lifetime in the range of 2 to 2.5 ns was recorded (Fig 7.14) and indicated that the equipment was performing optimally.

Following this, *N. crassa* cells expressing nuclear-targeted GFP were imaged using 830 nm two photon excitation. Although spatial resolution was considerably lower than for TPLSM or CLSM, nuclei were clearly resolved. Prior to measuring lifetime, the image was binned once (2x2 binning) to improve the signal to noise ratio and increase the fluorescence signal. Only nuclei were observed in the lifetime map obtained, and lifetime was generally in the

region of 2 to 2.5 ns. Lifetime from a region of the cell containing nuclei was graphed; this confirmed that average lifetime was approximately 2.1 ns (Fig 7.15). This was similar to the lifetime measurement for the GFP-labelled beads and provided confidence that lifetime measurements from living cells were correct. Small discrepancies could be accounted for by the fact that fluorescence lifetime is different depending on the environment of the probe.

Of primary interest to this research was: (a) spatial resolution of mitochondria using FLIM; (b) fluorescence lifetime measurement of mitochondrion-selective probes, (c) differentiation of 2 fluorescent probes with similar excitation maxima within the same cell, and (c) differentiation of charged and non-charged membranes within the same cell based on differences in lifetime of a single dye.

Initially, the mitochondrion-selective probe Rhodamine 123 was imaged at 780 nm. Mitochondria were resolved, albeit poorly, and were visible in greater abundance at the hyphal tip. This was consistent with TPLSM and CLSM imaging. A lifetime map of *N. crassa* cells labelled with Rhodamine 123 yielded a lifetime measurement in the region of 1.5 ns for mitochondria at the hyphal tip. Background fluorescence, from dye in the surrounding media, had a longer wavelength than Rhodamine 123 which had accumulated in mitochondria, of 2 ns or greater. A region of the lifetime map was graphed, and supported the conclusion that mitochondrion-associated Rhodamine 123 had a lifetime of approximately 1.5 ns in hyphal tips, and dye in the media had a longer wavelength of 2 ns or higher (Fig 7.16).

Following this, cells of *N. crassa* expressing nuclear-targeted GFP were also labelled with the mitochondrion-selective probe DASPMI. Both probes have emission maxima close to 530 nm and cannot be spectrally resolved using TPLSM or CLSM because emission filters are insufficiently narrow. Excitation was performed at 840 nm, which represented a compromise between the optimal excitation wavelengths determined for both probes using TPLSM. As expected, mitochondria and nuclei could not be spatially resolved on the basis of intensity using the FLIM detectors (although they were resolved using CLSM which had far superior spatial resolution, see Fig 6.14). However, when lifetime was calculated and a lifetime map processed, nuclei were distinguishable with a lifetime of approximately 2.5 ns, compared with a shorter lifetime of approximately 1.2 ns for DASPMI. A region of the lifetime map was graphed and showed a series of peaks between 2 and 2.5 ns (which represented GFP in nuclei) and a second series of peaks between 1 and 1.5 ns which represented lifetime from DASPMI (Fig 7.17).

Finally, cells of *N. crassa* labelled only with DASPMI were imaged using FLIM. In Chapter 6, DASPMI was shown to cause more intense non-selective labelling of the plasma membrane compared with Rhodamine 123. Here, lifetime measurements were compared for DASPMI which had accumulated in the charged mitochondrial membrane compared with dye which had accumulated in the plasma membrane. These regions of the cell were anticipated to have distinct local environments which might cause variations in the dye's lifetime. Fluorescence intensity, recorded using the FLIM detectors, enabled spatial resolution of the plasma membrane, septum and spherical mitochondria within the cell. Lifetime for this region was calculated and a lifetime map drawn. Lifetime was distinct for all 3 regions of the cell; DASPMI in the plasma membrane had the longest lifetime (approximately 2.5 ns), followed by dye in the septum (approximately 1.7 ns), and dye which had accumulated in the mitochondria had the shortest lifetime(approximately 1.2 ns). These observations were supported by the lifetime graph plotted for a region of the cell comprising septum, plasma membrane and mitochondria (Fig 7.18).

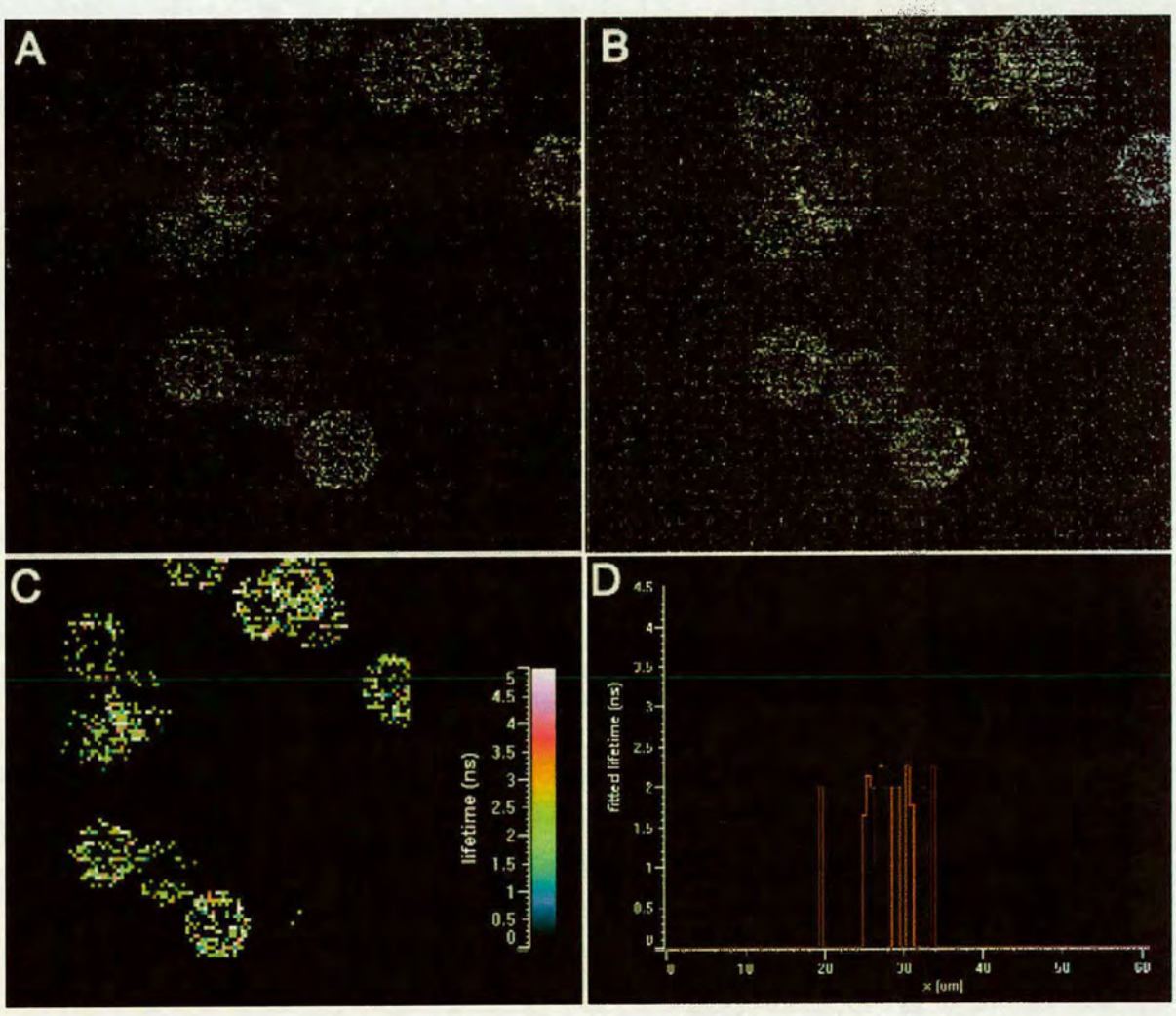

Figure 7.14: Initially lifetime was measured in GFP-labelled beads with a known lifetime of 2.2 ns. Lifetime gates were set so that the first gate provided an intense signal (A) and each subsequent gate provided intensity of approximately half the previous gate. Consequently, fluorescence signal was lowest in gate four (B). Three groups of beads were spatially resolved in each of the four gates. The image was binned, and a lifetime map was constructed from the information provided by the time gates and indicated that the beads had a lifetime of approximately 2.5 ns (C). Note that following binning, no background fluorescence was observed. A lifetime graph was plotted from these data and confirmed that lifetime for the GFP beads was between 2 and 2.5 ns (D).

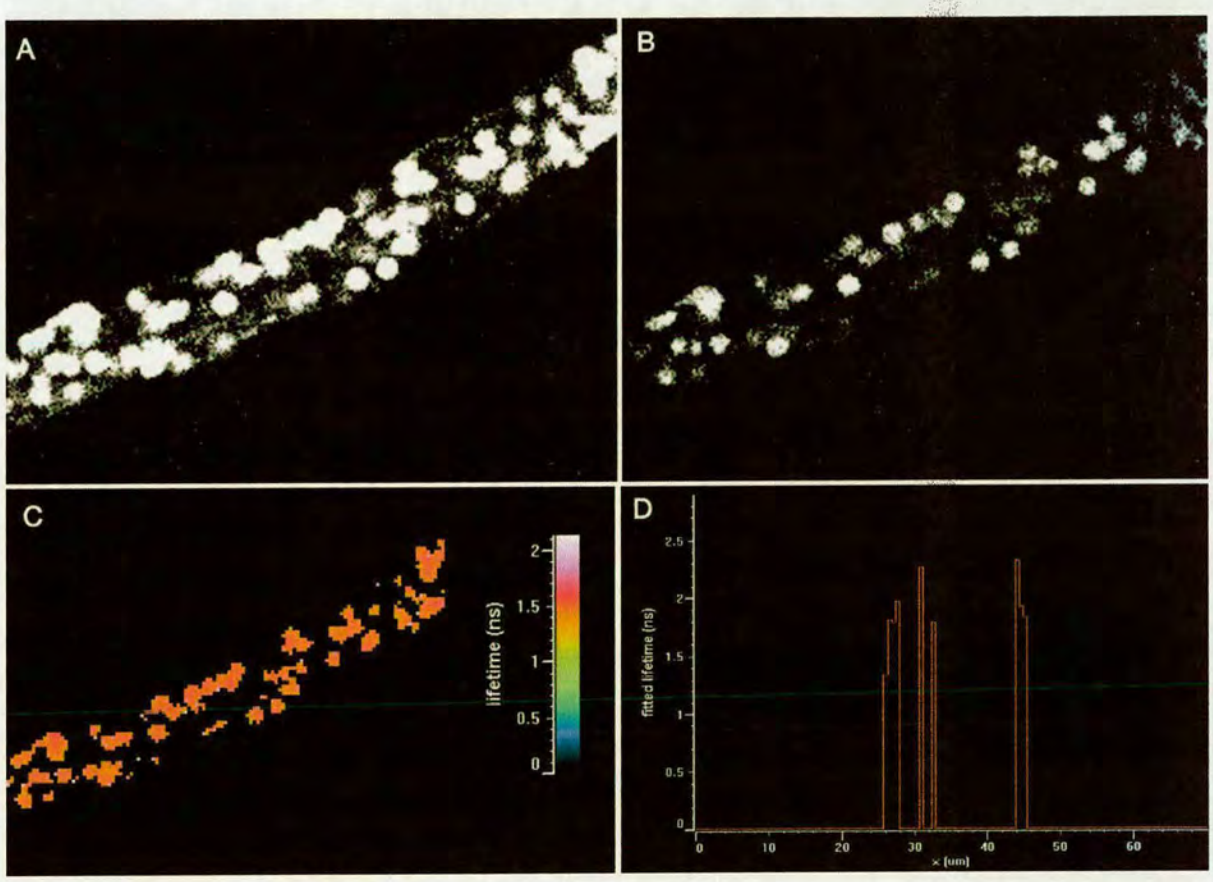

Figure 7.15: Lifetime was measured in cells of *N. crassa* expressing nuclear-targeted GFP. This was done for comparison between lifetime in live cells and inanimate beads, and to ensure that lifetime measurements were similar. Lifetime gates were set so that the first gate provided an intense signal (A) and each subsequent gate provided intensity of approximately half the previous gate. Consequently, fluorescence signal was lowest in gate four (B). The cell was spatially resolved, and an abundance of spherical nuclei were observed within the cell. The image was binned, and a lifetime map was constructed from the information provided by the time gates. Fluorescence lifetime values had a wider range in GFP in nuclei of live cells compared with GFP-labelled beads. The average lifetime of nuclear-targeted GFP was approximately 2 ns (C). A lifetime graph was plotted from these data and confirmed that lifetime for nuclear-targeted GFP was between 1.5 and 2.5 ns, with the majority of recorded lifetime falling within the range of 2 to 2.5 ns (D). This was very similar to the lifetime recorded in GFP-labelled beads.

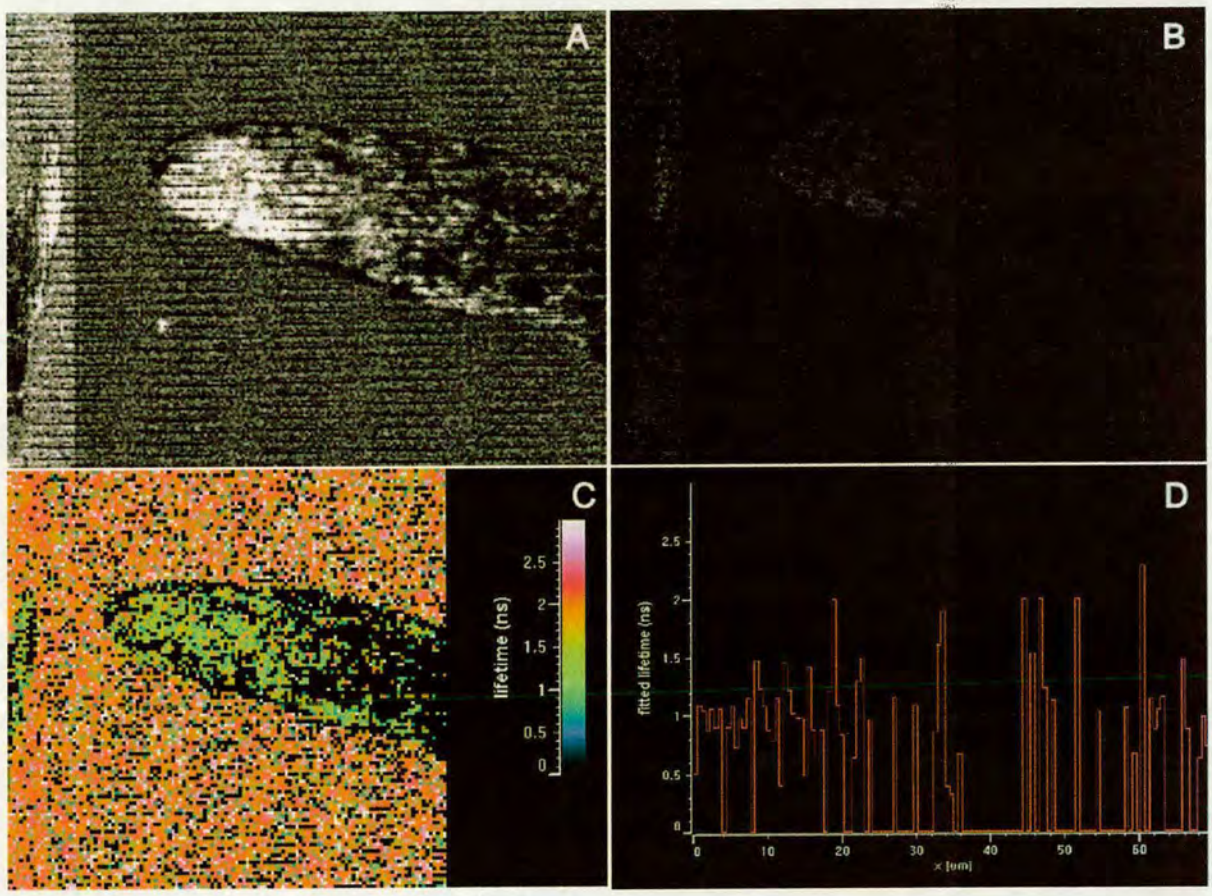

Figure 7.16: Fluorescence lifetime imaging of mitochondrion-selective probes was of primary interest to this research. Here, cells of *N. crassa* labelled with Rhodamine 123 were imaged. Lifetime gates were set so that the first gate provided an intense signal (A) and each subsequent gate provided intensity of approximately half the previous gate. Consequently, fluorescence signal was lowest in gate four (B). The cell was spatially resolved and a group of mitochondria were observed at the tip, although individual mitochondria were not resolved. Background fluorescence was high in the intensity images from all four time gates. Following binning, a fluorescence lifetime map was constructed and indicated that Rhodamine 123 in mitochondria had a shorter lifetime (1.5 ns) compared with Rhodamine 1234 in the surrounding media (2 ns and higher) (C). A lifetime graph was plotted from these data and confirmed that lifetime for mitochondrion-associated Rhodamine 123 was in the range of 1 to 1.5 ns, and extra-cellular Rhodamine 123 had a longer wavelength of above 2 ns (D).

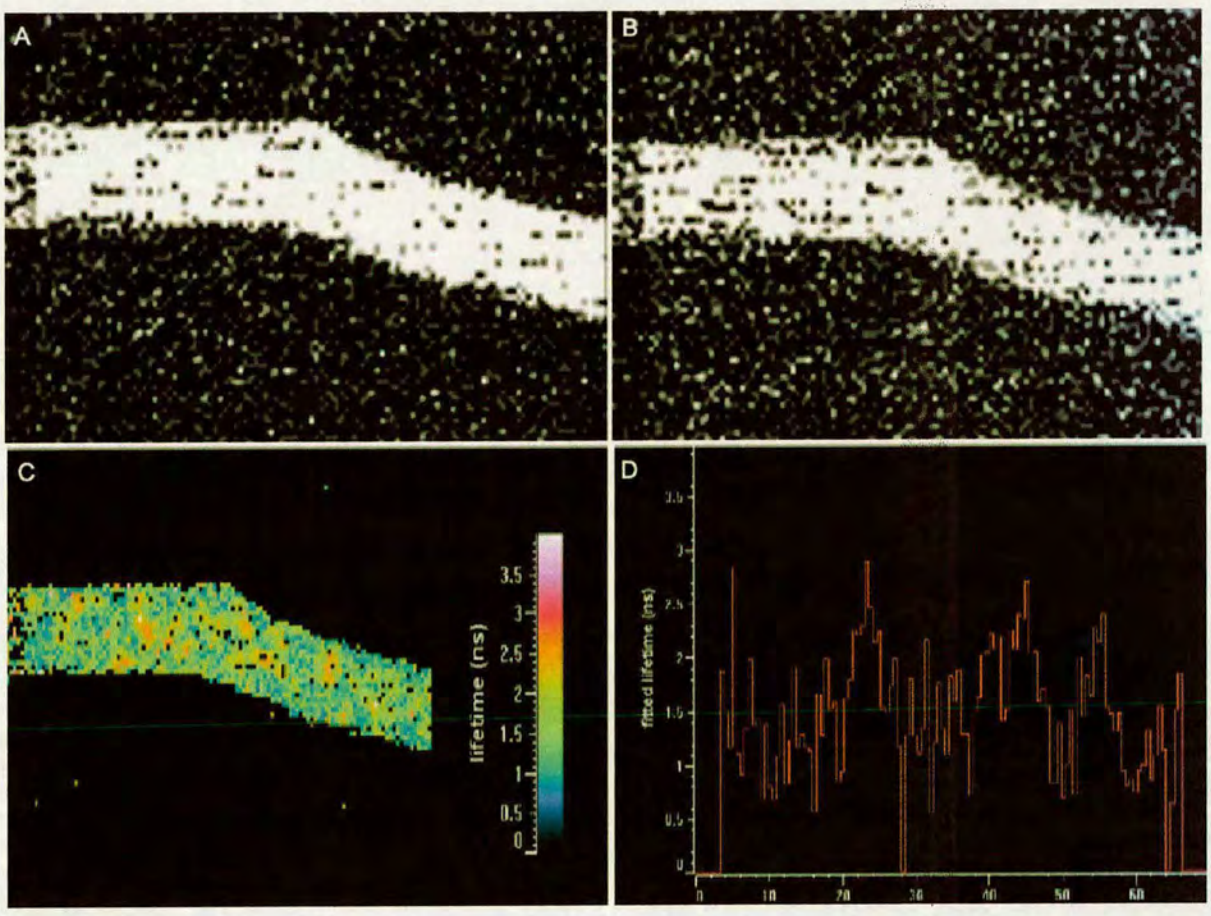

Figure 7.17: The fluorescent probes DASPMI and GFP have similar emission wavelengths and could not be distinguished using emission filters. Here, cells of *N. crassa* expressing nuclear-targeted GFP were co-labelled with DASPMI and imaged. Lifetime gates were set so that the first gate provided an intense signal (A) and each subsequent gate provided intensity of approximately half the previous gate. Consequently, fluorescence signal was lowest in gate four (B). The cell was spatially resolved, but neither mitochondria (labelled with DASPMI) nor nuclei (labelled with GFP) could be distinguished. Following binning, a fluorescence lifetime map was constructed and both mitochondria and GFP were clearly resolved. GFP (shown in yellow) had a longer lifetime (between 2 and 2.5 ns) than DASPMI, shown in blue/green (which had a lifetime of approximately 1.2 ns) (C). A lifetime graph was plotted from these data and produced a series of lifetime peaks of 1 to 1.5 ns and 2 to 2.5 ns. These were arranged in groups, coinciding with regions of the cells containing either mitochondria or nuclei (D).

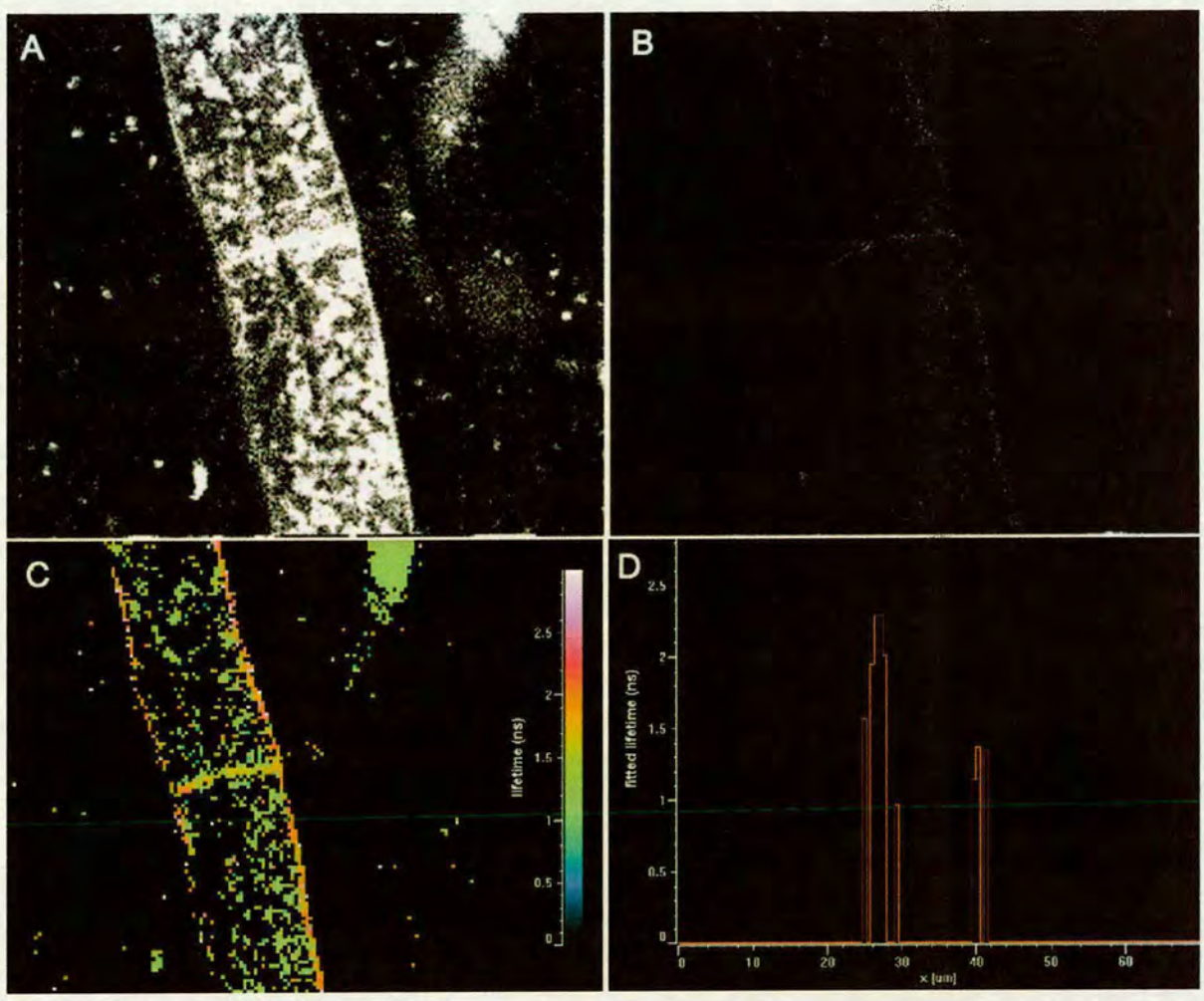

Figure 7.18: Potentiometric probes are more selective in their labelling of membranes with high electrochemical gradients. The potentiometric probe DASPMI is less selective than some others (including Rhodamine 123), and was found to intensely label both the plasma membrane and septa, as well as mitochondria. Here, regions of cells surrounding septa were selectively imaged in *N. crassa* labelled with DASPMI. Lifetime gates were set so that the first gate provided an intense signal (A) and each subsequent gate provided intensity of approximately half the previous gate. Consequently, fluorescence signal was lowest in gate four (B). The cell membrane, a septum, and an abundance of spherical mitochondria were spatially resolved in the sub-apical cell. Following binning, a fluorescence lifetime map was constructed. All 3 regions of the cell were observed to have different lifetimes: the plasma membrane (shown in red) had the longest lifetime at approximately 2.5 ns; the septum (shown in orange) had the next longest lifetime of approximately 1.5 ns, and mitochondria (shown in yellow/green) had the shortest lifetime of approximately 1 ns (C). A lifetime graph was plotted from these data for a region of the cell containing plasma membrane, septum and mitochondria. Three distinct peaks at 1, 1.5 and 2.5 ns were plotted, corresponding to mitochondria, septum and plasma membrane respectively (D).

7.4 Discussion

7.4.1 Two Photon Laser Scanning Microscopy

A basic parameter of fluorescence is the fluorescence excitation cross-section. Although one photon absorption spectra are well documented for a wide range of molecules, little is known about two photon absorption cross spectra for biologically useful fluorophores (Smith, 1986; Xu et al., 1996), although this is an area of active research. In the present study, the initial aim was to successfully excite several vital fluorescent probes in live-cells of filamentous fungi, and to identify excitation wavelengths which successfully excited dyes without causing observable photodamage to the imaged samples.

In the present study, the tunable ti:sapph laser was used to successfully excite both calcafluor, which is typically excited by UV light, and FM4-64, which requires excitation at much longer wavelengths (typically 514 nm for single photon excitation). One of the commonly reported benefits of 2 photon excitation of UV-excitable dyes is improved cell viability because UV light is relatively more harmful to live cells (Maiti et al., 1996). In this study, it was not possible to compare cell viability for single photon UV excitation with 2 photon excitation. However, the UV excitable dye, calcafluor, was successfully excited and imaged in living fungal cells. An obvious conclusion, therefore, is that 2 photon excitation of filamentous fungi labelled with UV-excitable dyes is possible and may be preferential to excitation using UV light.

Some authors agree that two photon excitation should be performed at the longest possible wavelength in order to minimise the level of phototoxicity from the infra-red laser. This is because shorter wavelengths (700 - 800 nm) cause the excitation of endogenous cellular absorbers in the UV region, whose excitation can lead to photo-oxidation processes creating destructive reactive oxygen species (Cunningham et al., 1985; Tyrell and Keyse, 1990; Konig et al., 1996). This view has been further supported by work with laser tweezers which use infra-red lasers to optically trap nano- and micrometer sized particles. Some studies found that with wavelengths above 800 nm, cells could be manipulated for over 15 min without observable damage being caused. However, the use of wavelengths in the region of 700 - 800 nm led to cell death within several seconds (Konig, 2000).

In the present study, comparatively long wavelengths were initially used to excite nuclear-targeted GFP and Rhodamine 123 in *N. crassa*. Interestingly, at 950 nm and 880 nm, GFP-labelled cells fractured within 12 s of scanning. Shortening the wavelength to 810 nm led to considerably improved cell viability, and cells could be imaged for extended time periods with no observable photodamage. The reasons for this are not clear, although it is likely that a combination of several factors are involved: 1) at extended wavelengths (from approximately 900 nm upwards) infra-red transmission through the Nikon objectives was up to 70% lower than at 800 nm which would lead to less light reaching the sample. Consequently, laser power would have to be greatly increased to excite the sample. Any continuous wave light, would reach the sample and could be potentially damaging, and at 950 nm certain UV absorbing molecules may be excited by 3 photon excitation and release photo-damaging products. Furthermore, irradiation of samples with longer infra-red wavelengths can lead to sample heating due to increased absorption of water within the cell. Although this is not a problem at shorter wavelengths, where water is very transparent, at 930 nm and above, water absorption could cause significant increases in temperature and even lead to boiling within the cell (Denk et al., 1995; Svoboda and Block, 1994). This observation is consistent with the results observed in the present study. Finally, the 2 photon cross-spectra shows maxima at 810 nm for wild type GFP, and 780 nm for Rhodamine 123.

Although excitation at 810 or 780 nm may be inherently more photodamaging, the greater quantum yield of fluorescence at this wavelengths for the probes used would enable the laser power to be significantly reduced, and this may lead to the improved cell viability observed. In the experimental set up at the COSMIC imaging facility, Edinburgh, power readings of laser light at sample were not possible, and it would certainly be helpful to understand how much light was irradiating the sample. Recent advances in laser technology have lead to the commercial release of a new generation of tunable ti:sapph lasers (e.g. Coherent Chameleon, released Spring 2003) that automatically tune to wavelengths within a 715 - 950 nm spectrum. The associated software enables the user to quickly run the laser along its tunable wavelength and produce a 2 photon excitation and emission spectra for a given fluorescent probe. These technological advances would enable the biologist to determine appropriate excitation cross spectra for any dye, and one would anticipate a significant step forward in our understanding of 2 photon excitation of biologically useful probes within the coming year. Placing a power meter above the objective and running the laser from its minimum to maximum wavelengths would also provide correlatory information regarding the power available at sample.

The theoretical maximum spatial resolution for CLSM is slightly greater than for TPLSM under optimal imaging conditions (e.g. when the sample is close tot he coverslip). In the present study, sample preparation had been optimised for confocal microscopy prior to TPLSM. Consequently, no differences in spatial resolution was observed under identical imaging conditions. However, increased rates of photobleaching and photodamage were observed for TPLSM. This is in contrast to the results reported by some authors (Denk et al., 1995; Billinton and Knight, 2001). This anomaly is probably due to differences in experimental design and the comparison of what exactly is being photobleached. Previously in this chapter the differences between optical sectioning using a confocal and 2 photon laser scanning microscope were compared. For continuous wave, single photon excitation, a region above and below the focal region of the laser was irradiated. For TPLSM, only the focal region of the laser was irradiated.

Many authors who conclude that photobleaching with 2 photon excitation is lower than for single photon have compared 3-D data series. In this case, it is likely that photobleaching will be lower, because for CLSM the whole sample is continually irradiated to some extent throughout the acquisition period. For TPLSM, only the thin optical section being imaged is irradiated. Consequently, bleaching rates would be anticipated to be considerably decreased. In the present study, single optical sections were compared. Photobleaching rates within the section at the plane of laser focus will, of course, be photodamaged at a rate at least comparable to CLSM. Therefore, photobleaching for single optical sections may well be greater in TPLSM compared with CLSM, and better for 3-D data series. Few systematic comparisons of CLSM and TPLSM exist in live-cell studies currently exist. As technological advances improve the accessability, usability, and cost of TPLSM systems, these vital questions should soon be answered.

7.4.2 Fluorescence Lifetime Imaging Microscopy

In general, probes that have the same emission wavelength usually do not have the same lifetimes, so they can be distinguished if the microscope has enough resolution in the time domain. The number of probes that can be imaged at the same time depends upon the concentration and lifetime of each probes and on the dynamic range of their lifetimes. In the spectral domain, the dynamic range allows for not more than two or three probes to be simultaneously imaged, with each probe necessarily having a dedicated photomultiplier tube for its collection. However, given that a typical lifetime resolution is in the sub-nanosecond range, with a dynamic range of 10 nanoseconds, it might be possible to distinguish between 10 or more probes within this time period as long as they remain spatially discrete and provide a high signal level (Draaijer et al., 1995).

Recording probes with differing lifetimes can be achieved with only a single detector and one excitation wavelength, and spectral differentiation following emission is not necessary. Because no bandpass filters are required, detector sensitivity is increased and the entire spectral band is detected. Signals from mixtures of probes can be easily deconvolved using basic image processing packages. Recently, new dyes have been developed specifically for lifetime imaging microscopy (Sauer et al., 1993).

Bleaching of fluorophores is a major source of image deterioration, and all fluorescent compounds are subject to photobleaching to some extent. Fluorescent signals can be protected if the specimen is mounted in an anti-fade agent. Unfortunately, these agents tend to be toxic and cannot be used in live-cell research (Cyzmmek, 1994). However, because fluorescence lifetime is independent of intensity, photobleaching is only a problem if the dye is bleached to such an extent that no measurement can be made (Daiijer et al., 1995).

In the present study, a series of basic experiments were performed to establish whether or not the potential benefits of FLIM could be advantageous in live-cell imaging of fungal hyphae. A common problem associated with imaging vital dyes is non-selective and background staining. In Chapter 6, for example, Rhodamine 123 was found to stain the cell's surrounding media. Consequently, contrast was lost and image resolution suffered. It is well established that the lifetime of a dye can vary depending on the local environment as a consequence of how much energy is lost by the excited electron to the environment prior to fluorescence emission (Murata et al., 2000; Lakowicz and Berndt, 1997).

Recent studies have demonstrated that protein-protein interactions causing fluorescence resonance energy transfer (FRET) lead to an increase in fluorescence lifetime (Murata et al., 2000), and variations in cellular pH levels can cause changes to some vital probes (Lin et al., 1999).

For the data shown, it was clear that the lifetime of Rhodamine 123 was longer in the extracellular media, and decreased upon accumulation of dye in the charged mitochondria. This was very interesting; for the first time, the lifetime of a mitochondrial probe has been shown to change upon accumulation in a charged membrane. Due to the low fluorescence signal, it was not clear whether lifetime differences existed between dye in the charged mitochondrial membrane and the non-charged plasma membrane. Nevertheless, these data support the current opinion that significant lifetime differences are found for vital probes in different environments. This view was further supported by the observation that the lifetime of DASPMI varied between 3 different membranes within the cell, namely: the mitochondrial membrane; plasma membrane and septum.

This result is potentially very significant. In Chapter 6, an assay for mitochondrial activity was developed using Rhodamine 123. However, this was not ideal because a) it was difficult to ensure the fluorescence signal did not saturate the detector and decrease sensitivity, b) high background fluorescence increased noise, c) some of the dye may have washed out of the mitochondria upon treatment with fungicide or pharmaceutical agents. The possibility that an assay for mitochondrial activity could be developed using FLIM would solve all of the inherent problems associated with intensity imaging. The use of lifetime measurements to analyse cellular and sub-cellular environments holds great promise for cell biologists with a wide variety of potential applications.

Finally, FLIM was used to resolve DASPMI and GFP within the same cell. From Chapter 6, these dyes could not be distinguished on the basis of their spectral properties. However, from the data presented in Chapter 7, both dyes were clearly resolved using lifetime measurements, with DASPMI having a significantly shorter lifetime (1.2 ns) compared to GFP (2 ns). The lifetime map created for DASPMI/GFP samples enabled the spatial resolution of nuclei and mitochondrial membranes which had not been possible with TPLSM or CLSM. Some authors have recently reported success using FLIM to discriminate between different probes in animal cells and cell extracts. For example, a lipophilic stain and a nuclear stain were successfully resolved in fixed fibroblasts where previously these probes could not be spectrally or spatially resolved using fluorescence intensity microscopy (Hermann et al., 2001).

Much of the current literature involving FLIM concerns measurements made using fixed samples or probes in media. The present study, in which live fungal cells were imaged using FLIM, is the first study in which lifetime measurements have been performed on filamentous fungal cells, and is one of very few studies in which live cells have been successfully imaged with FLIM. Recent technological advances in excitation lasers (both modulated LEDs and ti:sapph lasers), PMT detectors and image capture cards are making FLIM more accessible. Not only is spatial and temporal resolution increasing all the time, but cost is decreasing while usability and resolution improve. It is likely, therefore, that FLIM will become a commonplace and valuable tool for the study of cellular and sub-cellular events in cell biology over the next few years.

Chapter 8

Future Work

> In our endeavour to understand reality we are somewhat like a man trying to understand the mechanism of a closed watch. He sees the face and the moving hands, even hears it ticking, but he has no way of opening the case. If he is ingenious, he may form some picture of a mechanism which is responsible for all the things he observes, but he may never be quite sure that his picture is the only one that explains his observations.
>
> Albert Einstein, 1938

8.1 Future Work

The aim of this thesis was to study fungicide/fungus interactions on the micro-scale. Such studies offer a novel and under-exploited opportunity to further understand the complexities of the immediate interaction between fungicide, host and pathogen. It has been shown that many of these localised interactions, often occurring over very short time periods, may have far wider implications for the development of application regimes of fungicides to crop plants than had previously been appreciated. However, this thesis covers a large subject area, and many techniques were developed or designed to achieve this aim. Naturally, many of the areas covered could be improved upon by further research. Technological advances, particularly in the field of light microscopy, have also equipped us with a variety of new tools that can be used to improve our understanding of these localised events through the study of live cells. In the following section, possible areas of further research are suggested that would complement or build upon the present study.

8.1.1 Droplet and Deposit Characteristics

Building upon the work started in Chapter 3 of the present study, further research could usefully aim to improve our current understanding of how single droplets applied to leaves under laboratory conditions compare to those applied under field conditions. In this thesis, it has been demonstrated that even relatively small changes to the formulation of azoxystrobin can profoundly affect the wettability and spread characteristics of these formulations on the surface of wheat. Despite the increasing popularity of single-droplet studies (particularly for the analysis of fungicide uptake rates), it appears that few researchers have sufficiently considered the physicochemical properties of the droplets they apply to the leaf. If it is the case, as the present study suggests, that these properties can vary greatly, then the interpretation of much of the published research in this area becomes problematic.

In the present study, AT-SEM was used to qualitatively compare the physical characteristics of single droplet deposits of azoxystrobin on the wheat leaf surface. No attempts were made to explore the differences in uptake rate, biological activity, or absolute quantity of active ingredient deposited. This information would be very useful. Should it be shown that changes in fungicide formulation have little or no effect on the redistribution and biological efficacy of the fungicide, then the results of small-scale studies can be properly understood and interpreted. It is more likely, as we have seen, that small formulation differences will play a major role in the redistribution and efficacy of these compounds. After all, these are the very reasons that agrochemical companies invest so heavily in exploring new adjuvants systems for use with their active ingredients.

A better understanding of the properties of droplets which have been manipulated for the purposes of small-scale research would certainly lead to an improvement in the design and execution of future experiments. Furthermore, they may lead to a better understanding of micro-scale events in the uptake, distribution and efficacy of the active ingredients used, which might benefit fungicide formulation chemistry in its pursuit of new adjuvants.

Certain experiments (particularly those involving radiolabelled active ingredients) do not lend themselves to potter tower and track sprayer applications for reasons of cost, and health and safety considerations.

Methods that would help achieve the goal of improving our understanding of single droplet application might include:

- a comparison of the uptake rates of radiolabelled droplets using combustion analysis and scintillation counting to discover whether certain commonly used compounds (particularly alcohols) do significantly increase the uptake rate of single droplets
- SEM studies of deposit and fungus on the host surface or CLSM of fungi in petri dish culture to ascertain whether biological efficacy is improved when certain formulants are used.

8.1.2 Micro-scale of Infection Biokinetics

Much of the current research related to the biological efficacy of fungicidal active ingredients, including azoxystrobin, has involved large scale studies in glasshouses or field trials. In Chapter 4, techniques were developed to enable the observation of short time-scale, micro-scale interactions between pathogen and fungicide deposit. Of particular interest was the observed biological activity of the fungicide in regions distant to the droplet deposit. The observations were made over relatively short time periods. This research met with partial success, and repetition of the presented data with further refinements to the techniques employed would potentially be beneficial. Further research that would build upon the studies presented in Chapter 4 is described below.

The first significant observation was that established colonies of *Puccinia recondita* were apparently unaffected by single droplets of field-rate azoxystrobin. Work by Hart et al. (1995) has described hyphal collapse in *P. recondita* following treatment with azoxystrobin, although the experimental conditions involved greater quantities of fungicide and a longer time period between treatment and imaging to facilitate hyphal collapse. It would be interesting to repeat Hart's work, which benefited from track-spray application of fungicide, and serially reduce the period of time between treatment and observation to determine how long azoxystrobin takes to inhibit established colonies of this fungus.

In the present study, established colonies were used because time limits inhibited the observation of less well established colonies; the likelihood of locating any of the limited number of hyphae in the same place as the applied deposit were low, and it would therefore have taken too long to perform these experiments. It would, however, be of great value to the agrochemical community to understand the time frame and scale of inhibition of young colonies by azoxystrobin.

The obvious benefit from this kind of research, is that application regimes could be developed which are more sympathetic to the interactions between fungicide, host and pathogen, as opposed to, or in conjunction with, the weather conditions and foliar uptake rates of the fungicide, which is currently the focus.

Due to the difficulties in observing inhibition of established *P. recondita* colonies, established *B. graminis* colonies were used instead. Although this was more successful, it was impossible to establish whether fungicide translocation occurred entirely through the leaf, or in combination with redistribution processes through the mycelial mat. This could be explored by growing fungal cells on leaf replicas or in culture, and applying (either locally or by microinjection) radiolabelled axozystrobin to distal parts of the mycelium. These samples could then rapidly be cryo-preserved, sectioned, combusted and scintillation counted to analyse the extent of fungicide translocation through the fungal colony. In the present study, no attempt was made to study the uptake of fungicide active ingredient from dry deposits into the fungal cell. The exploitation of foliar uptake paths of fungicides has been an area of great interest to the agrochemical industry, yet no real effort appears to have been made to improve uptake into the cells of the target organism. It might, for example, be the case that certain adjuvant systems could be identified or developed that improve uptake into fungal cells and enable yet further reductions to application rates. A development of the above techniques might help provide these answers. Instead of applying solubilised active ingredient, fungal inhibition could be compared on fabricated leaf surfaces using dry, partially dry or wet droplet deposits. The introduction of different adjuvants might lead to an increase in fungal inhibition or increases in translocation through the mycelium.

Finally, an increased zone of inhibition was observed for germinating spores compared to established colonies of *B. graminis*. This was probably due to the energy requirements of the fungus at different stages in its life cycle, and the possibility that established colonies were comparatively tolerant to the fungicidal effects of azoxystrobin. Repetition of both these sets of experiments, but using altered dose rates of active ingredient, would provide valuable information regarding the susceptibility of different cell types to varying concentrations of the active ingredient.

8.1.3 Uptake and Translocation

Combustion analysis and scintillation counting are established techniques for the study of uptake rates of radiolabelled fungicide. Consequently, the experiments performed in Chapter 5 required relatively little technique development. However, some improvements could have been made to the experimental design which would have provided more information about the spatial location of fungicides within the leaf and on the leaf surface. Furthermore, phosphorimaging equipment with considerably improved resolution (e.g. less than 5 μm resolution compared with 100 μm in the present study) is available which would further improve spatial resolution.

The greatest practical limitation in the present study, was the poor combustion of polyvinylsiloxane impression material. Although the subtraction of combusted leaf material from a treated sheet of paper provided the means to estimate the quantity trapped within the polyvinylsiloxane, this was far from ideal. It would therefore be beneficial to compare the results obtained in the present study, with results using the same techniques but adopting cellulose acetate (which combusts well) as the stripping medium.

In the present study, phospohrimaging was used in conjunction with polyvinylsiloxane wax stripping techniques to compare fungicide which had been taken into the leaf with that still residing on the leaf surface. To properly quantify the amount of fungicide in these regions, combustion analysis is a preferred method. It would therefore be interesting to cut the leaf and associated cellulose strip into small portions (e.g. 500 μm2 sections) following freeze drying, and use combustion analysis and scintillation counting to properly quantify the amount of fungicide in regions of the leaf relative to the applied droplet.

One of the most interesting findings presented here was that basipetal movement of azoxystrobin occurs on a scale which is significant for the short-term protection of the plant, before the fungicide becomes xylem-mobile. During the course of these experiments, it was observed that dehydrating the plant prior to treatment, and thoroughly watering it after treatment, caused a substantial increase in the rate of fungicide movement. It would be of great interest to properly explore this phenomenon, as well as different environmental conditions (such as frost, flood, wind damage etc) to improve our understanding of the role of the environment on fungicide translocation and activity. Although some studies have investigated these variables, none have correlated the differences in observed translocation with potential differences to biological activity. This information may prove valuable in refining the application guidelines and recommended application rates of azoxystrobin.

8.1.4 Fungicide Uptake and Mitochondrial Dysfunction

Although mitochondria have been extensively imaged in animal cell studies, live-cell imaging of mitochondria in filamentous fungi has received little attention. In the present study, mitochondrial morphology, spatial location and physiology were analysed using CLSM, and mitochondrial dysfunction following the application of FCCP and azoxystrobin was observed. Confocal LSM offers excellent spatial resolution, however, temporal resolution is relatively poor compared to wide-field deconvolution microscopy and Nipkow spinning disk microscopy. These limitations in temporal resolution make it difficult to explore fast cellular processes, such as mitochondrial movement though septal pores and mitochondrial division, and impossible to take 4-D (x,y,z and t) data sets of mitochondria in fast growing species (e.g. *N. crassa.*

Further live-cell imaging studies of mitochondria in filamentous fungi would be of academic interest, to further visualise mitochondrial structure and dynamics in living cells. The use of wide-field deconvolution microscopy and Nipkow spinning disk microscopy would enable ultra-fast acquisition of 4-D data sets, and it would be of particular interest to further investigate the volume of cellular regions occupied by mitochondria, their interaction with other organelles, and movement within hyphae at greater temporal resolution. Furthermore, if these studies were combined with anti-GFP immunolabelling to localise GFP with transmission electron microscopy, the local organisation and fine structure of mitochondria could be imaged at the ultrastructural level and correlated with data collected at high temporal resolution in live cells.

In the present study, the uptake rate of azoxystrobin was measured by applying azoxystrobin to cells labelled with Rhodamine 123. Although a fast uptake rate was calculated, consistent with diffusion into the cell, uptake rate was not compared for different dose rates of the fungicide. It would be beneficial to measure uptake rate at a variety of doses and compare not only uptake rate but differences in the effect on mitochondrial biology and cell viability. Furthermore, the assay for mitochondrial activity which was developed in this study for filamentous fungi provides a convenient method for comparing the efficacy of different fungicidal active ingredients and adjuvant systems. It would, for example, be interesting to compare uptake rates of azoxystrobin in a variety of commercially important adjuvant systems and investigate whether uptake rate or activity are altered for low dose treatments with azoxystrobin.

Finally, a variety of differences in morphology and spatial location of mitochondria were identified following treatment with azoxystrobin. It was unclear whether the relocation of mitochondria was due to energy deficiency and the failure of the ATP-driven tubulin network, or due instead to mitochondria swelling and becoming detached from the cytoskeleton. Our current understanding of the cytoskeleton in filamentous fungi is far from complete. The application of various pharmacological agents (e.g. Latrunculin A or benomyl) which disrupt the cytoskeleton, in combination with live cell imaging of fluorescently labelled filamentous fungi, could be used to investigate the role of the cytoskeleton in regulating the spatial organisation and movement of mitochondria within hyphae. Furthermore, the *Nkin* tubulin deficient mutant of *N. crassa* could be used to help determine the role of tubulin in the organisation of mitochondria in filamentous fungi. For example, treatment of this mutant with azoxystrobin should not lead to the redistribution of fungal mitochondria unless their relocation following treatment with fungicide was due to their detachment from the cytoskeleton.

8.1.5 New Techniques in Live-Cell Imaging

In the final part of this study, new imaging techniques were used to observe filamentous fungi. The primary aim was to investigate whether these new techniques could provide an opportunity to overcome problems associated with CLSM, improve existing techniques available for live-cell imaging, and offer new methods to further our understanding of the biology and physiology of mitochondria in filamentous fungi and their dysfunction after application of fungicidal agents.

The most significant conclusion from this research, was that live-cell imaging of filamentous fungi can be performed using 2 photon laser light as an excitation source. Because cell viability can be maintained, it should be possible to take advantage of the inherent benefits of 2 photon imaging such as; imaging deeper into tissue than was previously possible, and imaging with 2 photon FLIM. Further research that would build upon the studies described in this thesis are described below.

Because of the improved depth of penetration reported for 2 photon microscopy, TPLSM could be applied to the study of foliar uptake of fungicides. By developing fluorescent analogues of existing active ingredients, or identifying fluorophores with similar properties to active ingredients (e.g. dihydrorhodamine 123 has a similar molecular weight and hydrophobicity to azoxystrobin), these compounds could be applied to leaf surfaces and imaged as they enter the plant.

Because the infrared laser can penetrate substantially further into thick tissue than the single photon laser, and because collection of scattered light from deep tissue is significantly improved due to modifications in the collection path, it should be possible to visualise and measure the uptake rate of fungicide analogues *in vivo* and in real time.

Furthermore, it has thus far not been possible to perform live cell imaging studies on fungal cells *in planta* due to the limited depth of penetration of the single photon laser. If a far infrared wavelength was selected (i.e. 950 nm or above), significantly improved laser penetration of the sample should be possible. This would be improved further if the ti:sapph laser was used to pump an oscillator and increase the excitation wavelength to above 1050 nm. If live-cell imaging of filamentous fungi *in planta* was proved to be possible, it is plausible that fungal cells could be labelled with a potentiometric mitochondrial marker, and a fluorescent active ingredient could be applied to the leaf surface, enabling live, real-time observation of the entire process of pathogen inhibition by a fungicide, from application, through uptake, to mitochondrial membrane disruption. This series of experiments would currently prove challenging due to technical limitations. However, laser and microscope manufacturers are improving the excitation and detection of fluorescent markers, and dye manufacturers are currently designing new fluorophores specifically for 2 photon excitation. The next generation of lasers, pumped oscillators, detectors and probes could well make these experiments possible.

Finally, lifetime imaging of filamentous fungi by FLIM was successfully performed in this study, and was considered to offer an entirely new perspective on the design of live-cell imaging experiments. Differences in environment between different membranes was demonstrated to change the lifetime of DASPMI sufficiently to resolve the dye in different regions of the hyphae. Therefore, mitochondrial membrane potential, and changes to membrane potential following the application of fungicidal agents, could be measured using FLIM in preference to CLSM. The significant advantage of this approach is that lifetime is independent of fluorescence intensity. Consequently, mitochondrial membrane depolarisation could be followed more accurately (because photobleaching would no give a false positive result, as is the case with intensity measurement). Fluorescence lifetime imaging microscopy could also be used to study organelle dynamics, by enabling the visualisation of several dyes that have similar emission spectra.

Chapter 9

References

Alberts, B., Bray, D., Lewis, J., Raff, M., Roberts, K. and Watson, J.D. (1994) Molecular Biology of the Cell. Garland Publishing Inc., New York pp 255-317.

Altmann, R. (1925) Die Elementarorganismen und ihre Beziehungen zu den Zellen. *American Journal of Anatomy*: 36, 131-142.

Amchenkova, A.A., Bakeeva, L.E., Chenstov, Y.S., Skulacev, V.P. and Zorov, D.B. (1988) Coupling membranes as energy-transmitting cables in filamentous mitochondria in fibroblasts and mitochondria clusters in cardiomycetes. *Journal of Cell Biology*: 107, 481-495.

Ammerman, E., Lorenz, G., Scelberger, K., Wenderoth, B., Sauter, H. and Rentzea, C., (1992) BAS 490F - a broad-spectrum fungicide with a new mode of action. Proceedings of Brighton Crop Protection Conference: 1, 403-410.

Anderson, N.H. and Girling, J. (1983) The uptake of surfactants into wheat. *Pesticide Science*: 14, 399-404.

Anke, T. and Steglich, W. Natural products in crop protection. In: Schlunegger, U.P. ed. (1989) Biologically Active Molecules, Identification, Characterisation and Synthesis. Springer-Verlag, Berlin and Heidelberg pp 1-29.

Arima, K., Imanaka, H., Kousaka, M., Fukuda, A. and Tamura, G. (1964) Pyrrolnitrin: a new antibiotic substance, produced by Pseudomonas. *Agricultural Biological Chemistry*: 28, 575-576.

Auger, J., Leonce, S., Jouannett, P. and Ronot, X. (1993) Flow cytometric sorting of living, highly motile human spermatazoa based on evaluation of their mitochondrial activity. *Journal of Histochemistry and Cytochemistry*: 41, 1247-1251.

Baker, C.J., Stavely, J.R., Thomas, C.A., Sasser, M. and MacFall, J.S. (1983) Inhibitory effects of Bacillus subtilis on Uromyces phaseoli and on development of rust pustules on bean leaves. *Phytopathology*: 73, 1148-1152.

Baker, E.A. Chemistry and morphology of plant epicuticular waxes. In: Cutler, D.F., Alvin, K.L., and Price, C.E. eds. (1992) The Plant Cuticle, Linnaeus Society Symposium Series no. 10. Academic Press, London pp 139-165.

Baker, E.A., Hayes, J., Hunt, G.M. and Butler, R.C. (1992) Physicochemical properties of agrochemicals: their effect on foliar penetration. *Pesticide Science*: 34, 167-182.

Baker, E.A. and Holloway, P.J. (1971) Scanning electron microscopy of waxes on leaf surfaces. *Micron*: 2, 364-380.

Bartlett, D.W., Clough, J.M., Godwin, J.R., Hall, A.A., Hamer, M. and Parr-Dobrzanski, B. (2002) Review: the strobilurin fungicides. *Pest Management Science*:58, 1-14.

Baummann, O. and Murphy, D.B. (1995) Microtubule-associated movement of mitochondria and small particles in Acanthamoeba castellanii. *Cell Motility and Cytoskeleton*: 32, 305-317.

Becker, W.F., von Jagow, G., Anke, T. and Steglich, W. (1981) Uedemansin, strobilurin A, strobilurin B and myxothiazol: new inhibitors of the bc1 segments of the respiratory chain with an E-B-methoxyacrylate system as common structural element. *FEBS letters*: 132, 329-333.

Beckett, A., Read, N.D. and Porter, M. (1984) Variations in fungal spore dimension in relation to preparatory techniques for light microscopy and scanning electron microscopy. *Journal of Microscopy*: 136, 87-95.

Bennett, R.N. and Wallsgrove, R.M. (1994) Secondary metabolites in plant defence mechanisms. *New phytology*: 127, 617-633.

Bereiter-Hahn, J. (1990) Behaviour of mitochondria in the living cell. *International Review of Cytology*: 122, 1-63.

Bereiter-Hahn, J. and Voth, M. (1994) Dynamics of mitochondria in living cells: shape changes, dislocations, fusions and fission of mitochondria. *Microscopical Research Techniques*: 27, 198-219.

Bertrand, H., Sachs, M.S., Metzenberg, R.L. and Bhandary, U.L. (1983) Cytochrome oxidase subunit V gene of Neurospora crassa: DNA sequences, chromosomal mapping, and evidence that the cya-4 locus specifies the structural gene for subunit V. *Molecular and Cellular Biology*: 9, 566-577.

Betz, W.J., Mao, F. and Smith, C.B. (1996) Imaging exocytosis and endocytosis. *Current Opinion in Neurobiology*: 6, 365-371

Billinton, N. and Knight, A.W. (2001) Seeing the wood through the trees: a review of techniques for distinguishing green fluorescent protein from endogenous autofluorescence. *Analytical Biochemistry*: 291, 175-197.

BioRad (2003) http://www.Bio-Rad.com

Biscoe, T.J. and Duchen, M.R. (1992) Mitochondrial funciton in type I cells isolated from rabbit arterial chemoreceptors. *Journal of Physiology*: 450, 13-31.

Bowser, D.N., Minamikawa, T., Nagley, P. and Williams, D.A. (1999) Role of mitochondria in calcium regulation of spontaneously contracting cardiac muscle cells. *Biophysical Journal*: 75, 2004-2014.

Bracker, C.E., Murphy, D.J. and López-Franco, R., (1997) Laser microbeam manipulation of cell morphogenesis in growing fungal hyphae. *The International Society for Optical Engineering*: 2983, 67-80.

Brackhage, A.A. (2000) Differential expression of the Apsergillus fumigatus pksP gene detected in vitro and in vivo with green fluorescent protein. *Eukaryotic Cell*: 69, 6411-6418.

Brent, K.J., (1985) One hundred years of fungicide use. In: Smith, I.M. ed. (1985) Fungicides for crop protection, 100 years of progress. Croydon, UK pp 11-22.

Briggs, G.C. and Bromilow, R.H. Influences of physiochemical properties on uptake and loss of pesticides and adjuvants from the leaf surface. In: Stock, D. and Davies (1992) pp 1-26.

Briggs, G.C. and Bromilow R.H. Influence of physicochemical properties on uptake and loss of pesticides and adjuvants from the leaf surface. In: Holloway, P.J., Rees, R.T. and Stock, D. eds. (1994) Interactions Between Adjuvants, Agrochemicals and Target Organisms. Springer-Verlag, Berlin pp 1-26.

Brunelli, A., Minuto, G., Monchiero, M. and Gullino, M.L., (1996) Efficacy of strobilurin derivatives against grape powdery mildew in Northern Italy. Proceedings of Brighton Crop Protection Conference: 1, 137-142.

Bullough, D.A., Ceccarelli, E.A., Roise, D. and Allison, W.S. (1989) Inhibition of the bovine heart mitochondrial F1-ATPase by cationic dyes and amphipathic peptides. *Biochemistry and Biophysics Acta*: 975, 377-383.

Cairney, J.W.G. (1992) Translocation of solutes in ectomycorrhizal and saprotrophic rhizomorphs. *Mycological Research*: 96, 135-141.

Carefoot, G.L. and Sprott, E.R. (1967) Famine on the Wind. Rand McNally and Co. Chicago.

Carver, T.L.W., Ingerson-Morris, S.M., Thomas, B.J. and Zeyen, R.J. (1995) Early interactions during powdery mildew infection. *Canadian Journal of Botany*: 73, 632-639.

Chen, L.B. (1989) Construction of the endoplasmic reticulum. *Journal of Cell Biology*: 109, 2045-2055.

Chen, L.B. (1990) Detection of individual fluorescently labelled reovirions in living cells. Proceedings of the National Academy of Science: 87, 6579-6583.

Childs, G.V. (1996) http://cellbio.utmb.edu/cellbio/mitoch/

Clough, J.M., Vivienne, A.M., de Fraine, P.J., Fraser, T.E.M., Godfrey, C.R.A., Godwin, J.R. and Youle, D. (1995) The synthesis of fungicidal -Methoxyacrylates. Eighth International Congress of Pesticide Chemistry Options, 59-71.

Clough, J.M. and Godfrey, C.R.A. (1996) Azoxystrobin: a novel broad-spectrum systemic fungicide. *Pesticide Outlook*: 7, 16-20.

Clough, J.M., De Fraine, P.J., Godfrey, C.R.A. and Rees, S.B. Strobilurin analogues as inhibitors of mitochondrial respiration in fungi. In: Bentley, P.H. and O'Hanlon, P.J. eds. (1997) Anti-infectives, Recent Advances in Chemistry and Structure-Activity Relationships. Royal Society of Chemistry pp 176-179.

Clough, J.M. and Godfrey, C.R.A. (1998) Fungicidal Activity, ed. D.H. Hudson and J. Miyamoto. John Wiley and Sons Ltd, London, 1998: 109-141.

Collins, T.J. and Read, N.D., (1997) Apressorium induction by topographical signals in six cereal rusts. *Physiological and Molecular Plant Pathology*: 51, 169-179.

Cormack, B. (1998) Green fluorescent protein as a reporter of transcription and protein localisation in fungi. *Current Opinions in Microbiology*: 1, 406-410.

Correa, A. and Hoch, H.C. (1995) Identification of thigmoresponsive loci for cell differentiation in Uromyces germlings. *Protoplasma*: 186, 34-40.

Cossarizza, A. and Salvioli, S. (2000) Analysis of mitochondria during cell death. *Methods of Cell Biology*: 63, 467-486.

Couchman, J.R. and Rees, D.A. (1982) Fibronectin has a dual role in locomotion and anchorage of primary chick fibroblasts and can promote entry into the division cycle. *European Journal of Cell Biology*: 27, 402-410.

Cox, M.F. (1989) The spreading of a liquid on a rough surface. *Journal of the American Oil Chemistry Society*: 66, 367-374.

Cubitt, A.B., Heim, R., Adams, S.R., Boyd, A.E., Grossm, L.A. and Tsien, R.Y. (1995) Understanding, improving and using green fluorescent proteins. *Trends in Biochemical Sciences*: 20, 448-455.

Cunningham, C.C., Leclerc, N., Flanangan, L.A., Lu, M., Jamney, P.A. and Kosik, K.S. (1995) Microtubule-associated protein 2c reorganises both microtubules and microfilaments into distinct cytological structures in an actin-binding protein-280-deficient melanoma cell line. *Journal of Cell Biology*: 136, 845-857.

Czymmek, K.J., Whallon, J.H. and Klomparens, A., (1994) Confocal microscopy in mycological research. *Experimental Mycology*: 18, 275-293.

Davis, R.H. and de Serres, F.J. Genetic and microbiological research techniques for Neurospora crassa. In: Tabor, H. and White, C. eds. (1970) Methods in Enzymology, Vol 17. Metabolism of Amino Acids and Amides. Academic Press, New York pp. 79-143.

Davis, D.G., Mullins, S., Stolzenberg, G.E. and Booth, G.D. (1979) Permeation of organic molecules of widely differing solubilities and of water through isolated cuticles of orange leaves. *Pesticide science*: 10, 19-31.

Deacon, J.W. (1997) Modern Mycology. Third Edition. Blackwell Science, London.

Deegan, R., Bakajin, O., Dupont, T., Huber, G., Nagel, S. and Witten, T., (1997) Capillary flow as the cause of ring stains from dried liquid drops. *Nature*: 389, 827-829.

Denk, W. (1993) Oscillatory flow in the cochlea visualised by a magnetic resonance imaging technique. Proceedings of the National Academy of Science: 90, 1595-1598.

Denk, W. (1994) Two-photon scanning photochemical microscopy: mapping the ligand-gated ion channel distributions. Proceedings of the National Academy of Science: 91, 6629-6633.

Denk, W.J., Piston, D.W. and Webb, W.W. Two-photon molecular excitation in laser-scanning microscopy. In: Pawley, J.B. ed. (1995) Handbook of Biological Confocal Microscopy. Plenum Press, New York pp 445-459.

DeWaard, M.A. Management of resistance to pesticides. In: Zodoks, J.C. ed. (1994) Modern Crop Protection: Developments and Perspective. Wageningen, Berlin pp 53-60.

Diaz, G., Setzu, D.S., Zucca, A., Isola, R., Diana, A., Murru, R., Sogos, V. and Gremo, F. (1999) Subcellular heterogeneity of mitochondrial membrane potential: relationship with organelle distribution and intercellular contacts in normal, hypoxic and apoptotic cells. *Journal of Cell Science*: 112, 1077-1084.

Dixon, G.K., Copping, L.G. and Holloman, D.W. (1995) Antifungal Agents: Discovery and Mode of Action. Bios Scientific Publishers, Oxford.

Doble, A., Hubert, J.P. and Blanchard, J.C. (1985) Pertussis toxin pretreatment abolishes the inhibitory effect of riluzole and carbachol on D-[3H] aspartate release from cultured cerebellar granule cells. *Neuroscience Letters*: 140, 251-254.

Draaijer, A. cited in: Draaijer, A., Sanders, R. and Gerritsen, H.C. Fluorescence lifetime imaging, a new tool in confocal microscopy. In: Pawley, J.B. ed. (1995) Handbook of Biological Confocal Microscopy. New York pp 19-37.

Drubin, D.G., Jones, H.D. and Wertman, K.F. (1993) Actin structure and function: roles in mitochondrial organisation and morphogenesis in budding yeast and identification of the phalloidin-binding site. *Molecular Biology of the Cell*: 4, 1277-1294.

Duchen, M.R., Valdeolmillos, M., O'Neill, S.C. and Eisner, D.A. (1990) Effects of metabolic blockade on the regulation of intracellular calcium in dissociated mouse sensory beurones. *Journal of Physiology*: 424, 411-426.

Duchen, M.R. and Biscoe, T.J. (1992) Relative mitochondrial membrane potential and [Ca2+] in type I cells isolated from the rabbit carotid body. *Journal of Physiology*: 450, 33-61.

Duchen, M.R., McGuinness, O., Brown, LO.A. and Crompton, M (1993) On the involvement of a cyclosporin A sensitive mitochondrial pore in myocardial reperfusion injury. *Cardiovascular Research*: 27, 1790-1794.

Duchen , M.R. Fluorescence-monitoring cellular chemistry in vivo. In: Stamford, J. ed. (1993) Monitoring Neuronal Function. IRL Press, Oxford pp 231-60.

Duchen, M.R. (1999) Contributions of mitochondria to animal physiology: from homeostatic sensor to calcium signalling and cell death. *Journal of Physiology*: 516, 1-17.

Eckert, J.W. Historical development of fungicide resistance in plant pathogens. In: Delp, C.J. ed. (1988) Fungicide Resistance in North America. APS Press, Minnessota pp 1-3.

Edwards, D, Abbot, G.D. and Raven, J.A. Cuticles of early land plants: a palaeoecophysiological evaluation. In: Kersteins, G. ed. (1996) Plant Cuticles: an Integrated Functional Approach. BIOS Scientific Publishers, Oxford pp 1-32

Emaus, R.K., Grunwald, R. and Lemasters, A. (1986) Rhodamine 123 as a probe of transmembrane potential in isolated rat-liver mitochondria: spectral and metabolic properties. *Biochemistry et Biophysica Acta*: 850, 436-448.

Felsenstein, F.G. (1994) Recent evolution and current status of sensitivity of Erysiphe graminis f. sp. tritici to fenpropimorph in different european regions. *Fungicide Resistance*:60, 337-340.

Fernadez-Abalos, J.M., Fox, H., Pitt, C., Wells, B. and Doonan, J.H. (1998) Plant adapted green fluorescent protein is a versatile vital reporter for gene expression, protein localisation and mitosis in the filamentous fungus Aspergillus nidulans. *Molecular Microbiology*: 27, 121-130.

Fischer-Parton, S., Parton, R.M., Hickey, P.C., Dijksterhuis, J., Atkinson, H.A. and Read, N.D., (2000) Confocal microscopy of FM4-64 as a tool for analysing endocytosis and vesicle trafficking in living fungal hyphae. *Journal of Microscopy*: 198, 246-259.

Foy, C.L., (1969) Pesticide formulations research. *Advanced Chemical Series*: 86, 55-62..

Foy, C.L. (1989) Adjuvants for Agrochemicals. CRC Press, Boca Raton, Florida pp 1-15.

Foy, C.L., Chow, P.N.P. and Grant, C.A., Appendix to: Foy, C.L. ed. (1992) Adjuvants for Agrochemicals. CRC Press, Boca Raton, Florida pp 691-715.

Fuller, M.T. (1993) The Devlopment of Drosophilla melanogaster. Cold Spring Harbour Laboratory Press, New York pp 71-147.

Gehmann, K., Nyfeler, R., Leadbetter, A.J., Nevill, D. and Sozzi, D., (1990) CGA 173506: a new phenylpyrrole fungicide for broad spectrum disease control. Proceedings of Brighton Crop Protection Conference: 2, 399-406.

Georgopolous, S.G. (1967) Tolerance of fungi to inorganic fungicides. *Annual Review of Phytopathology*: 5, 109-130.

Georgopolous, S.G. and Dovas A. Approaches to resistance risk management. In: Hewiit, H.G., Tyson, D., Holloman, D.W., Smith, J.M., Davies, W.P. and Dixon, K.R. eds. (1995) A Vital Role for Fungicides in Cereal Production. BIOS Scientific Publishers, Oxford.

Georgopolous, S.G., The genetics of fungicide resistance. In: Lyr, H. ed. (1995) Modern Selective Fungicides. Gustac Fischer Verlag, New York pp 39-52.

Geyer, U. and Schonherr, J. (1989) Pesticide formulations, innovations and developments. Proceedings of American Chemical Society Symposium: 371, 22-33.

Glass, N.L., Jacobson, D.J. and Shui, K.T. (2000) The genetics of hyphal fusion and vegetative incompatibility in filamentous ascomycete fungi. *Annual Review of Genetics*: 34, 165-168.

Godwin, J.R., Anthony, V.M., Clough, J.M. and Godfrey, C.R.A. (1992) ICIA5504: a novel, broad spectrum, systemic B-methoxyacrylate fungicide. Proceedings of Brighton Crop Protection Conference: 1, 259-264.

Godwin, J.R., Young, J.E. and Hart, C.E. (1994) ICIA5504: effects on developments of cereal pathogens. Proceedings of Brighton Crop Protection Conference: 1, 259-264.

Godwin, J.R., Young, J.E., Woodward, D.J. and Hart, C.A. (1997) Azoxystrobin: effects on the development of grapevine downy mildew. Proceedings of the ANPP Cinquieme Conference Internationale sur les Maladies des Plantes, 871-878.

Godwin, J.R., Bartlett, D.W. and Heaney, S.P. Azoxystrobin: implications of biochemical mode of action, pharmokinetics and resistance management for spray programmes against Septoria diseases of wheat. In: Lucas, J.A., Bowyer, P. and Anderson, H.M. eds. (1999) Septoria on Cereals: a Study of Pathosystems. CABI, Wallingford pp 299-315.

Gold, R.E., Ammerman, E., Kohle, H., Leinhos, G.M. and Lorenz, G., (1995) The synthetic strobilurin BAS 490F: profile of a modern fungicide. Proceedings of Brighton Crop Protection Conference: 1, 89-96.

Goodson, H.V., Kang, S.J. and Endow, S.D. (1996) Molecular phylogeny of the kinesin family of microtubule motor proteins. *Journal of Cell Science*: 107, 1875-1884.

Goransson, A., (1995) A new method for spectral measurements of x-rays from a laser-produced plasma using differential absorption. Diploma paper, Lund Reports on Atomic Physics, 1-75.

Gow, N.A.R. and Gadd, G. (1995) The Growing Fungus. Chapman and Hall, London

Gull, K. Form and function of septa in filamentous fungi. In: Smith, J.E. and Berry, D.R. eds. (1978) The Filamentous Fungi Vol. 3. Developmental Mycology. Edward Arnold, London pp 73-93.

Hammond-Kossack, K.E. and Jones, J.D.G. (1996) Resistance gene-dependent plant defense responses. *Plant Cell*: 8, 1173-1791.

Harold, F.M., (1997) How hyphae grow: morphogenesis explained? *Protoplasma*: 197, 137-147.

Hart, C.A. and Price, C.E., (1979) Biological applications of scanning electron microscopy to the study of pesticide formulations. *Pesticide Science*: 10, 341-357.

Hart, C.A. and Young, B.W. (1987) Scanning electron microscopy and cathodoluminescence in the study of the interactions between spray droplets and leaf surfaces. *Aspects in Applied Botany*: 14, 127-140.

Hart, C.A. (1995) Azoxystrobin, a new broad spectrum fungicide. Zeneca Agrochemicals Product Literature pp 4-5.

Hartley, G.S. and Graham-Bryce, I.J., (1980) Physical Principles of Pesticide Behaviour. Academic Press, London.

Hawes, C., Crooks, K., Coleman, J. and Satiat-Jeunemaitre, B. (1995) Endocytosis in plants: fact or artefact? *Plant Cell and Environment*: 18, 1245-1252.

Heaney, S.P. and Knight, S.C., (1994) ICIA5504: a novel broad-spectrum systemic fungicide for use on fruit, nut and horticultural crops. Proceedings of Brighton Crop Protection Conference: 2, 509-516.

Heggeness, M.H., Simon, M. and Singer, S.J. (1978) Reported in Proceedings of the National Academy of Science, USA: 75, 3863.

Hermann, G.J., King, E.J. and Shaw, J.M. (1997) The yeast gene, MDM20, is necessary for mitochondrial inheritance and organisation of the actin cytoskeleton. *Journal of Cell Biology*: 137, 141-153.

Hermann, P., Murata, S. and Lakowicz, J.R. (2001) Texture analysis of fluorescence lifetime images of nuclear DNA with effect og fluorescence resonance energy transfer. *Cytometry*: 43, 94-100.

Hewit, A.J. (1998) The international BCPC spray classification system including a drift potential factor. Proceedings of the Brighton Crop Protection Conference: 5, 371-380.

Hewit, A.J., Hermansky, C., Valcore, D.L. and Bryant, J.E. (1998) Modelling atomisation and deposition of agricultural sprays. Proceedings of ILASS, USA: 97, 178-182.

Hicke, L., Zanolari, B., Pypaert, M., Rohrer, J. and Reizman, H. (1997) Transport through the yeast endocytic pathway occurs through morphologically distinct compartments and requires an active secretory pathway and Sec18p/N-ethylmaleimide-sensitive fusion protein. *Molecular Biology of the Cell*: 8, 13-31.

Hickey, P.C., (2001) Imaging vesicle trafficking and organelle dynamics in living fungal hyphae. Ph.D. thesis, University of Edinburgh.

Hickey, P.C., Jacobson, D.J., Read, N.D. and Glass, L.N. (2002) Live-cell imaging of vegetative hyphal fusion in Neurospora crassa. *Fungal Genetics and Biology*: 37, 109-119.

Higuchi, T., Prodrug, molecular structure and percutaneous delivery. In: Roche, E.B. ed. (1997) Design of Biopharmaceutical Properties through Prodrugs and Analogs. American Pharmaceutical Association, Washington pp 409-421.

Hoch, H.C., Staples, R.C., Whitehead, B., Comeau, J. and Wolfe, E.D., (1987) Signalling for growth orientation and differentiation by surface topogrophy in Uromyces. *Science*: 235, 1659-1662.

Hoffman, J. and Mendgen, K., (1998) Endocytosis and membrane turnover in the germ tube of Uromyces fabae. *Fungal Genetics and Biology*: 24, 77-85.

Holloway, P.J. cited in Juniper, B.E., and Jeffree, C.E. (1983) Plant Surfaces. Edward Arnold, London.

Holloway, P.J. Plant Cuticles: Physiochemical characteristics and biosynthesis. In: Percy, K.E., Cape, J.N., Jagels, R. and Simpson, C.J. eds. (1994) Air Pollutants and the Leaf Cuticle. NATO, Berlin pp 1-15.

Holloway, P.J., The chemical and physical characteristics of leaf surfaces. In: Preece, T.F. and Dickinson, C.H. eds. (1971) Ecology of Leaf Surface Micro-Organisms. Academic Press, London pp 39-54.

Holloway, P.J., (1986) Use of the SGE syringe. *International Labnote*: 11, 15-17.

Holloway, P.J., Structure and histochemistry of plant cuticular membranes: an overview. In: Cutler, D.F., Alvin, K.L. and Price, C.E. (1982) The Plant Cuticle. Linnaeus Society Symposium Series no. 10. Academic Press, London pp 1-32.

Holloway, P.J., Wong, W.W., Partridge, C., Seaman, H.J. and Perry, R.B. (1992) *Pesticide science*: 34, 109-118.

Holloway, P.J., (1994) Structure and chemistry of plant cuticles. *Pesticide Science*: 37, 203-206.

Holloway, P.J. Plant cuticles: Physiochemichal characteristics and biosynthesis. In: Percy, K.E., Cape, J.N., Jagels, R. and Simpson, C.J. eds. (1994) Air Pollutants and the Leaf Cuticle. NATO, Berlin pp 1-15.

Howard, R.J., Ferrari, M.A., Roach, D.H. and Mahoney, N.P., (1991) Penetration of hard surfaces by a fungus employing enormous turgor pressures. Proceedings of the National Academy of Science, USA: 88, 11281-11284.

Humphreys, S.P. (1991) The effect of foliar pathogens on the movement and accumulation of triazole fungicides in wheat. Ph.D. thesis, Lancaster University.

Huttenen, S. Epiphytic microbes and deposited compounds. In: Kersteins, G. ed. (1994), Plant Cuticles an Integrated and Functional Approach. BIOS Scientific Publishers, Oxford pp 301-316.

Institut des Cereals et des Fourrages, cited in Bartlett, D.W., Clough, J.M., Godwin, J.R., Hall, A.A., Hamer, M. and Parr-Dobrzanski, B., (2002) Review: the strobilurin fungicides.*Pest Management Science*: 58, 1-14.

Isaac, S., (1992) Fungal-Plant Interactions. Chapman and Hall, London.

Jackson, O. and Taylor, B. (1996) Plant-microbe interactions: Life and death at the interface. *Plant Cell*: 8, 1651-1668.

Jennings, D.H. Nitrogen and phosphorous metabolism in fungi. In: Boddy, L., Marchant, R. and Read, D.J. eds. (1989) Nitrogen, Phosphorous and Sulphur Utilisation by Fungi. Cambridge University Press, UK pp 1-31.

Jeffree, C.E. Structure and ontogeny of plant cuticles. In: Kersteins, K. ed. (1996) Plant Cuticles: an Integrated and Functional Approach. BIOS Scientific Publishers, Oxford pp 33-75.

Jeffree, C.E. and Read, N.D. Ambient- and low- temperature scanning electron microscopy. In: Hall, J.L. and Hawes, C.R. (1991) Electron Microscopy of Plant Cells. Academic Press pp 313-413.

Joseph-Horne, T., Holloman, D.W. and Wood, P.M. (2001) Fungal respiration: a fusion of standard and alternative components. *Biochemica et Biophysica Acta*: 1504, 179-195.

Juniper, B.E., and Bradley, D.E., cited in Hallam, N.D., and Juniper, B.E. The anatomy of the leaf surface. In: Preece, T.F. and Dickinson, C.H. eds. (1971) Ecology of Leaf Surface Micro-Organisms. Academic Press, London pp 39-54.

Juniper, B.E., and Jeffree, C.E. (1983) Plant Surfaces. Edward Arnold, London.

Kaprelyants, A.S. and Kell, D.B. (1992) Rapid assessment of bacterial viability and vitality by Rhodamine 123 and flow cytometry. *Journal of Applied Bacteriology*: 72, 410-417.

Karpuk, V.V., (1996) Contribution of exo- and endocytosis to the relationships between pathogenic fungi and host plants. *Journal of Plant Physiology*: 43, 763-772.

Keen, N.T., (1992) Gene-for gene complementarity in plant-pathogen interactions. *Annual Review of Genetics*: 24, 447-463.

Kirkwood, R.C. (1993) Use and mode of action of adjuvants for herbicides: a review of some current work. *Pesticide Science*: 38, 93-102.

Knight, S.C., Anthony, V.M., Brady, A.M., Greenland, A.J., Heaney, S.P., Murray, D.C., Powell, K.A., Schulz, M.A., Spinks, C.A., Worthington, P.A. and Youle, D., (1997) Rationale and perspectives on the devlopment of fungicides. *Annual Review of Phytopathology*: 35, 349-72.

Knogge, W., (1996) Fungal infection of plants. *Plant Cell*: 8, 1711-1722.

Kobayashi, M., Matsuo, Y., Takimoto, A., Suzuki, S., Maruo, F. and Shoun, H. (1996) Denitrification, a novel type of respiratory metabolism in fungal mitochondria. *Journal of Biological Chemistry*: 271, 16263-16267.

Kong, J. and Xu, Z. (1998) Massive mitochondrial degeneration in motor neurons triggers the onset of amyotrophic lateral sclerosis in mice expressing a mutant SOD1. *Journal of Neuroscience*: 18, 3241-3250.

Konig, H., Moll, J., Ponta, H. and Herrlich, P. (1996) Trans-acting factors regulate the expression of CD44 splice variants. *European Molecular Biology Journal*: 15, 4030-4039.

Konig, K. (2000) Multiphoton microscopy in life sciences. *Journal of Microscopy*: 200, 83-104.

Kunoh, H., Inoue, E. and Kobayashi, I. (1988) Biocontrol of dollar spot disease by using commercial, antagonistic microbe complexes. *Journal of Japanese Turf Science*: 25, 113-119.

Krulik, G.A. (1980) Light transmission in wondow-leaved plants. *Canadian Journal of Botany*: 58, 1591-1600.

Lacowicz, J.R., Szmacinski, H., Nowaczyk, K., Berndt, K.W. and Johnson, M. (1992) Fluorescence lifetime imaging. *Annals of Biochemistry*: 202, 316-330.

Lakowizc, J.R. and Berndt, K.W. (1997) Lifetime selective fluorescence imaging using an r1 phase-sensitive camera. *Review of Scientific Instruments*: 61, 2557.

Leinhos, G.M.E., Gold, R.E., Duggelin, M. and Guggenheim, R. (1997) Development and morphology of Uncinula necitor following treatment with the fungicide kresoxim-methyl and penconazole. *Mycological Research*: 101, 1033-1046.

Lin, H.J., Szmacinski, H. and Lakowicz, J.R. (1999) Lifetime based pH sensors: indicators for acidic environments. *Annals of Biochemistry*: 269, 162-167.

Lopez-Franco, R., Bartnicki-Garcia, S. and Bracker, C.E. (1994) Pulsed growth of fungal hyphal tips. Proceedings of the National Academic Sciences USA: 91, 12228-12232.

Lopez-Franco, R., Howard, R.J. and Bracker, C.E. (1995) Satellite spitzenkorper in growing hyphal tips. *Protoplasma*: 188, 85-103.

Lorang, J.M., Touri, R.P., Martinez, J.P., Sawyer, T.L., Redman, R.S., Rollins, J.A., Wolpert, T.J., Johnson, K.B., Rodriguez, R.J., Dickman, M.B. and Ciuffetti, L.M. (2001) Green fluorescent protein is lighting up fungal biology. *Applied and Environmental Microbiology*: 67, 1987-1994.

Lorenz, G., Saur, R., Schelberger, K., Forster, B., Kung, R. and Zobrist, P. (1988) Long term monitoring results of wheat powdery mildew sensitivity towards fenpropimorph and strategies to avoid the devlopment of resistance. Proceedings of the Brighton Crop Protection Conference: 1, 171-176.

Lucas, J.A. (1998) Plant Pathology and Plant Pathogens. Blackwell Science, Oxford.

Lyr, H. (1995) Modern Selective Fungicides. Gustav Fischer Verlag, New York pp 584-602.

Lyr, H., Russell, P.E. and Sisler, H.D. (1995) Modern Fungicides and Antifungal Compounds. Intercept Longhurst, Andover, UK.

Maiti, S., Shear, B., Williams, R.M., Zipfel, W.R. and Webb, W.W. (1996) Measuring seratonin distribution in live cells with three-photon excitation. *Science*: 275, 530-532.

Maloney, P.C. and Schattschneider, S., (1980) Voltage sensitivity of the proton-translocating adenosine 5'-triphosphatase in Streptococcus lactis. *FEBS Letters*: 110, 337-340.

Markham, P. Organelles of filamentous fungi. In: Gow, N.A.R. and Gadd, G.M. (1995) The Growing Fungus. Chapman and Hall, London pp 75-78.

Maynard, R.A., Womac, A.R. and Kirk, I.W. (1996) Nozzle classification factors for ground applications. ASAE Annual Meeting, paper number 961074.

McCall, M., (1988) Quantitative modelling of the effects of physical and chemical parameters on the foliar penetration of pesticides and its potential for predicting field behaviour. *Aspects of Applied Biology*: 21, 185-201.

McDougal, J. (1996) Agrochemical Service, Wood Mackenzie on-line database. Edinburgh.

McWhorter, C.G. and Wills, G.D. In: Hodgson, R.H. ed. (1982) Adjuvants for Herbicides. Weed Science Society of America, Champaign, Illinois pp 119-133.

Mendgen, K., Welter, K., Scheffold, F. and Knauf-Beiter, G. (1992) High pressure freezing of rust infected plant leaves. In: Mengen K., Lesemann, D.E., eds. (1992) Electron Microscopy of Plant Pathogens. Springer Verlag, Heidelberg pp 31-42.

Mendgen, K. and Deising, H., (1993) Infection structures of fungal plant pathogens - a cytological and physiological evaluation. *New Phytologist*: 124, 193-213.

Michea-Hamzehpour, M. and Turian, G. (1987) GMP-stimulation of the cyanide-insenstitive mitochondrial respiration in heat-shocked conidia of Neurospora crassa. *Experientia*: 43, 439-440.

Mignotte, F., Tourte, J. and Mounolou P. (1989) Segregation of mitochondria in the cytoplasm of Xenopus vitellogenic oocytes. *Biology of the Cell*: 60, 97.

Molecular Probes (2003) http://www.probes.com

Moore, A.L. and Siedow, J.N. (1991) The regulation and nature of the cyanide-resistant alternative oxidase of plant mitochondria. *Biochemica et Biophysics Acta*: 23, 121-140.

Morgan-Hughes, J.A., Schapira, A.H., Cooper, J.M., Holt, I.J., Harding, A.E. and Clark, J.B. (1990) The molecular pathology of respiratory-chain dysfunction in human mitochondrial myopathies. *Biochemica et Biophysica Acta*: 1018, 217-222.

Murata, T., Kakinuma, Y. and Yamato, L. (2000) ATP-dependent affinity change of Na+ binding sites of V-ATPase. *Journal of Biological Chemistry*: 21, 48337-48340.

Musilek, V., Cerna, J., Sasek, V., Semerdzieva, M. and Vondracek, M., (1969) Antifungal antibiotic of the Basidiomycete Oudemansiella mucida. *Folia Microbiology*: 14, 377-387.

Nevill, D., Nyfeler, R. and Sozzi, D., (1988) CGA142705: a novel fungicide for seed treatment. Proceedings Brighton Crop Protection Conference 1: 65-72.

Nicholson, R.L., Yoshioka, H., Yamaoka, N. and Kunoh, H. (1988) Preparation of the infection court by Erysiphe graminis. *Experimental Mycology*: 12, 336-349.

Noga, G., Wolter, M., Barthlott, W. and Perry, W. (1991) Quantitative evaluation of epicuticular wax alterations as induced by surfactant treatment. *Angew Botanik*: 65, 239-252.

Oerke, E.C., Dehne, H.W., Schonbec, F. and Weber, A., (1994) Crop Protection and Crop Production. Elsevier, Amsterdam.

Oliver, J.F., Huh, C. and Mason, S.G. (1977) Microspreading studies on rough surfaces by scanning electron microscopy. *Journal of Colloid and Interface Science*: 59, 480-487.

Oliver, J.F. and Mason, S.G. (1980) Liquid spreading on rough metal surfaces.*Collids on surfaces*: 1, 79-104.

Osbourn, A.E. (1996) Preformed antimicrobial compounds and plant defence against fungal attack. *Plant Cell*: 8, 1821-1831.

Parton, R.M. and Read N.D. Calcium and pH imaging in living cells. In: Lacey, A.J. ed. (1999) Light Microscopy and Biology: a Practical Approach. 2nd edition. Oxford University Press, UK.

Pawley, J.B. Fundamental limits in confocal microscopy. In: Pawley, J.B. ed. (1995) Handbook of Biological Confocal Microscopy. Plenum Press, New York pp.19-37.

Pearse, R.F.W., Hayes, T.L., Camp, A.S. and Amer, N.M. (1966) Electron microscopy of living insects. *Science*: 154, 1185.

Percy, K.E. and Baker, E.A., (1990) Effects of simulated acid rain on epicuticular wax production, morphology, chemical composition and on cuticular membrane thickness in two clones of Sitka spruce (Picea sitchensis (Bong.) Carr.) *New Phytologist*: 116, 79-87.

Perin, M.S., Fried, V.A., Mignery, G.A., Jahn, R. and Sudhof, T.C. (1989) Phospholipid binding by a synaptic vesicle protein homologous to the regulatory region of protein kinase C. *Nature*: 345, 260-263.

Petit, P.X. (1992) Analysis of the membrane potential of rat- and mouse- liver mitochondria by flow cytometry and possible applications. *European Journal of Biochemistry*: 194, 389-397.

Piston, D.W. and Webb, W.W. (1991) Three dimensional imaging of intracellular calcium activity using two photon excitation of the fluorescent indicator dye indo I. *Biophysics Journal*: 59, 156-159.

Piston, D.W., Kirby, M.S., Cheng, H. and Lederer, W.J. (1994) Two photon excitation imaging of three-dimensional calcium-ion activity. *Applied Optics*: 33, 662-669.

Pohland, A.E., (1993) Mycotoxins in review. *Food Additive Contamination*: 10, 17-28.

Pollastro, S., Faretra, F., Di Canio, V. and de Guido, A. (1996) Characterisation and genetic analysis of field isolates of Botryotinia fuckeliana (Botrytis cinerea) resistant to dichlofluanid. *European Journal of Plant Pathology*: 102, 607-613.

Porter, K.R. and Bonneville, M.A. In: Lea, A. and Febiger, G. eds. (1973) Fine Structure of Cells and Tissue. University Press, Philadelphia, USA.

Prasher, D.C., Eckenrode, V.K., Ward, W.W., Prendergast, F.G. and Cormier, M.J. (1992) Primary structure of the Aequoria victoria green fluorescent protein. *Gene*: 111, 229-233.

Pridzun, L., Sasse, F., Reichenbach, H. Inhibition of fungal acetyl-coA carboxylase: a novel target discovered with the mycobacterial compound sorophen. In: Dixon, L.G. Copping, D. and Holloman, W. eds. (1995) Antifungal Agents Discovery and Mode of Action. BIOS Scientific Publishers, Guildford, UK: BIOSpp 99-109.

Raven, J.A. (1984) Physiological correlates of the morphology of early vascular plants. *Botanical Journal of the Linnaeus Society*: 88, 105-126.

Read, N.D. Low-temperature scanning electron microscopy of fungi and fungus-plant interactions. In: Mendgen, K. and Lesemann, D.E. eds. (1992) Electron Microscopy of Plant Pathogens. Springer-Verlag, Berlin pp 17-29.

Read, N.D, Kellock, L.J., Knight, H. and Trewavas, A.J. Contact sensing during infection by fungal pathogenes. In: Callow, J.A. and Green, J.R. (1992) Society for Experimental Biology Seminar Series 48; Perspectives in Plant Cell Recognition. Cambridge University Press, Cambridge pp 137-172.

Read, N.D. Cellular nature and multicellular morphogenesis of higher fungi. In: Ingram, D.S. and Hudson, A. (1994) Shape and Form in Plants and Fungi. Cambridge University Press, Cambridge, UK pp 251-269.

Read, N.D., Trewavas, A.J. and Knight, M.R. (1997) Transduction of Ca2+ signals in plant cells and compartmentalisation of the Ca2+ signal. *Transactions of the Biochemical Society*: 24, 971-974.

Read, N.D., Fischer, S. and Parton, R.M. (1998) Imaging Spitzenkorper, pH and calcium dynamics in growing fungal hyphae. *Pesticide Science*: 54.

Read, N.D. and Hickey, P.C. The vesicle trafficking network and tip growth in fungal hyphae. In: Geitmann, A., Cresti, M. and Heath, I.B. eds. (2001) Cell Biology of Plant and Fungal Tip Growth. IOS Press, UK pp 137-148.

Reichard, D.L. (1977) Spray droplet size distributions delivered by air blast orchard sprayers. American society of agricultural engineers: 20, 232-233.

Reiderer, M. and Schneider, G., (1990) The effect of environment on the permeability and composition of Citrus leaf cuticles. *Planta*: 180, 154-165.

Ribchester, R.R., Mao, F. and Betz, W.J. (1994) Optical measurements of activity-dependent membrane recycling in motor nerve terminals of mammalian skeletal muscles. Proceedings of the Royal Society of London (Biology): 255, 61-66.

Riederer, M. and Schreiber, L. Waxes - the transport barriers of plant cuticles. In: Hamilton, R. ed. (1999) Waxes: Chemistry, Molecular Biology and Functions. Oily Press, Dundee pp 131-157.

Riederer, M. and Schonherr, J. (1990) Effects of surfactants on water permeability of isolated plant cuticles and on the the compositon of their cuticular waxes. *Journal of Pesticide Science*: 29, 85-94.

Riederer, M. and Schonherr, J. Partitioning and transport of organic chemicals between the atmospheric environment and leaves. In: Trapp, S. and McFarlane, C. eds. (1999) Plant Contamination. BIOS Scientific Publishers, Oxford, UK pp 98-122.

Robards, A.W. (1978) A comprehensive freezing, fracturing and coating system for low temperature scanning electron microscopy. *Scanning Electron Microscopy*: 2, 325-344.

Roberson, R.W., (1992) The actin cytoskeleton in hyphal cells of Sclerotinium rolfsii. *Mycologia*: 84, 41-51.

Robertson, N.F., (1958) Experimental control of hyphal branching and branch form in hyphomycetous fungi. *Journal of the Linneaus Society*: 56, 207-211.

Salo, E., Bagu, J. and Walsh, W. (1989) Regeneration and pattern formation in planarians; local origin and and role of cell movements in blastema formation. *Development*: 107, 69-76.

Salvioli, S. (2000) Opposite role of changes in mitochondrial membrane potential in different apoptotic processes. *FEBS Letters*: 469, 186-190.

Sauer, M., Schulz, A., Seeger, S., Wolfrum, J., Arden-Jacob, J., Deltau, G. and Drexhage, K.H. (1993) Design of multiplex dyes. *Physical Chemistry*: 97, 1734-1737.

Schapira, A.H., Gu, M., Taanam, J.W., Tabrizi, S.J., Seaton, T., Cleeter, M. and Cooper, J.M. (1998) Mitochondria in the etiology and pathogenesis of Parkinson's disease. *Annals of Neurology*: 44, 89-98.

Scheffer, R.P., (1991) Role of toxins in evolution and ecology of plant pathogenic fungi. *Experientia*:47, 804-811.

Schreiber, L., Kirsch, T. and Riederer, M., (1996) Transport properties of cuticular waxes of Fagus sylvatica, L. and Pice abies (L) Karst.: estimation of size selectivity and tortuosity from diffusion coefficients of aliphatic molecules. *Planta*: 198, 104-109.

Schneider, E.F. and Dickert, K.J., (1994) Health costs and benefits of fungicide use in agriculture: a literature review. *Journal of Agromedicine*: 1(1), 19-37.

Schonherr, J. and Baur, P., (1996) Effects of temperature, surfactants and other adjuvants on rates of uptake of organic compounds. In: Kersteins, G. ed. (1996) Plant Cuticles. BIOS Scientific Publishers, Oxford pp 135-155.

Schonherr, J. (2001) Foliar nutrition using inorganic salts: laws of cuticular penetration. Proceedings of the International Symposium on Foliar Nutrition of Perennial Fruit Plants: 594, 1-7.

Schumann, G.L., (1991) Plant Diseases: their Biology and Social Impact. APS Press, St Paul, Minnesota.

Schwinn, F.J., (1992) Significance of fungal pathogens in crop production. *Pesticide Outlook*: 3, 18-25.

Shepherd, V.A., Orlovich, D.A. and Ashford, A.E. (1993a) Cell to cell transport via motile tubules in growing hyphae of a fungus. *Journal of Cell Science*: 105, 1173-1178.

Shepherd V.A., Orlovich, D.A. and Ashford, A.E. (1993b) A dynamic continuum of pleimorphic tubules and vacuoles in growing hyphae of a fungus. *Journal of Cell Science*: 104, 495-507.

Simon, V.R. and Swayne, T.C. (1995) Actin-dependent mitochondrial motility in mitotic yeast and cell-free systems: identification of a motor activity on the mitochondrial surface. *Journal of Cell Biology*: 130, 345-354.

Silcox, D. and Holloway, P.J., (1986) Epidermal stripping techniques and their application to studies on the foliar penetration of nonionic surfactants. *Aspects of Applied Biology*: 11, 19-28.

Silcox, D. and Holloway, P.J. In: Chow, P.N.P., Grant, C.A., Hinshelwood, A.M. and Simundsson, E. eds. (1989) Adjuvants and Agrochemicals, Volume, Mode of Action and Physiological Activity. CRC Press, Inc., Boca Raton pp 115-128.

Siller, I. and Turscanyi, G. (2002) http://www.ktg-gua.hu/tgabor/fasjismeret/fung/

Singer-Kruger, B., Frank, R., Crausaz, F. and Riezman, H. (1993) Partial purification and characterisation of early and late endosomes from yeasts: identification of four novel proteins. *Journal of Biological Chemistry*:268, 14376-14386.

Skepper, J.N. (2003) Properties of the demarcation membrane system in living rat mehakaryocytes. *Biophyiscal Journal*: 84, 2646-2654.

Smith, D. and Onions, A.H.S., (1983) A comparison of some preservation techniques for fungi. Transactions of the British Mycological Society: 81, 535-540

Smith, F.D. History of benzimidazole use and resistance. In: Delp, C.J. ed. (1988) Fungicide Resistance in North America. APS Press, St Paul, Minnesota pp 23-24. Smith, W.K. (1986) Adaptive relationship between leaf water repllency, stomatal distribution and gas exchange. *American Journal of Botany*: 76, 465-469.

Spellig, T. (1996) Green fluorescent protein as a new vital marker in the phytopathogenic fungus Ustilago maydis. *Molecules, Genes and Genetics*: 252, 503-509.

Staub, T. (1991) Fungicide resistance: practical experience with anti-resisitance strategies and the role of integrated use. *Annual Review of Phytopathology*: 29, 421-442.

Steurbaut, W., (1993) Adjuvants for use with foliar fungicides. *Pesticide Science*: 38, 85-91.

Steffens, J.J., Pell, E.J. and Tien, M., (1996) Mechanisms of fungicide resistance in phytopathogenic fungi. *Current Opinion in Biotechnology*: 7, 348-355.

Stierl, R., Mark, M., Schrof, W. and Butterfield, E.J. (2000) Activity of the new BASF strobilurin fungicide, BAS 500F, against Septoria tritici on wheat. Proceedings of Brighton Crop Protection Conference, 259-264.

Stock, D., Briggs, G., Bardsley, R.A. and Daniels, A. (1998) New formulation approaches to fluquinazole for enhanced curativity and increased disease spectrum. Proceedings of Brighton Crop Protection Conference, 107-114.

Stock, D and Briggs, G (2000) Physicochemical properties of adjuvants: values and applications. *Weed Technology*: 14, 978-806.

Stock, D. and Davies, L.E., (1992) Foliar penetration of agrochemicals: limitations imposed by formulation type and some interactions with adjuvants. In Stock and DAvies book. 27-52.

Subramanian, S., Matejuk, A., Zamora, A., Vandenbark, A.A. and Offner, H. (2003) Oral feeding with ethinyl estradiol suppresses and treats experimental auto-immune encephalomyelitis in SJL mice and inhibits the recruitment of inflammatory cells into the central nervous system. *Journal of Immunology*: 170, 1548-1555.

Suelmann, R., Sievers, N. and Fischer, R. (1997) Nuclear traffic in fungal hyphae: in vivo study of nuclear migration and positioning in Aspergillus nidulans. *Molecular Microbiology*: 25, 757-769.

Suhling, K., Seigel, J., Phillips, D., French, P.M.W., Leveque-Fort, S., Webb, S.E.D. and Davis, D.M. (2001) Imaging the environment of green fluorescent protein. *Biophysical Journal*: 83, 3589-3595.

Suzuki, F., Isono, K., Nagatsu, J., Mizutani, T., Kawashima, Y. and Mizuno, T., (1965) A new antibiotic, polyoxin A. *Journal of Antibiotics*: 18, 131.

Svoboda, K. and Block, S.M. (1994) Force and velocity measured for single kinesin molecules. *Cell*: 77, 773-784.

Szmacinski, H., Lakowicz, J.R., Johnson, M.L., (1994) Fluorescence lifetime imaging microscopy; homodyne technique using high-speed gated image intensifier. *Methods in Enzymology*: 240, 723-748.

Take, M.E. (1996) An FSCBG sensitivity study for decision support systems. ASAE Annual Meeting, paper number 961037.

Terry, T.M. (2003) http://www.sp.uconn.edu/terry/images/ets/

Thompson, C.J., Movva, N.R., Tizard, R., Crameri, R., Davies, J.E., Lauwereys, M. and Botterman, J. (1987) Characterisation of the herbicide-resistant gene bar from Streptomyces hygroscopius. *European Molecular Biology Organisation Journal*: 6, 2519-2523.

Tiburzy, R., Noll, U. and Reisener, H.J. (1990) Resistance of wheat to Puccinia recondita f sp. tritici: histological investigation of resistance caused by the Sr5 gene. *Physiological and Molecular Plant Pathology*: 36, 95-108.

Tomlin, C.D.S. (1994) The Pesticide Manual, 10th Edition. British Crop Protection Council, Farnham, UK.

Tomlin, C.D.S. (2002) The Pesticide Manual, 12th edition. British Crop Protection Council, Farnham, UK.

Tukey, H.B. Leaching of substances from plants. In: Preece, T.H. and Dickinson, C.H. eds. (1971) Ecology of Leaf Surface Micro-Organisms. Academic Press, New York pp 67-80.

Tyrell, R.M. and Keyse, S.M. (1990) Oxidant stress leads to transcriptional activation of the human heme oxygenase gene in cultured skin fibroblasts. *Molecular and Cellular Biology*: 10, 4967-4969.

Umbach, A.L. and Siedow, J.N. (2000) The cyanide-resistant alternative oxidases from the fungi Pichia stipitis and Neurospora crassa are monomeric and lack regulatory features of the plant enzyme. *Archives of Biochemistry and Biophysics*: 378, 234-245.

United Nations (2000) World Population Prospects: The 2000 Revision-Annex Tables. United Nations, New York.

US Environmental Protection Agency (1996) Office of Pollution Prevention and Toxic Substances, Harmonised Test Guidelines. Washington DC, USA.

Van Valkenberg, J.W. Terminology, classification and chemistry. In: Hodgson, R.H. ed. (1982) Adjuvants for Herbicides. Weed Science Society of America, Champaign, Illinois.

Vanderleyden, J., Peters, C., Verachtert, H. and Bertrand, H. (1980) Substrate kinetics of the alternative oxidase of Neurospora crassa. *Biochemical Journal*: 186, 1009- 1011.

Vida, T.A. and Emr, S.D., (1995) A new vital stain for visualising vacuolar membrane dynamics and endocytosis in yeast. *Journal of Cell Biology*: 128, 779-792.

Voet, D and Voet, J., (1995) Biochemistry, 2nd Edition. John Wiley and Sons, Inc., New York.

Walker, J.E. (1994) The mechanism of ATP synthesis. *Biochemist*: 16, 31-35.

Wallace, D.C. (1999) Mitochondrial diseases in man and mouse. *Science* 283: 1483-1488.

Ward, W.W. In: Chalfie, M. and Kain, S. eds. (1998) Green fluorescent Protein: Proteins, Applications and Protocols. Wiley, New York pp 45-75.

Wattanabe, T., Yagamuchi, I., (1992) Studies in wetting phenomena on plant leaf surfaces. 3: retention model for droplets on solid surfaces.*Pesticide Science*: 34, 273-279.

Watts, C. (1985) Rapid endocytosis of the transferin receptor in the absence of bound transferin. *Journal of Cell Biology*: 100, 633-637.

Wenzel, T.N.J. (1949) Resistance of solid surfaces to wetting by water.*Physics of Colloid Chemistry*: 53, 1466.

Wettstein-Knowles, P. Biosynthesis and genetics of waxes. In: Hamilton, R.J. ed. (1997) Waxes: Chemistry, Molecular Biology and Functions. Oily Press, Dundee pp 91-130.

Wiggins, T.E. and Jager, B.J. (1994) Mode of action of the new methoxyacrylate antifungal agent ICIA5504. *Biochemical Society Transactions* 22: 68.

Williams, W.P., Sagers, J.B., Hanten, J.A., Davis, F.M. and Buckley, P.M. (1993) Transgenic corn evaluated for resistance to fall armyworm and southwestern corn borer. *Crop Science*: 37, 957-962.

Wiseman, B.R. (1985) Insect resistance to two recently released sweet corn inbreds, GTS1 and GTS2. *Journal of Entomoligcal Science*: 20, 16-19.

Wood Mackenzie (1997) cited in Clough, J.M., Vivienne, A.M., de Fraine, P.J., Fraser, T.E.M., Godfrey, C.R.A., Godwin, J.R. and Youle, D. (1995) The synthesis of fungicidal -Methoxyacrylates. Eighth International Congress of Pesticide Chemistry Options: 59-71.

Worthington, P.A., (1988) Antibiotics with antifungal and antibacterial activity against plant diseases. *Natural Products Report*: 5, 47-66.

Xu, C., Zipfel, W., Chear, J.B., Williams, R. and Webb, W. W. (1996) Multiphoton fluorescence of excitation: new spectral windows for biological non-linear microsocpy. Proceedings of the National Academy of Science, USA: 93, 10763-10768.

Yaffe, M.P. (1996) Microtubules mediate mitochondrial distribution in fission yeast. Proceedings of the National Academy of Science, USA: 93, 11664.

Yaffe, M.P. (1999) The machinery of mitochondrial inheritance and behaviour.*Science* 283: 1493-1497.

Yoshikami, D. and Okun, L.M. (1984) Staining of living presynaptic nerve terminals with selective fluorescent dyes. *Nature*: 310, 53-56.

Ziogas, B.N., Baldwin, B.C. and Young, J.E. (1997) Alternative respiration - a biochemical mechanism of resistance to azoxystrobin (ICIA 5504) in Septoria tritici. *Pesticide Science*: 50, 28-32.

Ziogas, B.N. and Georgopolous, S.G. (1979) The effect of carboxin and of phenoyltrifluoroacetone on cyanide-sensitive and cyanide-resistant respiration of Ustilago maydis mitochondria. *Pesticide Biochemistry and Physiology*: 11, 208-217.

Zoratti, M., Pietrobon, D. and Azzone, G.F. (1982) On the relative relationship between rate of ATP synthesis and H+ electrochemical gradient in rat-liver mitochondria. *European Journal of Biochemistry*: 126, 443-451.

Chapter 10

Appendix

10.1 Azoxystrobin Micro-Biokinetics

10.1.1 Curative Control of *Blumeria graminis*

Curative control of *Blumeria graminis* was measured after 1, 7 and 24 h. The results are shown in the table below (time = h, distance = μm, lat = laterally to the deposit, bas = basipetally to the deposit, acr = acropetally to the deposit).

time		lat	bas	acr
1	a	110	130	115
	b	140	165	145
	c	195	185	155
	mean	148.3333	160	138.3333
	stdev	43.10839	27.83882	20.81666
7	a	145	190	355
	b	160	215	365
	c	220	280	435
	d	265	300	490
	mean	197.5	246.25	411.25
	stdev	55.45268	52.18157	63.42647
24	a	na	7000	50000
	b	na	7700	40000
	mean	na	7350	off leaf
	stdev	na	494.9747	off leaf

10.1.2 Preventative Control of *Blumeria graminis*

Preventative control of *Blumeria graminis* was measured after 1, 3, 5 and 7 h. The results are shown in the table below (time = h, distance = μm, lat laterally to the deposit, bas = basipetally to the deposit, acr = acropetally to the deposit).

time		lat	bas	acr
0	a	0	0	0
	b	0	0	0
	c	0	0	0
	d	0	0	0
	e	0	0	0
	mean	0	0	0
	stdev	0	0	0
1	a	130	135	125
	b	135	145	140
	c	140	145	150
	d	155	155	150
	e	155	165	155
	mean	143	149	144
	stdev	11.51086	11.40175	11.93734
3	a	125	170	195
	b	145	200	220
	c	150	210	235
	d	165	230	260
	e	170	235	285
	mean	151	209	239
	stdev	17.81853	26.07681	34.89269
5	a	135	315	495
	b	145	345	515
	c	145	360	560
	d	160	365	585
	e	170	380	595
	mean	151	353	550
	stdev	13.87444	24.64752	43.58899
7	a	140	295	645
	b	150	320	690
	c	150	355	720
	d	165	375	735
	e	170	390	750
	mean	155	347	708
	stdev	12.24745	39.14716	41.62331

10.2 Azoxystrobin Uptake and Translocation in Wheat

10.2.1 Longitudinal Translocation of Azoxystrobin

Longitudinal Translocation of Azoxystrobin after 1 h

Longitudinal translocation of azoxystrobin was measured in wheat after 1, 3, 5 and 7 h. The results after 1 h are shown in the table below (distance = distance form deposit centre in μm, values = pixel intensity from phosphorimager).

distance	a	b	c	d	e	f	g	h	I	mean	stdev
-35	0	0	0	0	0	0	0	0	0	0	0
-34	0	0	0	0	0	0	0	0	0	0	0
-33	0	0	0	0	0	0	0	0	0	0	0
-32	0	0	0	0	0	0	0	0	0	0	0
-31	0	0	0	0	0	0	0	0	0	0	0
-30	0	0	0	0	0	0	0	0	0	0	0
-29	0	0	0	0	0	0	0	0	0	0	0
-28	0	0	0	0	0	0	0	0	0	0	0
-27	0	0	0	0	0	0	0	0	0	0	0
-26	0	0	0	0	0	0	0	0	0	0	0
-25	0	0	0	0	0	0	0	0	0	0	0
-24	0	0	0	0	0	0	0	0	0	0	0
-23	0	0	0	0	0	0	0	0	0	0	0
-22	0	0	0	0	0	0	0	0	0	0	0
-21	0	0	0	0	0	0	0	0	0	0	0
-20	0	0	0	0	0	0	0	0	0	0	0
-19	0	0	0	0	0	0	0	0	0	0	0
-18	0	0	0	0	0	0	0	0	0	0	0
-17	0	0	0	0	0	0	0	0	0	0	0
-16	0	0	0	0	0	0	0	0	0	0	0
-15	0.00	0.00	0.00	0.00	0.00	0.00	0.00	0.00	0.00	0.00	0.00
-14	17.00	27	0	17	0	0	0	0	0	6.78	10.57
-13	22.00	38	8	10	0	13	0	19	0	12.22	12.64
-12	22.00	42	9	18	3	34	0	19	0	16.33	14.91
-11	25.00	37	11	45	17	22	32	9	28	25.11	11.87
-10	17.00	56	20	55	33	56	47	40	18	38.00	16.63
-9	56.00	79	25	65	52	89	52	54	45	57.44	18.70
-8	69.00	89	68	61	71	94	66	64	60	71.33	12.04
-7	74.00	106	96	78	87	108	79	79	75	86.89	13.25
-6	75.00	138	124	85	102	134	91	83	93	102.78	23.40
-5	107.00	215	157	121	116	140	99	108	102	129.44	37.23
-4	147.00	214	238	175	143	172	144	142	125	166.67	37.47
-3	231.00	209	255	221	207	228	228	208	199	220.67	17.12
-2	247.00	254	254	226	250	215	242	234	232	239.33	13.52
-1	241.00	255	255	204	236	226	236	226	195	230.44	20.54
0	233.00	255	255	232	231	252	252	254	217	242.33	14.18

distance	a	b	c	d	e	f	g	h	I	mean	stdev
1	250.00	236	255	173	237	240	247	201	236	230.56	26.51
2	200.00	149	193	106	255	158	182	125	177	171.67	44.06
3	145.00	116	139	85	246	117	124	84	126	131.33	47.83
4	108.00	84	121	61	190	91	102	74	111	104.67	37.20
5	83.00	78	91	51	143	73	91	62	89	84.56	25.82
6	61.00	52	73	40	116	60	76	71	87	70.67	21.94
7	68.00	62	65	47	78	52	75	51	79	64.11	12.07
8	61.00	37	36	32	81	36	50	20	80	48.11	21.61
9	61.00	47	33	28	61	31	50	9	51	41.22	17.22
10	59.00	11	41	10	59	15	25	0	55	30.56	23.28
11	55.00	9	32	5	50	0	29	23	31	26.00	19.05
12	55.00	11	15	0	54	1	23	24	11	21.56	20.41
13	36.00	15	13	0	31	2	8	14	5	13.78	12.41
14	13.00	21	20	0	21	0	11	13	6	11.67	8.31
15	5.00	24	0	0	18	0	9	0	1	6.33	8.99
16	14.00	4	16	0.00	0	0	12	0	5	5.67	6.60
17	0.00	0.00	0.00	0.00	0.00	0.00	0.00	0.00	0.00	0.00	0.00
18	0.00	0.00	0.00	0.00	0.00	0.00	0.00	0.00	0.00	0.00	0.00
19	0.00	0.00	0.00	0.00	0.00	0.00	0.00	0.00	0.00	0.00	0.00
20	0.00	0.00	0.00	0.00	0.00	0.00	0.00	0.00	0.00	0.00	0.00
21	0.00	0.00	0.00	0.00	0.00	0.00	0.00	0.00	0.00	0.00	0.00
22	0.00	0.00	0.00	0.00	0.00	0.00	0.00	0.00	0.00	0.00	0.00
23	0.00	0.00	0.00	0.00	0.00	0.00	0.00	0.00	0.00	0.00	0.00
24	0.00	0.00	0.00	0.00	0.00	0.00	0.00	0.00	0.00	0.00	0.00
25	0.00	0.00	0.00	0.00	0.00	0.00	0.00	0.00	0.00	0.00	0.00
26	0.00	0.00	0.00	0.00	0.00	0.00	0.00	0.00	0.00	0.00	0.00
27	0.00	0.00	0.00	0.00	0.00	0.00	0.00	0.00	0.00	0.00	0.00
28	0.00	0.00	0.00	0.00	0.00	0.00	0.00	0.00	0.00	0.00	0.00
29	0.00	0.00	0.00	0.00	0.00	0.00	0.00	0.00	0.00	0.00	0.00
30	0.00	0.00	0.00	0.00	0.00	0.00	0.00	0.00	0.00	0.00	0.00
31	0.00	0.00	0.00	0.00	0.00	0.00	0.00	0.00	0.00	0.00	0.00
32	0.00	0.00	0.00	0.00	0.00	0.00	0.00	0.00	0.00	0.00	0.00
33	0.00	0.00	0.00	0.00	0.00	0.00	0.00	0.00	0.00	0.00	0.00
34	0.00	0.00	0.00	0.00	0.00	0.00	0.00	0.00	0.00	0.00	0.00
35	0.00	0.00	0.00	0.00	0.00	0.00	0.00	0.00	0.00	0.00	0.00
36	0.00	0.00	0.00	0.00	0.00	0.00	0.00	0.00	0.00	0.00	0.00
37	0.00	0.00	0.00	0.00	0.00	0.00	0.00	0.00	0.00	0.00	0.00
38	0.00	0.00	0.00	0.00	0.00	0.00	0.00	0.00	0.00	0.00	0.00
39	0.00	0.00	0.00	0.00	0.00	0.00	0.00	0.00	0.00	0.00	0.00
40	0.00	0.00	0.00	0.00	0.00	0.00	0.00	0.00	0.00	0.00	0.00
41	0.00	0.00	0.00	0.00	0.00	0.00	0.00	0.00	0.00	0.00	0.00
42	0.00	0.00	0.00	0.00	0.00	0.00	0.00	0.00	0.00	0.00	0.00
43	0.00	0.00	0.00	0.00	0.00	0.00	0.00	0.00	0.00	0.00	0.00
44	0.00	0.00	0.00	0.00	0.00	0.00	0.00	0.00	0.00	0.00	0.00
45	0.00	0.00	0.00	0.00	0.00	0.00	0.00	0.00	0.00	0.00	0.00

Longitudinal Translocation of Azoxystrobin after 3 h

Longitudinal translocation of azoxystrobin was measured in wheat after 1, 3, 5 and 7 h. The results after 3 h are shown in the table below (distance = distance form deposit centre in μm, values = pixel intensity from phosphorimager).

distance	a	b	c	d	e	f	g	h	I	j	mean	stdev
-35	0	0	0	0	0	0	0	0	0	0	0	0
-34	0	0	0	0	0	0	0	0	0	0	0	0
-33	0	0	0	0	0	0	0	0	0	0	0	0
-32	0	0	0	0	0	0	0	0	0	0	0	0
-31	0	0	0	0	0	0	0	0	0	0	0	0
-30	0	0	0	0	4	0	0	0	0	0	0.4	1.264911
-29	3	0	0	0	0	0	0	0	0	0	0.3	0.948683
-28	6	9	3	2	13	9	20	6	8	0	7.6	5.796551
-27	18	21	12	14	31	11	21	13	7	14	16.2	6.811755
-26	32	16	14	37	41	0	23	0	19	32	21.4	14.37745
-25	55	20	2	32	60	0	41	25	20	47	30.2	20.67634
-24	50	42	13	8	80	0	36	20	17	21	28.7	23.7723
-23	57	52	6	31	75	20	44	13	42	26	36.6	21.40716
-22	46	57	19	45	85	3	64	36	38	37	43	22.85218
-21	76	54	20	42	61	23	52	43	68	43	48.2	17.94931
-20	74	76	24	24	85	0	76	0	66	57	48.2	32.96058
-19	73	66	24	54	93	22	81	34	66	51	56.4	23.97777
-18	73	84	31	71	102	0	90	48	76	47	62.2	30.71663
-17	97	85	39	38	102	38	117	50	87	70	72.3	29.49972
-16	89	92	42	57	106	42	129	41	85	95	77.8	30.62606
-15	90	101	57	82	96	48	130	22	96	90	81.2	30.83937
-14	105	99	79	94	116	66	132	73	99	95	95.8	19.76979
-13	96	101	60	73	140	78	156	75	98	95	97.2	30.07694
-12	110	84	64	87	135	80	187	89	106	96	103.8	35.02951
-11	117	120	91	103	144	92	200	100	121	122	121	32.13513
-10	130	129	98	120	150	68	218	133	136	133	131.5	38.21649
-9	124	144	108	126	159	97	221	117	164	136	139.6	35.56278
-8	140	156	110	131	170	111	215	139	200	145	151.7	34.73727
-7	168	172	142	143	190	139	210	164	245	165	173.8	33.37264
-6	212	212	163	166	229	178	207	191	255	197	201	28.4644
-5	255	210	209	185	233	210	219	222	242	235	222	20.03885
-4	255	222	219	219	234	233	213	247	229	221	229.2	13.37327
-3	255	255	255	255	255	235	255	255	232	246	249.8	9.065196
-2	244	255	255	255	255	236	255	255	227	255	249.2	10.16311
-1	215	252	246	234	255	255	234	255	228	255	242.9	14.28636
0	238	198	234	254	255	255	221	234	249	255	239.3	18.70264

distance	a	b	c	d	e	f	g	h	I	j	mean	stdev
1	249	255	255	255	255	251	190	221	255	255	244.1	21.71763
2	255	255	255	255	255	231	234	255	255	255	250.5	9.513149
3	255	253	234	255	239	200	241	221	231	248	237.7	17.35287
4	255	241	236	239	234	159	190	246	212	206	221.8	29.82095
5	203	208	200	223	213	111	221	209	249	175	201.2	36.85648
6	164	167	153	207	200	93	136	176	193	151	164	33.75401
7	150	148	126	180	194	89	176	145	157	140	150.5	29.78534
8	135	124	111	157	175	69	98	131	130	135	126.5	29.4854
9	129	121	91	145	159	37	84	133	119	128	114.6	35.27101
10	112	121	82	138	148	40	45	119	92	106	100.3	36.12032
11	113	119	97	119	121	38	66	88	106	95	96.2	26.67
12	111	112	69	111	138	18	52	94	84	84	87.3	34.56733
13	111	105	50	108	142	37	79	99	76	93	90	30.74989
14	110	107	51	68	135	0	56	70	97	106	80	38.98718
15	98	108	41	80	113	36	47	70	83	107	78.3	28.96761
16	82	75	38	64	110	0	56	74	85	82	66.6	30.17431
17	89	93	73	71	96	33	55	48	78	53	68.9	21.06841
18	78	91	36	62	113	0	29	32	82	30	55.3	35.24848
19	74	62	61	52	88	0	59	36	73	53	55.8	24.19274
20	71	85	62	65	87	0	8	20	60	66	52.4	31.38719
21	62	79	62	4	82	0	15	48	74	49	47.5	30.7544
22	40	71	78	22	70	0	0	46	45	53	42.5	27.88169
23	52	70	40	41	85	0	36	5	57	41	42.7	26.09406
24	66	61	46	48	33	0	4	0	36	25	31.9	24.37417
25	79	79	34	8	6	0	40	8	66	35	35.5	30.51502
26	56	68	51	0	43	0	0	11	10	43	28.2	26.5154
27	48	55	15	0	27	0	0	29	0	13	18.7	20.5375
28	42	59	29	13	45	8	11	15	6	9	23.7	18.82699
29	21	43	36	15	8	0	0	0	9	3	13.5	15.42905
30	36	43	0	0	0	0	37	0	0	0	11.6	18.76285
31	31	38	14	5	21	6	8	13	7	8	15.1	11.39639
32	12	25	17	0	0	0	0	0	0	21	7.5	10.20076
33	24	19	2	2	14	3	21	1	17	23	12.6	9.559172
34	21	2	8	12	1	16	21	2	17	11	11.1	7.694876
35	14	9	0	12	0	0	4	19	9	2	6.9	6.723921
36	13	9	0	0	0	0	0	0	6	1	2.9	4.748099
37	0	0	0	0	0	0	0	0	0	0	0	0
38	0	0	0	0	0	0	0	0	0	0	0	0
39	0	0	0	0	0	0	0	0	0	0	0	0
40	0	0	0	0	0	0	0	0	0	0	0	0
41	0	0	0	0	0	0	0	0	0	0	0	0
42	0	0	0	0	0	0	0	0	0	0	0	0
43	0	0	0	0	0	0	0	0	0	0	0	0
44	0	0	0	0	0	0	0	0	0	0	0	0
45	0	0	0	0	0	0	0	0	0	0	0	0

Longitudinal Translocation of Azoxystrobin after 5 h

Longitudinal translocation of azoxystrobin was measured in wheat after 1, 3, 5 and 7 h. The results after 5 h are shown in the table below (distance = distance form deposit centre in μm, values = pixel intensity from phosphorimager).

distance	a	b	c	d	e	f	g	h	I	j	k	mean	stdev
-35	0	0	0	0	0	0	0	0	0	0	0	0	0
-34	0	0	0	0	0	0	0	0	0	0	0	0	0
-33	0	0	0	0	0	0	0	0	0	0	0	0	0
-32	4	12	3	2	4	9	3	2	2	9	7	5.181818	3.487641
-31	5	9	2	0	9	12	4	13	21	12	0	7.909091	6.45685
-30	14	7	14	2	9	3	5	21	9	18	11	10.27273	6.051296
-29	0	8	0	8	8	11	0	43	28	59	17	16.54545	19.24767
-28	0	25	37	0	36	46	0	51	0	0	17	19.27273	20.51873
-27	15	42	31	0	61	27	0	41	0	28	45	26.36364	20.60229
-26	33	12	17	9	22	8	0	21	18	26	64	20.90909	16.96735
-25	0	42	20	45	17	28	19	33	12	41	32	26.27273	14.02919
-24	25	42	33	31	38	33	25	26	41	38	29	32.81818	6.258086
-23	6	32	43	29	92	41	21	48	24	56	55	40.63636	22.831
-22	32	36	33	64	82	39	13	76	4	55	42	43.27273	24.29441
-21	59	50	42	38	80	74	7	65	50	46	84	54.09091	21.97023
-20	68	52	41	8	103	52	23	79	47	57	57	53.36364	25.57058
-19	57	57	69	41	97	34	3	62	85	89	75	60.81818	27.27936
-18	34	11	70	56	98	62	43	103	78	74	78	64.27273	27.24368
-17	42	66	57	24	93	52	59	108	46	98	76	65.54545	25.8471
-16	64	71	76	28	111	79	19	97	88	111	94	76.18182	30.14902
-15	76	66	61	50	121	85	70	113	102	110	101	86.81818	23.83618
-14	92	71	93	15	119	84	85	107	92	120	93	88.27273	28.40807
-13	84	92	106	47	134	85	82	111	111	110	101	96.63636	22.5578
-12	74	117	105	69	148	94	76	112	113	111	115	103.0909	23.28285
-11	89	111	117	66	177	92	98	116	117	115	105	109.3636	27.41267
-10	112	111	122	29	219	103	108	140	129	116	93	116.5455	44.45079
-9	113	126	133	82	246	125	111	136	136	135	120	133	40.69152
-8	119	133	144	85	233	134	101	149	145	142	103	135.2727	38.69132
-7	134	130	157	92	214	158	130	170	161	150	125	147.3636	31.14249
-6	131	158	168	116	212	190	148	194	184	173	144	165.2727	29.05887
-5	154	187	193	142	212	235	176	219	210	210	171	191.7273	28.79615
-4	181	191	228	186	224	241	203	246	249	237	203	217.1818	25.17069
-3	223	223	255	238	252	246	235	236	255	232	237	239.2727	11.48992
-2	255	255	255	236	255	237	255	233	254	215	255	245.9091	13.64151
-1	255	255	255	209	246	233	255	228	255	217	241	240.8182	16.84529
0	249	228	251	205	223	221	219	235	255	222	218	229.6364	15.93281

distance	a	b	c	d	e	f	g	h	I	j	k	mean	stdev
1	249	255	255	217	212	255	255	255	255	233	221	242	17.63519
2	255	255	255	232	221	244	255	255	255	252	235	246.7273	12.09207
3	255	178	234	255	209	231	255	244	255	254	255	238.6364	24.97708
4	255	152	211	232	200	200	246	204	241	228	254	220.2727	30.76716
5	214	143	209	186	127	189	219	190	199	191	219	189.6364	29.82372
6	175	134	207	139	108	170	187	170	176	168	181	165	27.69476
7	150	124	175	120	105	143	158	158	164	139	147	143.9091	20.7868
8	139	120	156	110	96	131	135	143	150	135	133	131.6364	17.35669
9	116	106	144	106	82	110	121	127	131	119	117	116.2727	15.98806
10	124	101	131	79	91	111	108	131	127	126	108	112.4545	17.22999
11	108	79	131	97	78	116	83	124	122	106	105	104.4545	18.45732
12	103	56	115	94	82	106	76	120	116	115	94	97.90909	20.02725
13	112	93	96	94	89	96	52	111	102	106	52	91.18182	20.72592
14	93	66	115	73	78	79	45	117	98	99	89	86.54545	21.2902
15	88	56	102	68	65	99	46	105	84	111	80	82.18182	21.35331
16	76	29	93	84	73	91	60	96	84	98	48	75.63636	21.86903
17	84	38	80	55	74	85	62	80	56	96	55	69.54545	17.44915
18	48	66	93	68	50	83	38	55	70	80	85	66.90909	17.52401
19	60	46	55	46	59	68	36	91	75	78	61	61.36364	15.96416
20	68	43	84	57	47	66	18	62	71	69	66	59.18182	17.72466
21	0	47	73	45	42	52	31	68	82	52	74	51.45455	23.23086
22	69	38	32	59	14	51	26	60	56	37	45	44.27273	16.5897
23	46	28	41	24	25	34	22	64	73	42	41	40	16.40732
24	56	46	61	28	8	32	0	52	55	40	19	36.09091	20.51075
25	27	22	61	36	27	41	36	54	31	25	41	36.45455	12.25042
26	46	31	58	23	18	45	31	51	29	31	30	35.72727	12.41846
27	34	32	32	55	22	59	62	47	41	0	25	37.18182	18.29108
28	28	5	23	40	22	66	13	41	13	64	55	33.63636	21.14839
29	10	0	25	56	29	43	0	33	9	14	69	26.18182	22.66635
30	0	0	0	18	6	34	0	51	0	20	56	16.81818	21.31112
31	25	0	17	43	17	37	42	23	28	0	23	23.18182	14.54523
32	14	14	24	22	9	28	13	15	16	6	14	15.90909	6.441344
33	32	20	29	40	0	0	0	36	0	4	18	16.27273	16.08783
34	0	0	0	60	0	57	18	0	0	0	0	12.27273	23.48655
35	25	0	14	59	0	70	9	0	0	40	0	19.72727	25.69471
36	54	52	0	36	0	23	0	36	0	41	0	22	22.57875
37	27	55	25	29	0	0	0	5	0	47	0	17.09091	20.59347
38	3	11	15	0	0	0	20	13	42	0	0	9.454545	13.05652
39	0	0	0	0	14	12	32	14	18	13	8	10.09091	9.984533
40	19	33	40	0	0	0	0	15	0	0	0	9.727273	14.94718
41	54	28	41	0	0	0	38	5	28	0	0	17.63636	20.52449
42	36	0	0	0	0	0	29	14	0	15	0	8.545455	13.24661
43	41	14	16	11	11	9	12	14	2	18	9	14.27273	9.819276
44	34	14	12	13	15	9	21	2	3	0	0	11.18182	10.24518
45	22	0	6	0	0	0	0	20	0	32	0	7.272727	11.67125

distance	a	b	c	d	e	f	g	h	I	j	k	mean	stdev
46	27	8	0	0	2	14	0	21	9	13	0	8.545455	9.384707
47	12	17	0	14	6	3	7	0	4	25	0	8	8.124038
48	14	21	7	1	4	9	0	12	0	14	0	7.454545	7.160498
49	21	0	0	0	12	0	6	9	0	0	0	4.363636	7.018158
50	6	0	8	0	0	0	25	0	0	0	0	3.545455	7.659812
51	0	0	14	0	0	0	12	0	0	0	0	2.363636	5.277741
52	0	0	0	0	0	0	0	0	0	0	0	0	0
53	0	0	0	0	0	0	0	0	0	0	0	0	0
54	0	0	0	0	0	0	0	0	0	0	0	0	0
55	0	0	0	0	0	0	0	0	0	0	0	0	0
56	0	0	0	0	0	0	0	0	0	0	0	0	0
57	0	0	0	0	0	0	0	0	0	0	0	0	0
58	0	0	0	0	0	0	0	0	0	0	0	0	0
59	0	0	0	0	0	0	0	0	0	0	0	0	0
60	0	0	0	0	0	0	0	0	0	0	0	0	0
61	0	0	0	0	0	0	0	0	0	0	0	0	0
62	0	0	0	0	0	0	0	0	0	0	0	0	0
63	0	0	0	0	0	0	0	0	0	0	0	0	0
64	0	0	0	0	0	0	0	0	0	0	0	0	0
65	0	0	0	0	0	0	0	0	0	0	0	0	0
66	0	0	0	0	0	0	0	0	0	0	0	0	0
67	0	0	0	0	0	0	0	0	0	0	0	0	0
68	0	0	0	0	0	0	0	0	0	0	0	0	0
69	0	0	0	0	0	0	0	0	0	0	0	0	0
70	0	0	0	0	0	0	0	0	0	0	0	0	0
71	0	0	0	0	0	0	0	0	0	0	0	0	0
72	0	0	0	0	0	0	0	0	0	0	0	0	0
73	0	0	0	0	0	0	0	0	0	0	0	0	0
74	0	0	0	0	0	0	0	0	0	0	0	0	0
75	0	0	0	0	0	0	0	0	0	0	0	0	0
76	0	0	0	0	0	0	0	0	0	0	0	0	0
77	0	0	0	0	0	0	0	0	0	0	0	0	0
78	0	0	0	0	0	0	0	0	0	0	0	0	0
79	0	0	0	0	0	0	0	0	0	0	0	0	0
80	0	0	0	0	0	0	0	0	0	0	0	0	0
81	0	0	0	0	0	0	0	0	0	0	0	0	0
82	0	0	0	0	0	0	0	0	0	0	0	0	0
83	0	0	0	0	0	0	0	0	0	0	0	0	0
84	0	0	0	0	0	0	0	0	0	0	0	0	0
85	0	0	0	0	0	0	0	0	0	0	0	0	0
86	0	0	0	0	0	0	0	0	0	0	0	0	0
87	0	0	0	0	0	0	0	0	0	0	0	0	0
88	0	0	0	0	0	0	0	0	0	0	0	0	0
89	0	0	0	0	0	0	0	0	0	0	0	0	0

Longitudinal Translocation of Azoxystrobin after 7 h

Longitudinal translocation of azoxystrobin was measured in wheat after 1, 3, 5 and 7 h. The results after 7 h are shown in the table below (distance = distance form deposit centre in μm, values = pixel intensity from phosphorimager).

distance	a	b	c	d	e	f	g	h	I	j	k	mean	stdev
-35	0	0	0	0	0	0	0	0	0	0	0	0	0
-34	0	0	0	0	0	0	0	0	0	0	0	0	0
-33	0	0	0	0	0	0	0	0	0	0	0	0	0
-32	2	2	5	0	0	7	12	0	0	0	0	2.545454545	3.933538772
-31	1	4	6	0	0	2	2	4	1	0	6	2.363636364	2.292279532
-30	0	7	2	3	0	1	0	3	6	1	4	2.454545455	2.423371056
-29	12	14	11	5	0	0	15	0	12	6	0	6.818181818	6.161463817
-28	0	31	0	21	0	6	18	9	7	12	19	11.18181818	10.1076029
-27	0	25	22	5	23	2	13	4	33	22	0	13.54545455	11.86055341
-26	6	31	43	19	2	9	28	5	41	8	6	18	15.22497947
-25	51	41	12	41	32	9	17	21	32	9	22	26.09090909	14.29303708
-24	18	57	32	3	19	68	27	0	45	0	51	29.09090909	23.74217574
-23	41	61	47	0	0	37	57	0	27	0	13	25.72727273	24.17887884
-22	9	32	42	0	43	31	11	74	50	38	43	33.90909091	21.02595798
-21	29	25	43	68	37	47	36	52	23	55	45	41.81818182	13.63684848
-20	54	38	74	32	52	9	54	23	55	55	8	41.27272727	21.13334289
-19	56	22	47	8	45	60	66	45	71	37	45	45.63636364	18.50552743
-18	15	51	25	41	60	38	70	66	66	47	64	49.36363636	18.13434712
-17	69	98	68	50	52	46	66	48	84	91	50	65.63636364	18.48389963
-16	85	103	64	88	80	54	82	61	79	69	43	73.45454545	17.13104571
-15	74	82	88	89	87	75	65	66	85	71	89	79.18181818	9.271657692
-14	80	106	90	84	68	82	82	71	93	48	51	77.72727273	17.3268053
-13	94	119	92	97	101	93	66	89	84	94	45	88.54545455	19.15914213
-12	91	115	101	91	97	84	92	92	106	107	82	96.18181818	10.1470999
-11	105	119	106	111	111	98	69	101	106	110	84	101.8181818	14.09126099
-10	97	135	121	112	119	105	68	112	110	108	99	107.8181818	16.92819058
-9	106	133	117	116	131	116	112	116	117	107	111	116.5454545	8.571623374
-8	126	148	139	117	130	150	107	122	129	126	106	127.2727273	14.47128819
-7	142	170	153	140	139	159	116	139	143	150	122	143	15.3166576
-6	175	186	173	150	159	184	140	156	167	170	143	163.9090909	15.59778539
-5	212	217	204	195	189	184	180	172	194	193	177	192.4545455	14.22226168
-4	251	255	255	252	231	207	229	212	221	236	229	234.3636364	17.14218613
-3	246	255	255	255	255	255	255	255	255	255	255	254.1818182	2.713602101
-2	226	255	255	255	255	255	255	255	255	255	255	252.3636364	8.743828993
-1	215	255	255	255	255	255	237	249	255	255	250	248.7272727	12.45865891
0	217	255	255	255	255	255	231	241	255	255	242	246.9090909	12.90313563

distance	a	b	c	d	e	f	g	h	I	j	k	mean	stdev
1	223	255	255	255	255	255	233	245	255	255	250	248.7272727	10.955281
2	240	255	255	255	255	255	250	255	255	255	255	253.1818182	4.622081389
3	222	255	255	255	245	255	255	255	255	255	255	251.0909091	10.10400461
4	180	212	255	255	203	255	212	205	255	255	208	226.8181818	28.28362842
5	200	212	214	240	198	210	175	190	218	234	213	209.4545455	18.53301722
6	188	167	214	177	193	200	181	187	209	221	140	188.8181818	22.98616184
7	154	143	177	148	130	189	154	127	190	187	135	157.6363636	24.11751533
8	143	147	153	129	111	144	119	99	168	132	145	135.4545455	19.93170156
9	116	133	131	122	103	126	110	89	168	171	111	125.4545455	25.2085844
10	103	131	108	101	102	110	107	98	149	150	84	113	21.1896201
11	96	116	107	108	93	108	99	78	142	136	91	106.7272727	19.04253612
12	98	115	79	68	71	98	94	80	121	121	84	93.54545455	19.11734101
13	78	110	93	99	65	76	92	83	106	103	54	87.18181818	17.72466181
14	88	99	103	82	79	84	41	80	103	105	78	85.63636364	18.17840877
15	89	107	96	82	54	101	74	68	99	111	89	88.18181818	17.41733724
16	48	84	79	83	56	64	89	78	93	98	87	78.09090909	15.71276262
17	59	87	41	68	33	45	60	66	93	80	51	62.09090909	19.14917515
18	60	97	64	46	73	55	59	43	83	93	83	68.72727273	18.36894613
19	24	99	59	70	65	78	64	51	92	66	41	64.45454545	21.36990237
20	0	101	55	33	0	71	83	73	80	78	52	56.90909091	33.37200787
21	51	80	32	0	42	64	43	51	74	52	38	47.90909091	21.70462875
22	55	65	65	46	48	29	64	11	51	65	50	49.90909091	16.96734832
23	69	31	20	33	70	41	47	38	70	57	57	48.45454545	17.36872843
24	37	59	22	25	50	50	65	45	60	42	59	46.72727273	14.26948429
25	47	25	19	38	41	42	37	47	55	48	8	37	14.12798641
26	56	65	24	36	55	46	45	60	19	28	57	44.63636364	15.73704373
27	73	69	52	27	36	6	62	6	46	45	24	40.54545455	23.17051418
28	46	40	38	46	0	47	23	11	68	40	51	37.27272727	19.17858654
29	40	51	19	0	3	43	34	34	68	70	45	37	22.85169578
30	46	65	38	9	0	38	36	36	23	59	24	34	19.42163742
31	36	45	11	0	32	19	11	11	29	34	0	20.72727273	15.29765282
32	36	55	19	0	28	32	55	20	28	0	46	29	18.87855927
33	18	38	21	24	34	29	34	31	27	55	27	30.72727273	9.980890833
34	17	42	20	0	14	0	22	46	43	48	47	27.18181818	18.66450204
35	21	36	18	27	0	10	17	54	38	50	36	27.90909091	16.63402865
36	38	23	11	18	21	16	31	21	25	32	41	25.18181818	9.336146762
37	29	31	22	14	19	15	19	31	17	22	36	23.18181818	7.400245696
38	31	41	11	29	17	20	18	34	27	17	34	25.36363636	9.330302538
39	19	32	23	42	23	31	14	31	0	11	32	23.45454545	11.91103385
40	24	36	4	8	33	17	22	13	17	9	20	18.45454545	10.03357998
41	21	42	14	12	32	13	32	10	9	14	21	20	10.86278049
42	36	32	9	17	12	21	31	10	41	8	11	20.72727273	12.1498223
43	48	36	11	11	17	9	19	14	33	6	12	19.63636364	13.40352735
44	27	41	21	19	8	14	37	18	3	29	32	22.63636364	11.84291119
45	23	27	12	4	52	52	7	6	22	15	14	21.27272727	16.84690422

distance	a	b	c	d	e	f	g	h	I	j	k	mean	stdev
46	40	31	5	9	11	12	10	14	33	5	43	19.36363636	14.37548418
47	8	31	36	14	21	28	16	19	25	22	31	22.81818182	8.3763737
48	34	21	3	4	19	7	18	29	13	18	33	18.09090909	10.85775801
49	21	24	23	5	6	31	19	23	16	11	9	17.09090909	8.383967384
50	22	25	8	17	9	43	14	21	47	5	26	21.54545455	13.5378258
51	14	29	19	18	13	18	26	14	41	24	36	22.90909091	9.310795299
52	15	10	20	28	16	22	41	10	5	1	17	16.81818182	11.1069184
53	21	19	22	9	6	26	38	28	31	18	6	20.36363636	10.32736876
54	18	26	31	14	18	31	22	19	21	41	29	24.54545455	7.89130707
55	9	32	14	19	6	11	7	13	28	26	13	16.18181818	8.863613054
56	12	9	21	15	2	9	18	7	13	33	21	14.54545455	8.489565788
57	31	15	8	21	14	6	36	31	9	57	15	22.09090909	15.38476224
58	21	47	31	22	9	2	19	14	27	8	38	21.63636364	13.50757363
59	19	24	31	7	12	18	16	47	32	46	28	25.45454545	12.94865042
60	10	14	4	13	11	28	31	24	40	16	21	19.27272727	10.64979727
61	27	41	16	15	11	18	13	24	15	14	21	19.54545455	8.606551416
62	28	34	9	18	7	14	31	41	28	14	33	23.36363636	11.38659499
63	21	21	32	17	9	19	18	38	41	55	4	25	15.00666519
64	18	34	46	21	31	31	9	11	23	11	22	23.36363636	11.36021767
65	9	21	20	31	2	16	14	9	51	34	42	22.63636364	15.18072941
66	5	41	3	14	12	6	19	52	18	36	19	20.45454545	15.92082684
67	12	21	19	36	11	4	21	2	6	23	37	17.45454545	11.86055341
68	7	31	12	7	5	18	9	29	11	34	18	16.45454545	10.47247474
69	9	1	14	41	20	6	17	11	21	14	30	16.72727273	11.24358403
70	21	24	38	20	11	19	16	15	2	13	28	18.81818182	9.410825488
71	8	28	9	12	13	9	14	13	5	21	31	14.81818182	8.36442684
72	25	22	9	11	16	7	14	12	16	28	31	17.36363636	8.003408365
73	12	21	14	18	12	0	36	24	5	17	31	17.27272727	10.55548113
74	6	33	31	7	6	14	7	18	27	21	7	16.09090909	10.53996722
75	19	21	16	11	2	18	12	4	15	9	21	13.45454545	6.501748017
76	12	8	14	7	3	6	9	18	21	22	36	14.18181818	9.547965038
77	1	21	9	23	14	7	0	18	0	23	11	11.54545455	8.970659244
78	25	11	6	7	9	7	3	7	19	23	15	12	7.416198487
79	1	8	2	5	11	11	9	13	4	4	13	7.363636364	4.365151252
80	15	21	3	6	9	20	17	15	12	2	7	11.54545455	6.608534427
81	25	9	6	4	3	8	14	13	12	11	20	11.36363636	6.637359826
82	12	5	6	2	1	9	4	21	17	10	18	9.545454545	6.772940814
83	7	9	13	6	0	0	12	8	16	17	19	9.727272727	6.388910848
84	6	2	1	5	6	2	2	3	6	11	3	4.272727273	2.901410315
85	6	3	7	3	2	1	3	3	7	7	6	4.363636364	2.248231628
86	6	3	5	0	8	0	2	5	2	4	3	3.454545455	2.46429042
87	5	4	2	3	7	2	6	0	2	3	0	3.090909091	2.256304299
88	4	3	4	1	2	3	4	3	2	1	1	2.545454545	1.213559752
89	0	0	0	0	0	0	0	0	0	0	0	0	0

10.2.2 Lateral Translocation of Azoxystrobin

Lateral Translocation of Azoxystrobin after 1 h

Lateral translocation of azoxystrobin was measured in wheat after 1, 3, 5 and 7 h. The results after 1 h are shown in the table below (distance = distance form deposit centre in μm, values = pixel intensity from phosphorimager).

distance	a	b	c	d	e	f	g	h	i	j	mean	stdev
-10	0	0	0	0	0	0	0	0	0	0	0	0
-9	17	0	0	0	0	0	43	8.00	43	29	14	18.04932
-8	40	0	0	0.00	0	0	69	0.00	69	25	20.3	29.10918
-7	73	55	21	0.00	17	10	78	36.00	82	52	42.4	29.84106
-6	112	57	43	41.00	33	45	62	47.00	68	45	55.3	22.50457
-5	178	187	100	72.00	85	76	131	70.00	131	82	111.2	43.6267
-4	244	252	136	91.00	106	136	117	92.00	117	121	141.2	58.36437
-3	255	190	233	122.00	201	204	191	154.00	191	175	191.6	37.28628
-2	252	241	233	190.00	218	235	255	240.00	255	247	236.6	19.96219
-1	226	242	235	255.00	254	195	223	255.00	223	244	235.2	19.03097
0	226	228	213	231.00	215	203	214	250.00	214	247	224.1	15.33659
1	233	208	195	252.00	255	245	254	254.00	254	250	240	21.55097
2	158	191	238	238.00	209	205	255	255.00	255	213	221.7	32.27331
3	131	142	214	176.00	140	162	201	252.00	201	143	176.2	39.76542
4	100	71	182	135.00	103	82	130	213.00	130	113	125.9	43.65636
5	61	42	98	85.00	59	25	96	144.00	96	71	77.7	33.75747
6	42	25	52	47.00	46	13	52	119.00	52	38	48.6	27.8496
7	0	0	22	29.00	0	22	24	91.00	24	34	24.6	26.55477
8	0	0	3	17.00	0	17	18	65.00	18	0	13.8	19.87628
9	0	0	0	10.00	0	0	0	0.00	0	0	1	3.162278
10	0	0	0	0	0	0	0	0	0	0	0	0

Lateral Translocation of Azoxystrobin after 3 h

Lateral translocation of azoxystrobin was measured in wheat after 1, 3, 5 and 7 h. The results after 3 h are shown in the table below (distance = distance form deposit centre in μm, values = pixel intensity from phosphorimager).

distance	a	b	c	d	e	f	g	h	i	j	k	mean	stdev
-20	0	0	0	0	0	0	0	0	0	0	0	0	0
-19	0	0	0	0	0	0	0	0	0	0	0	0	0
-18	0	0	0	0	0	0	0	0	0	0	0	0	0
-17	0	0	0	0	0	0	0	0	0	0	0	0	0
-16	12	4	18	3	6	7	0	8	21	3	16	8.909091	6.891365
-15	20	2	17	30	0	14	17	21	6	0	8	12.27273	9.809087
-14	36	14	32	29	15	0	32	32	41	32	33	26.90909	12.07853
-13	50	32	55	57	0	73	0	65	83	47	37	45.36364	26.80027
-12	43	70	70	79	40	62	60	91	75	50	84	65.81818	16.56393
-11	65	82	80	76	62	101	56	91	91	78	84	78.72727	13.52842
-10	83	105	103	113	87	113	79	101	89	99	97	97.18182	11.47012
-9	105	134	122	108	65	139	87	119	112	89	111	108.2727	21.53644
-8	120	173	125	131	83	162	97	112	105	93	133	121.2727	27.90373
-7	150	215	162	148	93	198	105	147	136	120	156	148.1818	36.13258
-6	182	255	180	164	117	224	139	163	156	148	180	173.4545	38.58591
-5	187	255	205	199	144	249	143	207	191	150	215	195	38.19162
-4	200	255	226	236	173	254	177	255	245	170	255	222.3636	35.55917
-3	221	231	228	247	217	255	215	255	255	208	255	235.1818	18.59472
-2	255	219	240	231	242	255	255	242	251	232	255	243.3636	12.20879
-1	255	231	249	217	232	255	255	247	255	215	228	239.9091	15.72549
0	241	249	212	196	214	245	201	252	255	217	218	227.2727	21.50391
1	255	242	249	235	213	208	250	238	255	214	231	235.4545	17.16603
2	255	246	236	247	237	170	254	233	246	224	255	236.6364	24.23334
3	255	235	204	217	255	130	255	255	255	246	255	232.9091	38.44855
4	200	193	186	157	255	106	255	231	244	255	255	210.6364	50.63847
5	131	153	136	129	254	94	255	200	196	254	255	187	61.14082
6	184	134	120	96	199	79	232	195	161	209	210	165.3636	51.01426
7	168	96	113	84	163	56	198	159	140	175	177	139	45.25262
8	121	89	92	76	147	55	176	135	125	147	143	118.7273	36.41728
9	131	83	65	78	126	28	163	116	117	135	129	106.4545	38.65324
10	117	76	34	33	112	0	136	119	97	106	116	86	44.33509
11	96	45	14	17	98	0	112	93	106	112	92	71.36364	43.29728
12	61	28	52	38	62	0	71	69	76	75	87	56.27273	25.36963
13	34	38	19	29	41	0	51	46	57	50	42	37	16.2911
14	26	1	8	0	23	0	22	31	31	16	42	18.18182	14.35143
15	0	0	0	0	0	0	0	0	0	0	0	0	0

Lateral Translocation of Azoxystrobin after 5 h

Lateral translocation of azoxystrobin was measured in wheat after 1, 3, 5 and 7 h. The results after 5 h are shown in the table below (distance = distance form deposit centre in μm, values = pixel intensity from phosphorimager).

distance	a	b	c	d	e	f	g	h	i	j	mean	stdev
-20	0	0	0	0	0	0	0	0	0	0	0	0
-19	0	0	0	0	0	0	0	0	0	0	0	0
-18	0	0	0	0	0	0	0	0	0	0	0	0
-17	13.00	2	14	0	4	18	17	30	0	37	13.50	12.66886
-16	36.00	11	21	8	47	24	21	0	0	28	19.60	15.2403
-15	52.00	27	59	46	48	31	40	12	0	56	37.10	19.46764
-14	57.00	36	57	0	62	85	87	8	0	64	45.60	32.99562
-13	85.00	43	69	20	80	91	103	26	0	89	60.60	35.58776
-12	69.00	70	78	40	102	92	107	13	0	105	67.60	38.23669
-11	66.00	94	76	28	112	126	115	25	0	119	76.10	45.05663
-10	97.00	94	83	54	131	138	140	54	0.00	156	94.70	48.79219
-9	121.00	94	102	75	135	166	180	36	22	194	112.50	58.2528
-8	124.00	121	84	85	154	213	224	32	51	224	131.20	70.8877
-7	142.00	150	122	71	175	255	255	60	46	242	151.80	79.66011
-6	157.00	177	119	85	218	255	246	70	144	227	169.80	66.05856
-5	205.00	229	161	132	220	255	252	96	181	205	193.60	51.567
-4	255.00	230	217	162	255	255	255	124	196	207	215.60	44.89543
-3	255.00	190	255	189	255	255	255	219	217	218	230.80	27.5552
-2	241.00	255	246	255	255	255	255	237	255	250	250.40	6.785606
-1	255.00	255	226	255	255	255	255	240	255	228	247.90	11.97637
0	218.00	231	227	235	255	255	240	235	255	236	238.70	12.72836
1	245.00	231	250	255	255	255	255	236	255	255	249.20	8.978988
2	255.00	255	255	255	255	255	255	255	255	255	255.00	0
3	255.00	255	255	244	255	255	255	255	231	218	247.80	13.11318
4	246.00	251	215	255	255	255	255	232	200	176	234.00	28.05154
5	199.00	204	172	255	255	255	255	187	231	153	216.60	38.70745
6	164.00	167	149	241	255	247	207	142	241	125	193.80	49.70535
7	134.00	137	106	198	255	185	181	124	181	88	158.90	50.07206
8	105.00	111	111	157	215	149	156	83	153	89	132.90	40.37725
9	121.00	87	73	133	186	125	131	69	127	66	111.80	37.80594
10	97.00	87	94	116	158	111	121	64	98	71	101.70	26.89093
11	59.00	65	79	101	124	94	87	62	85	52	80.80	22.14999
12	71.00	63	21	97	119	89	89	37	50	4	64.00	36.19085
13	97.00	48	13	93	88	88	76	4	59	17	58.30	35.88887
14	79.00	46	0.00	59	94	47	85	0	45	0	45.50	35.63784
15	31.00	17	0	40	38	17	28	0	43	0	21.40	17.1153
16	13.00	2	0	12	26	14	3	0	55	0	12.50	17.19334
17	0	0	0	0	0	0	0	0	0	0	0	0
18	0	0	0	0	0	0	0	0	0	0	0	0
19	0	0	0	0	0	0	0	0	0	0	0	0
20	0	0	0	0	0	0	0	0	0	0	0	0

Lateral Translocation of Azoxystrobin after 7 h

Lateral translocation of azoxystrobin was measured in wheat after 1, 3, 5 and 7 h. The results after 7 h are shown in the table below (distance = distance form deposit centre in μm, values = pixel intensity from phosphorimager).

distance	a	b	c	d	e	f	g	h	i	j	mean	stdev
-25	0	0	0	0	0	0	0	0	0	0	0	0
-24	0	0	0	0	0	0	0	0	0	0	0	0
-23	0	0	0	0	0	0	0	0	0	0	0	0
-22	0	0	0	0	0	0	0	0	0	0	0	0
-21	2	0	4	0	0	3	0	0	0	9	1.8	2.785678
-20	9	4	11	0	0	7	5	0	6	12	5.4	4.247352
-19	0	13	0	5	0	14	16	0	8	0	5.6	6.29603
-18	8	20	0	16	0	0	10	0	3	17	7.4	7.552483
-17	20	23	0	33	0	0	18	25	0	22	14.1	12.09504
-16	24	27	14	24	0	0	42	21	40	42	23.4	14.73228
-15	36	33	13	25	13	13	79	36	6	6	26	20.89498
-14	14	37	23	20	20	20	88	76	36	47	38.1	24.08921
-13	47	27	32	61	22	22	101	38	41	65	45.6	23.25597
-12	92	52	42	73	70	70	121	59	75	62	71.6	20.94373
-11	87	65	69	79	84	84	135	82	79	76	84	18.2044
-10	112	74	65	83	74	74	171	92	105	94	94.4	29.22054
-9	139	97	82	92	94	94	219	116	111	88	113.2	38.63884
-8	176	106	85	107	117	117	255	122	126	116	132.7	46.27321
-7	213	107	117	142	138	138	255	147	162	133	155.2	42.95998
-6	250	144	149	144	153	153	245	195	195	152	178	39.15354
-5	255	187	152	172	187	187	238	242	240	163	202.3	35.69888
-4	255	237	164	223	228	228	255	245	249	178	226.2	29.76172
-3	232	231	186	255	255	255	255	236	252	209	236.6	22.28542
-2	215	255	222	255	255	255	255	231	249	255	244.7	14.96696
-1	219	255	230	255	247	247	255	255	236	255	245.4	12.2
0	186	200	237	241	241	207	255	226	255	255	230.3	23.55016
1	255	255	238	240	240	172	241	245	255	255	239.6	23.56353
2	227	255	255	255	255	255	134	251	232	255	237.4	35.87813
3	215	255	255	255	255	255	142	190	212	255	228.9	36.92005
4	153	255	255	255	255	255	105	119	177	255	208.4	59.80669
5	126	231	255	255	255	255	140	116	133	255	202.1	60.5499
6	94	211	226	209	209	209	76	83	107	207	163.1	60.35139
7	94	218	217	178	172	172	60	76	68	178	143.3	58.85244
8	102	178	181	154	161	161	28	55	79	164	126.3	52.75993
9	108	147	166	117	126	126	50	71	23	148	108.2	43.78539
10	119	119	154	92	99	99	0	31	41	124	87.8	45.8624
11	80	78	100	101	92	92	52	36	34	98	76.3	24.81149
12	96	83	107	78	89	89	15	0	31	79	66.7	35.23932
13	0	76	87	54	65	65	0	0	23	94	46.4	35.4209
14	0	75	99	40	45	45	4	0	0	69	37.7	34.11759
15	0	40	88	59	33	33	0	0	0	55	30.8	29.22602
16	0	55	68	31	13	13	6	0	0	62	24.8	25.84105
17	12	40	24	36	8	12	2	0	13	24	17.1	12.84095
18	0	32	6	0	33	0	0	0	0	11	8.2	12.63962
19	3	21	12	0	14	0	0	0	0	20	7	8.3666
20	9	13	3	15	0	0	4	0	0	6	5	5.347897
21	4	0	0	18	0	0	0	0	0	0	2.2	5.4
22	0	0	0	0	0	0	0	0	0	4	0.4	1.2
23	2	9	0	6	0	0	0	0	0	7	2.4	3.352611
24	0	0	0	0	0	0	0	0	0	0	0	0
25	0	0	0	0	0	0	0	0	0	0	0	0

10.2.3 Uptake of Azoxystrobin over 24 h

Area of Azoxystrobin Translocation

The area of the leaf surface and internal tissue in which azoxystrobin was present, was measured over a 24 h time course. Area was calculated in addition lateral and longitudinal measurements. These in the tables below.

		1h	6h	12h	18h	24h	1h	6h	12h	18h	24h
lat	a	1.6	2.6	2.8	3.1	4.7	1.8	3.2	3.3	3.5	4.3
	b	2	2.4	3.7	4.2	3.9	2.3	1.9	2.8	2.9	4.1
	c	2.2	3.2	3.6	4.6	4.5	2.4	2.2	2.6	3	3.7
	d	1.7	2.1	3	3.4	3.7	1.6	2.4	2.4	2.7	3.5
	e	1.5	3.4	2.9	3	4	1.8	2	2.7	3.3	3.4
	f	2	3	3.2	3.2	3.9	1.6	2.6	2.5	3.2	4
	mean	1.833333	2.783333	3.2	3.583333	4.16667	1.916667	2.383333	2.716667	3.1	3.83333
	stdev	0.273252	0.499667	0.374166	0.658534	0.392003	0.348807	0.475044	0.318852	0.269828	0.355903
bas	a	2.4	3.7	5	7.2	6.9	2.1	4	3.6	6	5.8
	b	1.9	3	4.6	7.4	7.4	1.8	3.6	4.8	4.8	6.8
	c	2	4.1	5.2	7.3	7.7	2.4	2.9	4	3.9	7.1
	d	2.3	3.7	4.8	6.8	7.3	2.2	3	5.2	5.5	7.3
	e	2.2	3.6	4.6	6.5	7.4	2.3	3.2	3.9	5.8	6.1
	f	2.5	3.8	4.7	6.7	6.5	2.7	3.5	5	6.1	6.9
	mean	2.216667	3.65	4.816667	6.983333	7.2	2.25	3.366667	4.166667	5.35	6.666667
	stdev	0.231661	0.361939	0.240139	0.365606	0.428952	0.301662	0.413118	0.66458	0.850294	0.588784
acro	a	3	9	12	22	52	1.9	3.8	8.7	10.9	31.8
	b	2.6	8.4	11.2	19.4	41.6	2.6	5.1	6.1	12.4	26.1
	c	2.5	7.9	13.1	24.6	37.2	2.2	2.9	7.2	14.1	22.8
	d	3.1	8.4	12.7	21.1	41.1	2	4.8	6.6	16.7	22.2
	e	2.9	8.8	10.9	20.5	48.1	2.4	4.4	5.8	13.2	32.6
	f	3	8.6	11	18.9	46.3	2.8	4.7	7	15.8	29
	mean	2.85	8.516667	11.81667	21.08333	44.38333	2.316667	4.283333	6.9	13.85	27.41667
	stdev	0.242899	0.381663	0.932559	2.056615	5.39682	0.348807	0.808497	1.027619	2.154762	4.446309

Stripped leaf								
	a	b	c	d	e	f	mean	stdev
1h	11	7	12	16	10	9	10.83333	3.060501
6h	18	21	19	24	17	15	19	3.162278
12h	25	19	22	28	23	22	23.16667	3.060501
18h	68	55	49	62	50	66	58.33333	8.164966
24h	112	98	124	89	101	72	99.33333	18.04069
Wax impression								
1h	8	7	11	16	9	10	10.16667	3.188521
6h	11	13	13	12	9	11	11.5	1.516575
12h	16	19	22	18	14	17	17.66667	2.73252
18h	33	29	36	34	28	31	31.83333	3.060501
24h	48	57	41	44	39	46	45.83333	6.369197

Combustion Analysis of Uptake

The quantity or radiolabelled fungicide that had been taken into the wheat leaf was measured using combustion analysis for leaves treated over a 24 h time course. The results are shown in the table below.

data set	control	1h strip	6h strip	12h strip	18h strip	24h strip
a	451.12	5.03	7.7	16.82	26.79	36.41
b	464.39	5.66	8.36	19.93	30.96	39.18
c	475.39	7.18	9.73	20.45	31.21	43.7
d	481.94	7.69	14.45	21.77	35.07	48.91
e	482.49	8.2	15.28	24.61	46.44	53.03
mean	471.07	6.752	11.104	20.716	34.094	44.386
st dev	13.3	1.352542	3.522759	2.834675	7.497735	7.052775
time	control	stdev	strip	stdev	wax*	stdev**
1	471.07	13.3	6.752	1.352542	464.318	13.3686
6	471.07	13.3	11.104	3.522759	459.966	13.75863
12	471.07	13.3	20.716	2.834675	450.354	13.59873
18	471.07	13.3	34.094	34.094	436.976	15.26781
24	471.07	13.3	44.386	44.386	426.684	15.05429

*wax = control - stripped

**stdev wax = root(square of stdev control + square of stdev strip)

10.3 Uptake of Azoxystrobin into Fungal Cells

Changes to growth rate and mitochondrial membrane potential in *Botrytis cinerea* was analysed after treatment with azoxystrobin. The results are shown in the following table.

time (s)	growth rate (microns/min)				
	a	b	c	mean	stdev
-18	5.8	7.1	6.2	6.366667	0.665833
-12	5.575	7.2	6.25	6.341667	0.816369
-6	5.581	7.25	6.2	6.343667	0.843724
0	5.744	7.2	5.4	6.114667	0.955534
6	5.621	6.35	5.35	5.773667	0.517185
12	5.17	5.2	5.1	5.156667	0.051316
18	4.639	4.25	3.75	4.213	0.445653
24	3.76	3.8	2.25	3.27	0.883572
30	3.01	2.7	1.8	2.503333	0.628517
36	2.156	1.55	1.35	1.685333	0.419697
42	1.129	0.83	0	0.653	0.584942
48	0	0	0	0	0
time (s)	fluorescence intensity (pixel int.)				
	a	b	c	mean	stdev
-18	243	255	228	242	13.52775
-12	240	255	231	242	12.12436
-6	246	255	238	246.3333	8.504901
0	241	255	234	243.3333	10.69268
6	243	255	233	243.6667	11.01514
12	246	250	228	241.3333	11.71893
18	234	238	221	231	8.888194
24	181	193	176	183.3333	8.736895
30	146	127	109	127.3333	18.50225
36	102	121	88	103.6667	16.56301
42	57	78	63	66	10.81665
48	40	63	56	53	11.78983

Chapter 11

Publications and Presented Posters

11.1 ICHC 2000

The following poster and accompanying abstract were presented at the Royal Microscopy Society's XIth International Conference of Histochemistry and Cytochemistry; Cell Biology and Imaging Tools for the New Century in York, UK (2000).

Imaging Mitochondrial Morphology, Distribution and Activity in Living Fungal Hyphae Using Confocal Microscopy

Samuel R. Swift[1], David W. Bartlett[2] and Nick D. Read[1]

[1]*Fungal Cell Biology Group, Institute of Cell and Molecular Biology, University of Edinburgh, Rutherford Building, Edinburgh, EH9 3JH, UK*

[2]*Bioscience, Phase III and Products, Zeneca Agrochemicals, Jealott's Hill International Research Centre, Bracknell, Berkshire, G42 6ET, UK*

Mitochondrial morphology, distribution and organisation have been analysed in living hyphae of *Aspergillus nidulans* and *Neurospora crassa* using a range of fluorescent probes imaged by confocal microscopy. Mitochondrial selective probes which have been used include: a) potentiometric dyes (Rhodamine 123, DASPMI and JC-1), b) non-potentiometric dyes (Mitotracker Green), c) lipophilic styryl dyes (FM 1-43 and FM 4-64) and d) GFP targeted to mitochondria. The advantages and disadvantages of each probe for analysing certain aspects of mitochondrial biology have been addressed. Relative measurements of mitochondrial membrane potential have been made in apical and sub-apical regions using Rhodamine 123, and the effects of the inhibitors azoxystrobin and FCCP on mitochondrial physiology have been assessed.

11.2 Scanning FAMS, 2001

The following poster and accompanying abstract were presented at the Foundation for Advances in Medicine and Science (FAMS) Scanning 2001 meeting in New York, USA (2001). The poster received the student scholarship award.

The abstract was published in:
Swift, S.R., Hart, C.A., Bartlett, D.W. and Read, N.R. (2001) Interactions between azoxystrobin and *Puccinia recondita, Blumeria graminis* and *Botrytis cinerea* on the microscale. Scanning 23: 153-154.